Segmented motor drive

- with multi-phase induction motor

Ph.D. Thesis

by

Flemming Buus Bendixen

Vestas Wind Systems A/S

December 2005

EF 952

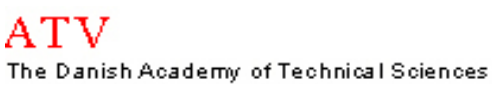

ISBN: 87-89179-60-9
December 2005

Printing: Uniprint

To my wife Luise,

my daughter Kirstine and the rest of my family.

Preface

This thesis is submitted, as partly fulfillment of the requirements for the Doctor of Philosophy, at the Institute of Energy Technology, Aalborg University, Denmark. The work has been carried out in the period January 2002 to December 2005.

The topic of the thesis is segmentation of motor drives by using multiple phases for induction motors. Before the project started some ideas (described in chapter 1.1) were discussed internally at Grundfos Management A/S (hereafter Grundfos). It was decided to start a Ph.D. project on the basis of these ideas. The Danish Academy of Technical Sciences (hereafter ATV) and Grundfos founded the project, and Aalborg University (hereafter AAU) took the academic responsibility.

After about 2 years some of the ideas in the project were evaluated and the ideas aimed better at very high power applications, the interest in the project seen from Grundfos point of view was thereby diminished. Therefore the project was transferred to Vestas Wind Systems A/S (hereafter Vestas), where the market naturally is more focused on high power applications.

I would like to thank Grundfos, Vestas, AAU and ATV for making this project financially possible.

I would also like to thank my supervisors: Pierré Vadstrup, Poul T. Frederiksen and Niels H. Petersen from Grundfos, Kenneth Krabbe from Vestas, Frede Blaabjerg and Peter O. Rasmussen from AAU.

During my project I visited Wisconsin Electric Machines & Power Electronics Consortium (WEMPEC) in Madison, Wisconsin for a 3½ month period. I would like to thank Professor Thomas M. Jahns and Professor Thomas A. Lipo for guidance and support. Besides guidance and support my wife and I would like to assign a special thank to Professor Thomas M. Jahns, his wife and charming children for taking good care of us during our stay.

Finally, I would like to thank all my colleagues from Vestas, Grundfos and Aalborg University for ideas, help, support and assistance. A special thank go to my friend Klaus Trangbaek for reviewing and correcting the thesis.

Reading guidance

In the end of Chapter 1 the outline of the thesis is specified. After the conclusion a list of references is included. In the thesis links are made to the references by the use of [x], where x is the number of the reference. A glossary of symbols and abbreviations is included to explain symbols, variables and the contracted form of often used words. The symbols and addreviations are all written in *italic*.

Abstract

This PhD project commences in modulation of motor drives, i.e. having the advantage of reducing the number of variants and improves the system reliability at error situations. Four different motor drive topologies with modular construction as common denominator are compared on a general level. The multi-phase motor is selected for further analysis. The project is limited to examine if increasing the number of phases can improve the characteristics for induction motor drives.

In the literature it is demonstrated that torque production in a six-phase motor can be increased, if a 3rd harmonic current with 1/6 amplitude is added to the 1st harmonic current. This claim is verified and the optimization of the motor design is extended to, beyond the stator tooth width, also to include the inner diameter of the stator. This means that the lamination sheet is optimized according to two geometrical dimensions. The possible torque increase proves to be strongly dependent on the physical dimensions in the initial three-phase motor. The torque increase according to the optimization is listed for a range of Grundfos motors, but in most cases the increase is only a few percent. In a single example with a six-pole motor a torque increase of 28.5% is however found. A plausible tendency is that when the number of poles is high the torque increase is also high, which is based on the trend that the stator yoke in these cases is small compared to the inner stator diameter.

A general multi winding model of the induction motor is set up. The model is able to calculate dynamical electric, magnetic and mechanic state variables, but initially it is used to calculate static characteristics in motors with different number of phases and different voltage supply shapes. This analysis show i.e. that the efficiency of the motor is not influence much by increasing the number of phases, regardless if the supply voltage is sinusoidal, sinusoidal with a 3rd harmonic component or square. The only exception is that the efficiency is lower if the number of phases is low (three) and at the same time the supply is sinusoidal with 3rd harmonic or square. Another tendency is that the torque ripple is decreased as the number of phases is increased, regardless of the supply type used. Torque ripple can be a source of acoustic noise generation, in this context a multi-phase motor can therefore be an advantage. According to various sources bearing currents, which in worst case conditions can destroy the bearings, on a multi-phase motor can be reduced considerably by using special pulse wide modulation strategies. This topic is however not analyzed further in this thesis.

A six-phase motor drive system is built in the laboratory, and a simple scalar control algorithm is implemented as a test example, to demonstrate the multi winding model. A good agreement between model and measurement is shown.

A more advanced control algorithm based on standard vector control is build for the six-phase motor. This control strategy enable, together with a return wire from the star-point of the motor back to the *mid-point* of the *DC-link* capacitors, a 3rd

harmonic current component in the motor. Controllers for the speed loop and current loops are designed. In addition to this a controller for stabilization of the *mid-point* potential in the *DC-link*, which is influenced by the third harmonic current, is developed. The control strategy is demonstrated on the build test system and a good agreement between simulation and measurements is found. Hereafter reliability in an error situation, where three phases are disabled online, is tested. This only yields a small speed disturbance, which is compensated by the speed controller. The consequence of the 3rd harmonic current, which in fact triples the number of poles on the motor, is demonstrated by driving the motor and a small load entirely with a 3rd harmonic current.

It is concluded that multi-phase motors are more redundant, have lower torque ripple, have possibility for low bearing current and can divide the power in more power-components than ordinary three-phase motor drives. They are therefore in particular qualified for big motor drives. Dependent on the lamination dimensions the torque production from a multi-phase motor can be increased by adding higher harmonic currents. This is in particular an advantage for multi-phase motors.

Resumé

Denne Ph.d.-rapport tager sit afsæt i en modulær opbygning af motordrev, som bl.a. har den fordel, at det kan nedbringe antallet af størrelsesvarianter og forbedre systemets pålidelighed under fejlsituationer. Der foretages en simpel sammenligning af fire forskellige drevtopologier med modulær opbygning som fællesnævner, hvoraf den flerfasede motor vælges til videre analyse. Projektet afgrænses til at undersøge, om flerfasede induktionsmotorer kan forbedre egenskaberne for motordrev sammenlignet med almindelige trefasede motordrev.

I litteraturen er det bl.a. påvist, at seksfasede motorer kan yde et højere moment end en traditionel trefaset motor, hvis en tredje harmonisk strøm med en sjettedel amplitude adderes til den første harmoniske strøm. I det nævnte tilfælde optimeres motordesignet i forhold til bredden af statortanden. Optimeringsprocessen udbygges til ligeledes at omfatte den indre diameter af statoren. Dermed er designet optimeret for to geometriske bliksnits parametre. Den mulige momentforøgelse viser sig at være stærkt afhængig af geometrien i den trefasede motor, som udgør sammenligningsgrundlaget. Momentforøgelsen for et større antal Grundfos-motorer beregnes ud fra de opstillede optimeringsbetingelser, men i de fleste tilfælde er momentforøgelsen imidlertid kun få procent. Et enkelt eksempel med en sekspolet motor viser dog en forøgelse på 28,5 %. En sandsynlig tendens er, at jo flere poler en motor har, jo mere kan momentet forøges, hvilket baseres på, at statoråget i disse tilfælde for det meste er lille sammenlignet med den indre diameter af statoren.

Der opstilles en generel flerviklingsmodel af induktionsmotoren, som kan bruges til at beregne de dynamiske elektriske, magnetiske og mekaniske forhold i motoren. Modellen bruges dog i første omgang til at udregne de statiske egenskaber i motorer med forskelligt antal af faser og forskellige spændingsforsyningsformer. Denne analyse viser bl.a., at virkningsgraden ikke påvirkes nævneværdigt ved en forøgelse af faseantallet, hverken ved spændinger der er sinusformede, sinusformede med tredje harmonisk indhold eller firkantede. Den eneste undtagelse er, at virkningsgraden formindskes, hvis faseantallet er lavt (tre), og forsyningsspændingen er firkantet eller sinusformet med tredje harmonisk. Der er en klar tendens til, at ripplen på momentet mindskes, hvis faseantallet forøges, uanset hvilken forsyningsspænding der bruges som udgangspunkt. Ripplen på momentet kan være en kilde til akustisk støjgenerering, hvorfor en flerfaset motor i denne sammenhæng kan være en fordel. Ifølge flere kilder kan lejestrømme, der i værste fald kan ødelægge lejerne på en flerfaset motor, også reduceres væsentligt ved at bruge specielle pulsbreddemodulationsstrategier. Dette bliver dog ikke nærmere behandlet i denne rapport.

Et seksfaset motordrevsystem opbygges i laboratoriet, og en simpel spændingsfrekvensstyring implementeres som testeksempel til eftervisning af flerviklingsmodellen. Der påvises en god overensstemmelse mellem model og måling.

En mere avanceret reguleringsstrategi baseret på en standard vektorregulering opbygges til den seksfasede motor. Sammen med en returleder fra motorens stjernepunkt til midtpunktet imellem mellemkredskondensatorerne muliggør reguleringen, at der kan løbe en tredje harmonisk strøm i motoren. Der designes regulatorer til hastigheds- og strømsløjfer. Desuden udvikles en regulator til stabilisering af midtpunktspotentialet i mellemkredsen, som påvirkes af den tredje harmoniske returstrøm. Regulatordesignet eftervises på det opbyggede testsystem, og der vises god overensstemmelse mellem simuleringer og målinger. Derefter testes robusthed overfor fejlsituationer ved, at tre faser afbrydes under drift, hvilket kun resulterer i en hastighedsforstyrrelse, som udkompenseres af hastighedsregulatoren. Virkningen af den tredje harmoniske strøm, der effektivt set tredobler poltallet på motoren, påvises ved at drive motoren og en mindre last udelukkende med en tredje harmonisk strøm.

Det konkluderes, at multifasede motorer er mere redundante, har lavere momentrippel, har mulighed for lavere lejestrømme og kan dele effekthåndteringen ud på flere effektkomponenter end almindelige trefasede motorer. De er derfor specielt velegnede ved større motordrev. Afhængig af blikgeometrien kan momentproduktionen desuden forøges for flerfasede motorer ved at addere højere harmoniske strømme. Dette er specielt en fordel for flerpolede motorer.

Table of Contents

1. Introduction

1.1 Motivation

The modern world we live in demands the use of energy in a steadily increasing rate. This is a sign on the fact that more and more people use electronic products for convenient automation and drive cars for transportation. In the short term this is a healthy development, and some say it is because people are getting richer. But energy prices increase, because the majority of energy production comes from fossil fuels. In the worst case the burning of fossil fuels will destroy our environment, because of global warming. It is however certain that all the fossil fuels will be used in a not so far away future. So it is important to use this resource as efficient as possible.

This calls attention to use the fuel in the best possible way, which means reducing the amount of energy used in any process, and thereby increasing the “lifetime” of the fuel. An example is extending the number of kilometers a car can drive on a liter of fuel. Another is to increase the efficiency of power conversion in electrical drives.

An even more sustainable way of solving the problem is to produce energy from unlimited sources. This could be producing electricity directly from the sunlight which is done in a solar cell, or from the wind which is done in wind turbines. Here the biggest challenge is to reduce the energy price so that it can compete with fossil fuels and ensure a stabile supply of energy when the wind is low.

It seems obvious that the producers of electronic components and energy are responsible for our common future, but they also face other challenges. Because the competition is hard the prices has to be low and the quality has to be high. In the end it is primarily the buyers who decide the specifications of the product. This thesis concentrates on electrical drives for various applications, and the project will focus on some of the challenges with these drives.

The electrical motor drive is widely used in both industry and domestic appliances. Advanced inverter drives ranges from sub-fractional horsepower to several millions

of horsepower. The applications of course also span from pumps, fans, conveyers to electric cars, propulsion, etc. These very different applications demand very different characteristics of the drive.

1.1.1 General characteristics for a good motor drive

The producers of electrical drives have numerous challenges, which go into different directions, blurring the picture of perfecting the characteristics of the motor drive. A motor drive is defined as a motor and an inverter. The following is a list of characteristics for a good motor drive.

- High reliability/robustness
- Fast dynamic shaft performance
- No service
- Long lifetime
- Easy to produce
- Low acoustic noise
- Low electromagnetic emission and high electromagnetic immunity [37].
- High efficiency
- Low standard unit cost
- Low use of materials
- Low weight
- No or minimal use of materials that are a threat against the environment.

The weight on each individual characteristic depends on the producer and on the application where the motor drive is used. This project can only contribute to a few of these always increasing demands.

1.2 Background of present project

The initial idea for this current project takes the starting point in the motor design field. Segmenting the stator in an electrical motor is a new trend in motor design reducing the weight, price and increases the efficiency [21], [22] and [23]. Segmenting the stator refers in this case to splitting the stator in smaller modules, enabling i.e. very high copper fill factors. Can the idea be transferred to the electronic part in an adjustable speed drive too? Meaning that, the electronic inverter is segmented in smaller modules. This was one of the initial ideas for this project. The electronics are becoming cheaper and cheaper, therefore using one power converter branch placed on each stator tooth becomes more and more attractive. The advantages could be some of the following:

- Lower *VA-rating* of the individual parts. Enabling the possibility of scaling the product when going toward high power units. Keeping a low voltage and current also help safety and complexity.

- Reuse the same power converter for a larger power range by varying the number of units. This leads toward lower prices because of mass production and a lower number of variants.
- The drive becomes more redundant because if a failure occurs in one module, the rest of the modules are not affected, so they can continue maybe at reduced power.
- More control flexibility. If all the modules measure electrical and magnetic properties, the information about the condition of the motor is redundant, which means that if a sensor fails, then the other can be used to estimate the failing component.
- Integration of motor and electronic. The integrated design of electronics and magnetic components enable easier access to measurements which can improve the control strategy hence the performance.
- At low load, parts of the system can be switched off, and inactive windings can maybe be used as sensors. If the load follows the speed, then at low speed the motor is only partly loaded. This overcapacity means that part of the windings can be used as sensors instead of active power producers. At low speed sensor less control becomes imprecise this problem could be minimized by the extra windings.
- Depending on design, higher efficiency, lower noise or higher torque/volume can be obtained if the number of phases is increased [1], [5].

1.2.1 Vision for segmented motor drive

Even though the ideal segmented motor drive might be utopia, it is inspiring to try to picture it in a vision. The vision for a completely segmented motor drive is illustrated on Figure 1. It shows a “black box” motor drive, which is made from several identical segments/modules. The tree curves below the text symbolize the tree-phase grid, and the arrow is a symbol of the mechanical rotation. The electrical power is blue (like the curves) and the mechanical power is red (like the arrow). Thereby in the segments/modules electrical energy is transformed to mechanical power (blue and red) in one integrated unit. The motor drive is shaped like an arrow, which symbolize a dynamic and innovative design.

It is indicated that the drive is redundant, if i.e. one segment fails only part of the motor fails and the motor is only partly damaged so the drive still is able to run. Segmenting the drive also means that the price for one segment can be reduced because of mass production. Furthermore the segmentation is a possible solution to the problem of having a range of different motor drive sizes. If one segment converts one unit of energy, ten segments will convert ten units etc. The drive looks simple, so it should also be simple to install for the user. Storage will also be easy because only one type of module exist, so the number of different production items is minimized. The knowledge about this module can be very specialized and deep in every business segment ranging from development and production to sales and service.

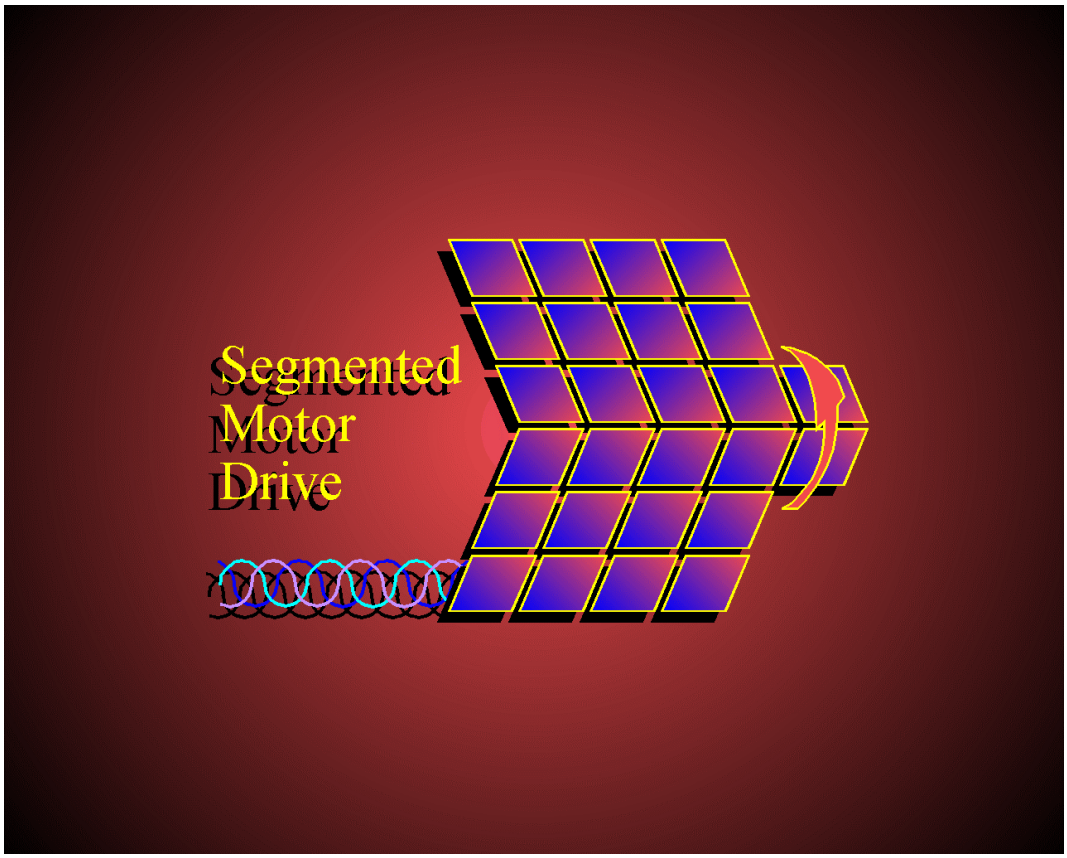

Figure 1	Vision for segmented motor drive illustrated by symbolic figure.

1.3 Topology analysis

Before analyzing which topology to continue working with for this Ph.D. project, some promising ideas have to be described. The best ideas from an intensive literature study, and some new ideas inspired by the trends are forming the project. They are described in the next section.

1.3.1 Multiphase motor

One way of segmenting a drive could be to build it in blocks of one, two or three phases. If two three phase blocks are chosen, the torque produced by the asynchronous motor can be increased. The shape of the flux density in the air-gap of the motor is made more square as a function of the rotor position. This is described

and analyzed in (see [4]). The idea is to inject a 3rd harmonic current into the stator windings which demands a fast and expensive current controller for each phase.

In general this principle can be extended to include any number of higher harmonics. The rule is that the total number of phases has to be at least two times higher than the number of harmonic current components injected. This in fact gives two phases seem from the harmonic current. On top of this the common star-point of the machine has to be returned to the *DC-link mid-point* (or an extra inverter branch) and carry current (like a normal two phase motor). If the star-point is not connected, the number of phases has to be at least three times as high as the highest harmonic current. Otherwise the harmonic component will only give pulsating torque. This is because the highest harmonic current needs three phases or at least two and a star point connection to produce nonzero mean torque. The harmonic current could be even, but then the flux distribution would not be symmetric around zero, so in general the first usable harmonic component is the third. So if for example the 3rd harmonic current has to produce torque, then a six-phase motor with star point connected to the midpoint of the *DC-link* voltage can be used. Alternatively, a nine-phase motor without a star-connection can be produced. In Figure 2 from the top a three-phase, a six-phase, a six-phase with 3rd harmonic and a nine-phase motor is shown. The two last drives are able to produce extra torque from 3rd harmonic current injection.

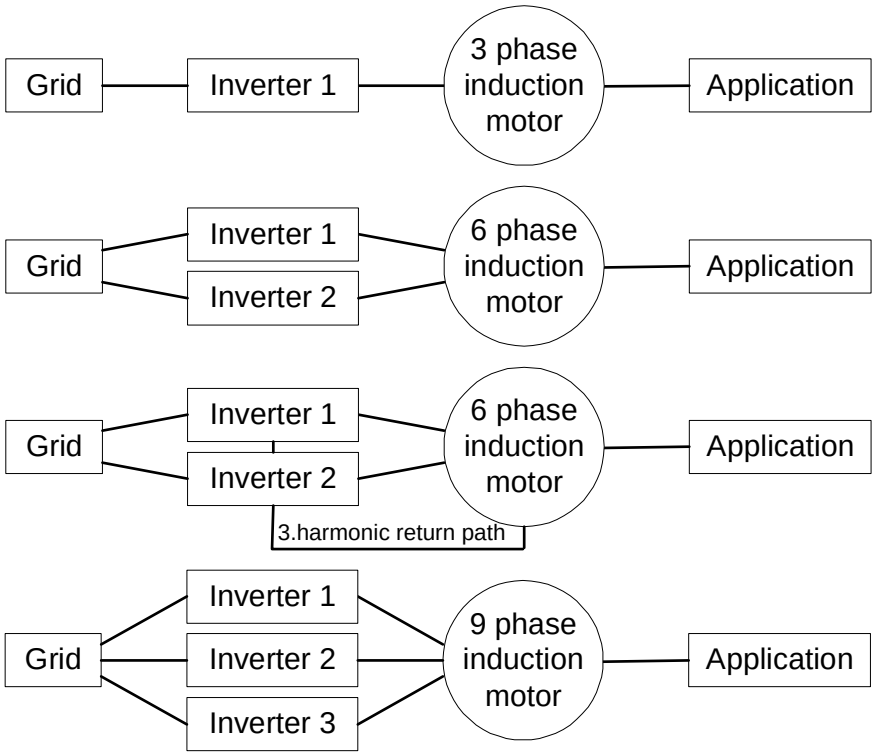

Figure 2 Segmenting the inverter and increase the number of phases of the motor.

In [5] a multiphase motor is also discussed. Here it is described that if the number of phases is high, then the motor can be supplied with a square-wave. The motor will have the same (or nearly the same) efficiency and performance, and the torque ripple will not be higher than for a standard three-phase supplied motor. This topology can be compared with a DC-motor with multiple commutators. If a simple supply like a square-wave voltage is used instead, in conjunction with multiple phases, then the current will also have a content of higher harmonics. It is not as controllable as if the current is regulated directly because the stator resistance and leakage inductance will low-pass filter the voltage. However it could be interesting to examine if the ripple torque could be comparable to the three phase sinusoidal supplied motor, and if the motor would be able to produce higher torque (or at least the same) for the same *RMS* value of the current.

The number of possible switch stages in a n-phase motor is 2^n. Therefore in some aspects the multi-phase motor can be compared to a multi-level inverter. The *PWM* switch frequency can be decreased if the number of different voltage levels is big. This means that at high phase numbers, the switch frequency can be very low, even simple six-step or square voltage switching. Low switch frequencies gives low switch loss, which increase the possible peak current in the switches. If i.e. the

number of phases is doubled and the same switches are used, then the *VA-rating* of this inverter is more than doubled, because the switch losses are much lower.

Using multi-phase motors gives the possibility to change the number of poles to extend the speed range [25], [26]. This is especially advantage if the application is electric vehicles because in this application mechanical gear change can be avoided if the motor can deliver high torque at low speed and in the same time is able to run fast at constant power. Generally motors with high pole numbers give high torque at low speed and motors with low pole numbers are able to run fast and maintain low iron loss.

Another advantage with i.e. six-phase motors is that the common-mode voltage can be canceled out using special *PWM* patterns [27], [29]. This nearly eliminates bearing currents which deteriorate the mechanics of the machine.

1.3.2 Multiple motors on the same shaft

Different motors have different advantages. A big induction motor usually has a high overload capability, and the permanent magnet motor usually has high efficiency. It is obviously a good idea to combine the two motors taking the best from both worlds, and the price could be competitive, especially at higher power levels, where the initial cost of one inverter becomes a smaller portion of the total cost of the system (see Figure 3). The motors can be coupled together on the same shaft or another mechanical connection, and the inverter/inverters of the motors can be coupled in many different ways.

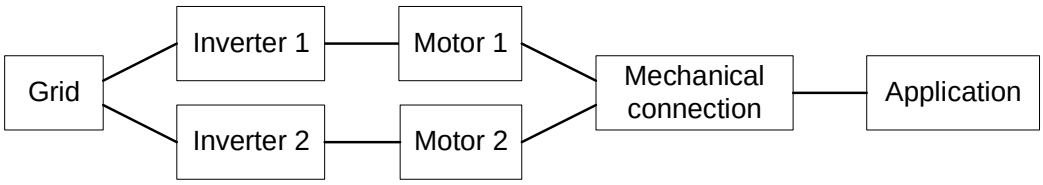

Figure 3 Multiple motors on same shaft.

If a permanent magnet motor and an induction motor are combined, the permanent magnet motor can supply mechanical power at low speed using a standard frequency inverter, because it has a high efficiency. When higher power is needed, the induction motor can be started, supplied directly from the grid or through a simple triac inverter. But if the induction motor is directly connected to the grid it has to run at or very near to fixed speed. Variable speed load can be reintroduced by using a power split device. A power split device is also used between the driving wheels in cars to distribute the power and enable different speeds of the wheels during curves.

New suggestions for applications for power split devices are hybrid vehicles. The main problem to solve in this idea is the control of the motors when the load is shared between them. Another important issue is to find the best topology combining the motors. It is also important to examine if the number of different motor sizes in the production can be reduced, as this could decrease the production cost and also increase the number of produced units with the same size.

Inverter 1 and 2 and or motor 1 and 2 could be identical, which could give all the mass production advantages mentioned in 1.2.1.

1.3.3 Delta pentagon

When a motor with several phases is needed, an inverter with several legs has to be built. All the switches in the inverter need gate drives, and therefore the price of the inverter increases when the number of switches increases.

An idea could therefore be to use the fact that the sum or difference between two sinusoidal voltages with the same frequency shifted by an angle, gives a sinusoidal voltage with a third angle. This may be used to make e.g. fifteen phases on the motor with only five legs in the inverter (see Figure 4). In the figure the five voltage supplies are named U1 to U5, and the motor phases are modeled by the impedances Z1 to Z15. Other combinations are maybe possible so one of the main tasks to solve with this idea is to examine different combinations of phase numbers on inverter and motor. This solution is not directly segmented electrically, but the link between inverter and motor is relaxed, so the optimal number of phases on the inverter probably can be selected together with the optimal number of phases on the motor.

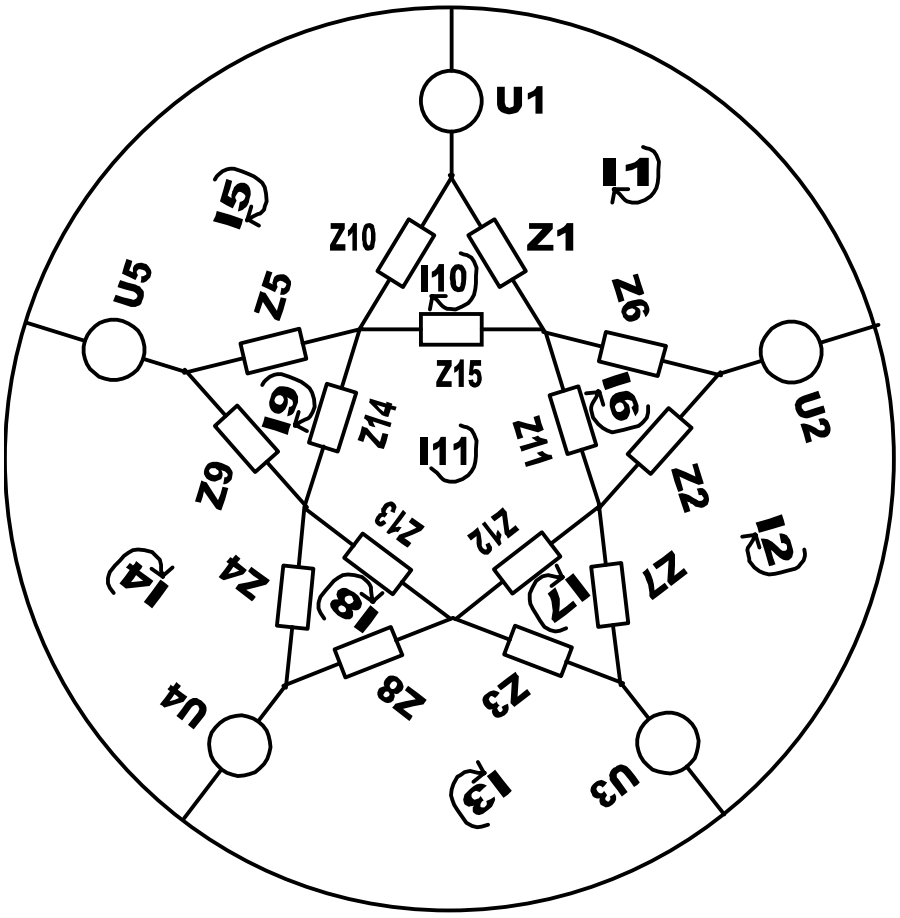

Figure 4	Delta pentagon with five supplies and fifteen windings (or phases).

1.3.4 Yoke winding

The stator winding in a motor decides the number of phases and poles. After the motor is produced, it can normally only be optimized for one specific combination of phases and poles. This is because the winding has to span one pole (or at least a big part of the pole, with a reduced pole pitch). Another issue is that the end winding is inactive, resulting in copper loss without torque production.

Instead of winding the motor around the tooth (or on the inside), it is possible to make a return path for the current on the outside of the yoke. This is actually how the original induction motor invention by Nicolas Tesla was created in 1887 [36] (see Figure 5). If this yoke winding is used, then the number of poles can be selected after production. Keeping in mind that then the motor (especially the yoke width) needs to be designed for the lowest number of poles. Actually it is possible to

change the number of poles in the application, which can be an advantage if the motor is an asynchronous motor. Even though the return path on the outside of the yoke is not active, it could be an attractive solution, because in many asynchronous motors the end wire is longer than the active part in the motor. It is even possible that the fill-factor can be higher because it is not dependent on the end winding (which it is in a standard motor). Stray fields from the return path will certainly appear but this will also be the case for an end-winded stator. The winding process has the potential to be much simpler if the yoke is split in segments, because the wires are winded directly on the stator. The yoke solution is not limited to a certain motor type, in could be used for both asynchronous and permanent magnet motors. Online change of pole numbers is not possible with permanent magnet motors, but it is still possible to produce motors with different number of phases.

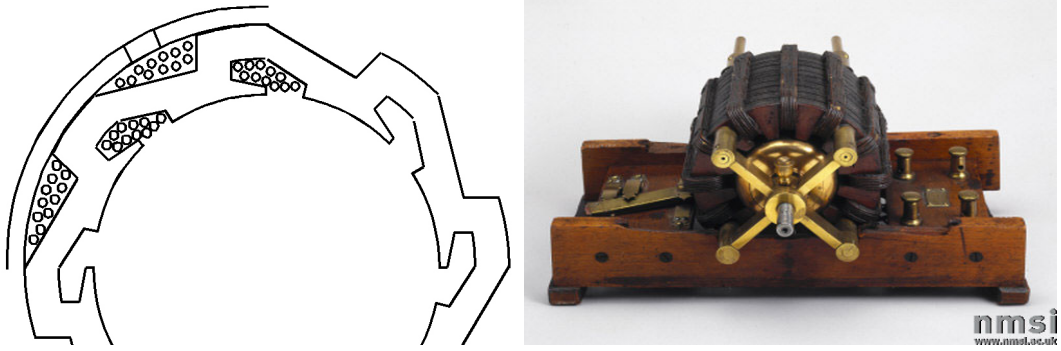

Figure 5	Example of a yoke wounded motor. Left schematic drawing and right original design by Nicolas Tesla 1887 [36].

The inverter to this type of motor could be integrated directly together with one tooth, in some kind of electrical to mechanical block segment. This is very closely related to the vision for the project. But scaling of the topology seems to involve some problems, because it either has to be along the axial length (resulting in the same solution as multiple motors on the same shaft) or around the circumference (resulting in mechanical imperfect air-gap).

1.4 *SWOT* analysis of suggested topologies

All the above-mentioned ideas have to be evaluated, and for this task a *SWOT* (strength, weakness, opportunities, threads) analysis is used. It is a simple schematic representation of the advantages and disadvantages of a topology.

Short description	Strength	Weaknesses	Opportunities	Threads
Multiphase motor.	The individual switches do not need as high a current rating, because they can share the current. Motor has better performance according to some references [1] & [5].	The number of gate drives is high. But it could be used in combination with the delta pentagon.	Square wave possible: use of slow IGBT's with low static loss. Maybe a simpler inverter with thyristors.	It could be expensive to produce a motor with more than 3 phases. The inverter might also cost more than a standard inverter. But keep in mind that the number of inverters could be higher (fewer variants) giving a lower price.
Multiple motors on same shaft.	At partial load only one motor is needed making the drive redundant. Modular build.	Expensive with more than one motor and/or inverter.	Better efficiency. More than one type/size of motor can be used.	Could be complicated to control.
Delta-pentagon	Use five phases to make fifteen. Or with another configuration use N phases to make M phases.	Difficult to control each phase individually.	Other configurations. Patentable. Connection with "Multiphase motor".	It could be necessary to use different numbers of windings! Maybe only 1st harmonic component.
Yoke winding	Small end windings depending on diameter/length ratio. High fill-factor in slot. Segmented. Pole change is possible. Control of each tooth.	Only ½*N*I is active. Magnetic noise from yoke winding. Weaker design with open yoke.	Could be connected with "Multiphase motor". Modular building blocks. Return/end-winding is independent of the number of phases.	Maybe difficult/expensive to produce. Wire/winding is longer than for a standard motor under certain conditions.

1.4.1 Selecting focus for the project

Since the ideas are compared and explained on different levels and since they do not solve the same problem, it is difficult to select one of them. Therefore it is important to study the final application, and compare the ideas at system level. But even though the ideas improve the drive or reduce the cost, it is uncertain that the idea with the highest value is the best idea. So another very important way to compare the ideas is to evaluate how likely it is that the idea will be a success. With these two tools in hand, the best idea can be selected.

Using the *SWOT* analysis as a reference and evaluating the chance of success, the topologies can be compared and the most qualified can be chosen.

The idea of "Multiphase motor" is one of the ideas with the highest potential, and it is already known to be an advantage according to the references.

The idea "Multiple motors on same shaft" is less attractive than "Multiphase motor", but it has a very good chance of success. For the idea "Multiple motors on same shaft" the greatest task, in developing this idea, is making the sharing controller. The motor and inverter can be made from standard components. Since the focus in this project is selected to be the connection between electronic and motor parts, the control is not in focus. A control algorithm evidently has to be made, but it is not the only focus area.

For the “Yoke winding” the main advantage lays in the production method (although new production lines and investments are needed), and in some areas like efficiency it could even be a disadvantage compared to a standard motor. This PhD. project is set to focus on science/development and not production, therefore this idea is rejected.

The “Delta-pentagon” is only an advantage if a high number of motor phases are needed. So it could be part of another topology like e.g. “Multiphase motor”. But since the “Delta-pentagon” needs asymmetrical windings (or another configuration with another number of input/output phases) it demands a deeper analysis. Further work however shows that extra torque from a multiphase motor demands higher harmonic content, which the delta-pentagon will have big problems supplying, at least if the phase shift of the harmonics in each motor phase has to be aligned. Since the potential of this solution is considered to be very small, it is chosen not to continue the work with the “Delta-pentagon” topology.

On the basis of the above discussion it is chosen to continue the work with the topology “Multiphase motor”.

1.5 Problem formulation

The selected topology obviously raises a lot of questions. To focus the further work the problem can be narrowed down to a single general question, which the rest of the report is concerned with.

“Can a multi-phase induction motor improve the general drive characteristics compared to a standard motor drive?”

1.6 Limitations in the project

It is essential to limit the scope of a Ph.D. project. Therefore a more narrow working area has been chosen. The following limitations are selected:

- The rotor position and stator currents are assumed to be known from measurements. In other words there will be no sensor-less control.
- It is assumed that a *DC-link* voltage is available. Rectifying, power factor correction and filtering of the grid voltage are not investigated.
- Matrix converters are not considered as a possible power electronic solution in this case.
- The power range interesting in the project is expected to be from a few kW and above. Segmentation of power inverters with lower power levels is considered to be too expensive, because of extra drivers, switches, calculation power demands etc.
- The theories throughout the thesis might as well apply for generator drives, like the ones used in wind turbines, but the focus are on motor drives.

- The selected motor type is induction motors. Switch reluctance motors are not considered because they usually have “hard to solve” problems with acoustic noise, which is considered to be critical in most applications. Permanent magnet motors are rejected simply to focus the project further.
- The application for the motor drive is any variable torque application using standard motors with integrated inverters [24]. Actually it is expected that the multi-phase induction-motor-drive can be used in the same applications as a standard three-phase, if the cost of extra phases can be compensated by improved drive characteristics.

1.7 Outline of the thesis

The outline of the thesis is described chapter by chapter in the following list:

1. **Introduction:** In the introduction the technical background and motivation for the project are first described. Then some general characteristics for a good motor drive are listed. The technical motivation and market desire are merged into a Vision for the project. The project is also limited due to resource reasons. Four topologies, taken directly from or inspired by an intensive literature study, are described and compared in a *SWOT* analysis. This gives the basis for the problem formulation “Can a multi-phase induction motor improve the general drive characteristics compared to a standard motor drive?” Limitations for the further work are set up.
2. **Design of six-phase induction motors:** In this chapter the static design of a six-phase motor with 3rd harmonic current injection is compared to a standard three-phase motor. The basis for this comparison is taken from the literature where the torque gain is discussed. The efficiency gain is also discussed. The static motor model calculating torque gain is optimized for more parameters than suggested in the literature. Potential extra torque gain is quantified for commercially available induction motors.
3. **Dynamic models for multiphase motors:** A three phase multi-winding model is first described. This state of the art model is expanded to multiple phases and used to compare multi-phase motors. The model is implemented in *Matlab*/*Simulink*, and parameters are taken from the *SPEED* motor design software (see Glossary of symbols page 7-152). The link to the *SPEED* software ensures that the dynamic model is established on the basis of well-known and well-tested design software. From the dynamic simulations several steady state values are calculated, including a simple model for flux density, iron losses and efficiency. The simulation model is used for comparing different fixed voltage supply shapes and motors with different number of phases. A test case example of a 3 kW induction motor is used to demonstrate and partly verify the theoretical calculations.
4. **Verification of a six-phase motor model:** A six-phase prototype motor, which is further described in Appendix C and D, is built and setup in a laboratory test bench. A simple *U/f control* principle is implemented in a *D-Space* system, and two standard three phase inverters are used to supply the

six-phase test motor. This is used to demonstrate and partly verify the dynamic model. The *D-Space* system is used as measurement system so first this function is checked. Measured and simulated values in two cases are compared. The first case is with sinusoidal voltage supply and no star-point connection. The second case is with sinusoidal voltage with 1/6 amplitude 3rd harmonic voltage where the star-point is connected to the *mid-point* of the *DC-link* capacitors.

5. **Controllers for a six-phase motor:** In this chapter the standard vector control strategy of a three-phase induction motor is first described. After this a vector control for a six-phase motor drive supplied by a six-phase inverter including speed and current loop is described and designed. This control strategy is suggested in the literature, but in addition to the six inverter-branches an extra branch is used to stabilize the voltage in the neutral point connection of the motor. The stability problem is analyzed and a new *mid-point* control algorithm is suggested, eliminating the need for an extra branch under certain conditions.
6. **Verification of control strategies:** The control strategy is implemented in a *D-Space* system. The speed loop and the current loops are tested. The entire control algorithm is tested and the new *mid-point* controller is tested. Then one kind of redundancy where three phases of the six-phase motor are turned off online is demonstrated. Finally it is demonstrated that the motor is able to run on a 3rd harmonic current as the only current source.
7. **Conclusion:** The thesis is summarized and a conclusion is made. New contributions mentioned throughout this thesis are listed. A small table listing the headline comparisons between three phase induction motors and six phase induction motors with 3rd harmonic current injection is setup and discussed. Recommendations for designing multi-phase induction motors are given together with advice to why, when and where to use multi-phase induction motors. Finally, suggestions for further work are discussed.

The thesis is supplemented with five appendices which are:

A. **Test system:** In this Appendix the test bench, the inverter, the motor and all other hardware are described. The *D-Space* and *Matlab*/*Simulink* controller diagrams are represented and discussed. Finally the control cockpit is pictured and notes are made.
B. **Simulation software:** In this Appendix the dynamic simulation program is included. The *Simulink* block diagram used for dynamic simulations is pictured. At last the steady state values calculated in chapter 3 and listed in Appendix E are explained.
C. **DQ-axis model of six-phase induction motor:** In this Appendix a dq-axis model of a six-phase induction motor is setup, discussed and parameters are found. At last the dq-axis model is compared to the multi winding model presented in chapter 3.

D. **Motor data:** In this Appendix the most relevant parameters for 3, 5, 6, 9 and 12 phased motors are listed. The color code used in the table is explained in Appendix B.

E. **Static results from dynamic simulations:** In this Appendix the steady state results calculated using the multi-winding model presented in chapter 3 is listed. The parameter names are explained in Appendix B.

2. Design of six-phase induction motors

2.1 Introduction

To answer if a multiphase induction motor can improve the general drive characteristics, first the system has to be analyzed. In this chapter the special case with six-phases is taken as an example of how higher harmonics can increase the maximum torque production. The torque gain is quantified according to previous work. The state of the art is given by [1], so the analysis in this chapter is mainly based on this work.

The efficiency gain, when increasing the number of phases to six, according to different references is discussed. In the next chapter this issue will be addressed further.

In the end of the chapter the torque gain is recalculated on the basis of a redesign of the motor with two degrees of freedom, where previous work is based on only one degree of freedom. It is found that redesigning the lamination gives extra torque gain.

2.2 State of the art motor design model

In this section the state of the art six-phase motor design calculations are presented. The calculations focus on the torque gain from a six-phase induction motor with a 3^{rd} harmonic current injected. Some discussion of the efficiency according to different references is also given.

2.2.1 Description

The model described in [1] can be used to analyze six-phased induction motors, where the current is controlled to contain both a fundamental and a 3^{rd} harmonic

component. This is done to improve the torque production. To realize that the torque can be improved using higher harmonics, and to quantify how much it can be improved, a simple model of the motor is analyzed here, starting with a standard three-phase motor, and extending it step by step, until the potential for the six-phase motor is explored.

2.2.2 The *MMF*

In [1] a standard full-pitch winding motor where the winding function looks like shown in Figure 6a is analyzed. The full pitch winding stator gives a winding function pictured in Figure 6b.

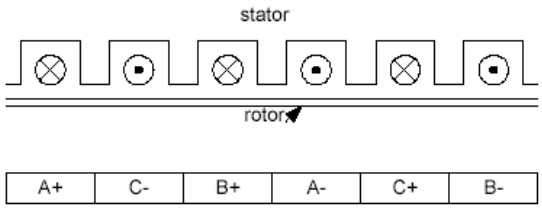

(a) Winding distribution.

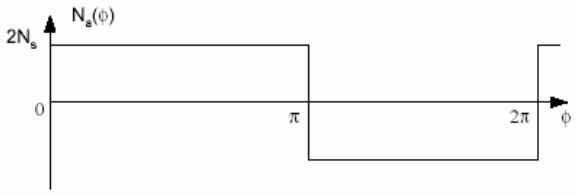

(b) Winding function.

Figure 6	Slot-wire diagram and winding function for a three-phase full pitch winding machine [1].

With this winding of a three-phased motor the *MMF* doesn't contain the even harmonics. The triple harmonics are also eliminated if the three phases are connected in a floating star point [10], which leaves the following harmonics 1, 5, 7, 11, 13, 17, 19 … If the supply current is sinusoidal the amplitude of the first three harmonics in the *MMF* have the relative amplitudes 100%, 20% and 14% if the

winding is full pitch as shown in Figure 6. The harmonics are in general 1/*h*, where *h* is the number of the harmonic [10]. The fifth harmonic is a negative sequence, which means that it produces negative torque for all positive speed. The seventh harmonic is a positive sequence, so it actually produces positive torque, but only if the speed is lower than 1/7 of synchronous speed, after this the torque production from the seventh harmonic is also negative (in a sense the seventh harmonic works like a generator) [38].

2.2.3 Zero sequence current

If the star point of the motor is connected i.e. to the midpoint of the *DC-link*, then a zero sequence current can be injected. The zero-sequence current will flow in the wire from the star-point back to the inverter. If a 3rd harmonic current with an amplitude of I_3 and a rotation angle of 3θ is injected in the phase wires, then the *MMF* of the zero sequence can be written like shown in equation (1) according to [1].

$$F_0 = \frac{4}{\pi}\frac{2N_s I_3}{3\cdot 2}\left(\cos(3\phi - 3\theta) - \cos(3\phi + 3\theta)\right) \quad (1)$$

Where:	*Var*	*Description*
	F_0	*Zero sequence MMF*
	ϕ	*Angular position along the air-gap.*
	θ	*Angular position of the electrical field.*
	N_s	*Number of turns in a slot.*
	I_3	*3rd harmonic stator current.*

This *MMF* produces a wave following the 1st harmonic *MMF*. It is three times as fast, but it also has to make three times as many waves as the 1st harmonic. If the 1st harmonic for example sees two poles, then the 3rd harmonic sees six poles. But unfortunately there is both a negative and a positive wave, and the summarized effect is a pulsating torque, with zero mean value, which of cause is undesirable. In a way the 3rd harmonic current only sees a single phased motor. In the physical positions $\phi = n\cdot\pi/3$ for any given integer *n*, $F_0 = 0$ hence the flux from the 3rd harmonic current is zero all the time, but the positions $\phi = n\cdot\pi/3 + \pi/6$ for any given integer *n*, the *MMF* is $F_0 = \frac{4}{\pi}\frac{2N_s I_3}{3}\sin(3\theta)\cdot\cos(n\cdot\pi)$. The *MMF* around the circumference of the air-gap is not rotating it has positions with zero amplitude all the time, which means that it does not create a rotating field.

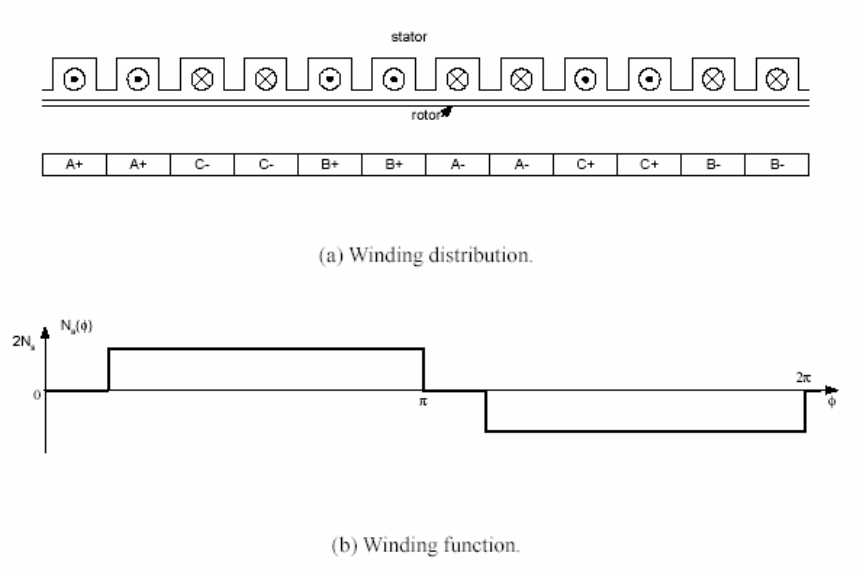

Figure 7	Slot-wire diagram and winding function for a three-phase distributed winding machine.

If a distributed winding like in Figure 7 is used, then the harmonic components are 96%, 5% and 3.7% compared to full pitch [10]. So the fifth and seventh components are reduced dramatically, but the 1st harmonic is nearly the same. So from the higher harmonic components point of view this motor is maybe all in all better. But just like with the full pitch winding motor a zero sequence current will again just give a pulsating torque.

Now three more currents are introduced, so that all in all six phases supply the motor. The motor configuration now is like a dual three-phase motor. The stator winding is shown in Figure 8. From the electrical point of view phase *X* is shifted thirty degrees back from phase *A, Y* is shifted thirty degrees back from phase *B* and *Z* is shifted thirty degree back from phase *C*.

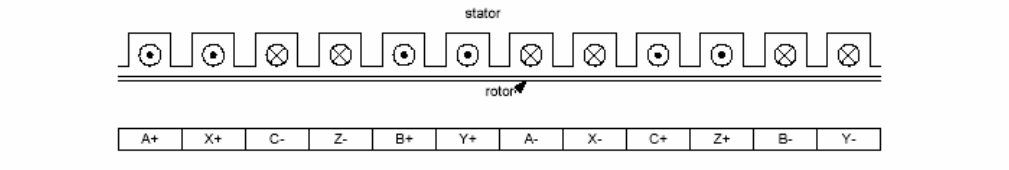

Figure 8	Slot-wire diagram for an asymmetric six-phase machine with full pitch windings.

This is basically the same as six independent full pitch windings (see Figure 6), therefore the 1st harmonic is again 100%. But the fifth and seventh harmonics do not produce any torque, the torque from the two three-phased systems cancel each other. In itself this is interesting (see chapter 3 and [6]) because the 1st harmonic *MMF* in increased by 4%, but if a zero sequence current is injected in each star-point of the two three-phase systems it becomes even more interesting. In practice the star-points of the two systems are connected and a neutral connection is made. If a standard *VSI* is used then the neutral can be connected to the midpoint of the capacitors (see also chapter 3). The zero sequence *MMF* can be summarized from the two systems, with 30^0 between with respect to both current phase and physical placement of the winding see (2).

$$\begin{aligned} F_0 = \; & \frac{4}{\pi}\frac{2N_s I_3}{3\cdot 2}\left(\cos(3\phi - 3\theta) - \cos(3\phi + 3\theta)\right) + \\ & \frac{4}{\pi}\frac{2N_s I_3}{3\cdot 2}\left(\cos(3(\phi + 30) - 3(\theta + 30)) - \cos(3(\phi + 30) + 3(\theta + 30))\right) \end{aligned} \tag{2}$$

Reducing to equation (3):

$$F_0 = \frac{8}{\pi}\frac{N_s I_3}{3}\cos(3\phi - 3\theta) \tag{3}$$

This *MMF* actually produces a positive torque all the time because the electrical and mechanical speeds follow each other. The 3rd harmonic field is now rotating around the circumference of the air-gap both in time and space, three times as fast at the fundamental harmonic. In other words the 3rd harmonic current creates three times as many poles as the 1st harmonic current, and it rotates with three times the speed. It is important to note that a zero sequence wire has to be connected to a neutral point, and the neutral point potential has to be stable, which complicates the inverter (see chapter 5). It also means that the *VA-rating* of the inverter has to be higher than in e.g. space vector modulation. The effect used in space vector modulation, where the voltage has a 3rd harmonic component, which gives up to 15% higher *VA-rating*, cannot be used if the star point voltage is fixed to half the *DC-link* voltage.

2.2.4 The flux density considerations

In motor design it is essential to avoid saturating the iron too much. Therefore an intensive analysis of the peak flux levels in the stator teeth (proportional to the peak

air-gap-flux) reveals that the best amplitude of the 3rd harmonic current is 1/6 of the 1st harmonic (see [1]). Using this value the 1st harmonic flux density can be increased by $2/\sqrt{3}$ or roughly a 15% increase for the same peak value of the flux density in the air gap (see Figure 9).

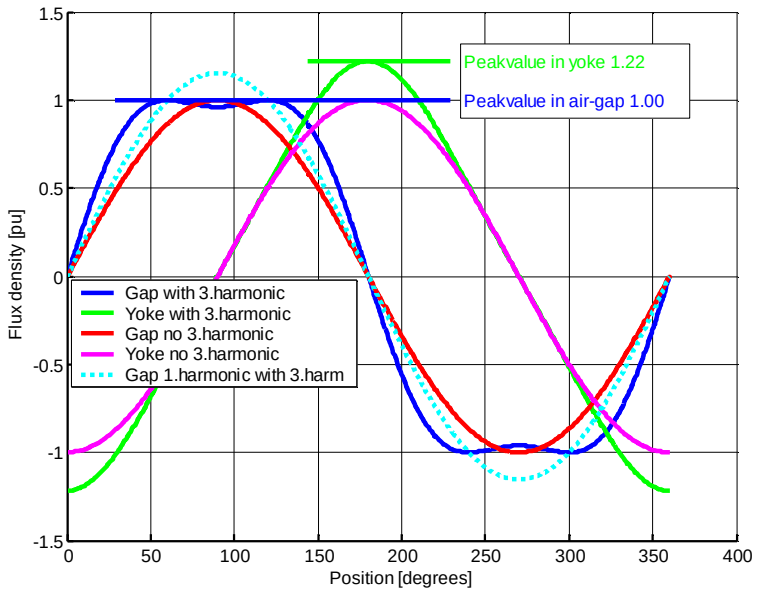

Figure 9	Flux density distribution in air-gap and yoke with and without 3rd harmonic injection. Blue means the flux density in the air-gap if a 3rd harmonic component is injected. Red means the flux density in the air-gap with only fundamental components. Cyan dotted means the waveform of the fundamental flux density in the air-gap if a 3rd harmonic component is injected. Green means the flux density in the yoke if a 3rd harmonic component is injected. Magenta means the flux density in the yoke with only fundamental components.

In Figure 9 the curves refers to the flux density along the angular positions in a two pole motor. The values are normalized to the per unit system.

The torque produced by the 1st harmonic current in an induction motor is proportional to the square of the amplitude of the 1st harmonic current ($T \sim I^2_{1.harm}$) [37], assuming linear behavior of the magnetic circuit, which means unsaturated iron. Therefore the six-phased motor, having a 15% higher 1st harmonic current, will have a 33% higher torque production from the 1st harmonic component alone. But the motor also has a positive torque production from the 3rd harmonic current, it is

found to be 2/27~7% (see [1]). So that all in all the total torque increase is 40% compared to a standard three phase motor without 3rd harmonic current.

But the drawback is the peak value of the flux density in the stator yoke, which hasn't been analyzed yet. Generally speaking the flux density in the yoke is the integral over one pole width of the flux density in the air-gap (see Figure 10). So with 1/6 3rd harmonic current injected, the peak value of the flux density in the yoke is increased by 22% (see equation (4)), because the flux density in the yoke is increased with both a factor $2/\sqrt{3}$ and $19/18$.

$$\text{Yoke peak flux increase} = \frac{\frac{2}{\sqrt{3}}\int_0^{\pi}\left[\sin(\theta)+\frac{1}{6}\sin(3\theta)\right]d\theta}{\int_0^{\pi}\sin(\theta)d\theta} = \frac{2\cdot 19}{\sqrt{3}\cdot 18} \approx 1.22 \qquad (4)$$

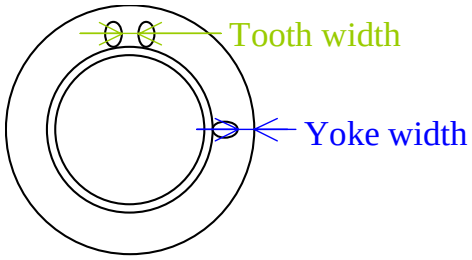

Figure 10	Showing where the highest flux densities in the teeth (green) and in the yoke (blue) are located.

It is nearly never acceptable to further increase the peak flux density in the stator yoke on a well designed motor, because the loss balance is shifted and the saturation level is increased, so a trade off has to be made. Figure 11 shows how big the torque gain is at different flux reduction factors *k*. The flux density in the air-gap is multiplied by *k*, which therefore also reduces the peak flux density in the stator yoke.

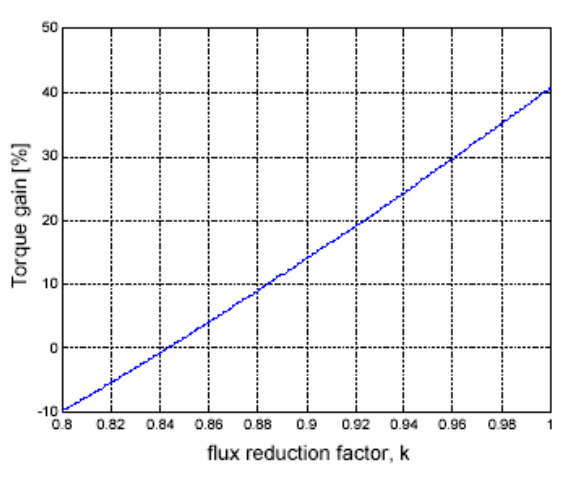

Figure 11	Torque gain in an asymmetrical six-phase machine with 3rd harmonic injection considering different reduction factors *k* in the air-gap flux to avoid saturation in the stator yoke flux.

Now if for example no increase in the peak value of the yoke flux density is acceptable, then the reduction factor has to be $\frac{\sqrt{3}\cdot 18}{2\cdot 19}\approx 82\%$ (reciprocal of equation (4)), and at this value the torque is actually decreased by 5.3% compared to a standard three phased motor! But if the flux is decreased by 22%, then the peak value of the flux in the teeth is also decreased by 22%, and this means that the potential of the iron is not used fully. To use the iron fully again the tooth width can be decreased, which gives more space for the windings, hence a better efficiency for the motor. Again this has to be quantified, so that the real value of the six phased motor with 3rd harmonic current injection can be revealed. So in Figure 12 a simplified model of the stator with slots and teeth is presented.

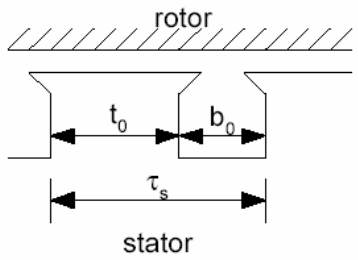

Figure 12	Simplified representation of stator slot and tooth.

A parameter γ can be defined as $\gamma = t_0 / \tau_s$. γ is the tooth width ratio for the initial motor design. After some calculations (see section 2.3.5) it is found that if the extra space from the thinner stator teeth is used for thicker windings, able to carry a higher current, the total torque gain can be summarized in Figure 13 see equation (20).

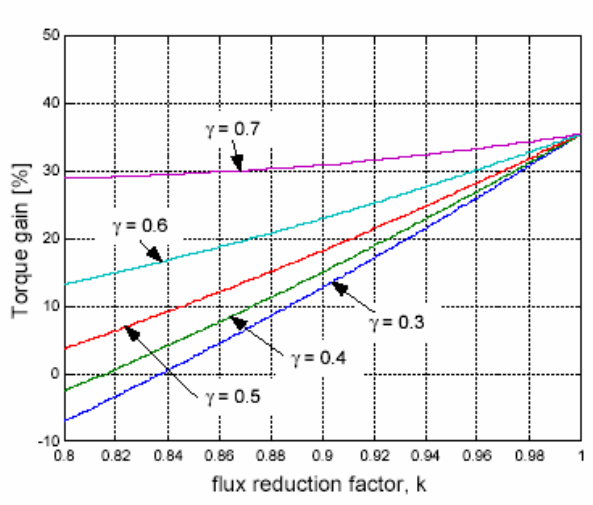

Figure 13	Torque gain in an asymmetrical six-phase machine with 3rd harmonic injection considering reduction in the air-gap flux to accommodate the stator yoke and increase in the surface current density [1].

Note that the amount of copper used is greater in the case with the new design because the stator slot area is increased (see also 2.3.2 & 2.3.3).

2.2.5 Summary

If no increase in peak yoke flux density is acceptable, *k* has to be 0.82. And if for example γ is 0.6, then the torque from the motor can be increased with approximately 15%!

2.2.6 Efficiency

In [1] the measured efficiency of a six-phased motor with 3rd harmonic current is compared with the measured efficiency of a standard three phase motor (see Figure 14). It was found that for all loads except overload (approximately 13Nm in [1]), the efficiency was lower for the six-phase motor with 3rd harmonic current, even though the effect of a smaller tooth was taken into account. A standard motor can normally only run for a few minutes in the overload condition otherwise the windings could

be overheated, which in the end could destroy the insulation and make a short circuit in the motor. For most applications this is not acceptable because the motor runs at part load most of the time. So it means that in this case the efficiency, of the induction motor with 3rd harmonic current injected, is lower than the efficiency of a standard three-phase motor for any working point.

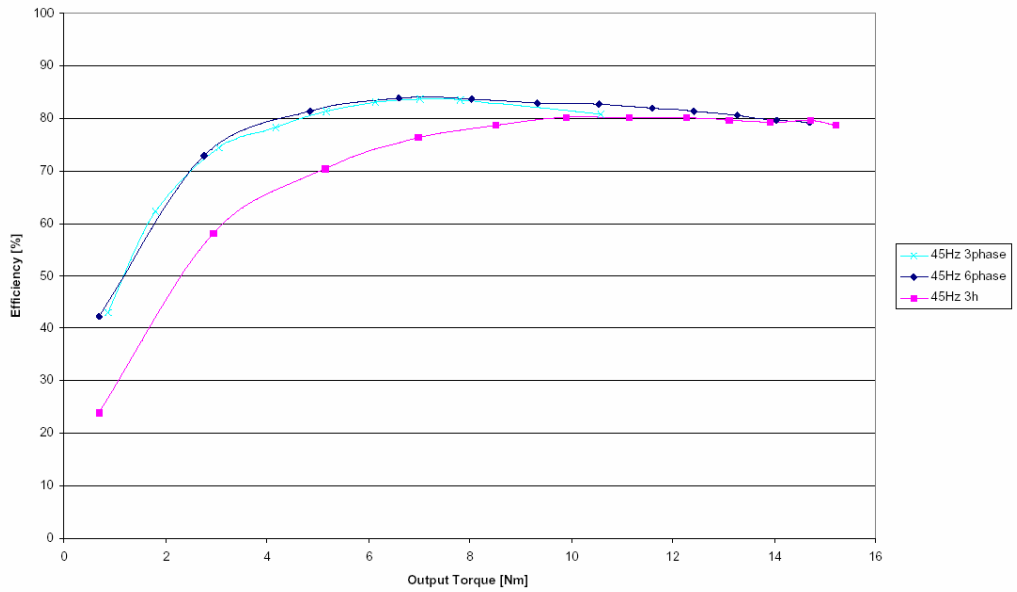

Figure 14	Measured efficiency at 45Hz for a six-phase machine. Comparison between the three-phase (3phase) machine and the six-phase machine with (3h) and without (6phase) 3rd harmonic current injection [1]. Nominal torque is about 13Nm.

In [1] it is suggested that the motor should be running without third order harmonic current injection when it runs at part load. This settles the efficiency at a point near to a standard three-phase motor (see also 3.5). 3rd harmonic current is only injected if the motor has to deliver peak torque.

So to summarize about the efficiency according to [1] it is only at overload conditions the efficiency of a six-phase motor with 3rd harmonic current is higher than a standard three-phase motor. But if the motor design geometry is optimized (i.e. as explained in 2.3.5) the efficiency could be improved (see chapter 3).

Efficiency without 3rd harmonic current

In [6] the efficiency of the multiphase induction motor is also analyzed. In this case the 3rd harmonic component is not injected. The conclusion is that the iron loss will

not be changed significantly, but the copper loss can be reduced by 8.5% if the number of phases is very high. At 6 phases the copper loss can be reduced by 6.7%. Another interesting feature about the multiphase machine examined in this paper is the torque ripple. It is concluded that torque ripple originated from the stator winding phase belts in the machine are reduced because the phase belts are attenuated by the higher number of phases like explained in 2.2.2. The elongation of the end windings are however not mentioned in this paper. This effect is rather complicated to analyze analytically because the end winding depends on a huge amount of factors including production methods. Therefore a case to case study using advance design programs like *SPEED* is recommendable.

2.3 Expansion of motor design model

In the following new calculations are done to expand the model from the state of the art analysis. There are two more effects on the motor design not mentioned in [1]. The first is that the end-windings have to be longer in a six-phased motor than in a standard three-phased motor. This is because the 3^{rd} harmonic component in the *MMF* needs to be as big as possible, the ideal is a full pitch winding. Therefore the stator resistance and end leakage inductance is bigger in a six-phased motor (see 2.3.2 and 2.3.3). The other effect is that if a third order harmonic decreases the peak flux density in the stator teeth, then the peak flux density in the rotor teeth is also reduced. This means more room for rotor bars and hence a lower rotor resistance.

2.3.1 Example

In the following section there is an example where the effects are calculated. The example has the characteristics shown in the table in Figure 15. The three-phase motor is the starting point for the calculations (called original). The six-phased motor is wound with the double number of windings in each slot, because the number of slots per phase is halved. The total number of wires per phase should be the same because the voltage is the same. This machine is build and is used as example throughout the rest of the thesis (called test in table). The width of the teeth in the six-phased motor is changed to take advantage of the lower peak flux density. The new widths are found by looking at dynamic simulations (see next chapter), decreasing the width until the peak flux density is the same as a three-phase motor. After this the stator and rotor resistances are recalculated in the motor design software *SPEED* (called optimized in table).

Note that the stator resistance and some of the other parameters for the optimized motor are calculated in the next section. The nominal power, speed and torque are not given for the build and the optimized six-phase motor because the performance of these motors is not qualified through test.

General information	Original	Test	Optimized	
Description	**3 ph. 3h.**	**6 ph. 3h.**	**6 ph. 3h.**	**Units**
Number of slots in stator	24	24	24	-
Number of slots in rotor	20	20	20	-
Number of windings/slot	39	78	78	-
Windings/phase	156	156	156	-
Number of phases	3	6	6	-
Pole number	2	2	2	-
Mechanical speed	2908			RPM
Shaft power	3010			W
Shaft torque	9.89			Nm
Stack length	140	140	140	mm
Rotor outer diameter	74.3	74.3	74.3	mm
Stator tooth width	3.6	3.6	3.08	mm
Rotor tooth width	4	4	3.42	mm
Stator yoke width	15.6	15.6	15.6	mm
Rotor yoke width	4.45	4.45	4.45	mm
Gamma γ	0.321	0.321	0.286	-
dcs/Dis	0.217	0.217	0.235	-
Viscose friction	3.04E-04	3.04E-04	3.04E-04	J*s
Moment of inertia	0.0025	0.0025	0.0025	kg*m*m
Frequency	50	50	50	Hz
Stator resistance/phase	2.251	4.719	4.440	Ohm
Radius to center of airgap	37.325	37.325	37.325	mm
Airgap length	0.35	0.35	0.35	mm
Main inductance	0.2033	0.2354	0.2354	H
Stator leakage inductance	0.00907	0.01814	0.01814	H
Rotor leakage inductance	0.00954	0.01908	0.01908	H
Leakage rotor bars	6.40E-07	6.40E-07	6.40E-07	H
Leakage rotor endring	3.11E-09	3.11E-09	3.11E-09	H
Rotor bar resistance	7.50E-05	7.50E-05	6.80E-05	Ohm
Rotor endring resistance	9.91E-07	9.91E-07	9.91E-07	Ohm

Figure 15 Datasheet for original three-phase machine, build six-phase machine and tooth-width optimized six-phase machine.

2.3.2 Stator end-winding

The winding design for the six-phase test motor is discussed in the following.

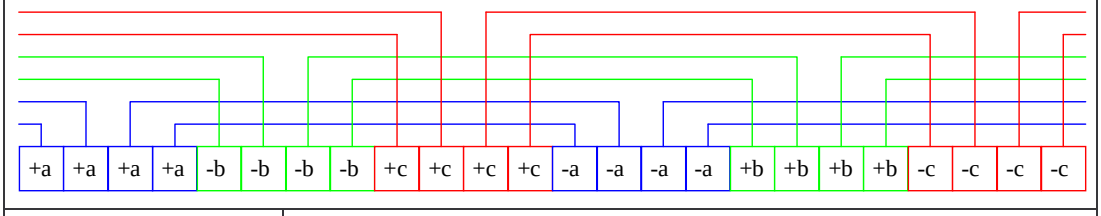

Figure 16 Winding (a) – three-phase winding with 4 slots phase belt.

The winding layout of the two cases is shown in Figure 16 and Figure 17. The three-phase motor has the winding diagram shown on Figure 16. The two six-phase motors have the winding diagram shown on Figure 17.

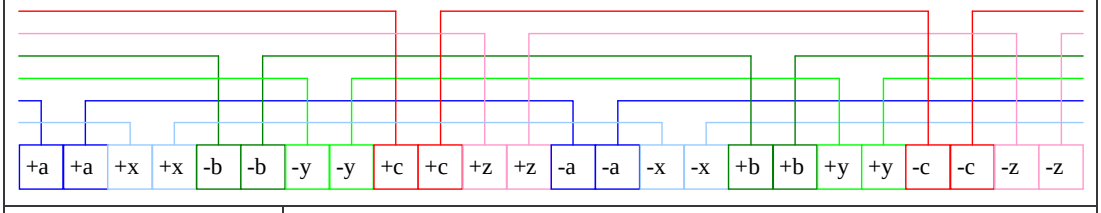

Figure 17 Winding (b) – six-phase winding with 2 slots phase belt.

If the slot fill factor is the same the resistance in the six-phased motor should be exactly twice the value of the three-phase motor. This can also be seen by realizing that if *A* and *X* (and *B* and *Y*, and *C* and *Z*) are connected in parallel then we again have the three-phased motor winding, but the end winding is increased. In the example the stator resistance is changed from 2.2510Ω to 2 x 2.3594Ω (or +4.8% calculated in *SPEED*). This also means that about 4.8% more copper is needed, which makes the motor more expensive. The end leakage inductance is also changed, but in this example the change is not computed. Detailed calculations can be done with the *SPEED* software.

2.3.3 Thinner stator teeth

The stator slot area can be increased by the 3rd harmonic flux effect as described in 2.2.4. This effect reduces the resistance to 2 x 2.2200Ω (or about -6.2%).

All in all the resistance is reduced by -1.4%. But it again raises the amount of copper used in the motor with about 6.2%. So that all in all about 11% more copper is needed.

2.3.4 Thinner rotor teeth

The rotor slot area can also be increased by the effect of the 3rd harmonic. This decreases the rotor-bar resistance from 1.0174Ω to 0.9223Ω (or -9.3%). This demands for 9.3% more copper/aluminum in the rotor bars. All calculations are carried out with the *SPEED* software.

The laminated iron has the same outer diameter, so no iron can be saved. And since the amount of electrical materials (copper, aluminum) is increased, the price of the complete motor is expected to increase also.

2.3.5 Re-design strategy

In [1] one way is chosen to re-design the motor geometry, when a 3rd harmonic flux is present, where the stator teeth are made smaller giving more room for copper. An alternative way to re-design the motor could be to increase the yoke width by moving the slots inward, which will decrease the air-gap radius. This would make it possible to use a higher flux reduction factor. It depends on the geometry (and thereby indirectly the number of poles) if this re-design method would be better than the one mentioned in [1]. If the yoke width is big compared to the stator inner diameter (indicating a low number of poles), then increasing the yoke width will mean a great reduction in the stator inner diameter, which will decrease the output torque. And vise versa. Output torque is proportional to the stator inner diameter squared [10].

$$T_e = \left(\frac{\sqrt{2}\pi}{4}\right) k_1 k_{is} \left(D_{is}^2 l_e\right) B_{g1} K_{s(rms)} \eta_{gap} \cos\phi_{gap} \tag{5}$$

Where:	***Var***	***Description***
	T_e	*Air-gap torque*
	k_1	*1st harmonic factor including pitch, distribution, slot opening, and skew.*
	k_{is}	*Stator lamination stacking factor.*
	D_{is}	*Stator inner diameter.*
	l_e	*Effective motor length.*
	B_{gl}	*Air-gap peak flux density.*
	$K_{s(rms)}$	*RMS current per unit length of stator circumference.*
	η_{gap}	*Rotor efficiency as seen from air-gap i.e. including rotor iron, copper and stray load losses.*
	$\cos\phi_{gap}$	*Cosine to angle between rotor current and rotor voltage.*

In the following it is assumed that rotor efficiency η_{gap} and rotor $\cos\phi_{gap}$ are not depending on D_{is}!

If the outer stator diameter is kept constant, it means that the inner stator diameter D_{is} added by two times the yoke width (d_{cs}) must be constant:

$$D_{is} + 2d_{cs} = const \tag{6}$$

Where:	Var	Description
	D_{is}	*Stator inner diameter.*
	d_{cs}	*Stator yoke thickness.*

Introducing a new stator inner diameter (D_{isn}) and yoke width (d_{csn}) gives:

$$D_{isn} = D_{is} + 2(d_{cs} - d_{csn}) \tag{7}$$

To give the same yoke peak flux density again, the yoke needs to be increased according to equation (8):

$$d_{csn} = d_{cs} \cdot \frac{2 \cdot 19}{\sqrt{3} \cdot 18} k \tag{8}$$

Where:	Var	Description
	k	*Flux reduction factor due to 3rd harmonic current.*

Equation (7) & (8) implies that:

$$D_{isn} = D_{is} + 2d_{cs}\left(1 - \frac{2 \cdot 19}{\sqrt{3} \cdot 18} k\right) \tag{9}$$

The torque is changed with the square of the diameter (see (5)) resulting in the torque factor given by (10).

$$\left(\frac{D_{isn}}{D_{is}}\right)^2 = \left(\frac{D_{is} + 2d_{cs}\left(1 - \frac{2 \cdot 19}{\sqrt{3} \cdot 18} k\right)}{D_{is}}\right)^2 = \left(1 + 2\frac{d_{cs}}{D_{is}}\left(1 - \frac{2 \cdot 19}{\sqrt{3} \cdot 18} k\right)\right)^2 \approx \left(1 + 2\frac{d_{cs}}{D_{is}}(1 - 1{,}22k)\right)^2 \quad (10)$$

But the tooth width is also changed, so the flux density in the stator teeth is increased as D_{isn} decreases. This effect also has to be taken into account. Therefore slot width b_{0n} has to be calculated as a function of γ, k, the yoke thickness d_{cs} and the inner stator diameter D_{is}. The equations are set up:

$$\begin{aligned} \tau_s = b_0 + t_0 \quad &\wedge \quad \tau_{sn} = b_{0n} + t_{0n} \\ \tau_s \cdot \gamma = t_0 \quad &\wedge \quad \tau_{sn} \cdot \gamma_n = t_{0n} \\ b_0 = (1 - \gamma)\tau_s \quad &\wedge \quad b_{0n} = (1 - \gamma_n)\tau_{sn} \end{aligned} \quad (11)$$

Where:	***Var***	***Description***
	τ_s	*Stator slot pitch width.*
	τ_{sn}	*Stator slot pitch width new design.*
	b_0	*Stator slot width.*
	b_{0n}	*Stator slot width new design.*
	t_0	*Stator tooth width.*
	t_{0n}	*Stator tooth width new design.*
	γ	*Stator slot pitch factor.*
	γ_n	*Stator slot pitch factor new design.*

If the diameter is changed, then the slot pitch is changed linearly with the diameter as shown in (12).

$$\tau_{sn} = \tau_s \cdot \frac{D_{isn}}{D_{is}} \quad (12)$$

If the stator teeth have to carry the same tooth flux density in the new design, then the new tooth width must obey equation (13).

$$t_{0n} = k \cdot t_0 \tag{13}$$

This means that the new slot pitch factor must comply with equation (14).

$$\gamma_n = \gamma \cdot k \cdot \frac{D_{is}}{D_{isn}} \tag{14}$$

And the new slot width is therefore given by equation (15).

$$b_{0n} = (1-\gamma_n)\tau_{sn} = \left(1-\gamma \cdot k \cdot \frac{D_{is}}{D_{isn}}\right)\tau_s \cdot \frac{D_{isn}}{D_{is}} = \left(\frac{D_{isn}}{D_{is}} - \gamma \cdot k\right)\tau_s \tag{15}$$

So the slot width is changed by the factor:

$$\frac{b_{0n}}{b_0} = \frac{\frac{D_{isn}}{D_{is}} - \gamma \cdot k}{1-\gamma} \tag{16}$$

The slot width is assumed to be proportional to $K_{s(rms)}$ (*RMS* current per unit length of the stator circumference), so collecting all the factors the total torque gain is:

$$Gain\% = \left(\frac{38k^2}{27}\frac{18}{19}\frac{\frac{D_{isn}}{D_{is}} - \gamma \cdot k}{1-\gamma}\left(\frac{D_{isn}}{D_{is}}\right)^2 - 1 \right) \cdot 100\% \tag{17}$$

Or depending only on the original design, the torque gain is as expressed by equation (18) using equation (10) and (17).

$$Gain\% = \left(\frac{38k^2}{27} \frac{18}{19} \frac{\left(1+2\frac{d_{cs}}{D_{is}}\left(1-\frac{2\cdot 19}{\sqrt{3}\cdot 18}k\right)\right)-\gamma\cdot k}{1-\gamma} \left(1+2\frac{d_{cs}}{D_{is}}\left(1-\frac{2\cdot 19}{\sqrt{3}\cdot 18}k\right)\right)^2 - 1 \right) \cdot 100\% \quad (18)$$

Where:	*Var*	*Description*
	k	*Flux reduction factor due to 3rd harmonic current.*
	d_{cs}	*Stator yoke thickness.*
	D_{is}	*Stator inner diameter.*
	γ	*Stator slot pitch factor.*
	γ_n	*Stator slot pitch factor new design.*

The torque gain (equation (18)), flux change and diameter change are pictured in Figure 18 and Figure 19. In Figure 18 the maximum possible torque gain is pictured as a function of γ and d_{cs}/D_{is}, which actually refers to different baseline motor geometries. Note that in the white areas the torque gain is more than 50%, but to get a high resolution in the rest of the plot, the areas are simply plotted as white. If e.g. $d_{cs}/D_{is} = 5\%$ and $\gamma = 0.5$ then the maximum torque gain is about 26%. This is possible because the flux in the motor is increased with 11% (see Figure 19 left), hence the tooth width is increased by 11% (see equation (13)) to maintain the same flux density in the teeth. At the same time the flux density in the yoke is increased so the diameter of the air-gap has to be decreased a few percent (see Figure 19 right). Taking the example from before it shows that the diameter has to be reduced by 3.8% (D_{isn}/D_{is}). The new slot pitch factor can be calculated by:

$$\gamma_n = \gamma \cdot k \cdot \frac{D_{is}}{D_{isn}} = 0.5 \cdot 1.11 \cdot \frac{1}{0.962} = 0.58 \quad (19)$$

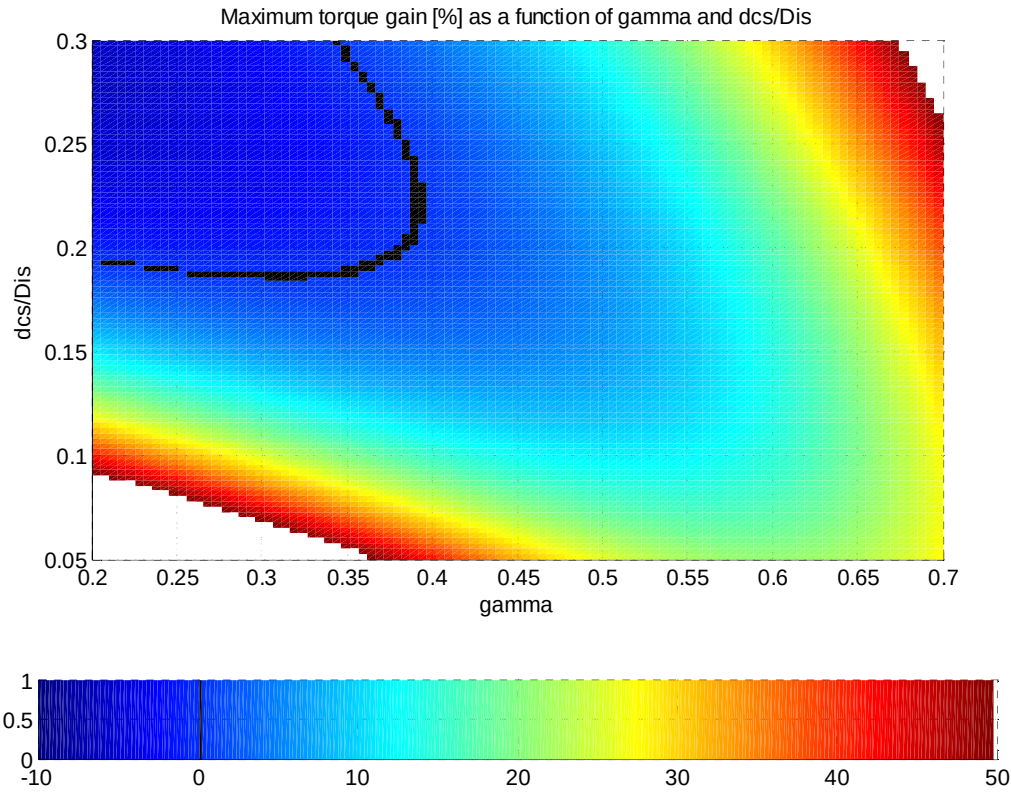

Figure 18	Torque gain as a function of the motor geometries γ and d_{cs}/D_{is}.

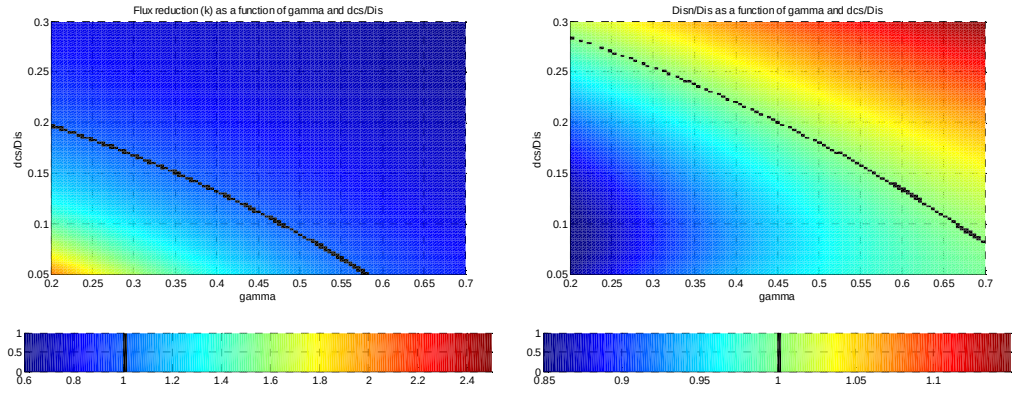

Figure 19	Flux reduction (left) and diameter reduction (right) as a function of the motor geometries γ and d_{cs}/D_{is}.

It is important to note that all motors on these curves have the same flux density in both teeth and yoke as the baseline three-phase motor, so all *k* values are realistic.

This is in contrast to the torque gain suggested in [1], where k values above 0.82 are only realistic if the yoke flux density can be increased! The difference is that the stator inner diameter is changed until the yoke flux density and teeth flux density are the same as for the baseline three-phase motor. Taking the example from before the torque gain according to the equation in [1] is only about 7%.

With fixed inner stator diameter, which is the same as if d_{cs}=0 (see equation (10) where D_{isn}=D_{is} and k is arbitrary), the gain looks like this:

$$Gain\% = \left(\frac{38k^2}{27} \frac{18}{19} \left(\frac{1-\gamma \cdot k}{1-\gamma} \right) - 1 \right) \cdot 100\% \tag{20}$$

This is the same as calculated in [1] (see Figure 13). Note that the percent gain from different factors cannot be added, the factors have to be multiplied. This gives a small difference compared to the curves and Gain expression used in [1].

Using the new torque gain calculation (equation (18)) and the gain calculated in [1] (equation (20)) on different Grundfos motors gives the following torque gains:

Poles	Stator slots	OD	Dis	dcs	γ	dcs/Dis	Disn/Dis	dcsn/dcs	gamman/ gamma	k	% Gain w. free Dis and γ	% Gain according to [1]
6,8,12	36	106.5	70.0	6.050	0.326	0.086	0.90	1.56	1.41	1.28	28.50	-2.46
4,6,8	36	170.0	110.0	15.400	0.429	0.140	0.96	1.15	0.99	0.95	5.55	1.87
4,6,8,12	24	106.6	65.0	9.200	0.445	0.142	0.96	1.13	0.96	0.93	5.49	2.67
2,4,6,8	24	93.1	55.0	7.850	0.384	0.143	0.94	1.20	1.04	0.98	5.36	-0.19
2	24	93.1	55.0	9.150	0.247	0.166	0.91	1.28	1.16	1.05	3.96	-4.95
2	24	93.1	55.0	9.150	0.247	0.166	0.91	1.28	1.16	1.05	3.96	-4.95
2	12	44.0	24.0	3.800	0.319	0.158	0.93	1.22	1.08	1.00	3.74	-2.69
2,4	16	69.5	40.0	6.850	0.356	0.171	0.95	1.14	0.99	0.94	1.63	-1.32
2	16	69.5	40.0	6.850	0.356	0.171	0.95	1.14	0.99	0.94	1.63	-1.32
4,6,8,12	36	135.0	75.0	16.400	0.411	0.219	1.01	0.99	0.81	0.81	1.03	1.01
2	24	135.0	75.0	13.800	0.312	0.184	0.94	1.15	1.00	0.94	0.17	-2.96
2,4	16	80.1	40.0	7.450	0.328	0.186	0.95	1.13	0.97	0.93	-0.01	-2.37
2,4	24	106.5	55.0	13.650	0.377	0.248	1.02	0.96	0.77	0.79	-0.15	-0.48
2	36	170.0	95.0	23.400	0.361	0.246	1.01	0.97	0.79	0.80	-1.00	-1.15
2,4	24	135.0	75.0	16.300	0.321	0.217	0.98	1.06	0.89	0.87	-2.12	-2.63
2,4	24	135.0	75.0	16.300	0.321	0.217	0.98	1.06	0.89	0.87	-2.12	-2.63
	Min	44.0	24.0	3.800	0.247	0.086	0.90	0.96	0.77	0.79	-2.12	-4.95
	Max	170.0	110.0	23.400	0.445	0.248	1.02	1.56	1.41	1.28	28.50	2.67
	Mean	108.9	62.8	11.350	0.346	0.179	0.96	1.15	0.99	0.94	3.48	-1.54

Figure 20 Torque gain for different Grundfos motors.

The torque gain according to [1] is very small (and even negative) in all cases using Grundfos motors. But it has to be noted that it is for fixed flux density in the yoke and teeth, because it is assumed that the three phase motors are already dimensioned "to the limit". This is not always the case, if i.e. the three-phase motor can be optimized, but then the six-phase motor can also be optimized.

Using the new calculations with free diameter and tooth width gives better values, but only one motor gives more than 6% torque gain. Grundfos motors might not represent asynchronous motors in general because Grundfos mainly use the motors for centrifugal pumps which demand high speed and low number of poles, which again means high d_{cs}/D_{is} values. This can also be seen on the table above, where motors with high pole number and low d_{cs}/D_{is} value give the highest torque gain. A general trend therefore seems to be that motors with high pole numbers have the greatest potential for torque increase.

The calculations above can be further expanded changing other motor parameters e.g. the slot-depth. This is not done in this thesis, but it shows that optimizing motors is a complex matter where changing only one parameter cannot optimize the six-phased motor. A full redesign of the machine taking also second order effects into account is needed to fully optimize the new six-phase motor.

2.4 Conclusion

Increasing the number of phases from three to six and injecting a 3rd harmonic current, chances the flux distribution in the motor. This has the consequence that the motor needs to be redesigned to take full advantage of the improvement. There exist many simple strategies to redesign the motor, but to fully optimize the new six-phased motor an advanced motor design software has to be used. This is illustrated by comparing the results from two strategies. In the first strategy (suggested in [1]) a 7% torque gain can be realized, but using a slightly more complicated strategy (calculated here) the torque improvement can be increased to 26%! In general the torque gain going from three to six phases very much depends on the geometry of the motor. In most practical cases a few percent torque gain is realistic. If the yoke width of the initial design is small compared to the air-gap diameter, which is usually the case if the number of poles is high, then the torque gain is highest.

3. Dynamic models for multiphase motors

3.1 Introduction

In this chapter the theoretical basis for a model of a motor with multiple phases is first set up. The model is a detailed dynamic model. The simulation program is discussed, and links are made to standard three phased motor design software. The link ensures that the dynamic model is founded on the basis of the well-known and well-tested motor design software *SPEED*, so it is expected that the simulation results are close to real values. Finally the simulation results for a steady state situation are calculated and some general trends are extracted, including a simple model for flux density, iron loss and efficiency. The whole process is described in general terms, but throughout the chapter an example of a 3kW motor is described. This example is used to demonstrate and partly verify the theoretical calculations. In the next chapter the test case is implemented in a laboratory set up.

3.2 Multiwinding model for three-phase motors

The simulation model, described in this subchapter, is taken from [2], [19], [40]. It is a complicated dynamic model of the induction motor, taking into consideration all the loops and windings in both the stator and rotor. The model is developed amongst other reasons to examine what happens if a rotor-bar is broken or has a higher resistance because of production failure or variation. The below presented model however assumes symmetry in the rotor bars and end-rings. It is a more precise and general model than the dq-axis model, because it doesn't assume that the stator windings have to be sinusoidally distributed. Actually by using this model the three phase dq-axis model can be extracted as a special case [19].

3.2.1 Assumptions

To make the multi-winding (*MWI*) model, the following assumptions are used.

- Iron loss is not an integrated part of the model. The loss is extracted from the shaft power after simulation. It is actually a widely used and accepted assumption, that iron loss can be subtracted like the mechanical loss, which is also used in the *SPEED* software. The iron loss is in this way overestimated, if instead it was added to the input power, it would have been under-estimated.
- Only non-zero reluctance across the air-gap. The iron has infinity permeability. But the length of the air-gap length can be corrected to accommodate saturated iron in a working point.
- The air-gap is an ideal cylinder. There are no stator or rotor slot-openings in the iron. The carter factor [10] is multiplied with the air-gap length to take these slotting effects into consideration.
- No end effect in air gap region. The model only takes the two lamination dimensions into account. The axial length is not considered. But in *SPEED* the air-gap length is increased according to the axial end fringing. And the *MWI* model is calibrated with the *SPEED* design. So the effect of end fringing is included in the air-gap length.
- The windings in stator and rotor have the radial and circular arc length zero. In other words the slots are modeled as points.
- Skewing of the rotor or stator is not possible. This normally has a noticeable impact on the machine performance. The main part of the effect is taken into consideration, because the magnetizing inductance is calibrated against the value calculated in the *SPEED* software, which include the skew effect. The effect can be included in the *MWI* model if the skewed slots are modeled like an arc line, but this is not done here.

3.2.2 Winding example

Figure 21 shows the lamination drawing of the 3kW test case on the left side, and on the right side the corresponding winding layout model is pictured. The example is just used to illustrate what the *MWI* model takes into consideration.

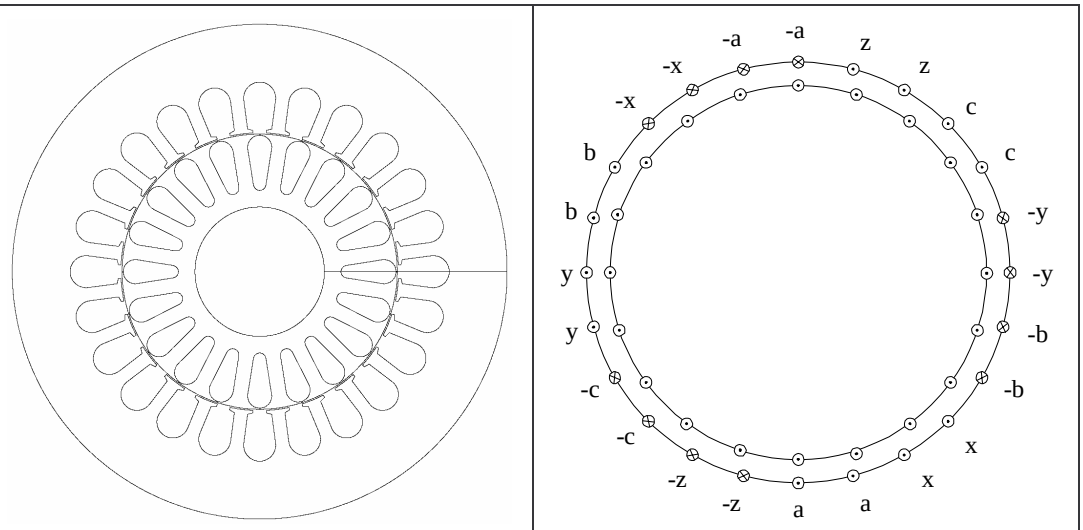

Figure 21 Figure of the 3kW lamination used in the test motor (left) and the 6 phase *MWI* model (right).

3.2.3 Model equations

The key element for developing the multiwinding model is the calculation of the coupling between the rotor and stator windings. The coupling is through a set of inductance matrices coupling the individual stator wires with the individual rotor loops (*MWI* equation 6.1).

$$\psi_s = L_{ss} i_s + L_{sr}(\theta_r) i_r$$
$$\psi_r = L_{rs}(\theta_r) i_s + L_{rr} i_r \qquad (21)$$

Where:	***Var***	***Description***
	ψ_s	*A vector with the stator flux linkages in each stator phase.*
	ψ_r	*A vector with all the rotor flux linkages in each rotor loop.*
	i_s	*A vector with the stator currents in each phase.*
	i_r	*A vector with all the rotor loop currents (see Figure 23).*
	θ_r	*The position difference between stator and rotor.*
	L_{ss}	*Magnetic coupling matrix between the individual stator phases.*
	L_{rr}	*Magnetic coupling matrix between the individual rotor loops/teeth.*
	L_{sr}	*Magnetic coupling matrix from the rotor currents to stator flux.*
	L_{rs}	*Magnetic coupling matrix from the stator currents to rotor flux.*

The first matrix L_{ss} can be expressed in this way:

$$L_{ss} = K_1 \cdot \frac{2\pi}{n} \begin{bmatrix} N_{s1}^T \cdot N_{s1} & N_{s1}^T \cdot N_{s2} & N_{s1}^T \cdot N_{s3} \\ N_{s2}^T \cdot N_{s1} & N_{s2}^T \cdot N_{s2} & N_{s2}^T \cdot N_{s3} \\ N_{s3}^T \cdot N_{s1} & N_{s3}^T \cdot N_{s2} & N_{s3}^T \cdot N_{s3} \end{bmatrix} + \begin{bmatrix} l_{sl1} & 0 & 0 \\ 0 & l_{sl2} & 0 \\ 0 & 0 & l_{sl3} \end{bmatrix} \quad (22)$$

Where:	***Var***	***Description***
	n	*The number of stator slots.*
	N_{sx}	*The column vector with the winding function for phase x [19]. It is the accumulated sum (where the mean value is removed) of a column vector with the number of wires in each slot in phase x (called w_{sik} in equation (25)). See also Figure 22.*
	l_{slx}	*The leakage inductance in phase x.*

K_l is the common inductance constant shown in equation (23).

$$K_l = \frac{ra \cdot l \cdot \mu_0}{d} \quad (23)$$

Where:	***Var***	***Description***
	ra	*The radius to the air-gap.*
	l	*The length of the rotor.*
	d	*The width of the air-gap.*
	μ_0	*Vacuum permability.* $\pi \cdot 4 \cdot 10^{-7}$

In Figure 22 the number of wires in each phase w_{sik} and the *MMF* function N_{sx} is shown for the three phase winding case (see 2.3.2).

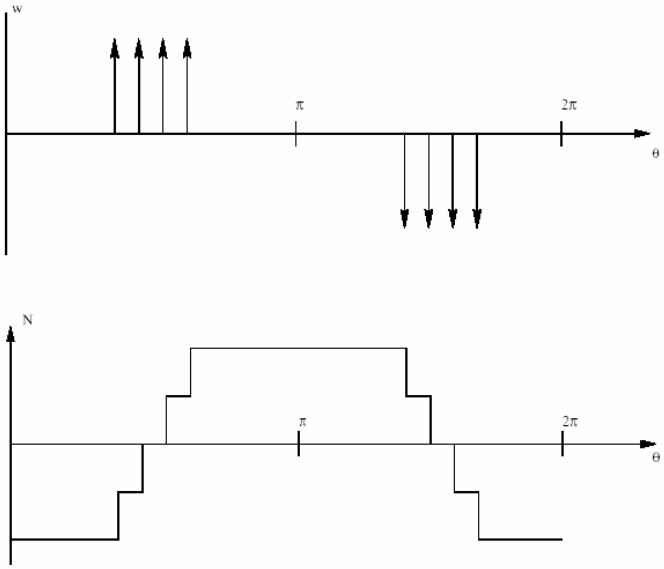

Figure 22	The number of wires in each slot from one phase and the *MMF* function [2], [19].

The matrix L_{rr} is the coupling inductance from one rotor loop to the others [19], [40]. It is defined by the angle positions of the rotor-bars and the common inductance constant K_l. Furthermore the inductances in the bars and endrings have to be taken into account. The definitions for the leakage inductances used in equation (24) are shown in Figure 23. The vertical impedances represent the rotor bar and the horizontal impedances represent the end-rings of the squirrel-cage.

The equations for rotor inductance are reduced because the bar inductances l_b for each loop are identical and the endring inductances l_e for each loop are identical. Note that it is also assumed that the circulating current in the endring i_e is zero. A more general rotor inductance matrix exist, with different inductances in each bar and endring, but this is not presented here, because the rotor is assumed to be symmetric.

$$L_{rr} = K_l \cdot \begin{bmatrix} \Delta\theta_1\left(1-\frac{\Delta\theta_1}{2\pi}\right) & -\Delta\theta_1\frac{\Delta\theta_2}{2\pi} & -\Delta\theta_1\frac{\Delta\theta_3}{2\pi} & \cdots & -\Delta\theta_1\frac{\Delta\theta_m}{2\pi} \\ -\Delta\theta_2\frac{\Delta\theta_2}{2\pi} & \Delta\theta_2\left(1-\frac{\Delta\theta_2}{2\pi}\right) & -\Delta\theta_2\frac{\Delta\theta_2}{2\pi} & \cdots & -\Delta\theta_2\frac{\Delta\theta_m}{2\pi} \\ -\Delta\theta_3\frac{\Delta\theta_2}{2\pi} & -\Delta\theta_3\frac{\Delta\theta_2}{2\pi} & \Delta\theta_3\left(1-\frac{\Delta\theta_3}{2\pi}\right) & \cdots & -\Delta\theta_3\frac{\Delta\theta_m}{2\pi} \\ \vdots & \vdots & \vdots & \ddots & \vdots \\ -\Delta\theta_m\frac{\Delta\theta_1}{2\pi} & -\Delta\theta_m\frac{\Delta\theta_2}{2\pi} & -\Delta\theta_m\frac{\Delta\theta_3}{2\pi} & \cdots & \Delta\theta_m\left(1-\frac{\Delta\theta_m}{2\pi}\right) \end{bmatrix} + \begin{bmatrix} 2\cdot(l_b+l_e) & -l_b & 0 & \cdots & -l_b \\ -l_b & 2\cdot(l_b+l_e) & -l_b & \cdots & 0 \\ 0 & -l_b & 2\cdot(l_b+l_e) & \cdots & 0 \\ \vdots & \vdots & \vdots & \ddots & \vdots \\ -l_b & 0 & 0 & \cdots & 2\cdot(l_b+l_e) \end{bmatrix} \quad (24)$$

Where:	*Var*	*Description*
	m	*The number of rotor loops, slots or bars.*
	$\Delta\theta_x$	*The angular difference between slot x and x+1.*

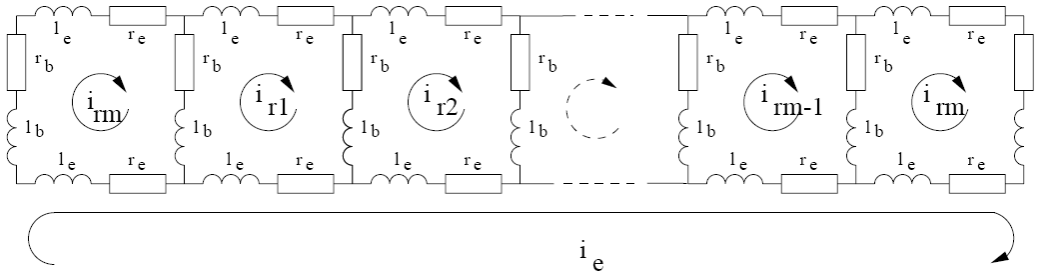

Figure 23 Definitions of parameters used in the rotor loop.

The last matrices L_{sr} and L_{rs} are dependent on the position of the rotor. They can be expressed with the following equation:

$$L_{srij}(\theta_r) = K_l \cdot \sum_{k=1}^{\frac{n}{2}} w_{sik} \cdot g(\theta_{sw}, \theta_{rj} + \theta_r, \theta_{r(j+1)} + \theta_r) \quad (25)$$

Where:	*Var*	*Description*
	i	*The stator phase number.*

j	*The rotor loop number.*
n	*The number of stator slots.*
m	*The number of rotor loops, slots or bars.*
θ_{rj}	*The position of the individual rotor loops.* $\theta_{r(m+1)} = \theta_{r1}$
θ_r	*The position difference between stator and rotor.*
w_{sik}	*The number of stator windings from each phase (i) in each individual stator slot (k).*
θ_{sw}	*The position of the stator windings. In symmetry:* $(k-1)\frac{2\pi}{n}$ *Where: k is the stator slot number. n is the number of stator slots.*

It is clear that the following relation applies:

$$L_{srij}(\theta_r) = L_{rsji}(\theta_r) \Leftrightarrow L_{rs}(\theta_r) = L_{sr}{}^{T}(\theta_r) \tag{26}$$

Where:	***Var***	***Description***
	L_{srij}	*Magnetic coupling matrix from the rotor currents to stator flux, matrix element i,j.*
	L_{rsji}	*Magnetic coupling matrix from the stator currents to rotor flux, matrix element j,i.*
	L_{sr}	*Magnetic coupling matrix from the rotor currents to stator flux.*
	L_{rs}	*Magnetic coupling matrix from the stator currents to rotor flux.*

The function *g* is defined as [19] , [40]:

$$g(\theta_s,\theta_{r1},\theta_{r2}) = \left\{\begin{array}{lrll} \theta_{r1}<\theta_{r2}: & -\frac{1}{2}\cdot(\theta_{r2}-\theta_{r1}) & if: & \theta_{r2}<\theta_s \vee \theta_{r1}>\theta_s+\pi \\ & \frac{1}{2}\cdot(\theta_{r2}-\theta_{r1}) & if: & \theta_s<\theta_{r1} \vee \theta_{r2}>\theta_s+\pi \\ & -\theta_s+\frac{1}{2}\cdot(\theta_{r2}+\theta_{r1}) & if: & \theta_{r1}\le\theta_s\le\theta_{r2} \\ & \theta_s-\frac{1}{2}\cdot(\theta_{r2}+\theta_{r1})+\pi & if: & \theta_{r1}\le\theta_s+\pi\le\theta_{r2} \\ \hline \theta_{r2}<\theta_{r1}: & -\frac{1}{2}\cdot(\theta_{r2}-(\theta_{r1}-2\pi)) & if: & \theta_{r2}<\theta_s \wedge \theta_{r1}>\theta_s+\pi \\ & -\theta_s+\frac{1}{2}\cdot(\theta_{r2}+(\theta_{r1}+2\pi)) & if: & \theta_{r2}\ge\theta_s \\ & \theta_s-\frac{1}{2}\cdot(\theta_{r2}+\theta_{r1}) & if: & \theta_{r1}<\theta_s+\pi \end{array}\right\} \tag{27}$$

Where:	***Var***	***Description***
	θ_{r1}	*The position of the first rotor loop, seen from a stator fixed position.*
	θ_{r2}	*The position of the second rotor loop, seen from a stator fixed position.*
	θ_s	*The position of the individual full pitch winding loops, seen from*

	a stator fixed position.

It can also be displayed in a graph like shown in Figure 24.

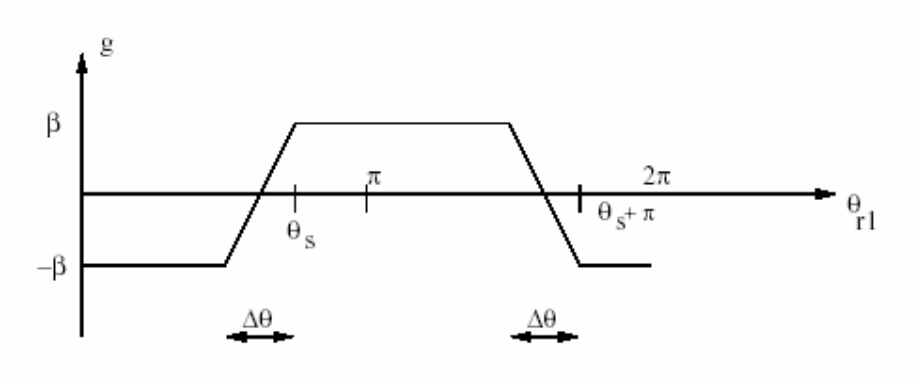

Figure 24	The g function, used for calculation of the mutual inductance between stator and rotor [19].

The definitions of the angles are shown in Figure 25.

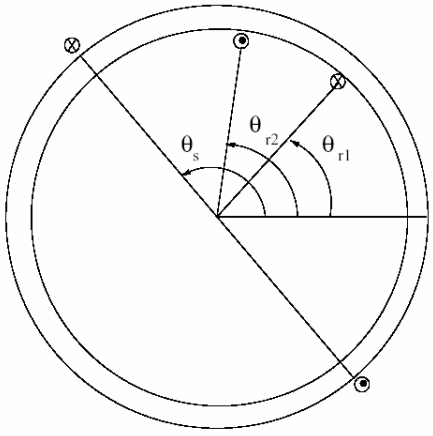

Figure 25	Definition of angles for calculation of the g function.

The next thing to consider is the voltage equations for both the stator and the rotor (28).

$$\frac{d}{dt}\psi_s = -R_s i_s + u_s$$
$$\frac{d}{dt}\psi_r = -R_r i_r \tag{28}$$

Where:	*Var*	*Description*
	ψ_s	*A vector with the stator flux linkages in each stator phase.*
	ψ_r	*A vector with all the rotor flux linkages in each rotor loop.*
	i_s	*A vector with the stator currents in each phase.*
	i_r	*A vector with all the rotor loop currents (see Figure 23).*
	u_s	*The voltage drop across a stator phase winding.*
	R_s	*The resistance matrix for the stator.* $\begin{bmatrix} r_s & 0 & 0 \\ 0 & r_s & 0 \\ 0 & 0 & r_s \end{bmatrix}$
	R_r	*The resistance matrix for the rotor. See definitions in Figure 23.* $\begin{bmatrix} 2\cdot(r_b+r_e) & -r_b & 0 & \cdots & -r_b \\ -r_b & 2\cdot(r_b+r_e) & -r_b & \cdots & 0 \\ 0 & -r_b & 2\cdot(r_b+r_e) & \cdots & 0 \\ \vdots & \vdots & \vdots & \ddots & \vdots \\ -r_b & 0 & 0 & \cdots & 2\cdot(r_b+r_e) \end{bmatrix}$

Now the electromagnetic torque can be calculated from expression (29):

$$M = i_s^T \cdot \frac{\partial}{\partial \theta_r} L_{sr}(\theta_r) \cdot i_r = i_r^T \cdot \frac{\partial}{\partial \theta_r} L_{rs}(\theta_r) \cdot i_s \tag{29}$$

Where:	*Var*	*Description*
	M	*Electromagnetic torque.*

And at last the mechanical equations:

$$\frac{d}{dt}\omega_r = \frac{(M - M_L)}{J}$$
$$\frac{d}{dt}\theta_r = \omega_r \quad (30)$$

Where:	*Var*	*Description*
	M_L	*Load torque.*
	i_s	*A vector with the stator currents in each phase.*
	i_r	*A vector with all the rotor loop currents (see Figure 23).*
	J	*Moment of inertia. (In test case 0.0025kg*m^2 noload and 0.0050kg*m^2 loaded with DC-motor)*
	ω_r	*The angular rotor speed.*
	θ_r	*The position difference between stator and rotor.*

3.2.4 Disadvantages

The following is a list of disadvantages of the model:

- The equations are only valid for three phases so an extension to more phases is needed.
- Calculation of design variables like flux density and iron loss are missing.
- The simulations are only valid at one saturation level, because the air-gap is fitted to a certain saturation level.
- Calculation of torque ripple from the stator and rotor slot openings is not possible.

3.2.5 Advantages

The following is a list of advantages of the model:

- Calculation of some part of the torque ripple is possible. The frequency content is expected to reflect real values. But the amplitudes are expected to deviate to some extend, because of saturation, iron loss and other nonlinearities.
- If the motor is not skewed the model is able to calculate the current ripple from the slots.
- It is possible to study the winding design intensively. For example examine non-sinusoidal winding distribution in the stator and rotor. This is not possible with a dq-axis model.
- Analyze the effects of broken rotor bars and end-ring segments (see also [30]), and the effects of variations in rotor bar and end-ring resistances. This is however not possible with the presented equations, but more general equations with different bars and endrings are presented in [19].

- Parameters are bounded more directly to physical parameters (compared to standard sinusoidal models) so they can be calculated from geometry, hence the model can be used for motor design if it is extended.

Note that it is not all the advantages with the model that are focused on in this project.

3.2.6 Conclusion

The *MWI* model has been described in the above section. It is a good and precise model for calculating dynamic performance of an induction motor, but static values of flux density and iron loss also have to be evaluated. Compared to the dq-axis model the *MWI* model is very flexible according to winding layout, this becomes an advantage when multi-phase motors are analyzed. The model only needs a small extension to be able to calculate on more than three phases. Furthermore a more precise link to the geometry is made in the following section.

3.3 Multiwinding model for f-phase motors

The model described in *MWI* has some disadvantages, and these disadvantages have to be handled in some way to be able to examine and analyze multiphase motors. The disadvantages mentioned in 3.2.4 are essential for a precise calculation of a multiphase motor, and they are all resolved in the following.

3.3.1 Theoretical calculations

Generally the equations are identical to the equations set up in 3.2, but the stator flux, current and voltage vectors are extended to f phases. Therefore the inductance matrices are also extended to f phases on the stator. The rotor variables flux, current and voltage are not extended, because all the loops in the rotor are already described. So the rotor inductances are also identical.

The inductance matrix for the coupling between the stator windings is extended to:

$$L_{ss} = K_l \cdot \frac{2\pi}{n} \begin{bmatrix} N_{s1}^T \cdot N_{s1} & N_{s1}^T \cdot N_{s2} & \cdots & N_{s1}^T \cdot N_{sf} \\ N_{s2}^T \cdot N_{s1} & N_{s2}^T \cdot N_{s2} & \cdots & N_{s2}^T \cdot N_{sf} \\ \vdots & \vdots & \ddots & \vdots \\ N_{sf}^T \cdot N_{s1} & N_{sf}^T \cdot N_{s2} & \cdots & N_{sf}^T \cdot N_{sf} \end{bmatrix} + \begin{bmatrix} l_{sl1} & 0 & \cdots & 0 \\ 0 & l_{sl2} & \cdots & 0 \\ \vdots & \vdots & \ddots & \vdots \\ 0 & 0 & \cdots & l_{slf} \end{bmatrix} \quad (31)$$

Where:	*Var*	*Description*
	n	*The number of stator slots.*
	N_{sx}	*The column vector with the winding function for phase x [19]. It is the accumulated sum (where the mean value is removed) of a column vector with the number of wires in each slot in phase x (called w_{sik} in equation (25)). See also Figure 22.*
	f	*The number of stator phases.*
	l_{slx}	*The leakage inductance in phase x.*

Stator to rotor inductances is extended to a bigger matrix, which is very easy to describe, the only thing to do is to extend w_{sik} to f phases, where i is the phase number and k is the slot number. One could say that there exists a vector with the number of wires in each stator slot as elements for all f phases.

3.3.2 Implementation in *Matlab*/*Simulink*

The *MWI* model is implemented in a block in *Simulink*. The equations in the simulink block are implemented in C code, to make the simulations faster. To start a dynamic simulation an m-file is first executed to initialize all the motor parameters. Then the reference either for the voltage or the current is setup in an m-file. The load torque is calculated externally and entered in the calculations. After this initialization the simulation can be started. In the example throughout this chapter, it is chosen to compare the performance of different motors based on a three-phase induction motor running at full load see Appendix D. The simulation makes the startup of the motor with no load (to decrease the simulation time), after 0.1s a step in the load is made so the torque is nominal. The different designs are compared for motors running in steady state, which is normally the case after 0.5-0.6s.

A useful property of the *MWI* model is that the shape of variables is much closer related to real values, than if a simple dq-axis model is used. The current is i.e. not only a sinusoidal curve. Therefore the *RMS*-value of the current is closer to real values.

3.3.3 Assumptions used for steady state values

In the following section the assumptions used for calculations of steady state values from variables are described. The complete list and description of steady state values is in Appendix B.

The torque ripple is calculated by the root mean square value of the shaft torque. Only the frequencies 40 to 1500 Hz are considered, because according to [20] mainly these frequencies can make noticeable audible noise from torque pulsations, higher frequencies are heavily damped by the mechanical system and lower frequencies are not hearable. Note that the amplitudes are only valid if saturation, iron loss, speed dependent load torque and other nonlinearities are not considered. So this value can only be used for comparison between different simulations.

The peak value of flux density in the rotor tooth (B_{rtpk}) is calculated on the basis of the flux linkage in one rotor loop ψ_r (see (21)) divided by the rotor tooth area.

The peak value of flux density in the stator tooth (B_{stpk}) is calculated on the basis of the flux linkage in one rotor loop ψ_r, divided by the stator tooth area, and multiplied by the number of rotor teeth divided by the number of stator teeth. This is only a rough assumption. To make it correct the leakage in the rotor has to be subtracted, and the leakage in the stator has to be added.

The peak value of the flux density in the stator yoke (B_{sypk}) is calculated by the basis of the flux density in the stator teeth. First the absolute values of the rotor flux linkages ψ_r are summed up for each time step. Then the result is divided by two (because of the negative values) and the number of poles and divided by the stator yoke area. In this way the total rotor flux per pole is assumed to run through the stator yoke at any given time and position. This is also only a rough assumption. To make it correct the leakage in the rotor has to be subtracted, and the leakage in the stator has to be added. The equation is calculated like this shown in equation (32).

$$\sum \left| \psi_r \right| / \left(2 \cdot A_{stator\_yoke} \cdot P \right) \tag{32}$$

Where:	***Var***	***Description***
	ψ_r	*A vector with all the rotor flux linkages in each rotor loop.*
	A_{stator_yoke}	*Area of the stator yoke. Length of stator times stator yoke width.*
	P	*The number of poles.*

The iron loss in the motor can be estimated on the basis of the three above mentioned peak flux densities in the motor (33). In this equation it is assumed that the iron loss is proportional to the peak value of the flux density squared. This assumption is good for hysteresis loss (assuming no minor loops) and fair for eddy

current loss [18], [35]. The eddy current losses of course also depend on how fast the flux is changing ($(dB/dt)^2$). But if i.e. the shape of the flux in the teeth becomes more square in shape resulting in higher *dB/dt*, the flux in the yoke becomes more triangular (see 2.2.4), hence a lower *dB/dt*. So that for the whole motor it is claimed that the flux shape is not very important only the peak value matters.

$$Fe = (Iron + SLL) \cdot \frac{Ro_{Tooth}\left(\frac{B_{rtpk}}{B_{rtpkr}}\right)^2 + St_{Tooth}\left(\frac{B_{stpk}}{B_{stpkr}}\right)^2 + St_{Yoke}\left(\frac{B_{sypk}}{B_{sypkr}}\right)^2}{Ro_{Tooth} + St_{Tooth} + St_{Yoke}} \tag{33}$$

Where:	***Var***	***Description***
	Iron	*Reference value of complete calculation of iron loss taken from the SPEED program.*
	SLL	*Reference value of stray load loss in the motor taken from the SPEED program.*
	Ro_{Tooth}	*Reference value of iron loss in the rotor tooth taken from SPEED.*
	St_{Tooth}	*Reference value of iron loss in the stator tooth taken from SPEED.*
	St_{Yoke}	*Reference value of iron loss in the stator yoke taken from SPEED.*
	B_{rtpk}	*The peak flux density in the rotor teeth.*
	B_{stpk}	*The peak flux density in the stator teeth.*
	B_{sypk}	*The peak flux density in the stator yoke.*
	B_{rtpkr}	*Reference value of peak flux density in the rotor teeth taken from the three phased reference simulation.*
	B_{stpkr}	*Reference value of peak flux density in the stator teeth taken from the three phased reference simulation.*
	B_{sypkr}	*Reference value of peak flux density in the stator yoke taken from the three phased reference simulation.*

For more details about output values see Appendix B.

3.3.4 The power supply input for the motor

There exist a range of different supplies to try. Square wave supplies of multiphase motors are interesting because this naturally reduce switching loss in the IGBT's but in the same time only increase the loss in the motor marginally [28], [31] and [32]. So in a way the hard to handle switching loss in the inverter switches is moved to the motor, where the heat is spread in a much bigger volume with a much bigger surface area. This could increase the *VA-rating* of the inverter considerably. The gain for the inverter is not examined here, but different types of square voltage supplies are tested on multiphase motors with different number of phases.

In chapter 2, [1], [4] a sinusoidal current with 3rd harmonic current injected is mentioned as a way to increase the torque production from the motor. A simpler version where the voltage has a 3rd harmonic component injected instead is also tested as a supply type.

The different types of supply are the input to the simulation. Figure 26 shows a principle circuit of how the motor is supplied, the resistor, inductor and electro magnetic force E_1 to E_n symbolize the n-phase motor, and the voltages U_1 to U_n represent the inverter. The star-point of the machine can be connected back to the supply or simply be floating.

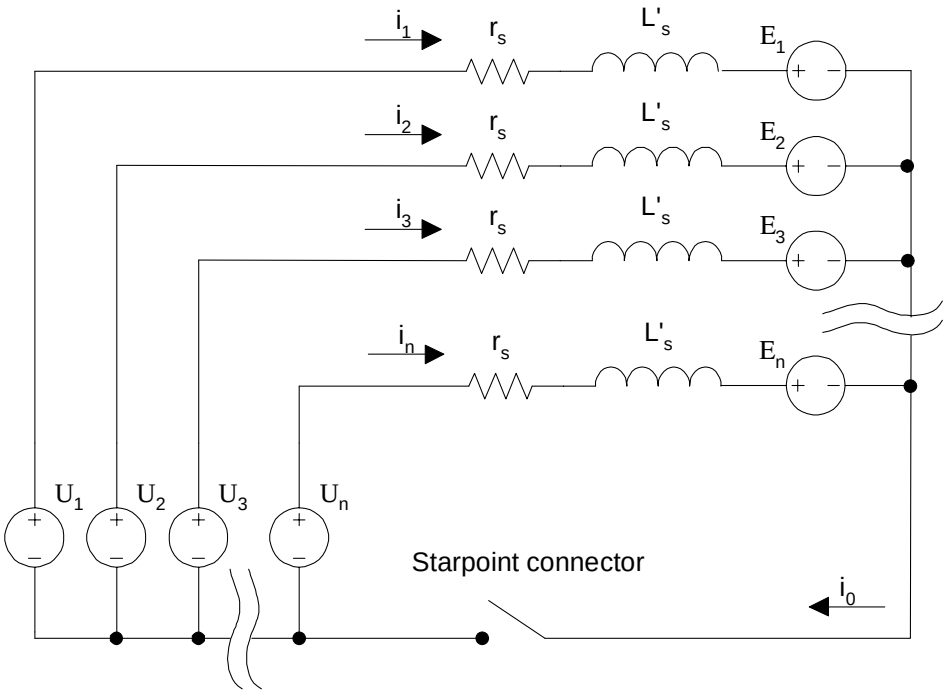

Figure 26 Equivalent control diagram for midpoint controller.

The first thing to do is to see if the simulation of the 3 phase motor with a sinusoidal supply matches the calculation in *SPEED*, or if there is something wrong in the link, or with the winding design. So a completely sinusoidal voltage for multiple phases is one supply type, this is the reference simulation for all the others. The other supply types used for the simulations are summarized in the table below:

Name	Source type	Connection
Sinus	Sinusoidal voltage	Star-point connected to midpoint of capacitor.
Sinusstj	Sinusoidal voltage	Floating star-point.
U3h6p0	Sinusoidal voltage with 1/6 3rd harmonic	Star-point connected to midpoint of capacitor.
U3h6p0stj	Sinusoidal voltage with 1/6 3rd harmonic	Floating star-point.
Square	Voltage: ½Udc, -½Udc.	Star-point connected to midpoint of capacitor.
Squarestj	Voltage: ½Udc, -½Udc.	Floating star-point.
Dead	Voltage: ½Udc, 0, -½Udc, 0. Zero in one phasebelt.	Star-point connected to midpoint of capacitor.
Deadstj	Voltage: ½Udc, 0, -½Udc, 0. Zero in one phasebelt.	Floating star-point.
Deadx2	Voltage: ½Udc, 0, -½Udc, 0. Zero in two phasebelts.	Star-point connected to midpoint of capacitor.
Deadx2stj	Voltage: ½Udc, 0, -½Udc, 0. Zero in two phasebelts.	Floating star-point.

Figure 27 shows the above-mentioned types of voltage supply.

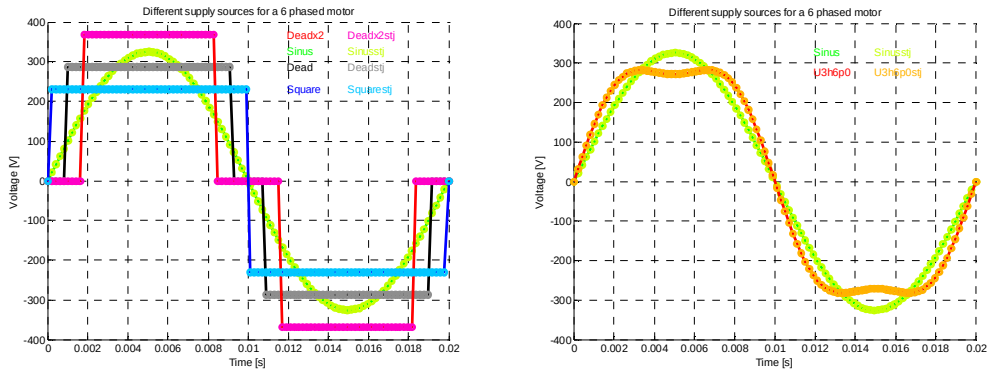

Figure 27	Different constant voltage supplies used for test simulations.

Beside these voltage supplies sinusoidal current supplies with and without 3rd harmonic component is simulated see chapter 5.

3.4 Dynamic results using test case

In this section some dynamic results are presented. The results come from a test case with the motor parameters described in Appendix E. The test case is used throughout the thesis and used to demonstrate and partly verify the theoretical calculations. The test case is implemented and tested in the laboratory (see chapter 4 and 6).

As mentioned the simulations have to reflect the steady state situation. All the variables have to stabilize, and in a motor the slowest variable is the speed. To avoid long simulation times, the motor is started up without load, and after 0.1 seconds the load is applied.

3.4.1 The three phase reference motor

The first simulation to examine is naturally the reference motor, which means a three-phased motor with sinusoidal voltage where the star-point is floating. Figure 28 to Figure 32 shows the simulation results for this case.

The currents in the stator and rotor (Figure 28) have a similar shape during a startup sequence, because they are closely linked through the inductance matrix. The amplitude is scaled differently, because the number of wires, phases and slots is not the same on the stator and rotor.

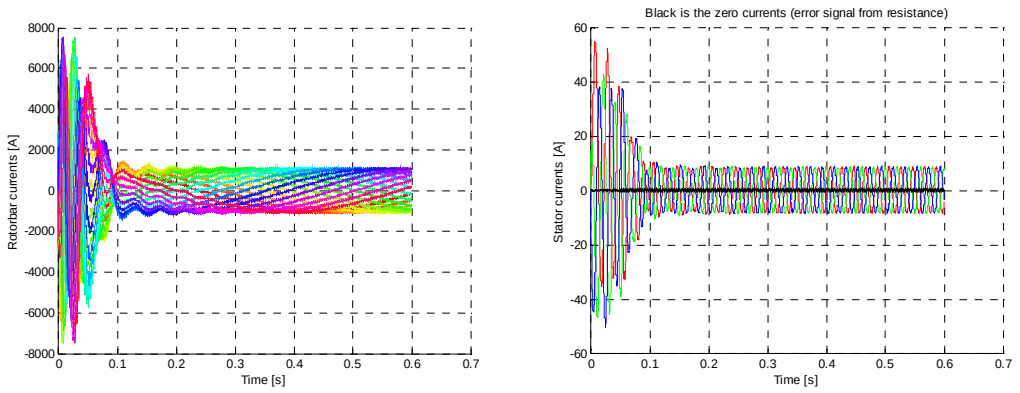

Figure 28	Simulation results for test case with sinusoidal voltage. Stator and rotor currents.

The effect of the slots passing each other gives a high frequency component in the current, both on the stator and the rotor (Figure 29). The rotor sees the 24 stator slots passing with 2920/3000*50Hz~48.7Hz, this gives 1168Hz. The stator sees the 20 rotor slots passing with 48.7Hz, this gives approximately 973Hz.

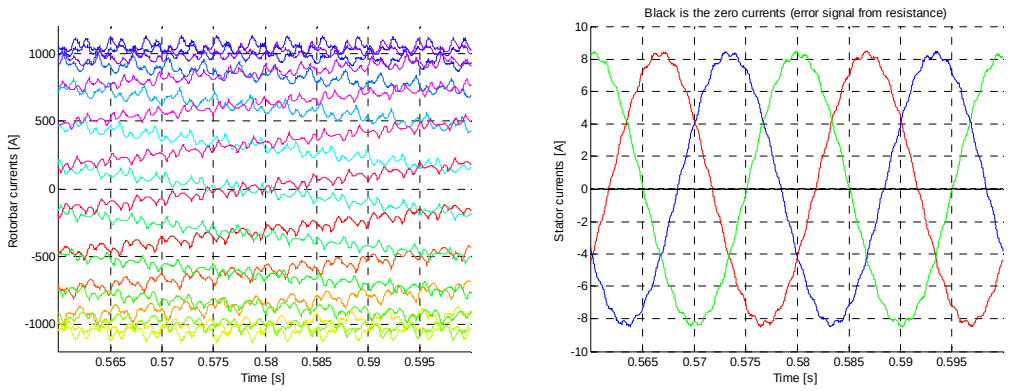

Figure 29	Simulation results for test case with sinusoidal voltage. Stator and rotor currents zoomed in.

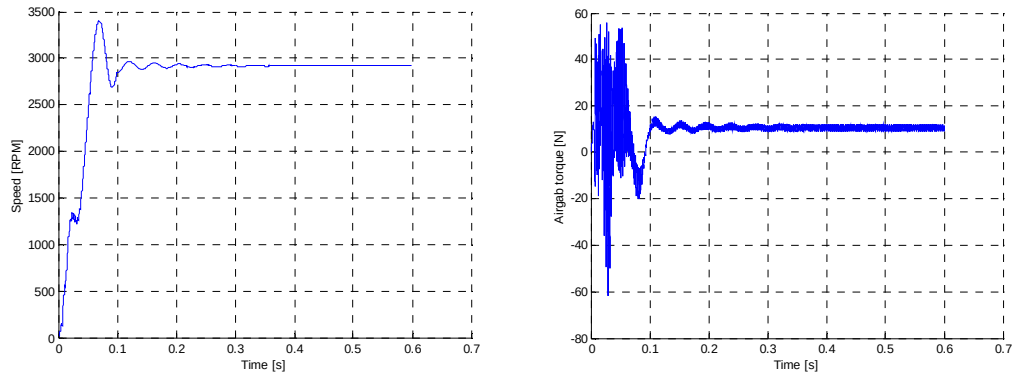

Figure 30	Simulation results for test case with sinusoidal voltage. Speed and torque.

The speed rises within 0.05s to 3000rpm, after this it makes an overshoot to about 3400rpm, where the dynamic torque for a short time actually becomes negative. This breaks the speed and when the load is applied the speed stabilizes to about 2920rpm (Figure 30).

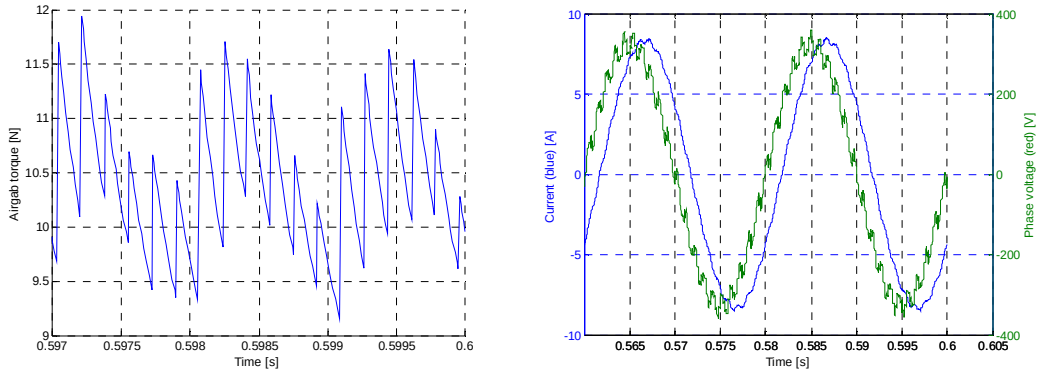

Figure 31	Simulation results for test case with sinusoidal voltage. Torque zoomed in and voltage and current for phase one.

The torque zoomed in (Figure 31, left) shows that it has a ripple depending on the stator and rotor slots passing each other (high frequency saw tooth shape). This frequency depends on the lowest common integer multiple of the number of slots on the stator (24) and rotor (20), in this case 120. This results in a frequency of 120*50Hz*2920rpm/3000rpm ~6000Hz, which means that the amplitude ripple is heavily filtered and damped through the rotor mechanical system. The ripple on the speed is therefore negligible.

In the right plot of Figure 31 the current and the voltage of a single phase is plotted together. The 20 slots from the rotor can be seen in both the current and the voltage. The voltage is the phase voltage, so it is the applied voltage minus the star-point voltage. To prevent these high frequencies the rotor can be skewed, which in effect means that the point windings on the rotor are stretched to an arc in the tangential direction. But this is not taken into account in this *MWI* model.

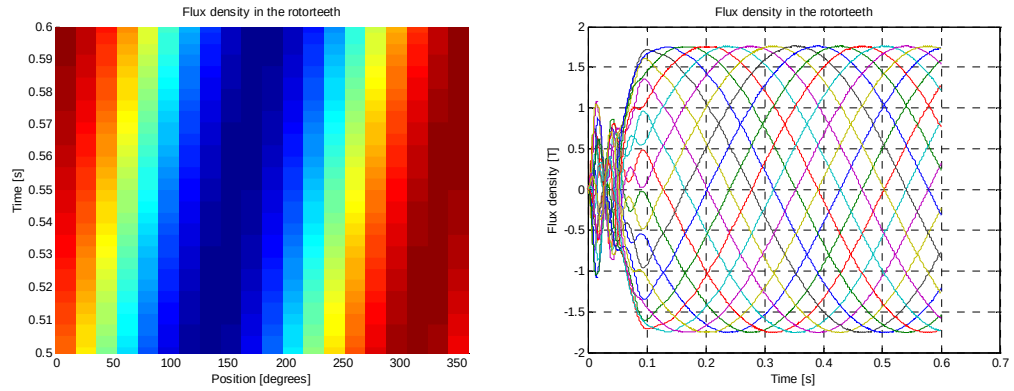

Figure 32	Simulation results for test case with sinusoidal voltage. Flux density in the rotor as a function of time and position and time curve for the 20 rotor slots.

Figure 32 shows the flux density in each rotor tooth as a function of time in two different plots. Looking at the right plot the flux density in each tooth is clearly close to a sinusoidal curve at steady state. The slip frequency of the rotor flux is calculated to (3000-2920)/3000*50Hz~1.33Hz, which fit nice with the frequency of the rotor flux.

3.4.2 Six phase motor with 3rd harmonic voltage

The next is a simulation of a six-phased motor with sinusoidal and 1/6 3rd harmonic voltage supply, where the star-point is connected to the *mid-point* of the *DC-link*. This is shown in Figure 33 to Figure 37.

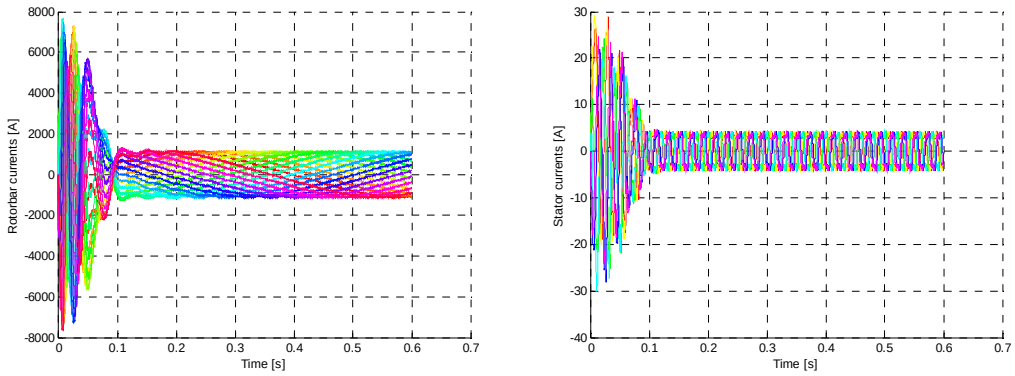

Figure 33	Simulation results for test case with sinusoidal voltage with 3rd harmonic content. Stator and rotor currents.

The stator and rotor current shapes in Figure 33 are again comparable in the rotor and the stator. But like in Figure 28 the amplitude differs, in this case there are 6 instead of 3 phases therefore the amplitudes of the stator currents are approximately halved.

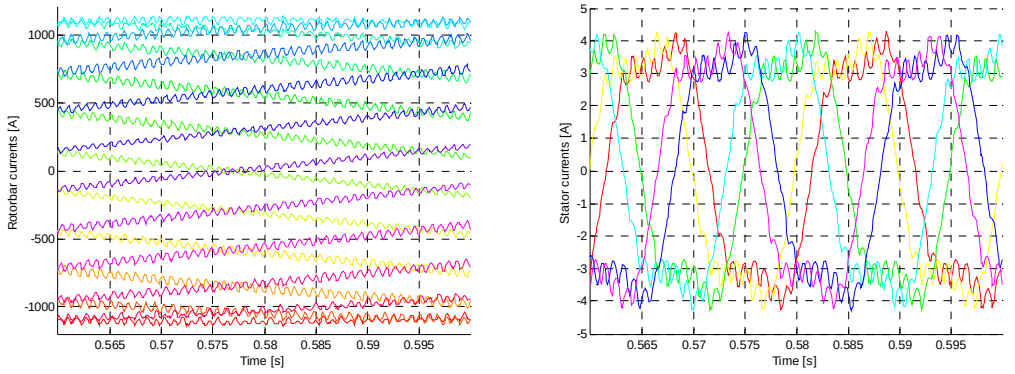

Figure 34	Simulation results for test case with sinusoidal voltage with 3rd harmonic content. Stator and rotor currents zoomed in.

Again, the effect of the slots passing each other gives a high frequency in the current, both on the stator and the rotor (Figure 34). The rotor sees the 24 stator slots passing with 2920/3000*50Hz~48.7Hz, this gives 1168Hz. The stator sees the 20 rotor slots passing with 48.7Hz, this gives approximately 973Hz. If the stator current in Figure 34 is compared to Figure 29, it is obvious that the ripple is increased. This is because in the six phase case the stator phase belts are only spanning 2 slots,

compared to 4 slots in the three phase case. It is also important to note that the 3rd harmonic current has an amplitude about 1/6 of the 1st harmonic, in the case where the supply voltage also has 1/6 3rd harmonic voltage added. This is not general the case it depends heavily on the motor design.

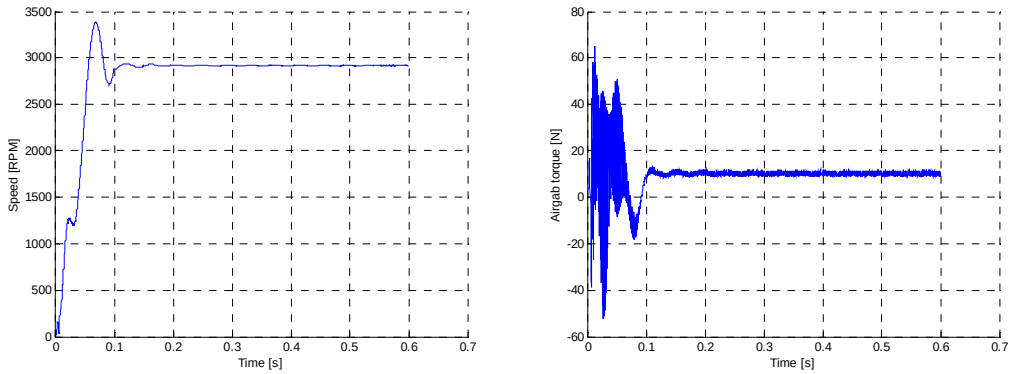

Figure 35	Simulation results for test case with sinusoidal voltage with 3rd harmonic content. Speed and torque.

The speed and torque curve in Figure 35 look a lot like the curves in Figure 30. So the transient response seems to be comparable on a large scale at least.

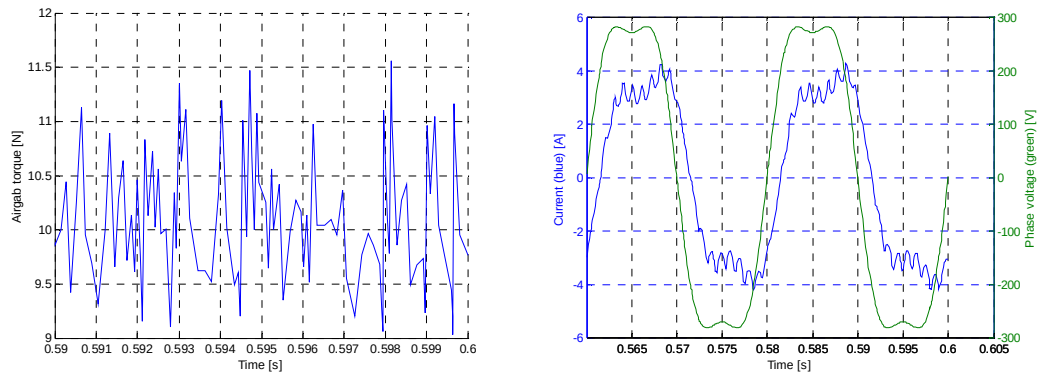

Figure 36	Simulation results for test case with sinusoidal voltage with 3rd harmonic content. Torque zoomed in and voltage and current for one phase.

The torque ripple plotted on the left half in Figure 36 again has some high frequency ripple. The phase voltage plotted in the right half of Figure 36 now only contains the

applied first and 3rd harmonic component, because the star-point is fixed. The current clearly has a 3rd harmonic component in this case.

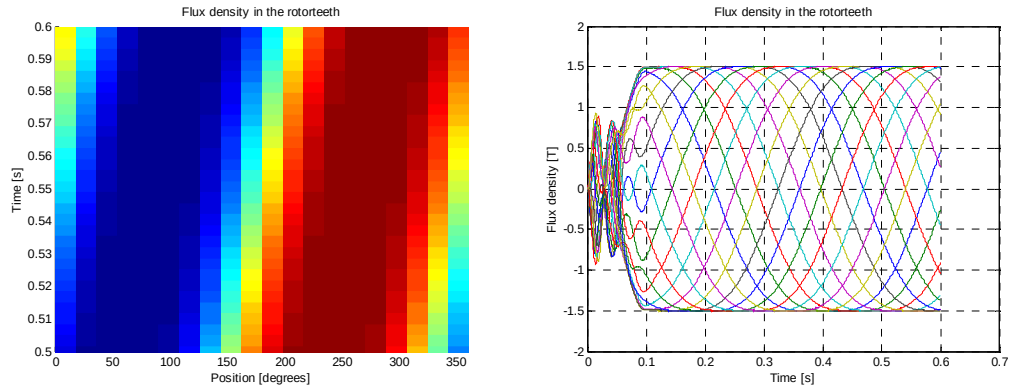

Figure 37	Simulation results for test case with sinusoidal voltage with 3rd harmonic content. Flux density in the rotor as a function of time and position and time curve for the 20 rotor slots.

The perhaps most interesting phenomenon is shown in Figure 37, where the rotor tooth flux densities are plotted as a function of time. One rotor tooth flux-density as a function of time now contains both a first and a 3rd harmonic component as expected. So even though the torque is the same, the peak value of the flux density is decreased from about 1.75T to about 1.5T!

Voltage, current and flux phase relationship

It is also noticeable that the first and 3rd harmonic of the voltage and also the flux are in phase with each other. So in this particular case a current controller is not needed to control the angle between the first and the 3rd harmonic current (see 5.3.2). But it is expected that in general the current is closer related to the flux than the voltage, mainly because of the leakage reactance and stator resistance (See equation (21) & (28)).

3.5 Steady state results from simulation cases

In this section some steady state characteristics are presented. They are calculated using the dynamic *MWI* model, which is expected to reflect perturbations accurately. The production variation of one topology could in some cases be higher than the simulated difference between two topologies. But the difference between two simulated topologies is expected to resemble the difference, between the same two topologies measured on produced units, on average. The Excel sheet with all the

static characteristics calculated from the dynamic variables, is attached in Appendix F. The reference simulation is on the green line in the top of the sheet. The rest of the simulations are of other examples with different combinations of phase numbers and voltage supply. Some of the main results are gathered in the table in Figure 38:

3	0.589	1.76	8.67	87.1	2820		Sinusoidal	To Udc½	
Ph	**Torq. rip**	**Brtpk**	**I p 3-ph**	**Eta**	**VA peak**	**Note**	**Voltage**	**Starpoint**	**Reference**
3	0.489	1.51	8.52	86.5	2305	-	Sinusoidal with 3.harm 1/6 amp.	To Udc½	
3	1.436	1.75	10.85	86.5	4063	-	Square	Floating	
3	0.536	1.76	8.51	87.3	3056	0	Sinusoidal	Floating	
5	0.581	1.51	8.95	87.1	2521	1	Sinusoidal with 3.harm 1/6 amp.	To Udc½	Toliyat
6	0.712	1.31	14.55	85.9	3492	-	Square	To Udc½	
6	0.679	1.42	11.21	86.9	2914	-	Square with zero	To Udc½	
6	0.507	1.51	8.58	87.3	2418	2	Sinusoidal with 3.harm 1/6 amp.	To Udc½	Lyra
6	0.581	1.54	9.61	86.9	3477	-	Square with zero	Floating	
6	0.566	1.69	11.98	87.4	5011	-	Square with 2xzero	Floating	
6	0.036	1.76	8.80	87.7	3391	-	Sinusoidal	Floating	
9	0.133	1.77	10.62	87.6	4491	-	Sinusoidal	Floating	
6	0.338	1.79	8.82	87.6	2993	-	Sinusoidal	To Udc½	
9	0.675	1.49	10.86	86.9	3060	-	Sinusoidal with 3.harm 1/6 amp.	To Udc½	
9	0.586	1.58	10.87	87.3	4182	3	Sinusoidal with 3.harm 1/6 amp.	Floating	Lipo
12	0.481	1.31	14.80	86.2	3552	-	Square	To Udc½	
12	0.539	1.37	12.21	86.7	3053	-	Square with zero	To Udc½	
12	0.338	1.37	11.55	86.9	3476	-	Square with zero	Floating	
12	0.649	1.42	12.29	87.0	3195	-	Square with 2xzero	To Udc½	
12	0.044	1.77	9.40	87.8	3620	-	Sinusoidal	Floating	
12	0.402	1.78	9.41	87.5	3194	-	Sinusoidal	To Udc½	
3	**0.581**	**1.75**	**8.71**	**85.9**	**2834**	**4**	**Sinusoidal**	**To Udc½**	**Winding a)**
6	**0.351**	**1.77**	**8.86**	**86.1**	**2996**	**5**	**Sinusoidal**	**To Udc½**	**Winding b)**
6	**0.557**	**1.50**	**8.71**	**85.6**	**2454**	**6**	**Sinusoidal with 3.harm 1/6 amp.**	**To Udc½**	**Winding b)**
6	**0.530**	**1.76**	**8.70**	**86.2**	**2451**	**7**	**Sinusoidal with 3.harm 1/6 amp.**	**To Udc½**	**Small teeth winding b)**

Figure 38 Main steady state results from dynamic simulations. The colors refer to the following:

Compared to reference
A lot better
A little better
Reference simulation for note -,0,1,2,3
Reference simulation for note 4,5,6,7
Same level or a little worse
A lot worse

In the first simulations (Note number: -, 0, 1, 2, 3) the end-winding is expected to be identical. This means that the phase resistance is linearly dependent on the number of phases, and it is therefore calculated with reference to the three phase motor $R_{ph}=R_3 \cdot ph/3$.

The last simulations (Note number: 4, 5, 6, 7) are only comparable to each other and closer related to a real producible motor than the simulations with the other note numbers, because the resistance is calculated in the *SPEED* program. In *SPEED* the end-winding is calculated on the basis of the winding design and geometric parameters (see 2.3.2). Winding a) and b) in the reference column refer to the windings in Figure 16 and Figure 17 respectively.

3.6 Discussion of steady state results

In Figure 38 the characteristics of the motor drives in the simulations, with a number in the note column, are discussed in the below section.

From Figure 38 some general trends can be concluded:

- If the star point is disconnected (floating) and the supply is a sinusoidal voltage, then the torque ripple is very low.
- Higher numbers of phases with sinusoidal supply increases the motor efficiency slightly and reduce the torque ripple.
- Completely sinusoidal voltage without any higher harmonics does not change the peak flux density in the stator and rotor tooth. This means redesign of the lamination geometry is not necessary.
- Square voltage supply with or without zero voltage gives high peak currents in the switches.
- Square voltage supply without zero voltage gives lower motor efficiency.
- Sinusoidal with 3rd harmonic with 1/6 amplitude gives low *VA-rating*.
- Square voltage supply with or without zero voltage gives high *VA-rating*. But note that this is without considering that the switching losses are considerably lower.

The following is a list with some comments to the simulations with note numbers.

0. The simulation with the note number 0 is nearly the same as the reference simulation. The only difference is that the star point in the reference simulation is connected to the midpoint of the *DC-link* in the inverter. It would perhaps be more correct to use the simulation with the note number 0 instead of the reference simulation, but the differences in the values are minimal. So the conclusions will not change. If the inverter has space vector modulation where a 3rd harmonic voltage is added in phase with the first, the *VA-rating* of the inverter could be decreased by about 15% [15]. So actually the minimum obtainable *VA-rating* is 3056 minus 15% ~ 2600 VA. One could argue that this would be the right *VA-rating* to be used as a reference for all the rest of the simulations!
1. This simulation is inspired by Professor H.A. Toliyat, who at a workshop at the IAS conference 2002 showed that a motor with five phases and a 3rd harmonic current injected would be able to provide higher torque per volume, than a standard three-phase motor. The characteristics are all comparable to the reference simulation, except the peak flux density in the rotor and the stator teeth, which is 0.25T lower! The lower peak flux density is an advantage because the width of the teeth can be decreased. The peak flux density is lower in both the stator and the rotor teeth. Therefore there is more room for copper in the stator wires and aluminum in the rotor bars, hence the efficiency can be increased. In sections 2.3.3 and 2.3.4 this is also described, although with the six-phase motor in mind, but this simulation compared with

the six-phase (note 2), shows that the difference is not that big! In the same time the inverter in simulation with note 1, at the given working point, could be made with an open loop voltage control, which is much simpler than the closed loop current regulated inverter suggested by Toliyat. But as mentioned in 3.4.2 this does not necessarily apply in all working points. The *VA-rating* is also better than the reference simulation. But the phase between the first and 3rd harmonic voltage could change in other working points, if the flux harmonics have to be aligned. So the peak voltage could increase a little.

2. The next important configuration is inspired by R. Lyra, who has written a PhD thesis [1] with 3rd harmonic current injection in six-phased motors. This simulation has 14% lower torque ripple, 0.25T lower peak flux density, the same peak current and 0.2 percent point higher efficiency. So the motor is slightly improved, although it needs redesign, just like in note 1, to take advantage of the lower peak flux density. The *VA-rating* is also better than the reference simulation. But again the phase between the first and 3rd harmonic voltage could change in other working points, if the flux harmonics have to be aligned. So the peak voltage could increase a little, but the *VA-rating* is still expected to be comparable or a little better.
3. The simulation with the note 3 is the only simulation with 3rd harmonic voltage and no star point connection. This simulation is inspired by Professor T.A. Lipo, who says that the 3rd harmonic current in a nine phased motor effectively sees a three phased motor with three times as many poles as the 1st harmonic current. The simulation shows that as expected the flux density in the teeth is lower, but the peak current in the phase is higher. The reason for the peak current to be higher is that the current is not controlled instead the voltage is shaped, just like in all the other cases, because this makes a much simpler inverter. It has to be mentioned that skewing the rotor would decrease this ripple considerably, which is of cause the case for all simulations, but in this case it is especially important because the nine-phased motor has a lower number of stator and rotor slots, 18 and 14 respectively. This is due to winding considerations. If the current at the same time is controlled, then the peak current value would be much lower. The configuration with nine phases is of course interesting, but compared to the five-phase motor (note 1) and the six-phased motor (note 2) the inverter with nine gate drivers could be too expensive. The most important detail about the nine-phase motor is that the return path to the star-point is not necessary even if a 3rd harmonic current is injected.
4. This simulation is a three-phase sinusoidal supplied reference for the last three simulations. The stator resistance is found by measurements in a heating test of the three-phase motor to make the calculations more realistic, therefore the stator resistance is changed from 2.00Ω (Note number: -, 0, 1, 2, 3) to 2.25Ω (Note number: 4, 5, 6, 7).
5. In this simulation a six-phase winding (Figure 17) is used. The geometry is the same as for the three phase case. The supply is still sinusoidal. The winding resistance if therefore changed to 2·2.36Ω (found using *SPEED*). But even though the resistance is higher, the motor efficiency is improved

0.2% point, and the torque ripple is reduced 40%! As expected the flux level is not changed, since there is no 3rd harmonic component.

6. In this simulation a 3rd harmonic voltage (resulting in a current) is injected. This reduces the efficiency a little because the *RMS* current is increased, but it also reduces the flux level in the teeth. The torque ripple is again only a little lower than the reference simulation.
7. In the last simulation the potential of the flux reduction gained in note 6 is used to reduce the teeth, and increase the stator and rotor slot areas. This gives a reduction of the stator resistance to 2·2.22Ω, and the rotor resistance from 1.02Ω to 0.92Ω. This gives 0.3% point higher efficiency and nearly 10% torque ripple reduction, compared to the reference simulation.

3.7 Conclusion

A dynamic model called the multi winding (*MWI*) model capable of calculating variables in both dynamic and steady state conditions is build. A close link to the commercially available motor design software called *SPEED* is made. This enables a high degree of accuracy to perturbations in the design, and a close connection to the physical dimensions and limitations. The dynamic simulation shows the startup sequence, and the effect of slots passing each other can be seen in the current, voltage, and torque signals. The flux-densities in all the individual teeth are calculated. A 3rd harmonic component can i.e. be seen in the rotor flux if a 3rd harmonic current is injected in the stator current of a six-phase motor. This is important when finding the limits in performance. The model can be used for any winding design with any number of phases.

From the steady state variables (calculated on the basis of the dynamic variables) earlier work done by Toliyat, Lyra and Lipo has been examined. 3, 5, 6, 9, 12 phased motors are compared on a general level to capture some trends.

In a more detailed level analysis (including accurate resistance calculations) it was found that a six-phase motor with sinusoidal supply has a 0.2% point higher efficiency and 40% lower torque ripple than a three-phase motor with sinusoidal supply. Increasing the slot width in the six-phase motor and injecting a 3rd harmonic voltage giving a 3rd harmonic current with 1/6 amplitude compared to the 1st harmonic current gives 0.3% point higher efficiency but only 10% lower torque ripple compared to the three phase motor.

In the simulations simple open loop voltage controllers are used instead of a close loop current controller, but it is expected that closed loop current control is needed at other working points. A close loop current vector controller is therefore designed in chapter 5.

On the basis of the above it is chosen to concentrate the further work on the six-phase machine. In the next chapter a six-phase induction motor is tested and compared to a *MWI* model of this specific motor.

4. Verification of a six-phase motor model

4.1 Introduction

In this chapter the *MWI* model described in chapter 3 is tested in a case with a six-phase motor. It is simplest to run the six-phase test motor with two frequency converters because six different angles/phases are needed. Two standard Danfoss VLT inverters are used, the VLT's are controlled using a *D-Space* system, programmed in *Matlab*/*Simulink* and managed by the control-desktop software. A simple voltage control algorithm is used in the verification process in this chapter. A more advanced current controller is designed and implemented in chapter 5 and tested in chapter 6. The test system is described in more details in Appendix A. Assumptions are discussed, and two different voltage supply situations are simulated and tested.

4.2 Test system

The test system is summarized in this section, and the complete description is in Appendix A. The test system consists of a three-phase rectified DC-voltage connected to two Danfoss VLT's. The VLT's have interconnected *DC-link* capacitors and the capacitor midpoint potential is also interconnected. This point is connected to the motor star-point (in case a return current is needed). The two VLT's make six phase voltages connected to the motor with a cable. The corresponding six currents from the motor are sampled and measured with a *D-Space* card in a computer. The VLT's are controlled with *PWM* running in optical fibers from the *D-Space* card. The six-phase motor is mechanically loaded with a permanent magnet synchronous motor. The load motor is connected to a drive from Siemens, which is also controlled with the *D-Space* card. More details about the test system can be found in Appendix A.

4.2.1 Assumptions and difference between simulation and test

There are a few assumptions and deviations between simulation and test that have to be mentioned here. They can explain the difference between measurements and simulations. The assumptions made in relation to the *MWI* model described in 3.2.1 are still valid. The most important are summarized here. Because of measurement difficulties of *PWM* voltages some assumptions are also made on the measurements.

Skewing

The rotor in the test motor is skewed by one rotor slot. This is not included in the *MWI* model. The effect is assumed to be that the rotor slot harmonics are considerably reduced on the stator current.

Nonlinear behavior

The BH-curve for iron is in the *MWI* model assumed to be linear and included in the air-gap (see 3.2.1). The BH-curve is in reality nonlinear [35] which amongst others cross couple the harmonics in the motor. An example is the harmonic current content in a saturated sinusoidal supplied motor [38].

Another nonlinear effect from the real BH-curve is the iron loss. This is also not modeled in the *MWI* model. The iron loss can however be subtracted from the shaft power or added to the input power to emulate the effect of the loss component.

The voltage

Phase voltage is not measured, it is assumed to be equal to the reference voltage. In the controller the duty cycles are calculated by dividing the reference voltage with the *DC-link* voltage and adding 0.5. The result is limited to a value between 0 and 1. The *PWM* switching times are calculated by the *D-Space* processors. The two VLT's have a 1.5µs build-in dead time between upper and lower switch activation to prevent short circuit. This gives a small asymmetry between positive and negative voltage. However this asymmetry is normally neglected, because if the switch frequency is 5kHz, the asymmetry is only in the per thousand range. Voltage drops across IGBT's and diodes are also neglected.

The assumptions about the voltage are validated by measuring one motor phase voltage (with an oscilloscope) and comparing this with the reference voltage in the *D-Space* system. A differential probe is inserted between one motor phase and the return wire from the star-point connection. In this situation the star-point of the motor is therefore returned to the *mid-point* of the *DC-link*. To synchronize the voltages the VLT's are disabled, which trigger both the *D-Space* measuring system and the Oscilloscope. The phase voltage is *PWM* modulated, so it has to be filtered to compare with the *D-Space* reference voltage. A fifth order filter with a resulting bandwidth of about 1000Hz is used. To avoid phase error the *Matlab* function

”filtfilt” is used. This function uses a special technique which involves forward & backwards filtering of the signal, the result is zero phase error for all frequencies.

In Figure 39, the voltages are compared. The filtered oscilloscope voltage is close to the reference voltage both in amplitude and shape.

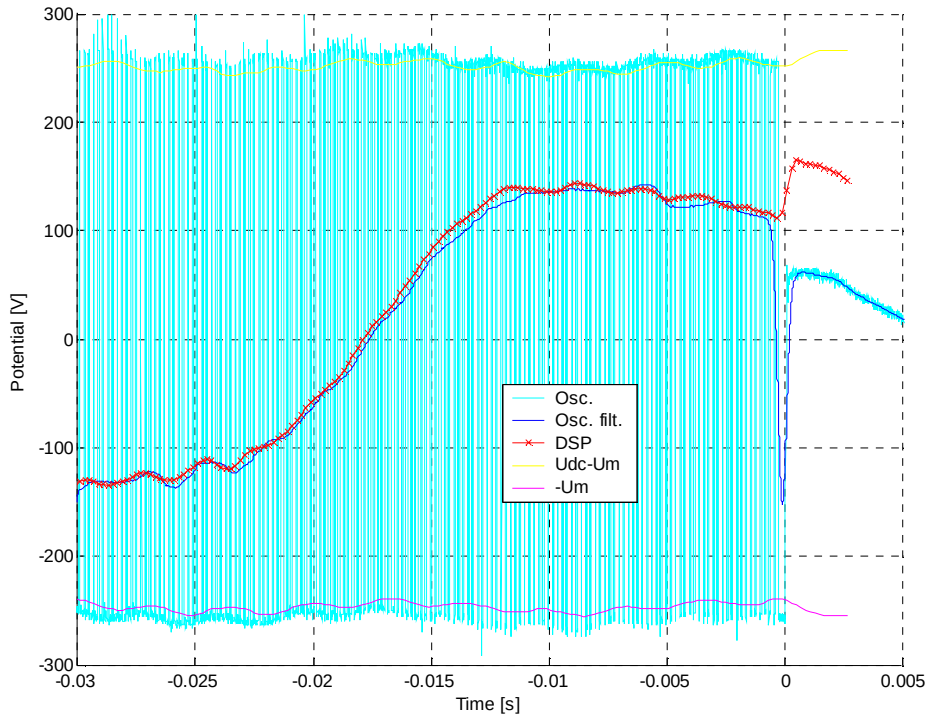

Figure 39	Phase voltage measured with oscilloscope (Osc.) and *D-Space* system (DSP). Filtered oscilloscope voltage (Osc. filt.). (Udc) and (Um) are used for comparison with peak values of the *PWM* (see Figure 58b).

Figure 40 is a zoom in of Figure 39, and it shows a close up of the voltage *PWM*. The voltage on the oscilloscope is sampled with 250kHz, and the *PWM* switch frequency is 5kHz.

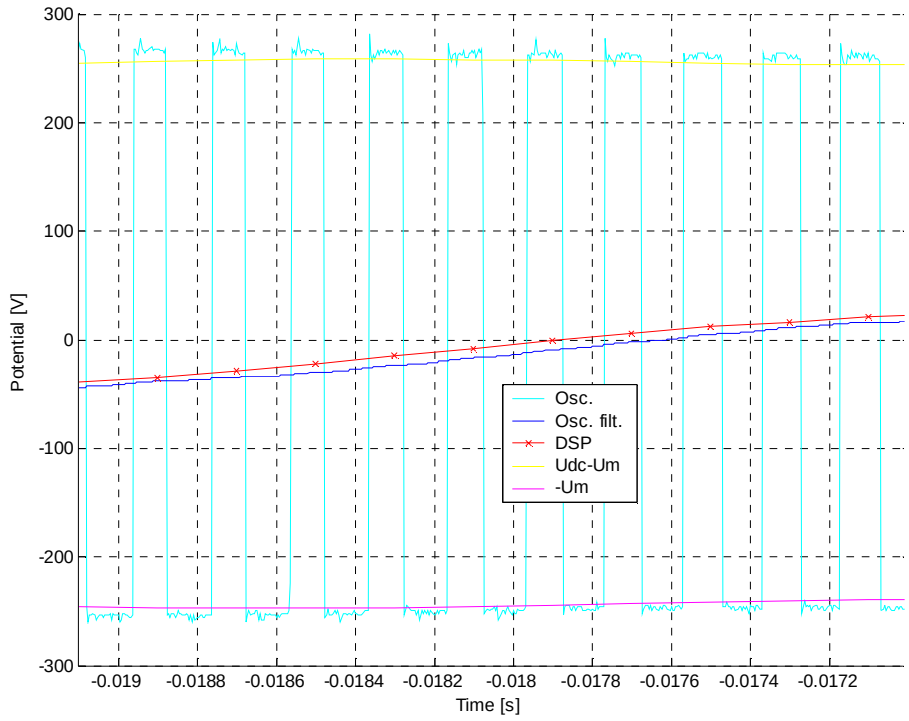

Figure 40	Zoom in of phase voltage measured with oscilloscope (Osc.) and *D-Space* system (DSP). Filtered oscilloscope voltage (Osc. filt.). (Udc) and (Um) are used for comparison with peak values of the *PWM* (see Figure 58b).

The maximum valid voltage is U_{dc}-U_m (see Figure 58b for definitions), and this voltage can be compared to the positive *PWM* voltage. The minimum voltage is $-U_m$ (see Figure 58b for definitions), and this voltage can be compared to the negative *PWM* voltage. Both U_{dc} and U_m are measured with the *D-Space* system. The difference between the extreme values measured with the oscilloscope and the *D-Space* measurements is a few percent, which could be due to the relative low amplitude precision of the oscilloscope combined with a non calibrated voltage measurement from the *D-Space* system. Since the reference voltage in the rest of the thesis mainly is used for control purpose, the difference is acceptable.

All in all it is concluded that the assumptions about the voltages are acceptable.

The current

The phase currents are measured using the *D-Space* system. This means that the currents are sampled at 5kHz. The current ripple due to *PWM* switching is therefore

not measured. It is assumed that the measured current describes the mean phase current.

Just like the voltage assumptions, the current assumptions are validated by measuring the current with a current probe attached to the oscilloscope. Also the current has a high ripple due to the *PWM* voltage. The filter described in the voltage section just above is again used to filter the oscilloscope measurement. In Figure 41 the measurements are compared for the same phase and situation as shown in the voltage verification case. The *D-Space* and the filtered oscilloscope measurement match each other very well in shape and amplitude, but there is a small offset due to the *PWM* ripple. This offset is further examined in the zoom see Figure 42.

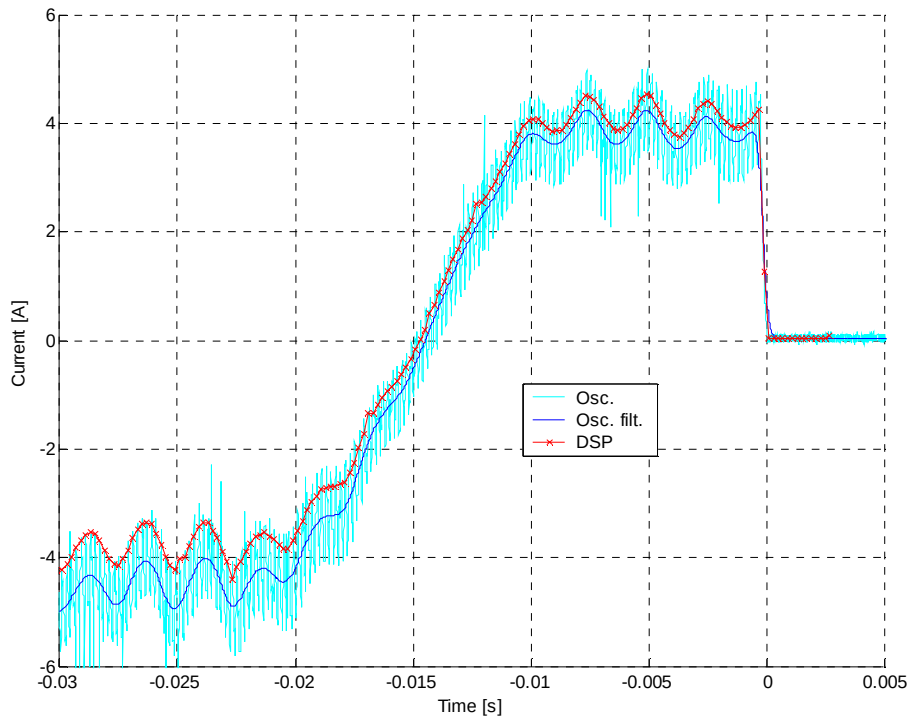

Figure 41	Phase currents measured with oscilloscope (Osc.) and *D-Space* system (DSP). Filtered oscilloscope voltage (Osc. filt.).

In Figure 42 it becomes clear that the current measured in the *D-Space* system is sampled at an imprecise time. The sampling is done in a time during the *PWM* where the voltage is positive (the current is rising), which is OK, but the problem is that the sampling is not at the center of the positive period, it is delayed about 30µs. This means that the *D-Space* current is about 0.3-0.5A above the real mean current.

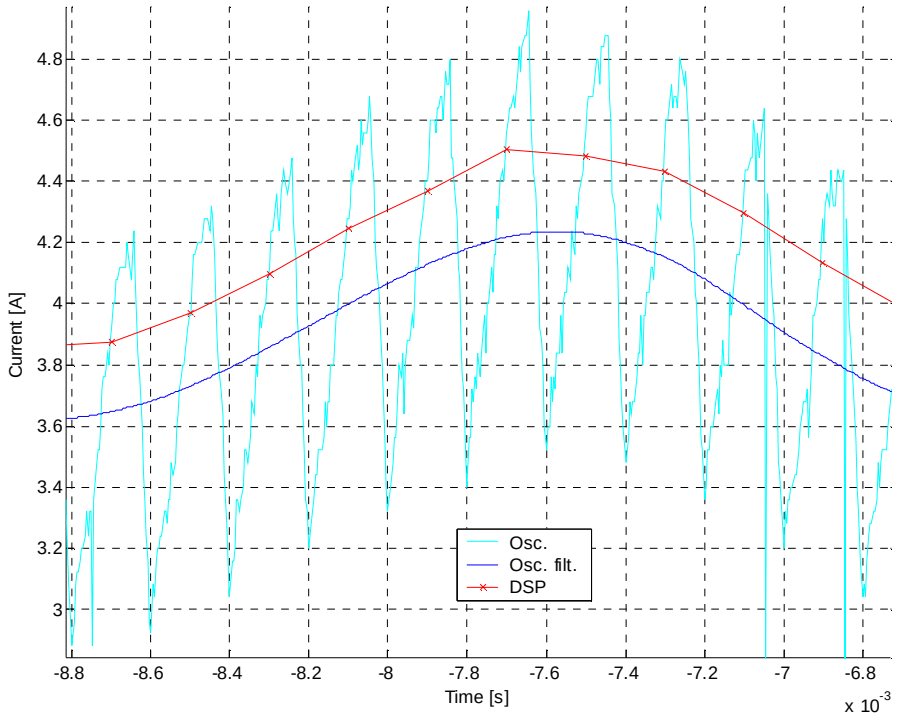

Figure 42	Zoomed phase currents measured with oscilloscope (Osc.) and *D-Space* system (DSP). Filtered oscilloscope current (Osc. filt.).

A solution to this problem is to sample the currents 30µs in advance, or even better to program the *PWM* generation and sampling directly in C-code. But the gain of doing this is not expected to be worth the effort, especially because the current shape and amplitude are so close to the real value. Instead the currents are simply offset calibrated so the currents are zero in mean value. If a fixed duty cycle (e.g. 50%) is entered on one phase, the current has to stabilize at zero mean current, because the DC-midpoint voltage simply will settle at the *DC-link* voltage times the duty cycle (see Figure 58b for definitions).

4.3 Comparison between measurements and *MWI*

Two different fixed voltage supply situations are compared. The first is with sinusoidal voltage and floating star-point. The second situation is with first and 1/6 3rd harmonic voltage. Here the star-point is connected to the *mid-point* in the *DC-link*. The voltage divide by frequency ratio is fixed in these cases to keep the flux-

density in the motor at the same level [9], [37]. In both cases the *D-Space* system and VLT's are used.

4.3.1 With sinusoidal voltage supply floating star points

The first case is with completely sinusoidal voltage supply and the star points disconnected so that no current floats from the motor back to the *DC-link* midpoint. A voltage and the corresponding current for simulation and measurement are pictured in Figure 43. The simulated time is offset -0.2453s, because the simulation first has to settle on steady state values.

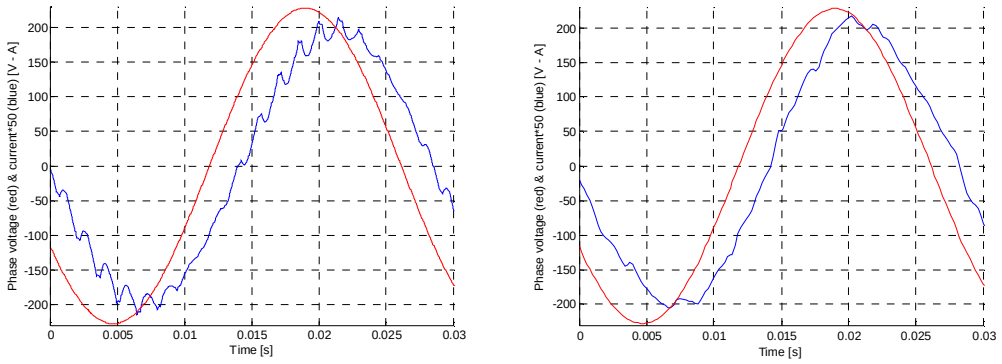

Figure 43	Simulated (left) and measured (right) stator current (blue) and voltage (red). The currents are multiplied with 50. Working point @ 35Hz, 10Nm, 161Vrms 1st harmonic.

The measured and simulated current fit very nicely, a main difference is the current ripple due to the rotor slots on the simulated current, which is dampened considerably on the measured curve because the rotor is skewed. Nonlinearities like saturation also cause some difference both in amplitude and in dampening the harmonic current contents. This can also be seen on a fast Fourier transformation (FFT) analysis of the currents which is performed in Figure 44.

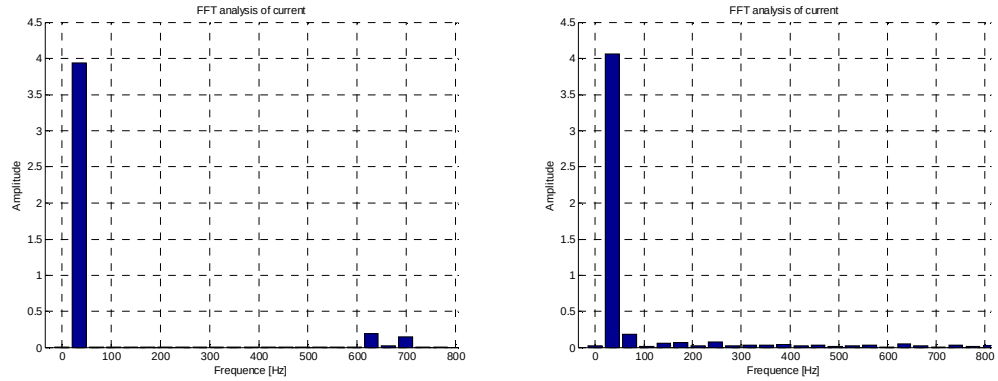

Figure 44	Simulated (left) and measured (right) peak stator current FFT analysis. Working point @ 35Hz, 10Nm, 161Vrms 1st harmonic.

The high frequency components near 640Hz and 700Hz comes from the rotor slots passing the stator slots, which as mentioned are minimized considerably by skewing the rotor one stator slot, more details about this can be found in section 3.4.

The six currents (colored) and the sum of the currents (black) are shown in Figure 45. There is a small difference between the two three-phase systems, especially for positive peak values. It could come from the measurement technique, see 4.2.1. The *PWM* generation for the second VLT is evaluated at a random time, depending on the simulation order of the different *Simulink* blocks. Because even though the measured/sampled current in the two three phased systems are synchronous with each other, the *PWM* switchings are not. This gives unsynchronized *PWM* generation and sampling. Looking at Figure 42 it can be seen, that the peak to peak current ripple is about 1.4A and the amplitude on the second order harmonic current is only about 0.2A. This means that the asymmetry could come from measurement error alone. The asymmetry is so small (a few percent) that it is assumed not to come from modeling error and it is not examined further.

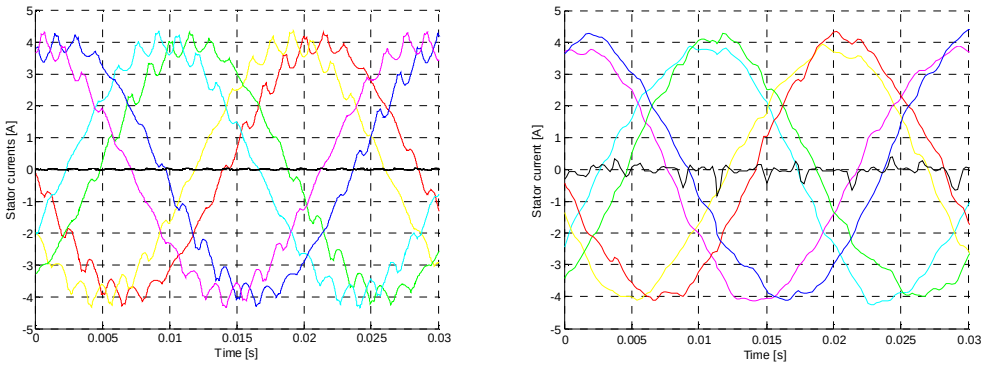

Figure 45	Simulated (left) and measured (right) stator currents. Working point @ 35Hz, 10Nm, 161Vrms 1st harmonic.

The synchronous speed at 35Hz is 2100RPM. The torque in the simulation is fixed to 10Nm. The torque on the load machine in the test setup is also set to 10Nm. The measured speed at this torque is 1993RPM and the simulated speed is 2000RPM. The main difference is probably the iron loss, stray load loss and ventilation loss, which reduces the speed in the measurement.

4.3.2 With sinusoidal and 3rd harmonic voltage supply

The second case is with sinusoidal with 1/6 amplitude 3rd harmonic voltage supply and the star points are connected so that a current can float from the motor back to the *DC-link* midpoint. A voltage and the corresponding current for simulation and measurement are pictured in Figure 46. The simulated time is offset -0.2647s, because the simulation first has to settle on steady state values.

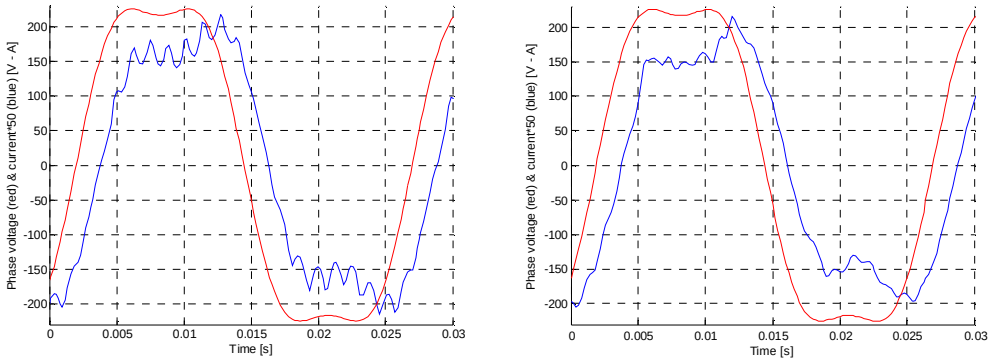

Figure 46	Simulated (left) and measured (right) stator current (blue) and voltage (red). The currents are multiplied with 50. Working point @ 40Hz, 10Nm, 184Vrms 1st harmonic, 30.7Vrms 3rd harmonic.

The measured and simulated current again fit very nicely, a main difference is the rotor slot ripple on the simulated current, this ripple is dampened considerably on the measured curve because the rotor is skewed. This can also be seen on a FFT analysis of the currents which is performed in Figure 44.

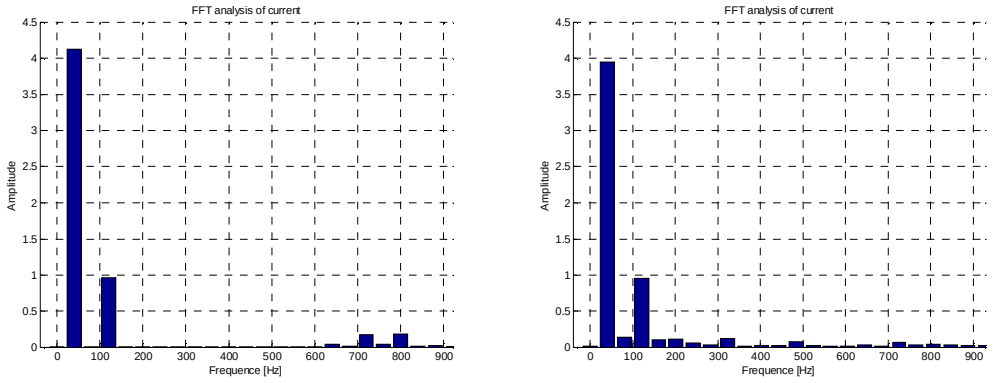

Figure 47	Simulated (left) and measured (right) peak stator current FFT analysis. Working point @ 40Hz, 10Nm, 184Vrms 1st harmonic, 30.7Vrms 3rd harmonic.

The six currents (colored) and the sum of the currents (black) are shown in Figure 48. The measured zero current has a slightly higher amplitude than the simulated.

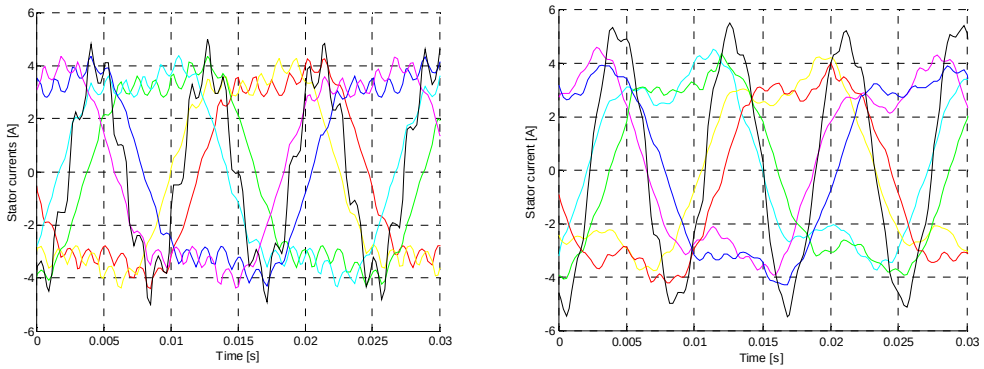

Figure 48	Simulated (left) and measured (right) stator currents. Working point @ 40Hz, 10Nm, 184Vrms 1st harmonic, 30.7Vrms 3rd harmonic.

The synchronous speed at 40Hz is 2400RPM. The torque from the simulation and test are fixed to 10Nm. The measured speed at this torque is 2290RPM and the simulated speed is 2295RPM. The main difference is probably also in this case the iron loss, which reduces the speed in the measurement.

The efficiency is not tested because it demands a very high degree of accuracy. The input power to the motor has to be measured with three power-analyzers. The voltage and the current have as shown in 4.2 high frequency ripple and the six-phase motor with return wire has six independent currents and voltages. In a three-phase motor it is only required to measure two voltages and currents. The shaft power can of course be measured by the speed and the torque independent of the number of phases. Another effective way to measure the efficiency is to measure the heat generated by the loss known as calorimeter measurements [34]. None of the very demanding practical methods are used to test the efficiency of the build six-phase motor. Partly because of the great effort it demands and partly because the result is not expected to be very valuable. The six-phase motor is not optimized in any way. The lamination is identical to the three-phase lamination the only difference between the three-phase motor and the build six-phase motor is the winding layout.

4.4 Conclusion

The *MWI* model gives an acceptable degree of accuracy in the six-phase motor case. The *MWI* model does not take skewing of the rotor into account. Skewing is done in the practical case to reduce the high frequency slot harmonics, resulting in less audible noise. Another important thing the *MWI* model does not consider is the nonlinear saturation of the iron. These two factors together with measurement error and the assumption that the voltage from the inverter is the reference voltage fully

explain the difference between model and measurements. Therefore the *MWI* model is a satisfactory model to use, when simulating the six-phase motor.

It is however important to note that the verification is only one single case, other cases could have other number of phases, other number of slots on stator and rotor, other winding distribution and so on, just to mention a few parameters. It is not certain that the *MWI* model works in all cases. This means that the *MWI* model is not verified except for the specific six-phase test case.

Now that the *MWI* model is build and tested, it can be used to make a more advanced controller for the six-phase motor. The control strategy is analyzed in the next chapter.

5. Controllers for a six-phase motor

5.1 Introduction

A standard rotor field oriented vector control strategy of a three-phase induction motor is described in the beginning of this chapter. After this the state of the art for a current controlled six-phase motor drive supplied by a six-phase inverter is presented [1]. It is a simplified form of a rotor field oriented vector control of traditional three-phase motors. Current controllers for the six-phase motor can now be designed using traditional linear control methods. Six controllers are necessary in this system, since the number of independent currents is six. The controllers consist of, two controllers of active current for the 1st harmonic, one controller for active 3rd harmonic current, two controllers of magnetization current for the 1st harmonic and one controller for the 3rd harmonic magnetization current. A speed controller, giving reference to the three active current controllers, is designed as an outer loop. The reference for the three magnetization current controllers is given directly.

In addition to the six inverter-branches, [1] uses an extra branch to stabilize the voltage in the neutral point connection of the motor. The stability problem is analyzed and a new control algorithm is suggested, eliminating the need for an extra branch under certain conditions.

5.2 Vector control of a three-phase induction motor

The heart of the vector controller is the transformation between rotating signals and stationary signals, which make the controller simpler, because it makes the electrical signals dc-values in steady state conditions. The second step is to make the system linear for the controller, and the torque and magnetizing current are thereafter controllable independently [11]. After the dq-axis transformation to a reference frame with stationary signals and the linearization of the motor, the controller is easy to design, because standard linear control strategies like root-locus plot and bode-plot can be used.

5.2.1 dq-axis transformation

The stator voltage equations transformed with the angle θ to the frame rotating with ω_{mr} (Figure 49) are shown in equation (34). In the equation everything is divided by R_s (see [11]).

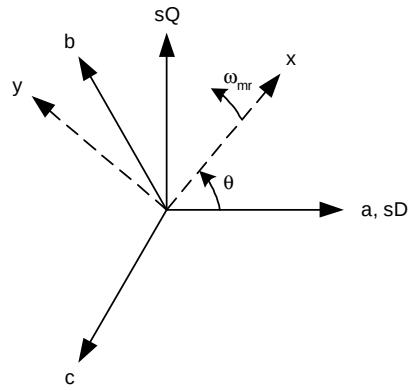

Figure 49 dq-axis transformation vector diagram [11].

$$T_s' \cdot \frac{di_{sx}}{dt} + i_{sx} = \frac{u_{sx}}{R_s} + \omega_{mr} \cdot T_s' i_{sy} - (T_s - T_s') \cdot \frac{d|i_{mr}|}{dt}$$
$$T_s' \cdot \frac{di_{sy}}{dt} + i_{sy} = \frac{u_{sy}}{R_s} - \omega_{mr} \cdot T_s' i_{sx} - (T_s - T_s') \cdot \omega_{mr} \cdot |i_{mr}| \quad (34)$$

Where:	***Var***	***Description***
	T_s	*Time constant for stator.* $T_s=L_s/R_s$
	T_s'	*Transient time constant for stator.* $T_s'=L_s'/R_s$ *Where:* $L_s'=L_s-L_m^2/L_r$
	ω_{mr}	*Angular speed of the rotor-flux-oriented reference frame.*
	u_{sx}	*Direct component of stator voltage.*
	u_{sy}	*Quadrature component of stator voltage.*
	i_{sx}	*Flux-producing stator current component.*
	i_{sy}	*Torque producing stator current component.*

These equations are linear differential equations, so they are relatively easy to handle, but the magnetizing current $|i_{mr}|$ is also a function of the rotor current (see (35)), so therefore this circuit also has to be considered.

$$|i_{mr}| = i_{sx} + j \cdot i_{sy} + (i_{rx} + j \cdot i_{ry}) \cdot (1 + \sigma_r) \quad (35)$$

Where:	*Var*	*Description*
	σ_r	*Rotor leakage factor. Rotor leakage inductance divided by magnetizing inductance.*
	j	*The complex operator.*

5.2.2 Rotor-flux-oriented control

One very used way to make a linear control system is to make a rotor-flux-oriented control [11]. With this strategy high dynamic performance, torque control and loss minimization is possible. A way to implement this strategy is presented in Figure 50.

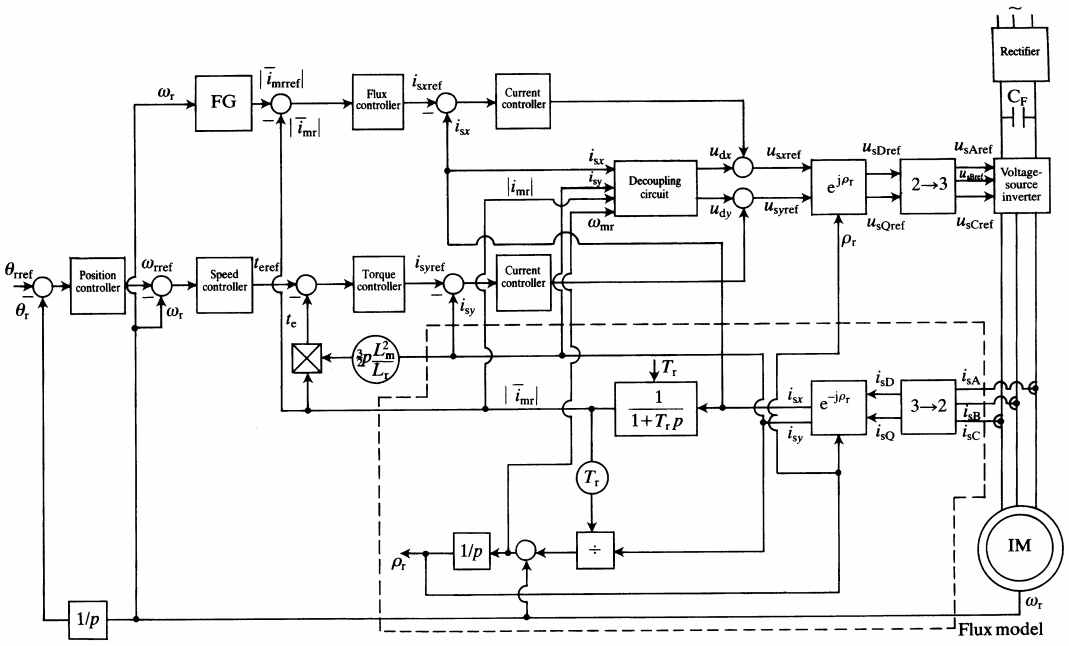

Figure 50 Control of a three phase induction motor-drive using rotor-flux-oriented vector control [11].

The blocks in the figure are described in the following.

5.2.3 Torque decoupling

In [11] the torque is expressed like shown in equation (36).

$$t_e = \frac{3PL_m^{\ 2}}{2L_r}|i_{mr}|i_{sy} \tag{36}$$

Where:	*Var*	*Description*
	t_e	*Electrical torque.*
	P	*The number of poles.*
	L_m	*The magnetizing inductance between stator and rotor.*
	L_r	*Self inductance of the rotor, transformed to stator side parameter. Equal to the rotor leakage plus the magnetizing inductance.*
	$\|i_{mr}\|$	*Rotor magnetizing current.*
	i_{sy}	*Torque producing stator current component.*

The rotor magnetizing current is defined as:

$$|i_{mr}| = i_{sx} + j \cdot i_{sy} + \left(i_{rx} + j \cdot i_{ry}\right) \cdot (1 + \sigma_r) \tag{37}$$

Now the idea is to keep the magnetizing current constant. This is equivalent to keeping the flux level constant in the machine. Under this condition the torque is a linear function of the torque producing current i_{sy}, hence it is easy to make a controller. The rotor magnetizing current can be changed, but then the gain in the designed torque controller has to be compensated to give the same performance. This is the same as scheduling the open loop gain.

5.2.4 Flux model

Now looking at the rotor circuit, the voltage equation for this circuit (eq. (38)) gives a key to calculating both the flux or magnetizing current and the slip, which will be analyzed later.

$$0 = R_r \cdot \left(i_{rx} + j \cdot i_{ry}\right) + L_m \cdot \frac{d|i_{mr}|}{dt} + j \cdot (\omega_{mr} - \omega_r) \cdot L_m \cdot |i_{mr}| \tag{38}$$

Where:	*Var*	*Description*
	R_r	*Rotor resistance matrix.*
	ω_r	*The angular rotor speed.*
	ω_{mr}	*Angular speed of the rotor-flux-oriented reference frame.*

Magnetizing current

From the real part of equation (38) the rotor magnetizing current (or flux) can be calculated as the stator current in the *x*-direction filtered with the rotor time constant. The equation is shown equation (39) [11].

$$T_r \frac{d|i_{mr}|}{dt} + |i_{mr}| = i_{sx} \tag{39}$$

Where:	***Var***	***Description***
	T_r	*Rotor time constant = L_r/R_r.*
	$\|i_{mr}\|$	*Rotor magnetizing current.*
	i_{sx}	*Flux-producing stator current component.*

Sometimes this filter is ignored so $|i_{mr}| = i_{sx}$ is assumed. This is the case later on in the six-phase controller.

Slip relationship

The other equation that can be extracted from the complex part of (39) is the slip relationship [11].

$$\omega_{mr} = \omega_r + \frac{i_{sy}}{T_r |i_{mr}|} \tag{40}$$

With this relationship the necessary angular field speed can be calculated from currents and rotor angular speed. As mentioned in (36) the current i_{sy} is proportional to the torque, therefore the field speed has to be increased to keep the same rotor speed if the load on the motor is increased.

5.2.5 Voltage feed forward

The *VSI* is the most used inverter type, so the current controller has to set a voltage reference for the *VSI*. It is possible to use the output form the current controller for the *x* and *y* axis directly to set a voltage reference, but the two axes are not decoupled from each other. In [11] a feed forward strategy is described, assuming ideal inverter, without any delay. The strategy is to split the applied voltage (see equation (34)) in two terms, one term is the voltage drop across a transient inductance and the stator resistance, and the second term is the rotor voltage. It is

also assumed that $|i_{mr}|$ does not change in time. This gives the equations shown in (41).

$$
\begin{aligned}
u_{sx} &= \hat{u}_{sx} + u_{dx} = L_s' \cdot \frac{di_{sx}}{dt} + R_s i_{sx} - \omega_{mr} \cdot L_s' i_{sy} \\
u_{sy} &= \hat{u}_{sy} + u_{dy} = L_s' \cdot \frac{di_{sy}}{dt} + R_s i_{sy} + \omega_{mr} \cdot L_s' i_{sx} + (L_s - L_s') \cdot \omega_{mr} \cdot |i_{mr}| \\
\hat{u}_{sx} &= L_s' \cdot \frac{di_{sx}}{dt} + R_s i_{sx} \\
\hat{u}_{sy} &= L_s' \cdot \frac{di_{sy}}{dt} + R_s i_{sy} \\
u_{dx} &= -\omega_{mr} \cdot L_s' i_{sy} \\
u_{dy} &= \omega_{mr} \cdot L_s' i_{sx} + (L_s - L_s') \cdot \omega_{mr} \cdot |i_{mr}|
\end{aligned}
\tag{41}
$$

Where:	***Var***	***Description***
	$\hat{u}_{sx}$	*Direct component of stator voltage drop across resistance and leakage.*
	$\hat{u}_{sy}$	*Quadrature component of stator voltage drop across resistance and leakage.*
	u_{dx}	*Direct component of stator decoupling voltage.*
	u_{dy}	*Quadrature component of stator decoupling voltage.*

The voltages u_{dx} and u_{dy} can be calculated and fed forward in advance, before the input to the *VSI*. But it is problematic to calculate $\hat{u}_{sx}$ and $\hat{u}_{sy}$ in advance because they depend on the differentiated value of the current, and a differentiation is normally sensitive to noise. So this is normally ignored.

5.2.6 Current controller

If the feed forward voltage is 100% correct, then the motor seen from the controller is reduced to a simple first order system, and a linear current controller is easy to construct.

$$
\begin{aligned}
\frac{i_{sx}}{\hat{u}_{sx}} &= \frac{1}{L_s' \cdot s + R_s} \\
\frac{i_{sy}}{\hat{u}_{sy}} &= \frac{1}{L_s' \cdot s + R_s}
\end{aligned}
\tag{42}
$$

Where:	***Var***	***Description***
	s	*The differential operator (d/dt).*

5.3 Vector control of a six-phase induction motor

In [1] a six-phase induction motor is controlled using a simplified form of the three phase rotor flux oriented vector control principle described in 5.2. The vector control principle is extended to six phases and the diagram for the controller suggested in [1] is shown in Figure 51.

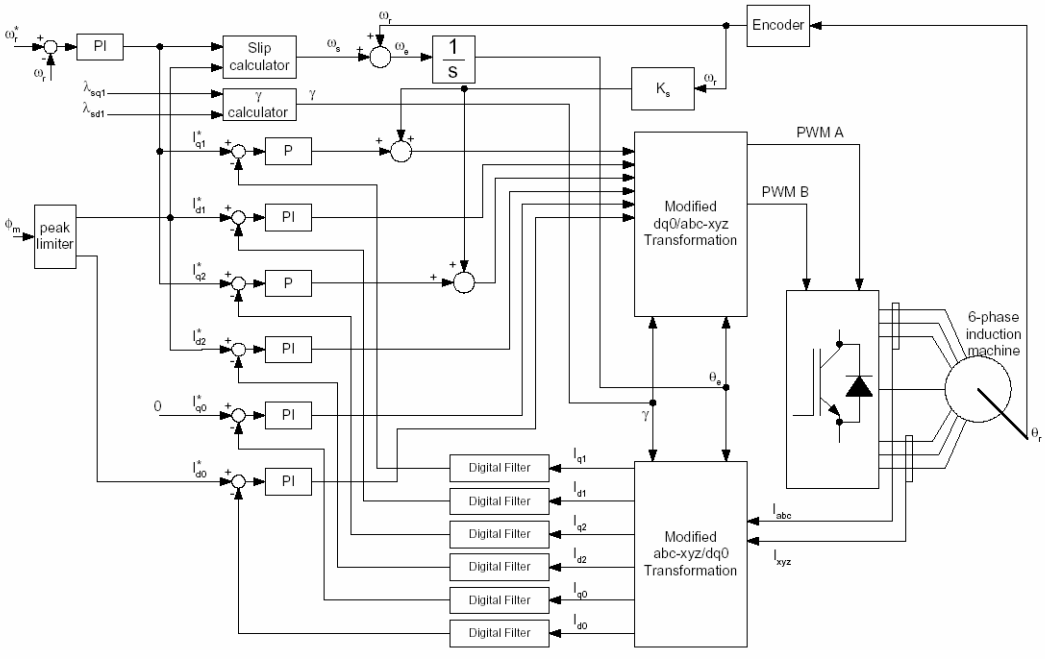

Figure 51 | Control of a six phase motor-drive [1].

In general terms it works like a simplified indirect rotor-flux vector control of a three phase induction motor. The controller consists of an advanced dq-axis transformation (transforming signals from stationary to rotating and vice versa), a slip compensator, six current controllers and a speed controller. The controller is explained and analyzed in more details below.

5.3.1 Six-phase dq-axis transformation

The vector diagram for the rotation of the 1st harmonic components is shown in Figure 52. The two dq-axis systems are shifted 30° just like the *abc*-axis system and the *xyz*-axis systems.

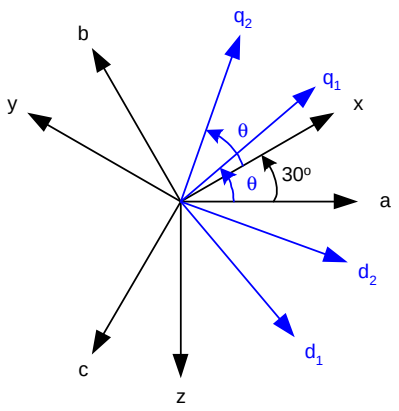

Figure 52	Six-phase vector diagram [1].

In Figure 53 the zero sequence or 3rd harmonic vector rotation diagram is shown. The rotation frequency is three times as fast as the 1st harmonic components, so the *x*, *y* and *z* axis are aligned, the same apply for the *a*, *b* and *c* axis.

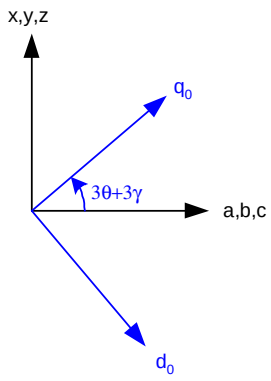

Figure 53	Six-phase vector diagram [1].

The transformation matrix suggested in [1] is shown in equation (43) and (44). The transformation from rotating to stationary coordinates:

$$\begin{bmatrix} f_{q1} \\ f_{d1} \\ f_{q0} \\ f_{q2} \\ f_{d2} \\ f_{d0} \end{bmatrix} = \frac{2}{3} \begin{bmatrix} \cos(\theta) & \cos(\theta-120°) & \cos(\theta+120°) & 0 & 0 & 0 \\ \sin(\theta) & \sin(\theta-120°) & \sin(\theta+120°) & 0 & 0 & 0 \\ \frac{\cos(3(\theta+\gamma))}{2} & \frac{\cos(3(\theta+\gamma))}{2} & \frac{\cos(3(\theta+\gamma))}{2} & \frac{\sin(3(\theta+\gamma))}{2} & \frac{\sin(3(\theta+\gamma))}{2} & \frac{\sin(3(\theta+\gamma))}{2} \\ 0 & 0 & 0 & \cos(\theta-30°) & \cos(\theta-150°) & \cos(\theta+90°) \\ 0 & 0 & 0 & \sin(\theta-30°) & \sin(\theta-150°) & \sin(\theta+90°) \\ \frac{\sin(3(\theta+\gamma))}{2} & \frac{\sin(3(\theta+\gamma))}{2} & \frac{\sin(3(\theta+\gamma))}{2} & -\frac{\cos(3(\theta+\gamma))}{2} & -\frac{\cos(3(\theta+\gamma))}{2} & -\frac{\cos(3(\theta+\gamma))}{2} \end{bmatrix} \begin{bmatrix} f_a \\ f_b \\ f_c \\ f_x \\ f_y \\ f_z \end{bmatrix} \quad (43)$$

Where:	***Var***	***Description***
	θ	*Angular position of the electrical field.*
	γ	*The angle between the 3rd harmonic and the 1st harmonic component (see 5.3.2).*
	$f_{a,b,c}$	*The rotating abc components.*
	$f_{x,y,z}$	*The rotating xyz components.*
	$f_{q1,q2}$	*The stationary q or torque producing components of the 1st harmonic. 1 for abc and 2 for xyz.*
	$f_{d1,d2}$	*The stationary d or flux producing components of the 1st harmonic. 1 for abc and 2 for xyz.*
	f_{q0}	*The stationary q or torque producing components of the 3rd harmonic.*
	f_{d0}	*The stationary d or flux producing components of the 3rd harmonic.*

The transformation from stationary to rotating coordinates is shown in equation (44):

$$\begin{bmatrix} f_a \\ f_b \\ f_c \\ f_x \\ f_y \\ f_z \end{bmatrix} = \begin{bmatrix} \cos(\theta) & \sin(\theta) & \cos(3(\theta+\gamma)) & 0 & 0 & \sin(3(\theta+\gamma)) \\ \cos(\theta-120°) & \sin(\theta-120°) & \cos(3(\theta+\gamma)) & 0 & 0 & \sin(3(\theta+\gamma)) \\ \cos(\theta+120°) & \sin(\theta+120°) & \cos(3(\theta+\gamma)) & 0 & 0 & \sin(3(\theta+\gamma)) \\ 0 & 0 & \sin(3(\theta+\gamma)) & \cos(\theta-30°) & \sin(\theta-30°) & -\cos(3(\theta+\gamma)) \\ 0 & 0 & \sin(3(\theta+\gamma)) & \cos(\theta-150°) & \sin(\theta-150°) & -\cos(3(\theta+\gamma)) \\ 0 & 0 & \sin(3(\theta+\gamma)) & \cos(\theta+90°) & \sin(\theta+90°) & -\cos(3(\theta+\gamma)) \end{bmatrix} \begin{bmatrix} f_{q1} \\ f_{d1} \\ f_{q0} \\ f_{q2} \\ f_{d2} \\ f_{d0} \end{bmatrix} \quad (44)$$

The transformation consists of two dq-axis transformations with 30-degree phase shift for the 1st harmonic and a zero sequence for the 3rd harmonic. In an ordinary three-phase dq-axis transformation the zero sequence does not exist, because the neutral connection of the motor doesn't exist. In a standard three phase motor without star-point connection the number of independent variables is two, because the third current is the sum of the two others. In a six-phase motor there exist six independent variables, one for each phase. Here the sum of the currents in the phases is not necessarily zero, because the current has the possibility to return in the star-

point connection. Therefore the number of independent axis is also six, two dq-axis for the 1st harmonic and one dq-axis for the 3rd harmonic component.

A complete dq-axis model of a six-phase induction motor with 3rd harmonic current injection is described in Appendix C.

5.3.2 3rd harmonic angle

In the transformation there is an angle called γ. This angle describes the angle between the first and the 3rd harmonic component. To align these two components the angle has to be:

$$\gamma = \tan^{-1}\left(\frac{h_q}{h_d}\right) \tag{45}$$

Where:	***Var***	***Description***
	h_d	*The d axis component of h.*
	h_q	*The q axis component of h.*

The variable *h* is a general variable it could be flux, current, voltage or any other describing variable. There are two possibly different dq-axis reference vectors for the 1st harmonic component, but only one 3rd harmonic vector component, so the 3rd harmonic component can only be aligned to one of those vectors (or maybe a linear combination of the two 1st harmonic vector components). If for example the following variables are given:

$$\begin{gathered} amp = h_q = h_d = f_{q1} = f_{q2} = f_{d1} = f_{d2} \Rightarrow \gamma = 45^\circ \\ f_{q0} = 0 \end{gathered} \tag{46}$$

The transformation from stationary to rotating components gives:

$$\begin{bmatrix} f_a \\ f_b \\ f_c \\ f_x \\ f_y \\ f_z \end{bmatrix} = \begin{bmatrix} \cos(\theta) & \sin(\theta) & \cos(3(\theta+45°)) & 0 & 0 & \sin(3(\theta+45°)) \\ \cos(\theta-120°) & \sin(\theta-120°) & \cos(3(\theta+45°)) & 0 & 0 & \sin(3(\theta+45°)) \\ \cos(\theta+120°) & \sin(\theta+120°) & \cos(3(\theta+45°)) & 0 & 0 & \sin(3(\theta+45°)) \\ 0 & 0 & \sin(3(\theta+45°)) & \cos(\theta-30°) & \sin(\theta-30°) & -\cos(3(\theta+45°)) \\ 0 & 0 & \sin(3(\theta+45°)) & \cos(\theta-150°) & \sin(\theta-150°) & -\cos(3(\theta+45°)) \\ 0 & 0 & \sin(3(\theta+45°)) & \cos(\theta+90°) & \sin(\theta+90°) & -\cos(3(\theta+45°)) \end{bmatrix} \begin{bmatrix} amp \\ amp \\ 0 \\ amp \\ amp \\ f_{d0} \end{bmatrix} \tag{47}$$

Reducing to:

$$\begin{bmatrix} f_a \\ f_b \\ f_c \\ f_x \\ f_y \\ f_z \end{bmatrix} = \begin{bmatrix} amp\sqrt{2}\sin(\theta+45°)+ f_{d0}\sin(3(\theta+45°)) \\ amp\sqrt{2}\sin(\theta+45°-120°)+ f_{d0}\sin(3(\theta+45°)) \\ amp\sqrt{2}\sin(\theta+45°+120°)+ f_{d0}\sin(3(\theta+45°)) \\ amp\sqrt{2}\sin(\theta+45°-30°)- f_{d0}\cos(3(\theta+45°)) \\ amp\sqrt{2}\sin(\theta+45°-150°)- f_{d0}\cos(3(\theta+45°)) \\ amp\sqrt{2}\sin(\theta+45°+90°)- f_{d0}\cos(3(\theta+45°)) \end{bmatrix} = \begin{bmatrix} amp\sqrt{2}\sin(\theta+45°)+ f_{d0}\sin(3(\theta+45°)) \\ amp\sqrt{2}\sin(\theta+45°-120°)+ f_{d0}\sin(3(\theta+45°)) \\ amp\sqrt{2}\sin(\theta+45°+120°)+ f_{d0}\sin(3(\theta+45°)) \\ amp\sqrt{2}\sin(\theta+45°-30°)+ f_{d0}\sin(3(\theta+45°)-90°) \\ amp\sqrt{2}\sin(\theta+45°-150°)+ f_{d0}\sin(3(\theta+45°)-90°) \\ amp\sqrt{2}\sin(\theta+45°+90°)+ f_{d0}\sin(3(\theta+45°)-90°) \end{bmatrix} \quad (48)$$

Resulting in:

$$\begin{bmatrix} f_a \\ f_b \\ f_c \\ f_x \\ f_y \\ f_z \end{bmatrix} = \begin{bmatrix} amp\sqrt{2}\sin(\theta+45°)+ f_{d0}\sin(3(\theta+45°)) \\ amp\sqrt{2}\sin(\theta+45°-120°)+ f_{d0}\sin(3(\theta+45°-120°)) \\ amp\sqrt{2}\sin(\theta+45°+120°)+ f_{d0}\sin(3(\theta+45°+120°)) \\ amp\sqrt{2}\sin(\theta+45°-30°)+ f_{d0}\sin(3(\theta+45°-30°)) \\ amp\sqrt{2}\sin(\theta+45°-150°)+ f_{d0}\sin(3(\theta+45°-150°)) \\ amp\sqrt{2}\sin(\theta+45°+90°)+ f_{d0}\sin(3(\theta+45°+90°)) \end{bmatrix} \quad (49)$$

Using this combination of values clearly gives aligned first and 3rd harmonics. The angle γ simply aligns the 3rd harmonic d-axis with the resulting dq-axis vector.

In the case of the six-phase motor the currents are controlled, hence $f_{q0,d0,q1,q2,d1,d2}$ are the current components. If the windings for the two three-phase systems are identical and if the motor performance has to be optimal, the two dq-axis current systems have to be identical. This means that $f_{q1}=f_{q2}$ and $f_{d1}=f_{d2}$. If furthermore a 3rd harmonic stator current is needed then $h_q= f_{q1}= f_{q2}$ and $h_d= f_{d1}= f_{d2}$ which align the 3rd harmonic d-axis current with the 1st harmonic current vector.

5.3.3 Slip relationship

For the controller suggested in [1] it is necessary to measure the speed of the motor. The reason is that the speed of the field injected into the induction motor has to be calculated. The angular field position is also used in the transformation above, and it is the integral of the field speed. The difference between the two speeds is called the slip speed, and it can be calculated from the slip relationship. This relationship can be calculated just like in standard vector control see equation (40).

$$\omega_s = \left(\frac{r_r}{L_m + L_{lr}} \right) \left(\frac{I_q}{I_d} \right) \tag{50}$$

Where:	*Var*	*Description*
	ω_s	*Slip speed.*
	r_r	*Rotor resistance.*
	L_m	*The magnetizing inductance between stator and rotor.*
	L_{lr}	*The leakage inductance in the rotor.*
	i_q	*The 1st harmonic component of q axis current.*
	i_d	*The 1st harmonic component of d axis current.*

In this case $i_q=i_{sq1}=i_{sq2}$ and $i_d=i_{sd1}=i_{sd2}$.

When the slip speed is calculated, the speed of the magnetic field can be calculated using equation (51):

$$\omega_e = \omega_r + \omega_s \tag{51}$$

Where:	*Var*	*Description*
	ω_s	*Slip speed.*
	ω_r	*The angular rotor speed.*
	ω_e	*Applied field speed to the stator windings.*

The speed of the magnetic field ω_e is integrated and the result is the field position θ_e, which is used in the transformation from rotating to stationary coordinates.

5.3.4 Speed controller

A standard PI controller is used for the speed control [8]. The input is the speed error and the output is the q-axis current or torque component of the current. The current loop makes a small delay in the torque response, but this is ignored in the following because the current loop is dimensioned to be much faster than the speed loop. It is assumed that the mechanical system can be described simply by inertia and viscous friction. In practical cases the load torque can depend on the speed in different powers. But this makes the system nonlinear, and then standard control design tools (like root locus plot) do not apply, to use these tools some kind of linearization has to be performed. The speed controller is dimensioned using the following first order open loop transfer function from i_q (torque) to speed:

$$\frac{\omega_r}{i_q} = \frac{\omega_r}{T \cdot k_t} = \frac{1}{k_t \cdot (Js + B)} \tag{52}$$

Where:	*Var*	*Description*
	k_t	*Torque constant going from q-axis current to torque. (In test case 0.28A/Nm)*
	J	*Moment of inertia. (In test case 0.0025kg*m^2 noload and 0.0050kg*m^2 loaded with DC-motor)*
	T	*Shaft torque.*
	B	*Viscous friction. (In test case 3.5*10^{-4}J*s at noload and 3.25*10^{-2}J*s at load)*
	i_q	*The 1st harmonic component of the q-axis current. Torque producing axis.*

The active current i_q is the common current reference for both 1st harmonic active currents. The reference for the 3rd harmonic current i_{q0} is 1/6 of i_q.

Note that in no-load condition only ventilation and rotational losses are included. In the simulations later on the iron loss and stray load loss are also included in the viscous friction. The iron loss and stray load loss are also dependent on the magnetization level, which can be lowered at no-load. Therefore the controller is designed using a worst case situation with a low viscous friction.

It is possible to use a simple constant gain controller, but it has fixed steady state amplification, so it will also have a steady state error on the speed signal. To avoid this, a controller with an integrator has to be used. This improves the system from a type 0 to a type 1 system with no steady state error for a step input in the speed [7]. It is therefore chosen to use a PI controller.

Assumptions and difference between linear control and simulation

- i_q is assumed to be proportional to torque (see 5.2.3 & 5.2.4).

Test case

The motor parameters for the test case are listed in chapter 2 Figure 15. In the six-phase motor case i_q is kept identical for both three phase subsystems. From this transfer function the root locus can be drawn using the matlab function “SISOTOOL”.

The speed controller has to work both with and without load. Therefore both situations are analyzed here. The open loop root locus is used to analyze the stability, by placing the zero and setting the gain of the PI-controller (see Figure 54). The closed loop step response can then be plotted to find the overshoot and rise time [8]. Both types of plot are needed, because even though the open loop root loci

indicate the damping factor and hence the overshoot, it is not valid in this analysis, because the zero is relatively close to the system pole, and this changes the step response [8]. In the load condition (test bench with DC-generator) the inertia is assumed to be doubled and the load torque is modeled entirely by viscous friction. By simple calculations from the desired shaft power 3010W at nominal speed 2908RPM, the viscous friction at load is $3010/(2908*\pi/30)^2=3.25*10^{-2}$J*s. The stability of the designed speed loop is only guaranteed if the load torque is a constant times the speed.

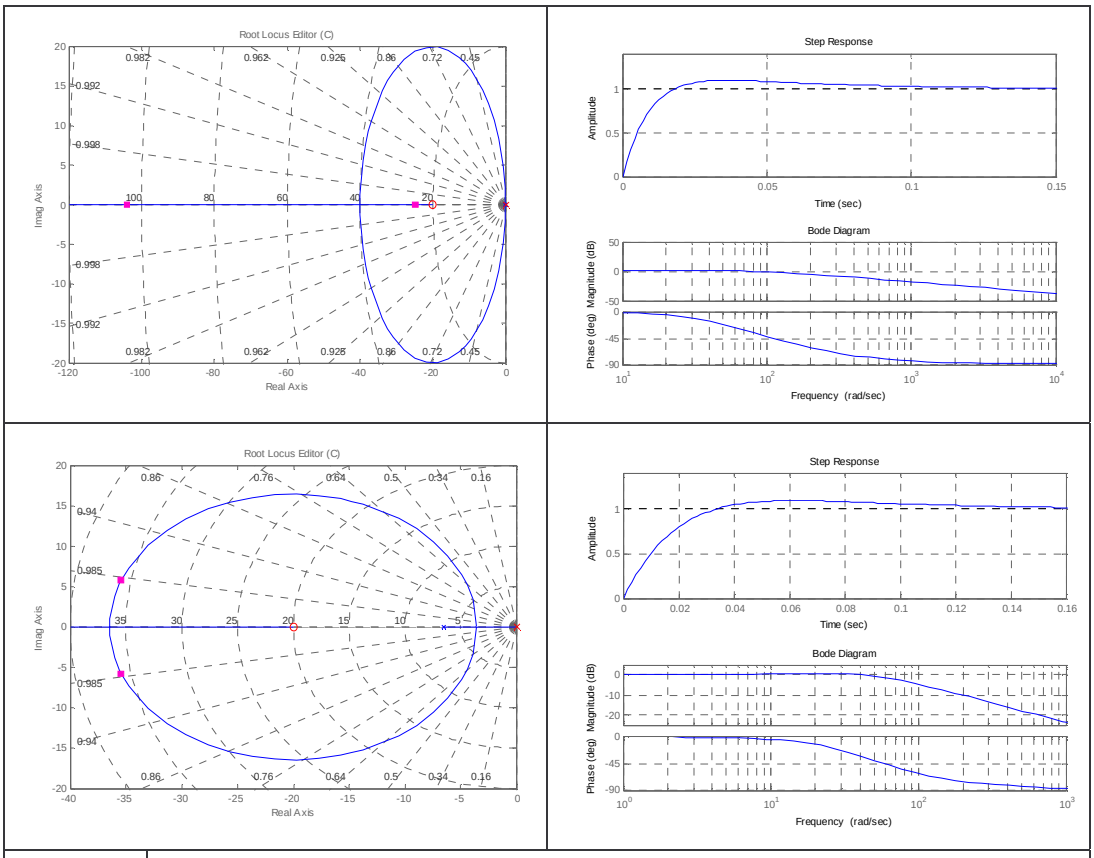

Figure 54 Left top: The root locus plot of the speed control loop in no-load condition. Right top: step response and closed-loop bode-plot of the speed control loop in no-load condition. Left bottom: The root locus plot of the speed control loop in load condition. Right bottom: Step response and closed-loop bode-plot of the speed control loop in load condition. X means open loop pole, O means zero and □ means closed loop pole.

The gain could be increased, but it will not improve the performance considerably, it will only amplify noise. The zero is placed in -20rad/s because the speed loop must

be slower than the current loop and in the same time have an acceptable response time.

The constructed PI-controller is shown on equation (53).

$$\frac{i_{q\_ref}}{\omega_{r\_error}} = \frac{0.09 \cdot s + 1.8}{s} \tag{53}$$

Where:	Var	Description
	ω_{r_error}	*The reference minus the measured angular speed.*
	i_{q_ref}	*Reference current to the inner current loop.*

It is also important to note that the torque in the real world has to be limited. Therefore the rise time for big step changes will probably be increased. To find the real rise time nonlinear time stepping simulations have to be used (see chapter 3 & 6).

5.3.5 Current controllers

The principle for the current controller is the same as for the speed controller, the electrical system can be modeled as six independent first order systems (see equation (54)), assuming that they are decoupled by feeding forward the electromotive voltage (see 5.2.5 & [7]). Therefore PI controllers are also used for the current controllers. So just like in [1] it is chosen to make a feed forward compensation of the voltage drop across the magnetizing inductance in the q-axis [7] & [11]. This means that compared to the feed forward voltages u_{dx} and u_{dy} suggested in equation (41), only the term $(L_s - L_s') \cdot \omega_{mr} \cdot |i_{mr}|$ is compensated, the cross couplings between the axis are not fed forward, therefore the performance is not expected to be as good as for the three phase vector control mentioned in 5.2.

$$\frac{\mathrm{i}}{\mathrm{v} - \mathrm{e}(\omega_r \cdot \mathrm{i}_d)} = \frac{1}{\mathrm{L'_s s} + \mathrm{r_s}} \tag{54}$$

Where:	Var	Description
	L'_s	*Transient stator inductance =* $L_m + L_{sl} - L_m^2 / (L_m + L_{rl})$ *[6]. (In test case 0.3049+0.01814-0.3049^2/(0.3049+ 0.01455)= 0.03199 H)*
	r_s	*Stator resistance in one phase. (In test case 4.719Ω)*
	v	*Stator voltage.*
	$\mathrm{e}(\omega_r \cdot \mathrm{i}_d)$	*Electromotive force. Voltage drop across the magnetizing inductance.*

i	*Stator current.*

Assumptions and difference between linear control and simulation

- Only partly cross coupling compensation between d- and q-axis. The term $(L_s - L_s') \cdot \omega_{mr} \cdot |i_{mr}|$ is fed forward in the voltage (see 5.3.5).

- i_d is assumed to be proportional to flux, no dynamic from rotor (see 5.2.4 equation(39)).

Test case

The controller is dimensioned using root locus like the speed controller (see Figure 55).

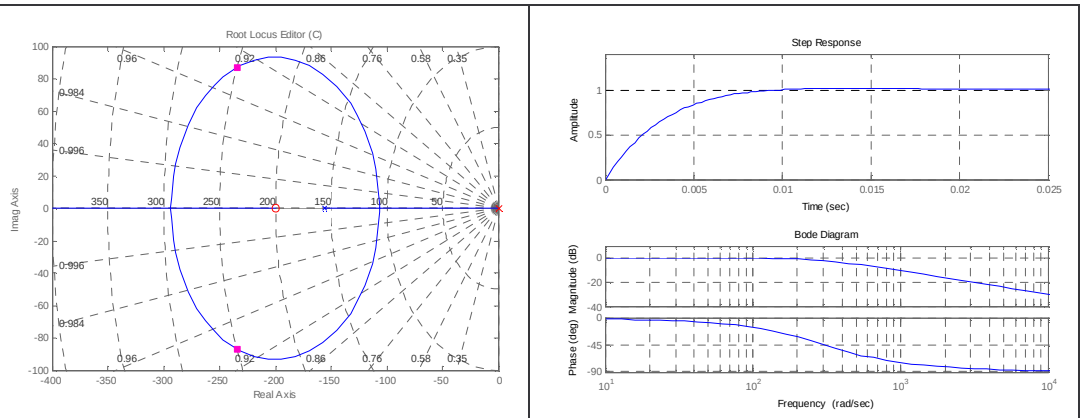

Figure 55	Left: The open loop root locus plot. Right top: Step response of the current control loop and Right bottom: Close-loop bode-plot of the current control loop.

This result in the PI controller shown in equation (55). The controller is identical for the four 1st harmonic current controllers: d1, d2, q1 and q2.

$$\frac{u_{ref}}{i_{error}} = \frac{9.438 \cdot s + 1888}{s} \tag{55}$$

Where:	***Var***	***Description***
	i_{error}	*The reference current subtracted with the measured current.*
	u_{ref}	*Reference voltage to the motor.*

It is important that the inner current loop is faster than the outer speed loop, therefore a factor of 10 is used to place the zero, and hence it is placed in -200rad/s. In this case the current loop response is only made 3-7 times faster, because it was found by test that the gain could not be increased further because of noise problems or maybe because of the cross coupling between the d- and q-axis. The response of the combined control system is shown on Figure 56.

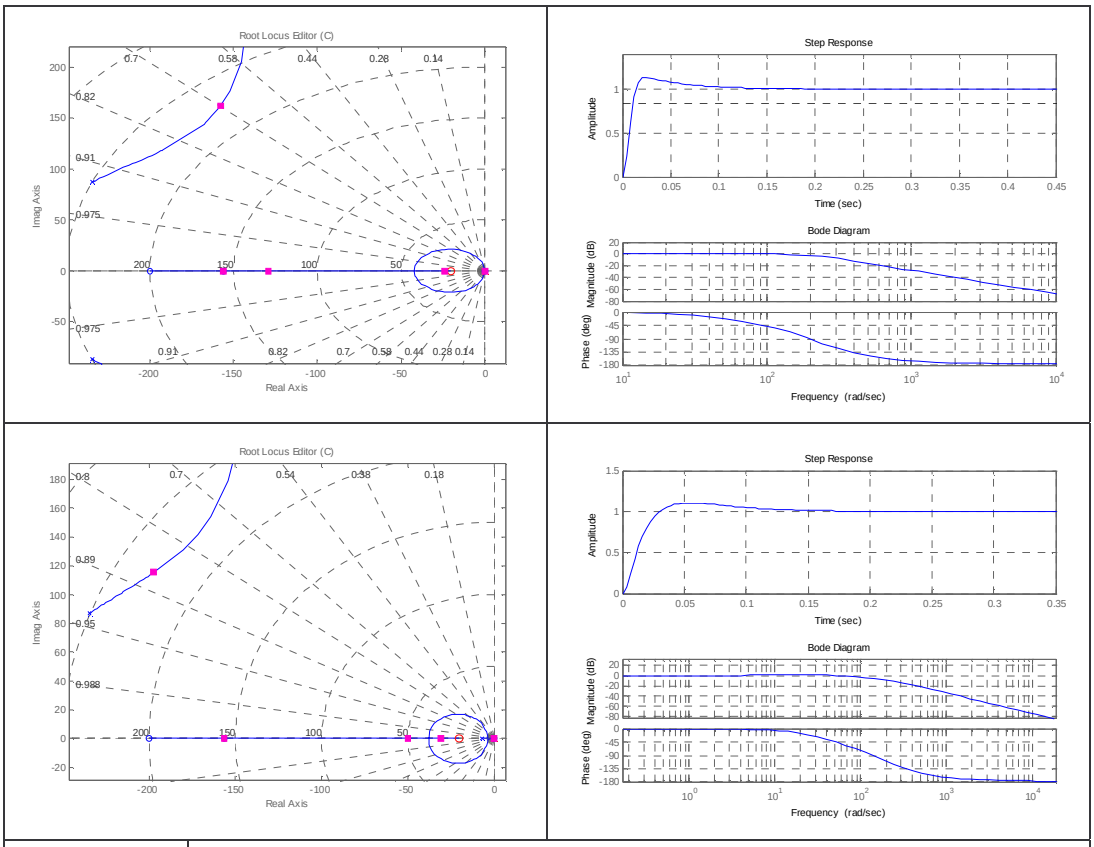

Figure 56 Left top: The root locus plot of the speed control loop in no-load condition including current loop model. Right top: Step response and closed-loop bode-plot of the speed control loop in no-load condition including current loop model. Left bottom: The open loop root locus plot of the speed control loop in load condition including current loop model. Right bottom: Step response and closed-loop bode-plot of the speed control loop in load condition including current loop model. X means open loop pole, O means zero and □ means closed loop pole.

The response of speed loop for the combined system is satisfactory and no further control design of this loop is needed.

A current controller with higher performance like an LQ controller [13] can be made, but the performance of the constructed current controller is good enough to test the performance of the six-phase motor.

5.3.6 3rd harmonic current controllers

The two 3rd harmonic currents id0 and iq0 also have to be controlled. In Appendix C a dq-axis model for the 3rd harmonic component is set up. This model has the same stator resistance as the 1st harmonic, and the transient inductance is also about the same as the 1st harmonic, so the same controller and parameters are chosen for the 3rd harmonic.

$$\frac{i}{v - e(\omega_r \cdot i_d)} = \frac{1}{L'_{s3}\, s + r_s} \tag{56}$$

Where:	*Var*	*Description*
	L'_{s3}	*Transient stator inductance =* $L_{m3} + L_{ls3} - L_{m3}^2 / (L_{m3} + L_{lr3})$ *[6]. (In test case* $0.06420+0.01814-0.06420^2/(0.06420+0.02629)=0.03679H$*)*
	r_s	*Stator resistance in one phase. (In test case 4.719Ω)*
	v	*Stator voltage.*
	$e(\omega_r \cdot i_d)$	*Electromotive force. Voltage drop across the magnetizing inductance.*
	i	*Stator current.*

Assumptions and difference between linear control and simulation

- The cross coupling is again not taken into consideration, so the performance is expected to deviate a little from the calculated.

Test case

In the test case the linear root locus and bode-plot looks like presented in Figure 57.

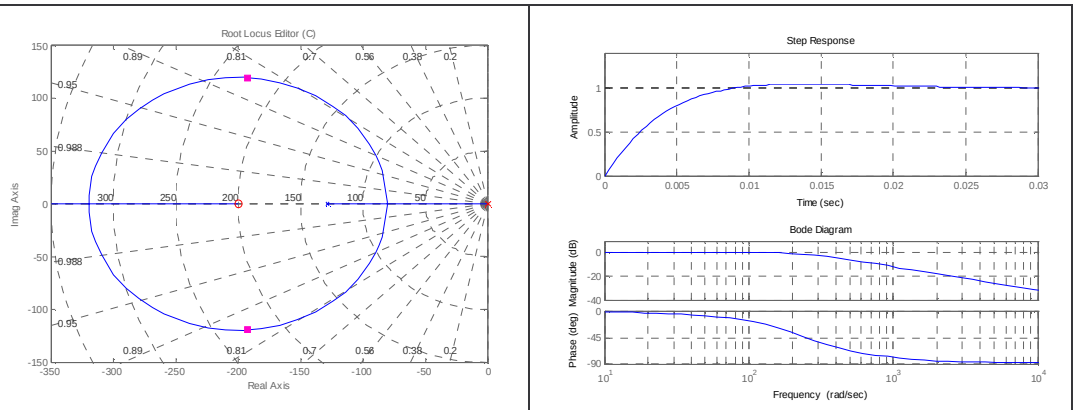

Figure 57	Left the open loop root locus plot, and right top step response and bottom close-loop bode-plot of the current control loop for the 3rd harmonic current.

5.4 Connection of the neutral-point of the motor

In a normal three-phase motor drive the neutral point of the motor is floating. This has the effect that the sum of the currents is always zero. The neutral-point voltage doesn't have to be fixed. This gives an extra control option, because the phase voltage is the voltage from the inverter leg minus the neutral-point voltage. So if the same voltage is added to both the inverter leg voltage and the neutral-point voltage, the phase voltage isn't changed. This fact is used in modern motor drives to improve the drive performance by decrease the necessary *VA-rating* or increase efficiency by injecting i.e. trapezoidal or 3rd harmonic voltage to all phases or by discontinuous modulation strategies [14], [15] & [16].

5.4.1 Problem with neutral connection due to 3rd harmonic current

To inject a 3rd harmonic current into a six-phase motor, the 3rd harmonic current need a return path, because the sum of the six currents is no longer zero, it is a 3rd harmonic current. A simple way of realizing this is to focus on the 3rd harmonic part of the motor which has two phases (one for each three-phase group). This two-phase motor need two wires, one for each phase and a return path to make a circulating magnetic field. This can also be expressed in equations. Using the transformation suggested in [1]. The six phase currents have to look like this:

$$\begin{bmatrix} i_a \\ i_b \\ i_c \\ i_x \\ i_y \\ i_z \end{bmatrix} = \begin{bmatrix} \cos(\theta) & \sin(\theta) & \cos(3(\theta+\gamma)) & 0 & 0 & \sin(3(\theta+\gamma)) \\ \cos(\theta-120°) & \sin(\theta-120°) & \cos(3(\theta+\gamma)) & 0 & 0 & \sin(3(\theta+\gamma)) \\ \cos(\theta+120°) & \sin(\theta+120°) & \cos(3(\theta+\gamma)) & 0 & 0 & \sin(3(\theta+\gamma)) \\ 0 & 0 & \sin(3(\theta+\gamma)) & \cos(\theta-30°) & \sin(\theta-30°) & -\cos(3(\theta+\gamma)) \\ 0 & 0 & \sin(3(\theta+\gamma)) & \cos(\theta-150°) & \sin(\theta-150°) & -\cos(3(\theta+\gamma)) \\ 0 & 0 & \sin(3(\theta+\gamma)) & \cos(\theta+90°) & \sin(\theta+90°) & -\cos(3(\theta+\gamma)) \end{bmatrix} \begin{bmatrix} i_{q1} \\ i_{d1} \\ i_{q0} \\ i_{q2} \\ i_{d2} \\ i_{d0} \end{bmatrix}$$

The sum of the motor currents (on the left side of the equal sign) is:

$$i_0(t) = \sum_{n=\{a,b,c,x,y,z\}} i_n = 3 \cdot \left(i_{q0} \cdot (\cos(3 \cdot (\theta+\gamma)) + \sin(3 \cdot (\theta+\gamma))) + i_{d0} \cdot (\sin(3 \cdot (\theta+\gamma)) - \cos(3 \cdot (\theta+\gamma))) \right)$$

$$\Updownarrow \qquad (57)$$

$$i_0(t) = 3 \cdot \sqrt{2} \cdot \left[i_{q0} \cdot \sin(3 \cdot \theta(t) + 3 \cdot \gamma + 45°) + i_{d0} \cdot \sin(3 \cdot \theta(t) + 3 \cdot \gamma - 45°) \right]$$

Where:	***Var***	***Description***
	i_{q0}	*3rd harmonic stator current in the q-axis.*
	i_{d0}	*3rd harmonic stator current in the d-axis.*
	i_0	*Current returning from the star-point of the motor.*
	γ	*The angle between the 3rd harmonic and the 1st harmonic component (see 5.3.2).*
	$\theta(t)$	*Position of the current vector as a function of time.*

$\theta(t)$ is the angular position of the electrical field as a function of time. i_0 is only zero if the amplitudes of the 3rd harmonics are zero. Or in other words it is not possible to inject a 3rd harmonic current without having a return path. The ideal amplitude of the zero current in the return path can now be calculated. The 3rd harmonic amplitude has to be 1/6 of the 1st harmonic (see chapter 2) and from equation (57) it is obvious that the amplitude of the return path current (sum of all six currents) is $3 \cdot \sqrt{2}$ times higher. All in all 0.71 times the 1st harmonic current.

5.4.2 State of the art in control of the neutral connection

If the neutral-point is connected directly to the *mid-point* of a split capacitor in the *DC-link*, the voltage across the two capacitors varies due to the 3rd harmonic current especially at low input frequencies. Another problem with the neutral connection to a split capacitor is that the midpoint potential can drift towards either U_{dc} or 0 voltage. This is caused partly by asymmetry and non linearity in the inverter (i.e. dead time). But also as explained later, drift in the natural integration from current to voltage in the capacitors. There are two obvious ways to control the voltage across the capacitors.

One way could be to have an extra inverter leg, and an inductance as filter as shown in Figure 57a. This is what is done in [1]. The disadvantage by the extra leg is that it cost extra money and two standard three-phase modules are not enough. Two extra transistors with diodes and gate-drivers and an inductor, are needed (Figure 57a). So even though it stabilizes the voltage completely and effectively, it would by a great advantage if the neutral connection can be stabilized without any extra components and cost.

The alternative solution is to skip the seventh branch and the inductor and control the midpoint voltage directly by the six existing branches (see Figure 57b). This has the disadvantage, compared to a seventh inverter leg that the *DC-link* capacitors are loaded with the 3rd harmonic current, which may reduce the lifetime of the capacitors. It also gives some limitations in the amplitude of the 3rd harmonic current at very low speed, because the voltage ripple on u_m may become high, limiting the applicable voltage to the motor. On the other hand the necessary voltage applied to the motor at low speed is also decreased because of the reduction in the induced voltage. It is also important to note that u_m is dictated by the zero sequence current, so if i_0 has even a very small DC value, u_m will drift towards either u_{dc} or zero. So u_m has to be measured and controlled carefully.

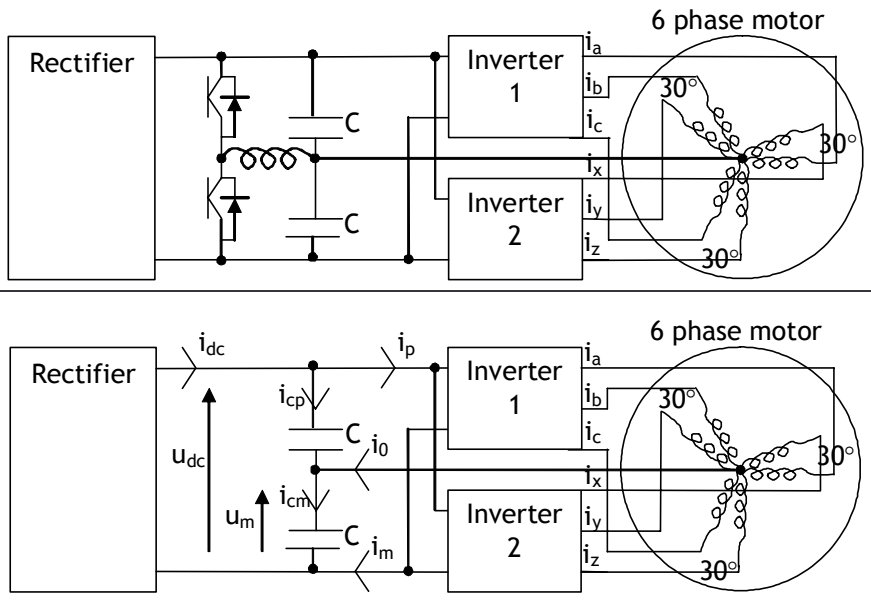

Figure 58 Control of a six-phase motor. (a) Two inverters with three phases and an extra branch used for voltage stabilization. (b) Two inverters with three phases. The six motor supply phases are here also used to stabilizing the voltage.

5.4.3 Analysis of voltage across *DC-link* split capacitors

Considering the electric circuit in Figure 58 b it can be seen that the midpoint potential u_m depends on the current in the return path i_0. From the circuit in Figure 57b, equation (58) can be set up:

$$u_m(t) = \frac{1}{2C}\int i_0(t)dt + \frac{u_{dc}(t)}{2} + U_0 \tag{58}$$

Where:	***Var***	***Description***
	u_m	*Potential across lower capacitor.*
	C	*Size of capacitors.*
	i_0	*Current returning from the star-point of the motor.*
	u_{dc}	*Potential in dc-link.*
	U_0	*Voltage in the lower capacitor at the time zero.*

The current i_0 is already known both from the given reference value (see equation (43)) and from current measurements, but the needed integration involves problems. U_0 is just the voltage across the capacitor in the start condition, so this is set to zero in the following. The directly integrated voltage can be calculated to:

$$u_{mi\,ref}(t) = \frac{3}{\sqrt{2}\cdot C}\int \left(i_{q0}(t)\cdot\sin(3\cdot\theta(t)+3\cdot\gamma+45°)+i_{d0}(t)\cdot\sin(3\cdot\theta(t)+3\cdot\gamma-45°)\right)dt + \frac{u_{dc}(t)}{2} \tag{59}$$

Where:	***Var***	***Description***
	$u_{mi\ ref}$	*Directly integrated potential across lower capacitor.*
	γ	*The angle between the 3rd harmonic and the 1st harmonic component (see 5.3.2).*
	i_{q0}	*3rd harmonic stator current in the q-axis.*
	i_{d0}	*3rd harmonic stator current in the d-axis.*
	$\theta(t)$	*Position of the current vector as a function of time.*

If the currents i_{d0} and i_{q0} are constant in time, the mean value of the integral is zero, hence $u_{mi\ ref}$ is ½u_{dc}, and this is the optimal value. But if the currents are changed dynamically, the capacitor voltage tends to drift out of control, dependent on when the currents are changed. This is very easy to realize, if i.e. i_{q0}=0, $\theta(t) = \omega_e \cdot t$, γ=0 and i_{d0} is 1 if the sign of $\sin(3\cdot\theta(t)+3\cdot\gamma-45°)$ is positive, and zero otherwise (see Figure 59). Then the integral will grow every positive half period and not decrease in the negative. The result would be that $u_{mi\ ref} = u_{dc}$, and the inverter will have no

possibility to give positive voltage, so it will have to stop. This is illustrated on the red curve in Figure 60.

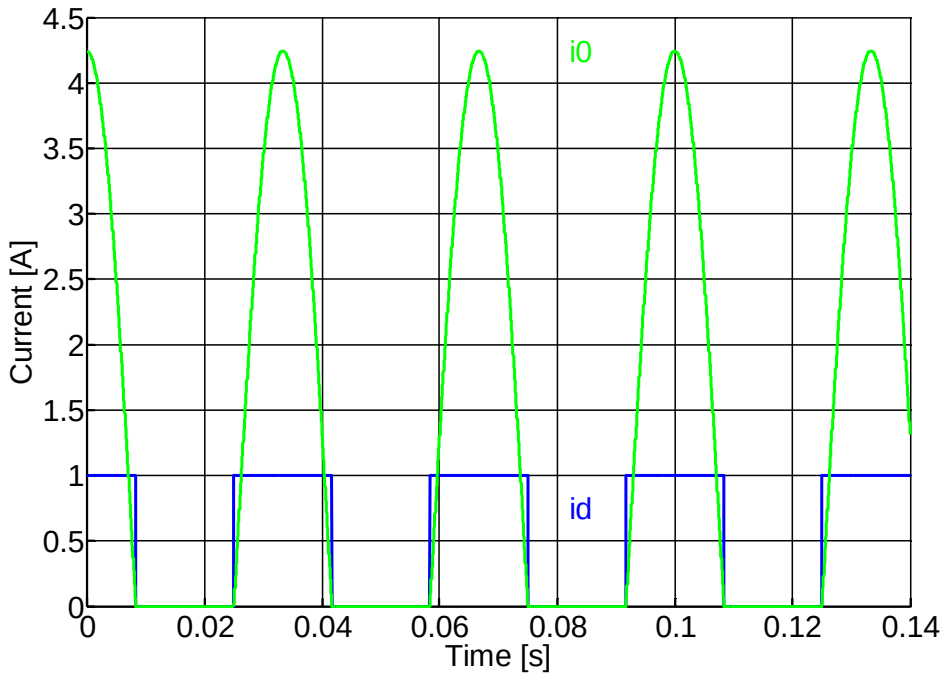

Figure 59	Illustration of return current i_0 under dynamically changing 3rd harmonic current i_d.

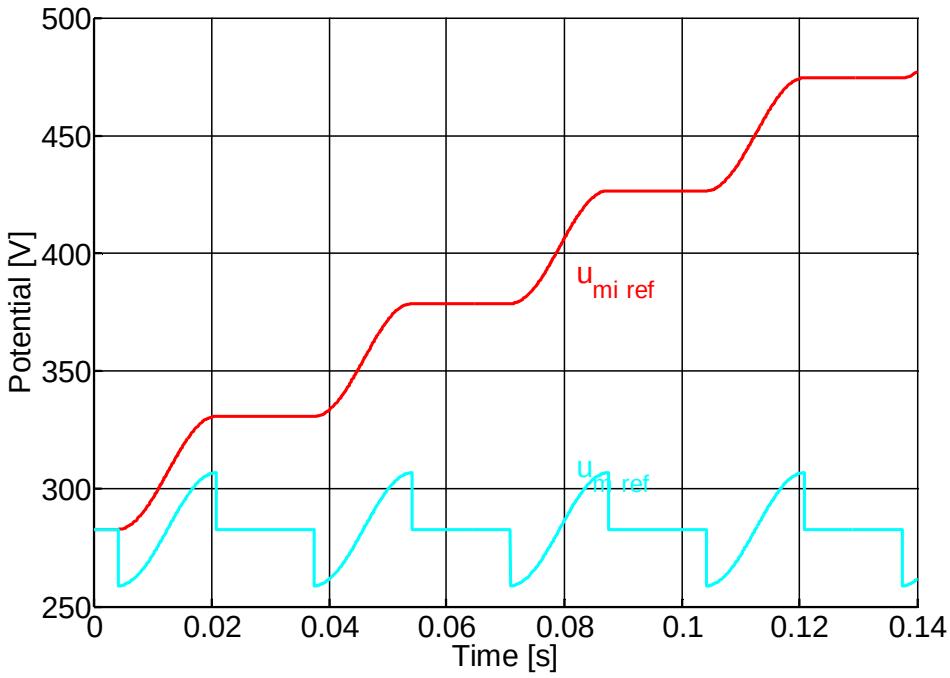

Figure 60	Resulting midpoint voltage under dynamically changing 3rd harmonic current. Using integration to find reference voltage $u_{mi\ ref}$, red curve. Using new solution where the reference voltage is found without integration $u_{m\ ref}$, cyan curve.

5.4.4 New solution

A new strategy is proposed where the integration is done analytically, which is possible since the integration is already calculated as an internal command in the controller. If it is assumed that the currents are constant in time, the integration can be solved. Using that $\theta(t) = \omega_e \cdot t$. (see equation (60)).

$$u_{m\,ref}(t) = \frac{-1}{\sqrt{2} \cdot C \cdot \omega_e(t)} \left(i_{q0}(t) \cdot \cos\left(3 \cdot \theta(t) + 3 \cdot \gamma + 45°\right) + i_{d0}(t) \cdot \cos\left(3 \cdot \theta(t) + 3 \cdot \gamma - 45°\right) \right) + \frac{u_{dc\,meas}}{2} \qquad (60)$$

Here $u_{m\ ref}$ does not drift, and the mean value is as close to ½$u_{dc\ meas}$ as possible. Now this predicted voltage $u_{m\ ref}$ can be used as a reference for the measured midpoint voltage $u_{m\ meas}$. The error signal is used in a controller and added to the reference voltages for all the six motor phases. In ideal steady state conditions the error signal

to the controller is zero, even though the midpoint voltage is oscillating depending on the 3rd harmonic current. The final control loop is shown in Figure 61.

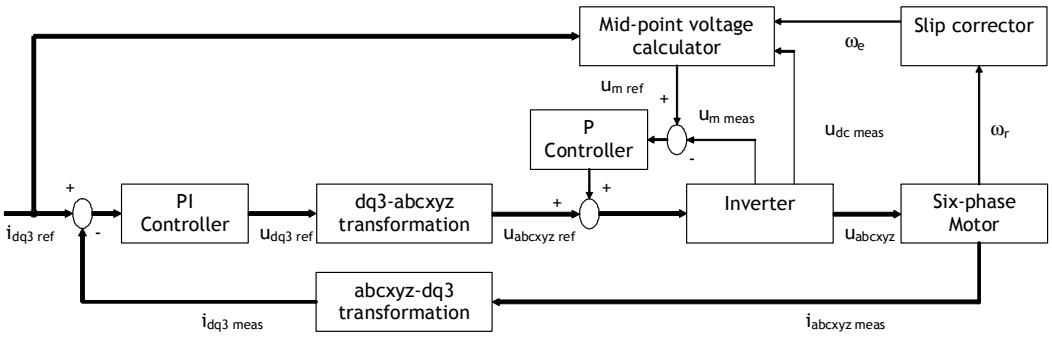

Figure 61 Diagram of the proposed control system for midpoint potential.

5.4.5 Dimensioning of the midpoint controller

A simplified diagram for the six-phase motor is shown in the left part of Figure 62. It is assumed that the motor is linear in behavior, which is a good approximation if the inductance is not saturated. Therefore superposition can be used. This gives the equivalent small signal diagram shown in the right part of Figure 62 [17].

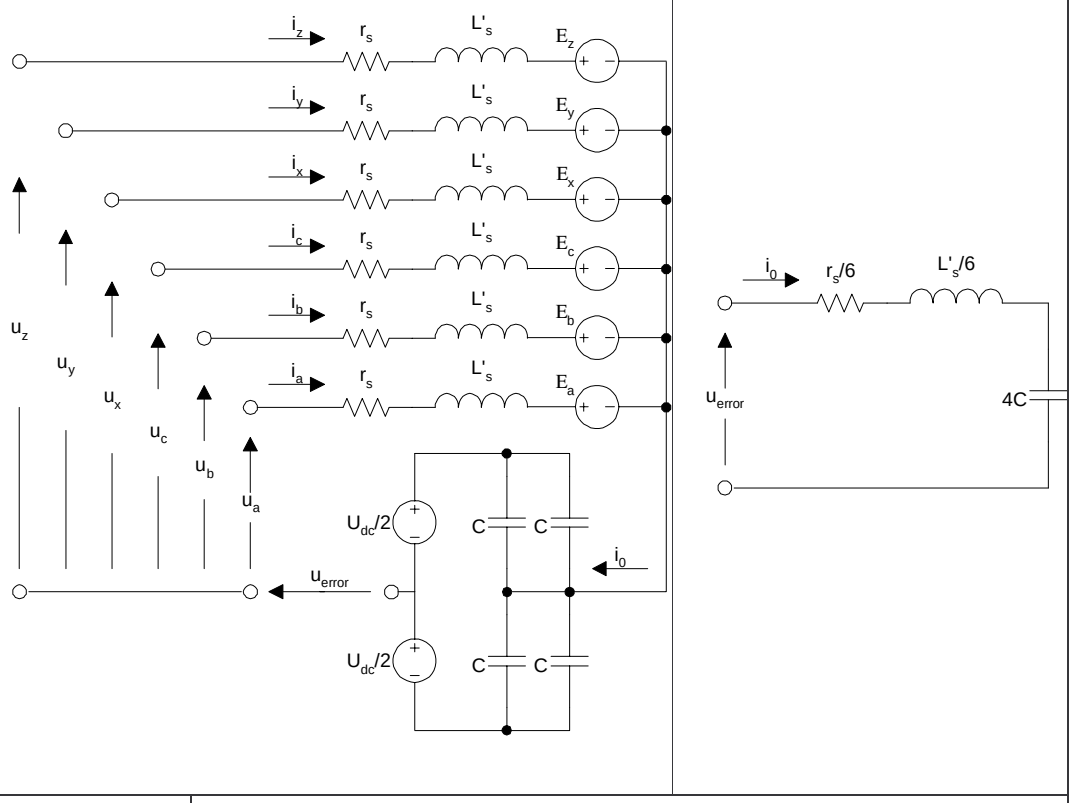

Figure 62	Left: Diagram of the six-phase motor with star-point connection. Right: Equivalent diagram of the motor seen from the midpoint controller.

The reason for having four capacitors is that two three-phase inverters are connected (see Appendix A). The control diagram for the midpoint controller is shown in Figure 63.

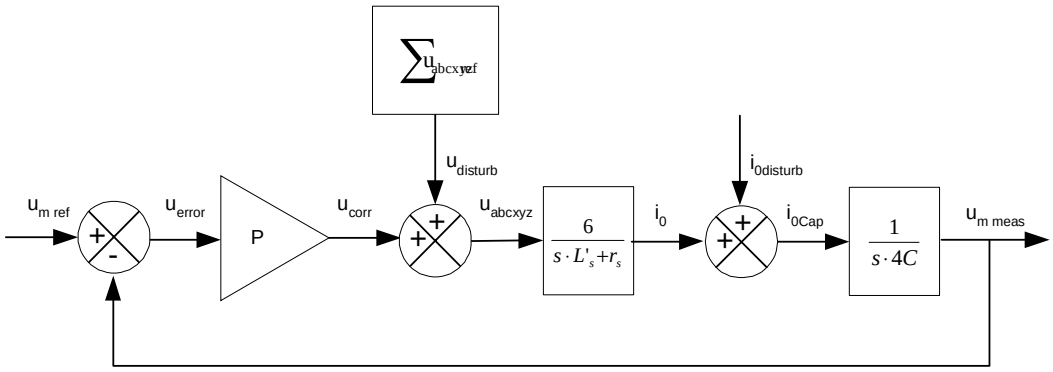

Figure 63 Equivalent control diagram for midpoint controller.

It is important to note that the number of independent inputs to the motor is the six currents (the zero current is not independent because it is the sum of the six currents), but seven conditions (the six currents and the midpoint voltage) have to be controlled. So not all the controllers can have integral action, and small steady state errors have to be accepted. For the midpoint controller it is therefore chosen to use a simple P-controller, which allows a small steady state error, but in simulation and practice it works well together with the six current controllers.

The transfer functions from different inputs to the midpoint voltage are shown in the table below. Note that the two first transfer functions are simple second order systems without zeros, where the damping and natural frequency are defined [8].

Transfer function	Damping	Natural frequency	Steady state gain
$\frac{u_{m\ \ meas}}{u_{m\ \ ref}} = \frac{\frac{3 \cdot P}{2 \cdot C \cdot L'_s}}{s^2 + \frac{r_s}{L'_s} s + \frac{3 \cdot P}{2 \cdot C \cdot L'_s}}$	$\zeta = r_s \sqrt{\frac{C}{6 \cdot P \cdot L'_s}} = \frac{0,21}{\sqrt{P}}$	$\omega_n = \sqrt{\frac{3 \cdot P}{2 \cdot C \cdot L'_s}} = 299\sqrt{P}$	$s=0 \Rightarrow \frac{u_{m\ meas}}{u_{m\ ref}} = 1$
$\frac{u_{m\ \ meas}}{u_{disturb}} = \frac{\frac{3}{2 \cdot C \cdot L'_s}}{s^2 + \frac{r_s}{L'_s} s + \frac{3 \cdot P}{2 \cdot C \cdot L'_s}}$	$\zeta = r_s \sqrt{\frac{C}{6 \cdot P \cdot L'_s}} = \frac{0,21}{\sqrt{P}}$	$\omega_n = \sqrt{\frac{3 \cdot P}{2 \cdot C \cdot L'_s}} = 299\sqrt{P}$	$s=0 \Rightarrow \frac{u_{m\ meas}}{u_{disturb}} = \frac{1}{P}$
$\frac{u_{m\ \ meas}}{i_{0disturb}} = \frac{\frac{s}{4 \cdot C} + \frac{r_s}{4 \cdot C \cdot L'_s}}{s^2 + \frac{r_s}{L'_s} s + \frac{3 \cdot P}{2 \cdot C \cdot L'_s}}$			$s=0 \Rightarrow \frac{u_{m\ meas}}{i_{0disturb}} = \frac{r_s}{6P}$

Assumptions and difference between linear control and simulation

- Linear model only valid for small signals, limitation of the voltage and currents are not in the linear control.
- The linear motor model is equivalent to a first order system (see Figure 62).

- The current controller is not assumed to have an influence on the linear *mid-point* control design, but it is taken into consideration in the simulation.

- Iron loss in the motor is neglected. It usually dampens oscillations in the system like a resistor.

Test case

In the test case P is selected to be 2, which gives a steady state gain for a common mode disturbance in the motor voltages of 0.5, and a steady state gain for a disturbance in the zero current of 0.4. The damping of the reference and disturbance voltage is only about 0.15, but together with the current control loop, the complete system is simulated and tested to give a very good performance (see 6.4). The bandwidth for the reference voltage is about 100Hz and the natural frequency is 67Hz. The natural frequency seems to be close to the supply voltage frequency, which is about 50Hz at nominal speed and power, but in measurements the system is stable, a reason could be that the iron loss dampens the system and that the current loop controllers also influence the circuit (see 6.4). Step responses and bode-plot for the three transfer functions are shown in Figure 64.

The unit step response for a current disturbance is compared with a simulation done with the *MWI* model. The simulation diagram is shown in Figure 65. In the simulation the mechanical system is removed and the machine is set to run at a fixed speed i.e. 2904RPM. Since the *MWI* model is non-linear (stator to rotor coupling depends on position), it is also a function of the input speed. This gives the main difference between the linear function and the *MWI* model, but the difference is so small that the simplified model (Figure 62) is acceptable for control purpose. As mentioned the control design might seem to be very oscillatory, but together with the current controllers (that also influence/damp the *mid-point* current) the control design is well suited (see 6.4).

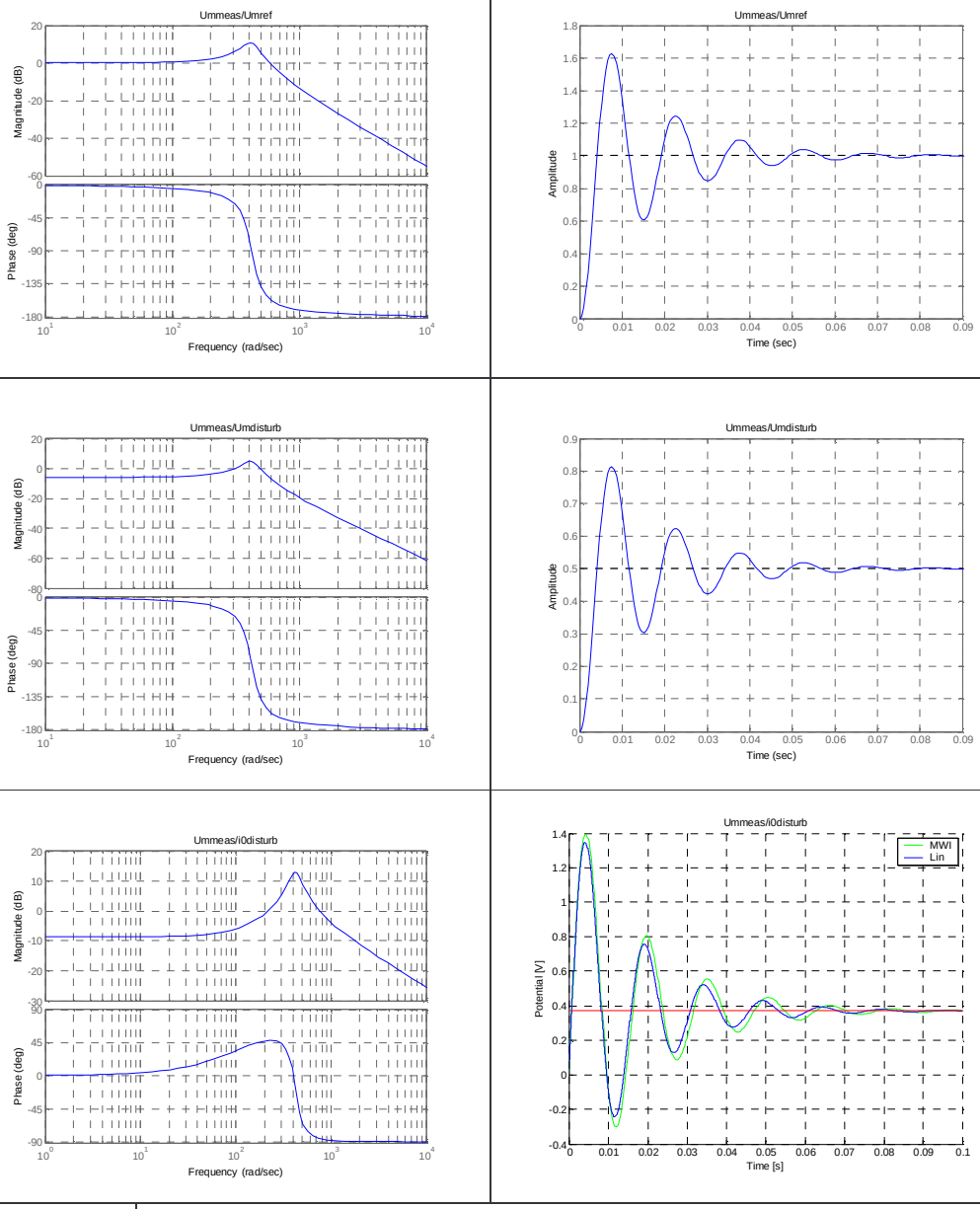

Figure 64	Left side bode-plots, and right side step responses for midpoint controller. Transfer function from voltage reference, voltage disturbance and current disturbance to midpoint voltage.

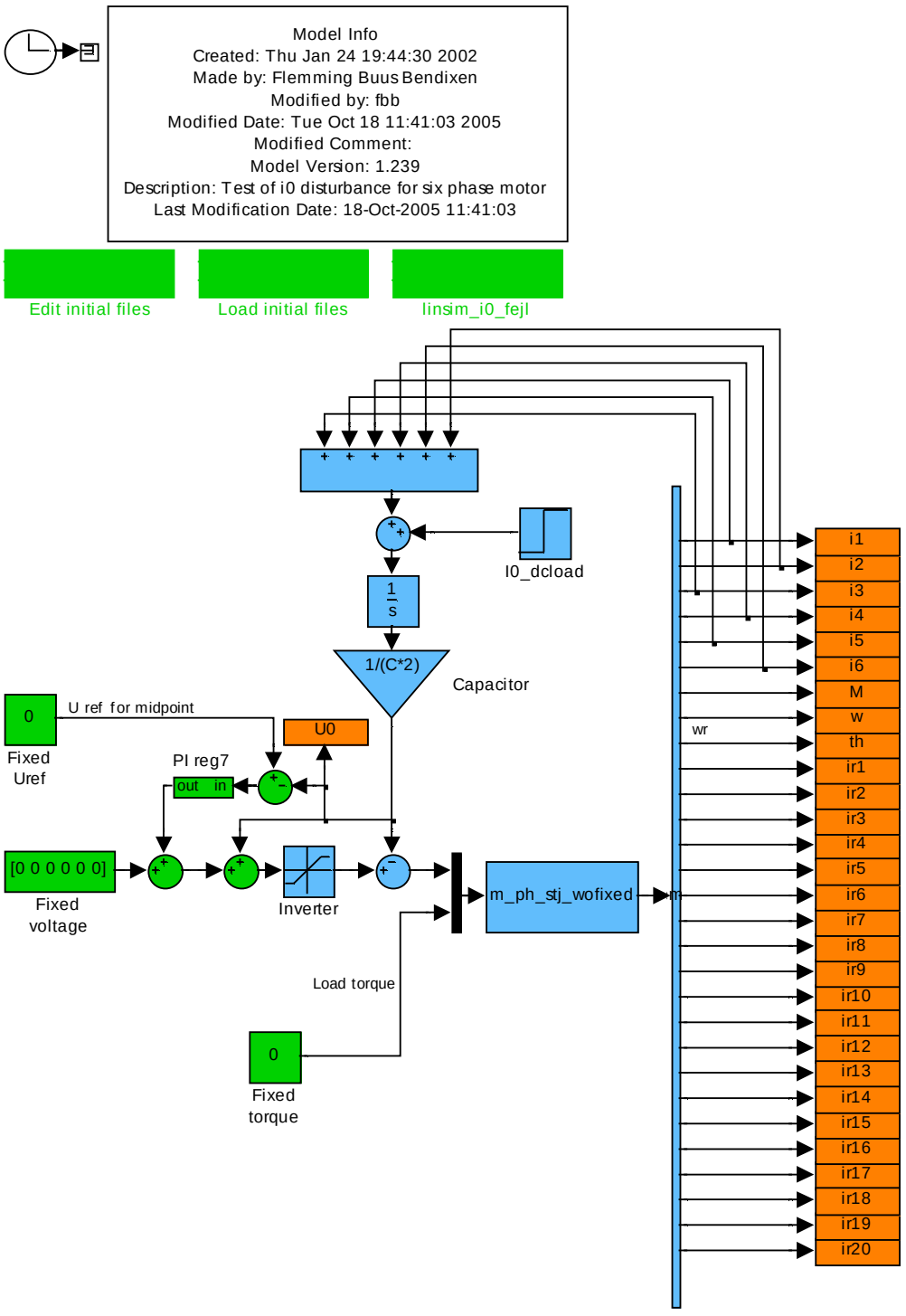

Figure 65 Simulation diagram to test *mid-point* controller.

5.4.6 Capacitor size

A problem with this new controller is that it depends on the size of the capacitor. This means that if the right value is not selected the error signal for the controller (u_{error}) will have a 3rd harmonic ripple, hence the correction voltage (u_{corr}) will have a ripple. But this problem is negligible. The reason is that the current controllers (especially for the 3rd harmonic currents) are designed to minimize this kind of error. The current controllers are more "powerful" than the midpoint controller.

The minimum size of the capacitors is calculated in equation (61). In the last equal sign it is assumed that the 3rd harmonic current is 1/6 of the 1st harmonic current (see chapter 2).

$$C_{\min} = \frac{I_{3\max}}{\sqrt{2} \cdot U_{rip} \cdot \omega_e} = \frac{I_{1\max}}{2 \cdot U_{rip} \cdot \omega_e} \tag{61}$$

Where:	*Var*	*Description*
	C_{min}	*Minimum capacitor size.*
	I_{3max}	*Maximum amplitude of the 3rd harmonic stator current.*
	I_{1max}	*Maximum amplitude of the 1st harmonic stator current.*
	U_{rip}	*Acceptable voltage ripples at the applied field speed.*
	ω_e	*Applied field speed to the stator windings.*

The maximum current in an induction motor is usually independent of the field speed, because it is mainly limited by temperature rise in the windings. The acceptable voltage ripple is settled by the *VA-rating* of the inverter. The needed voltage (to give maximum current) is nearly proportional to the field speed, because the backward electromotive force induced by the induction motor is proportional to the field speed. This gives in effect that the acceptable voltage ripple, to prevent the inverter to go into voltage limit, is inversely proportional to the field speed. So high field speed means low tolerance to voltage ripples and vice versa, but since the two factors are inverse proportional the capacitor size is not affected. Therefore the capacitor size might as well be found at maximum field speed, maximum current and from the maximum acceptable loss in voltage rating due to voltage ripple.

5.4.7 Asymmetric capacitor size

The two *DC-link* capacitors are not necessarily identical. If they are not, and the *DC-link* voltage has to be split equally between the two capacitors (u_m=u_{dc}/2), the *DC-link* voltage will begin to have an influence on the zero current. Equation (62) describes this dependency.

$$i_0(t) = \frac{C_m - C_p}{2} \frac{du_{dc}(t)}{dt} \tag{62}$$

Where:	***Var***	***Description***
	C_m	*Lower capacitor in Figure 58b.*
	C_p	*Upper capacitor in Figure 58b.*

There are two ways out of this problem. One is to calibrate so:

$$u_m(t) = \frac{C_p}{C_m + C_p} u_{dc}(t) \tag{63}$$

This means that the *VA-rating* has to be increased to give the necessary voltage in both positive and negative direction. The other is to let the *mid-point* controller deliver the alternating current calculated in (62), which depend in the ripple in the *DC-link*. This means that the motor windings has to carry a higher current, hence a lower efficiency of the motor.

5.5 Conclusion

In this chapter the control strategy of the six-phase motor with 3rd harmonic current injection is discussed and analyzed. The strategy builds on a strategy suggested in [1]. The elements in the controller is a transformation from the six axis (six phases) to three dq-axis, traditional slip relationship calculation, dimensioning of a speed and a current controller and finally a suggestion for a new controller that require fewer inverter components.

The traditional dq-axis transformation known from three phase motors is expanded to six phases. This gives four independent axes, and the 3rd harmonic current injected in the six phases also gives two more independent signals to control. The transformed signals have DC value under steady state conditions this helps the control design considerably. The other important element to ease the control design process is to make the motor linear seen from the controllers point of view. This is done using rotor field oriented vector control with simplified feed forward without cross coupling. Six PI controllers are now dimensioned using root-locus plots and step response. The same tools are used to design the speed controller.

The suggested new midpoint controller saves an inverter branch and an inductor, using a little extra computer power instead. A drawback could be a slightly reduced lifetime of the *DC-link* capacitors. And the two *DC-link* capacitors have to be nearly

identical to avoid an increase in the *VA-rating* of the inverter or a lower efficiency of the motor.

In this chapter the theory was set up. In the next chapter simulations and test of a 3kW six-phase motor is made combining the motor model described in chapter 3 and the control strategy described in this chapter.

6. Verification of control strategies

6.1 Introduction

First in this chapter three test cases are described. The cases use the theoretical motor model described in 3 and the control strategy described in chapter 5. In other words the developed tools are used in three simulation and test cases to verify the control strategy. The three cases test the speed loop, the current loops and the midpoint control loop. Simulations and measurements are compared in all the cases.

After this, failure redundancy is tested in a case where one converter is disabled. It is proven that the motor is able to continue running on only three phases. Other cases exist, i.e. one phase failure, half branch failure etc., but they are not examined here.

Finally it is proven that the 3rd harmonic current is able to produce torque even if the 1st harmonic current component is zero. It is shown that in this case the six-phase motor act much like a two phase (six-pole) motor with a return wire.

6.1.1 Assumptions and difference between simulation and test

In the simulation the following assumptions are used.

- Motor parameters are assumed to be known and constant.
- No magnetic saturation, mean value of inductances is used.
- Iron loss, ventilation, bearing loss and stray load losses are included in a common viscous friction load subtracted from the air-gap torque. In this case 145W @ 2908RPM. The viscous friction torque is assumed to be linear dependent on speed.
- No temperature dependent parameters. The simulations assume warm wires, which gives the highest resistance. In this case 4.44Ω.

- The motor is modeled using the *MWI* model described in chapter 3.
- In all tests and simulations the six-phase motor has 1/6 3rd harmonic injected, except if anything else is mentioned.

The simulation software is described in Appendix B and the test system is described in Appendix A.

6.2 Speed step

6.2.1 Assumptions and difference between simulation and test

- The load machine loads the motor with extra inertia ($4.8 \cdot 10^{-3} kg \cdot m^2$ according to data sheet)
- The load machine gives no extra viscous friction (at least very little compared to the viscous friction of the motor 145W at 2908RPM). The ventilation of the load machine is forced by a small motor with a fan.
- The mechanical coupling gives no extra inertia.
- The magnetization current is set to 2.5A.

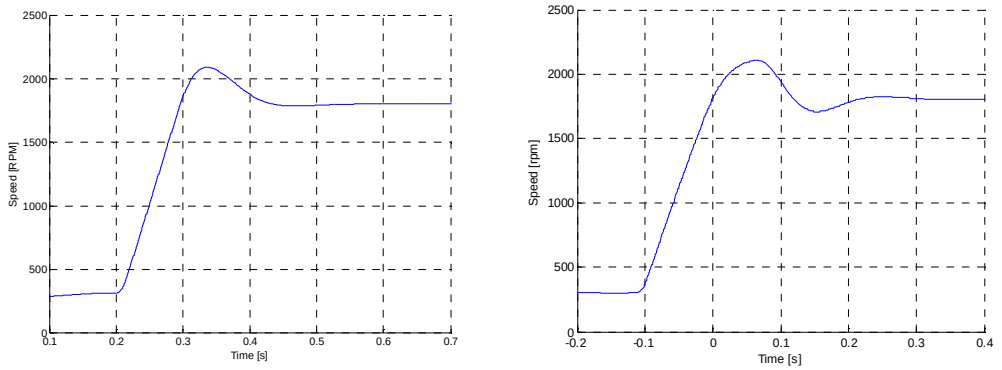

Figure 66	Simulated (left) and measured (right) speed during no-load startup sequence with passive load generator.

The speed loop is tested by a no-load startup sequence, where the speed is first 300RPM at a certain time (0.2s in simulation -0.1s in test) the speed reference is stepped to 1800RPM. In Figure 66 the speed response to this reference is shown for

both simulation and test. The oscillation seems to be less dampened in the measurement, which could be because of a rough mechanical model of the six-phase motor and load generator. It is however chosen not to examine this further, because the speed control loop is still stable with the physical system. Note that the controller implemented in the *D-Space* test system is exactly the same as in the simulation, so there is no need to verify the performance of the controller as the aim is simply to get a stable speed loop.

It is also important to note that the *DC-link* voltage is not controlled in the test setup, it is just a passive rectification, and this limits the deceleration capability because the power is fed back in the *DC-link* increasing the voltage toward or above trip limit level. Therefore speed steps with overshoot where deceleration is needed (the power changes direction) are difficult in the test setup. In this speed step test case an extra resistor (approximately 500Ω) is put in parallel with the *DC-link* capacitors to dissipate some of the power. This increased the ripple in the *DC-link* potential considerably.

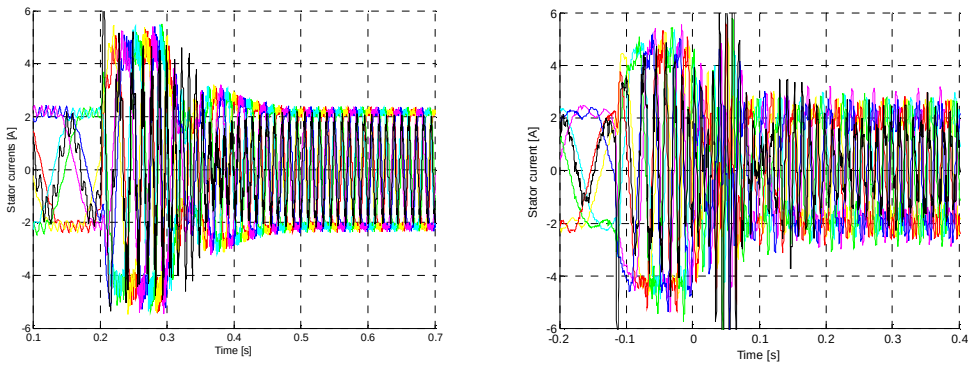

Figure 67	Simulated (left) and measured (right) currents during no-load startup sequence with passive load generator.

There is a small difference in the currents dynamic shape, which is due to the difference in the mechanical system, giving different current references.

The difference between simulation and test in the speed control loop is expected to come from a simplified mechanical model. But since the control loop is still stable and has an acceptable response, no further effort will be given to correct the model and or the controller. A very precise mechanical model is not the main point in the present thesis.

6.3 Current step

The current control loops are verified by stepping the i_d and i_q current individually keeping the other current fixed. The speed loop is deactivated. The idea is that fast current pulses of 40ms will only change the speed slightly, so the mechanical system is in a way decoupled, it only experiences the mean current.

6.3.1 Assumptions and difference between simulation and test

- In simulation the "ideal" reference voltage is applied to the motor, in the test a *PWM* voltage is applied (see 4.2.1).
- The currents are sampled with 5kHz on the *D-Space* system, but the currents have a higher frequency ripple due to the *PWM* voltage (see 4.2.1).
- The load machine gives a torque linear with the speed of 10Nm per 2000RPM. It also loads the six-phase motor with extra inertia ($4.8 \cdot 10^{-3} kg \cdot m^2$ according to data sheet) and extra viscous friction (assumed to be as big as the viscous friction from the six-phase motor). The measurement load torque is tuned until the speed from the simulation is reached.

6.3.2 i_d steps

i_d is pulse stepped between 2.5 and 3.5A every 40ms. i_q is fixed at 2.5A. The error signals from the current controllers are shown on Figure 68. As expected the two i_d currents are disturbed, but very quickly (within 10ms) controlled back toward zero error. This fit very nice with the expectation from the linear control design (see Figure 55). The i_q currents are also disturbed by the changing i_d currents, which is due to the fact that the two systems are not completely decoupled (see 5.2). The high frequency component of the error signals comes from the rotor slot passing the stator slots as mentioned in 3.4.2. There is also some cross coupling from the first to the 3rd harmonic currents, but at an acceptable level, and it also decade toward zero error very fast.

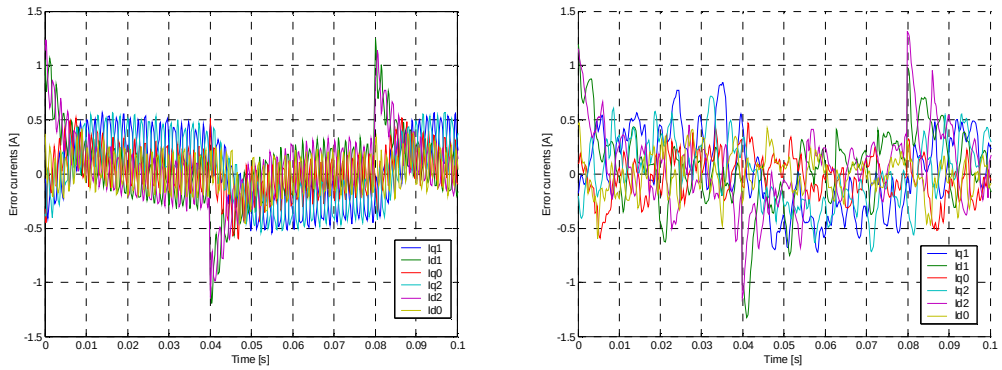

Figure 68	Simulated (left) and measured (right) dq-axis error currents during i_d steps. i_q is fixed.

On Figure 69 and Figure 70 the measured currents are shown in the stationary and rotating system. In the measurements for practical reasons the motor had to rotate in the opposite direction compared to the simulation, therefore the phase order is reverse on Figure 70. Note that the 3rd harmonic current is also step changed in both simulation and measurement to keep the amplitude factor 1/6.

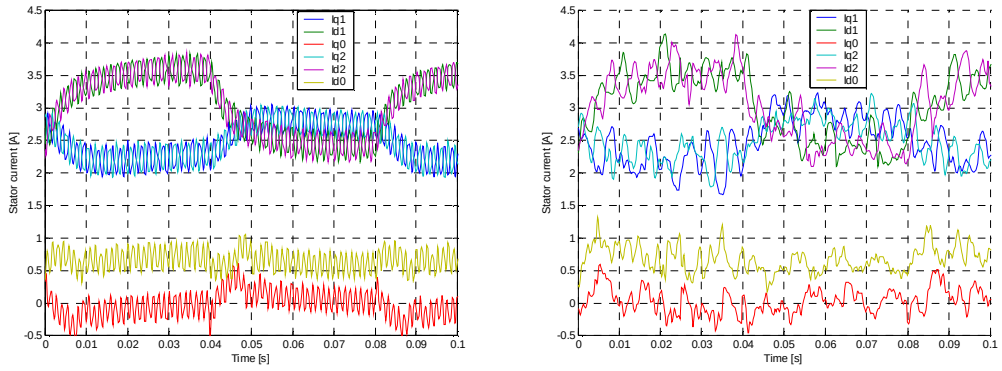

Figure 69	Simulated (left) and measured (right) dq-axis currents during i_d steps. i_q is fixed.

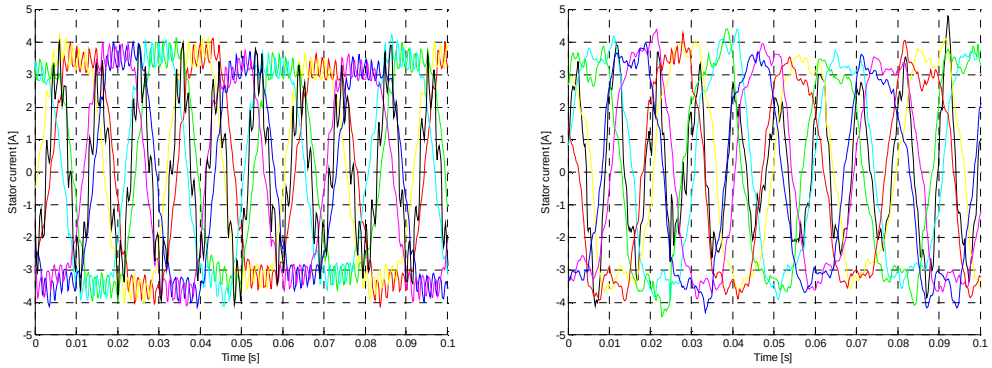

Figure 70	Simulated (left) and measured (right) currents during i_d steps. i_q is fixed.

A common difference between simulation and measurement are the higher frequency contents due to the slot harmonics. The difference is assumed to be due to saturation of the iron teeth and/or yoke and the fact that the real rotor is screwed one stator slot (see also 4.3).

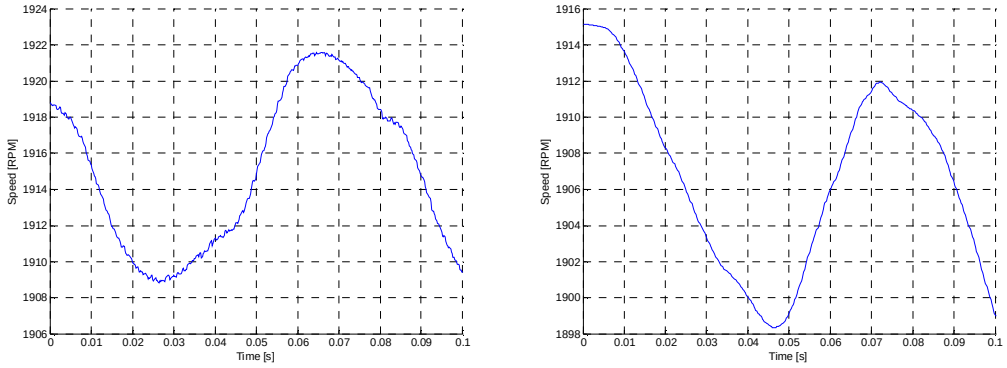

Figure 71	Simulated (left) and measured (right) speed during i_d steps. i_q is fixed.

Figure 71 show the simulated and measured speed. Although the level is not identical due to small differences in the mechanical model, the peak to peak value of the last top is more or less the same. The important thing in these figures is to note that the speed change less than 1%, so it is acceptable to say that the speed is constant.

6.3.3 i_q steps

i_q is pulse stepped between 2.5 and 3.5A every 40ms. i_d is fixed at 2.5A. The error signals from the current controllers are shown on Figure 72. As expected the two i_q currents are disturbed, but very quickly (within 10ms) controlled back toward zero error. This fits very nicely with the expectation from the linear control design (see Figure 55). The i_d currents are only disturbed marginally by the changing i_q currents. The high frequency component of the error signals comes from the rotor slot passing the stator slots as mentioned in 3.4.2. There is also some cross coupling from the first to the 3rd harmonic currents, but at an acceptable level, and it also decays toward zero error very fast.

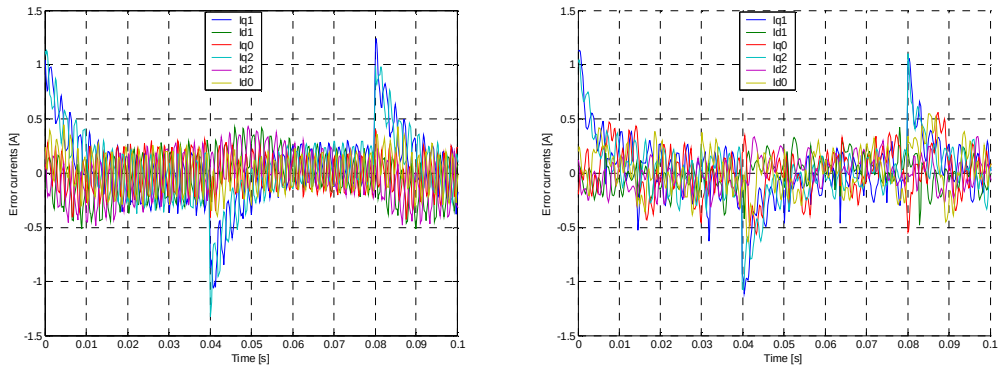

Figure 72	Simulated (left) and measured (right) dq-axis error currents during i_q steps. i_d is fixed.

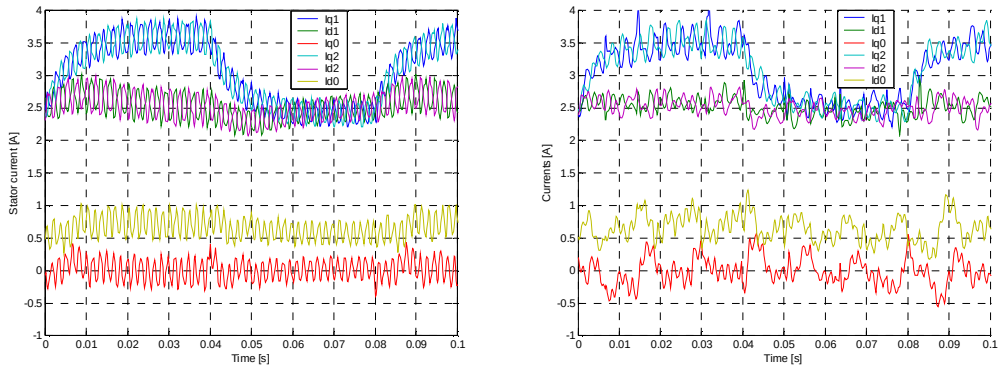

Figure 73	Simulated (left) and measured (right) dq-axis currents during i_q steps. i_d is fixed.

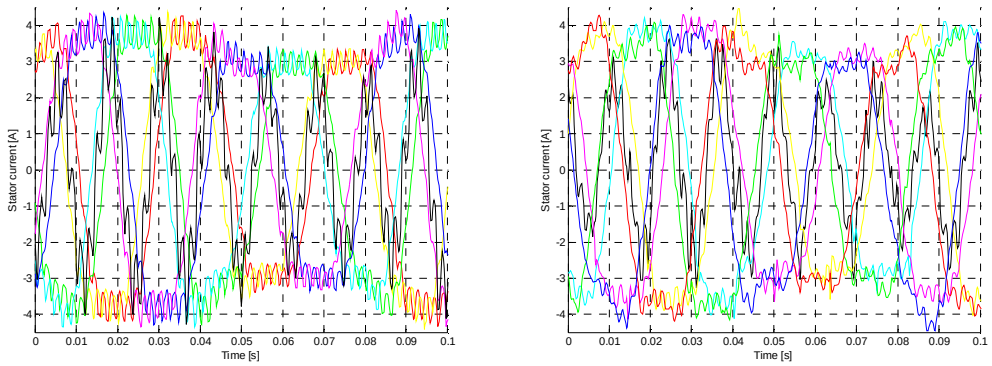

Figure 74	Simulated (left) and measured (right) currents during i_q steps. i_d is fixed.

On Figure 73 and Figure 74 the measured currents are shown in the stationary and rotating system. In the measurements for practical reasons the motor had to rotate in the opposite direction compared to the simulation, therefore the phase order is reverse on Figure 74. Note that the 3rd harmonic current is also step changed in both simulation and measurement to keep the amplitude factor 1/6.

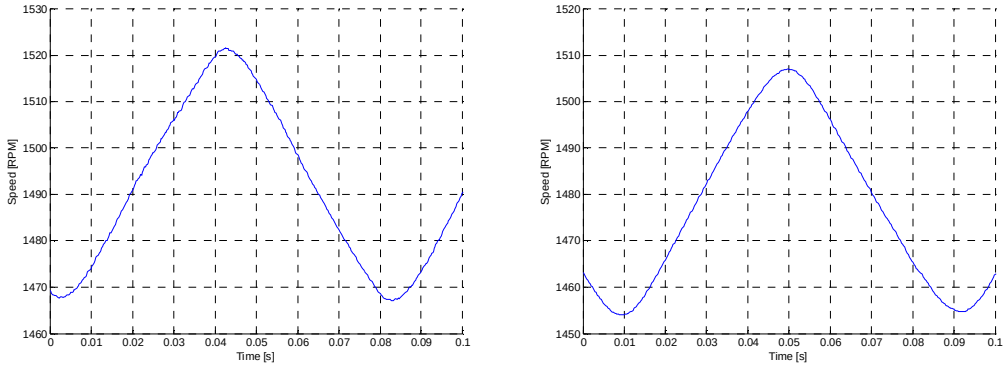

Figure 75	Simulated (left) and measured (right) speed during i_q steps. i_d is fixed.

Figure 75 show the simulated and measured speed. Although the level is not identical, the peak to peak value is more or less the same. The important thing in these figures is to note that the speed change is about 3%, so it is still acceptable to say that the speed is constant.

The torque and speed change much more when the active current is stepped, than when the magnetization current is changed, which is mainly due to better and

opposite decoupling of i_q. So if i_d is stepped i_q will counteract, but if i_q is stepped i_d will act in the same direction (see Figure 69 and Figure 73).

6.4 Midpoint controller

6.4.1 Assumptions and difference between simulation and test

- In simulation the “ideal” reference voltage is applied to the motor, in the test a *PWM* voltage is applied (see 4.2.1).
- The currents are sampled with 5kHz on the *D-Space* system, but the currents have a higher frequency ripple due to the *PWM* voltage (see 4.2.1).
- The capacitor size is assumed to be known.
- The motor model and parameters are assumed to be known and constant.

The midpoint voltage controller is simulated by subtracting an artificial dc offset current of 1.4A. The system is tested with nearly the same procedure as in the simulation where a constant current is applied at 0.5s. In practice a resistance of 177Ω is connected across the lower capacitor U_m at the time 0.7s. Without a midpoint controller the capacitors in the *DC-link* will integrate the current, until the asymmetry is so big that the motor has to stop (see 5.4.3). But with the new suggested controller, the midpoint voltage is stabilized, and the motor is able to continue to run. In the case of using the proposed control system, the controller corrects the motor currents so the motor now supplies the 1.4A in i_0 to the disturbance (with 0.23A dc for each phase see Figure 76). In the test and simulation the motor runs 1000RPM and it is loaded with about 7.5Nm.

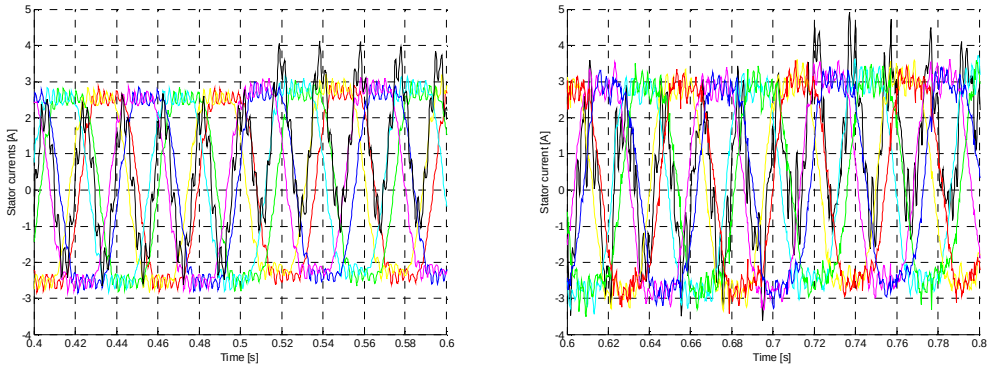

Figure 76	Simulation (left) and measurement (right) of six-phase motor drive with dc-controller. Asymmetry occurs at 0.5s in the simulation and at 0.7s in the test. Phase currents (colored) and zero current (black).

The *mid-point* of the *DC-link* will now be stabilized, which is shown in Figure 77, where the difference between the half *DC-link* voltage and the *mid-point* voltage is shown in both a simulation and a measurement. Despite the high amount of noise on the measured voltage, the figures show that the voltage will be stabilized, and that there is a high degree of correlation between model and test.

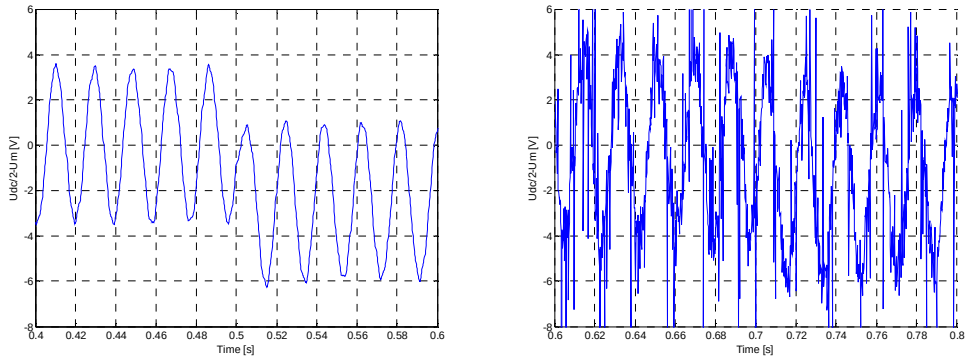

Figure 77	Simulation (left) and measurement (right) of six-phase motor drive with dc-controller. Asymmetry occurs at 0.5s in the simulation and at 0.7s in the test. Potential between half *DC-link* voltage and midpoint voltage.

In section 5.4.5 the damping of the midpoint voltage at a disturbance current step is much lower, which is because the midpoint controller is designed with open current loops. The current loops therefore help to damp oscillations.

Now the speed, current and midpoint control loops have been verified by comparing simulations and tests. There are a few other interesting features given by the six-phase machine that has to be examined. With the flexibility of the *D-Space* system these features are very easy to implement and study directly on the measurement system. Measurements will not be compared with simulations, because simulations are in this case actually more time-consuming to carry out and the model is already considered to be verified.

6.5 Redundancy

An interesting feature about the six-phase motor system is that it is redundant, which means that if a fail occurs the motor is able to continue to run, though at reduced power. This is an advantage if the motor is in very critical or costly processes that need to continue to be able to run, or at least close down slowly. The redundancy also gives the advantage that repair can be scheduled which gives smaller bills for repair because it is not time critical. Some examples are paper mills, heat/cool pump systems, all kinds of transportation, wind turbine generators, pumps in power plants etc.

Compared to motors with several individual three-phase windings multi-phase motors are more redundant. All the windings have a different vector angle, so it is possible to make a rotating field even if only two phases are still operating. The angles between the vectors could however be very low, so the torque production in this case is very low.

The redundancy in the six-phase system is tested simply by turning off the enable signals to one of the VLT's (see Figure 78). At the time 0s, the enable signal to the VLT supplying phase *abc* is disabled. The controller has no algorithm to detect this failure, so it responds by increasing the phase voltages in phase *abc* to increase the current in the phases. But the current in phase *abc* very quickly decay to 0A (note a small error in the current measurement see 4.2.1).

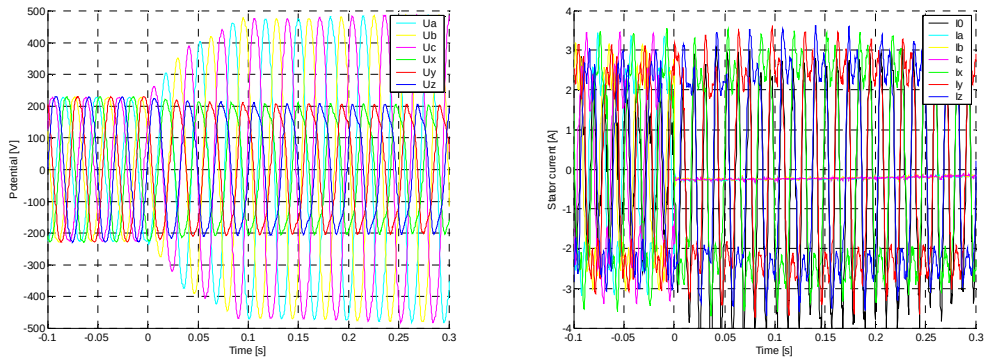

Figure 78	Voltage (left) and current (right) of six-phase motor during failure of three phases.

The three active phases continue uninterrupted, actually the torque producing current i_{q2} is doubled from 0.5A to 1A while i_{q1} becomes 0, which can be seen in Figure 79. The error in the 3rd harmonic current is increased because i_{q0} and i_{d0} are produced by all phases (see 5.3.1). So it would be more effective to remove the 3rd harmonic current in the case of this kind of failure.

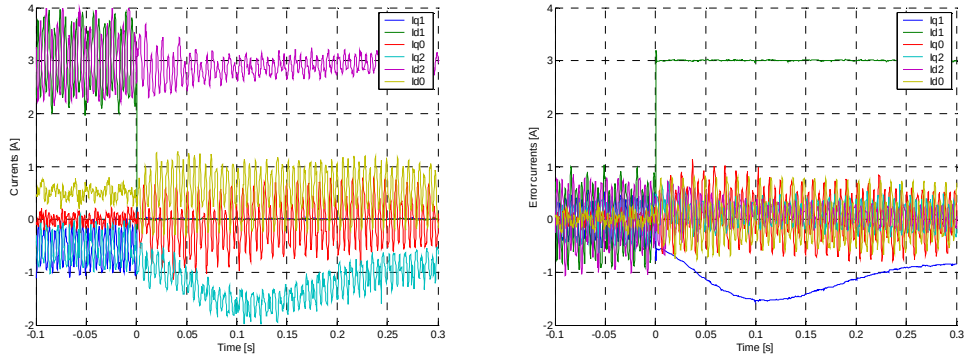

Figure 79	Transformed currents (left) and error currents (right) of six-phase motor during failure of three phases.

Since the torque is affected the speed is also perturbed, but the speed controller quickly corrects the error (see Figure 80 left). In the right curve on Figure 80 half the *DC-link* voltage minus the midpoint voltage is pictured. As the failure occurs the voltage amplitude increases mainly because the 3rd harmonic current can no longer

be controlled, but the *DC-link* controller still stabilize the *mid-point* voltage level to be around half the *DC-link* voltage.

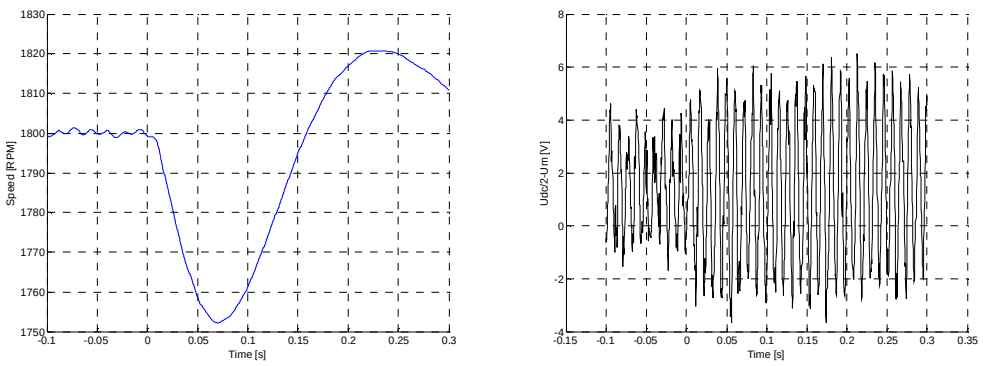

Figure 80	Speed (left) and *DC-link mid-point* voltage (right) of six-phase motor during failure of three phases.

The above example shows a very simple kind of redundancy, because the power capability will instantaneously be halved, but the interesting thing is that the build system is redundant without any additional coding/algorithms. Other kinds of failure redundancy are possible but more difficult to test, and they may need extra coding to protect the rest of the circuits. If i.e. only one branch fails, the motor should be able to continue on five phases. The return connection from the star-point actually becomes a valuable advantage in the six-phase motor, because it effectively decouples the six phases, by allowing any current flowing in the return path. In the extreme case the motor is able to run on only two phases, though at considerably decreased power rating.

6.6 Motor running only on 3rd harmonic current

The motor is run exclusively on the 3rd harmonic current, to show that the 3rd harmonic current actually produces torque. In this situation the current from phase *abc* and *xyz* are in phase in two groups (see 5.3.1) effectively giving two phases. The return wire here act as the return wire in a two phase motor. The two phase systems are shifted by 90°, also the same situation as in a two phase motor (see Figure 81).

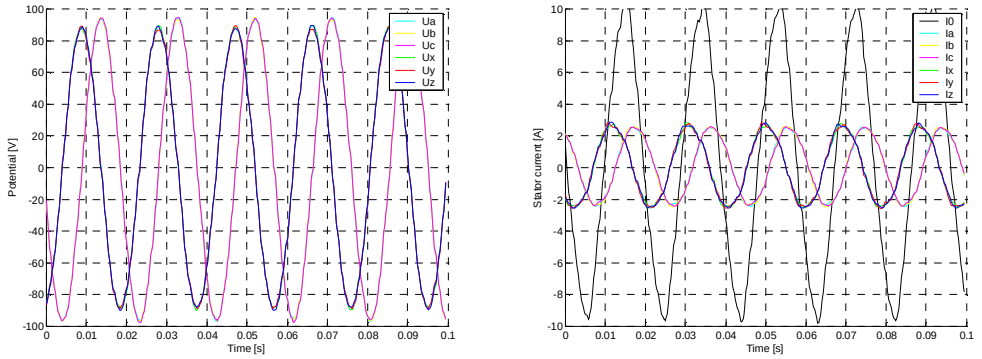

Figure 81	Voltage (left) and current (right) of six-phase motor running entirely on 3rd harmonic currents.

Figure 82 show the current and the current error in the dq-axis frame. As mentioned only the 3rd harmonic currents (i_{d0} & i_{q0}) are nonzero. There is some error in the 3rd harmonic components. This error is around 100Hz which is the double of the output frequency. This indicates an asymmetry between the two three phase systems, which could come from the fact that the 3rd harmonic current controllers are not cross decoupled (see 5.3.6), or it could come from the influence from the *mid-point* controller.

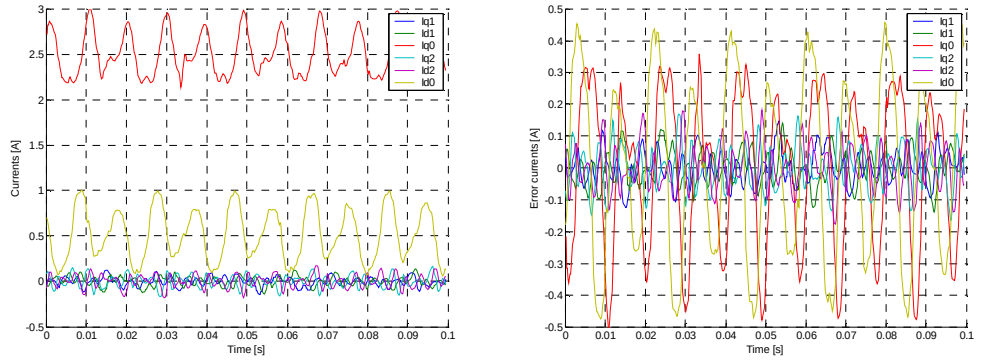

Figure 82	Transformed currents (left) and error currents (right) of six-phase motor running entirely on 3rd harmonic currents.

Figure 83 shows the speed and the load torque. The speed is around 1014RPM and the torque 1.54Nm neither vary notably. The torque level is not on the limit for torque from the 3rd harmonic current, but the return current is on the limit of what

the motor cable is able to transfer, and the *DC-link* voltage ripple is also considerable compared to the voltage and current rating of the capacitors. So the system was not pushed closer to the limit to avoid damage.

Note that the motor runs roughly 1000RPM, and the frequency of the current is around 50Hz, which indicate that the motor has 6 poles. This is also expected from the analysis in 2.2.3.

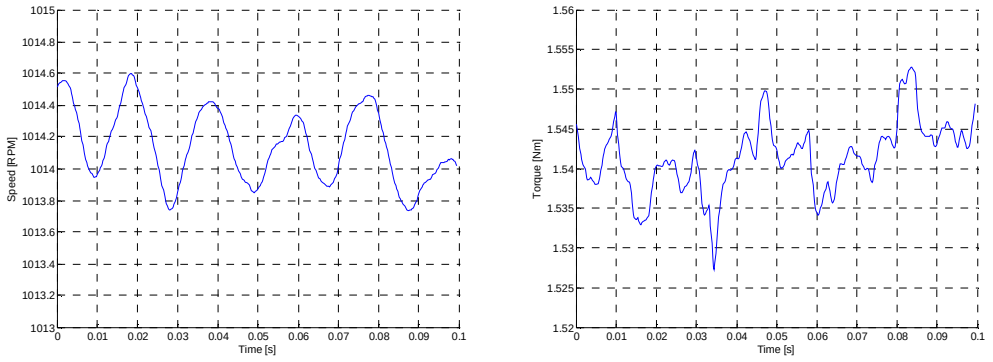

Figure 83	Speed (left) and load torque (right) of six-phase motor running entirely on 3rd harmonic currents.

The *mid-point* controller is also in this case able to control the midpoint voltage (see Figure 84) without ruining the performance of the current controllers. The voltage variation in the *DC-link mid-point* is in this case excessive (around 40V peak to peak).

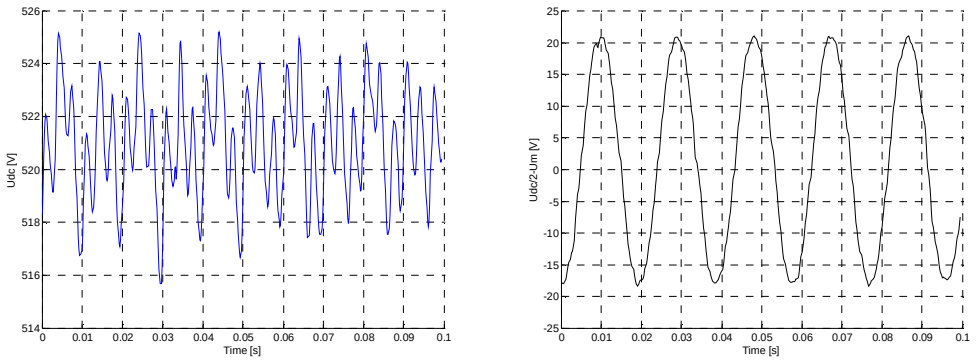

Figure 84	*DC-link* voltage (left) and *DC-link mid-point* voltage (right) of six-phase motor running entirely on 3rd harmonic currents.

As expected a six-phase motor is able to produce torque, even though the performance of the current controllers could be increased by cross decoupling.

6.7 Conclusion

In this chapter the controllers designed in chapter 5 are verified. Simulation and test results are compared.

The speed controller is tested by a speed reference step from zero (300RPM in test) to 1800RPM. The dynamic shape in the test is less dampened than in the simulation. This is expected to come from an imperfect model of the mechanical system. Especially data from the load machine are incomplete. But the mechanical system is not the focus area in this report. The simulation model is not improved and the controller is not redesigned, because the performance of the controller is acceptable.

The performances of the current controllers are validated. Two cases are tested. In the first case the magnetizing current i_d is pulse stepped between 2.5 and 3.5A every 40ms the active current i_q is fixed at 2.5A. In the second case the torque producing current i_q is pulse stepped between 2.5 and 3.5A every 40ms the magnetizing current i_d is fixed at 2.5A. There is a very nice match between measurement and simulation in these two cases. The current controllers are not perfectly decoupled as mentioned in 5.3.5 (especially when the magnetizing current is stepped), but even so the response time fits very nicely with the expectation from the linear analysis.

The *mid-point* controller is tested by a step in the zero current. The response of the nonlinear simulation and measurement fit very nicely. It is though noticeable that the response of the current disturbance is not like in the linear simulation, the damping in the linear simulation is much lower. But this is because the current controllers also have some influence on the *mid-point* voltage.

Furthermore redundancy is tested by a simple failure emulation procedure. In this procedure one of the VLT's is disabled, resulting in zero current in the three phases associated with this converter. The motor continues to run and in this situation the active VLT is able to take over the load without speed reduction.

It is proven that the 3rd harmonic current produces active torque. This is done by running the motor entirely on the 3rd harmonic current. In the test setup the motor produces about 1.54Nm @ 1000RPM, so even though this is not the limit to torque production from the 3rd harmonic current it surely proves the capability.

7. Conclusion

A summary of the thesis linking the introduction together with the analysis and results initiate this conclusion. In the second part of the conclusion, ideas and contributions gained during the thesis are described, analyzed and verified. Some recommendations for designing multiphase motors, recommendations for when and where to use multiphase motors and a table comparing various multi-phase motors with different supply is given in the third section. The final part of this chapter looks beyond the thesis, suggesting how to carry on the work on multiphase motors and segmented motor drives to continue the never ending spiral of improvements.

7.1 Thesis summary

The title of this project is segmented motor drive. Segmentation of the stator lamination can, with proper design, improve the motor efficiency. Segmentation of the inverter is expected to give higher redundancy, production advantages, etc. Four topologies having a segmentation strategy in common are described in the introduction. On the basis of a *SWOT* analysis it is selected to focus the work on multiphase induction motors. The problem formulation for the thesis: “Can a multiphase induction motor improve the general drive characteristics compared to a standard motor drive?” is stated.

As an example and as a motivating starting point the static design of a six-phase motor with 3rd harmonic current injected is analyzed in the second chapter. The idea with this topology is to increase the 1st harmonic flux in the air-gap by adding a 3rd harmonic flux (current) with the same peak flux-density in the stator teeth as a result. A drawback is that the yoke flux-density is increased, demanding redesign of the motor lamination. The state of the art in this area is described and analyzed. It was found that according to the state of the art a torque increase is generally possible even though it depends heavily on the initial lamination design. Taking 16 Grundfos motors as examples the maximum extra torque production was 2.67% if the yoke was already saturated with flux. An extra lamination dimension (the air-gap diameter) is set free to investigate the influence of a more complete redesign. It was

found that using the same Grundfos motors as mentioned before the maximum torque gain was now considerably increased to 28.5%. Under the same conditions, several motors have more than 5% torque gain. Grundfos motors with a low yoke thickness compared to air-gap diameter have the greatest potential for the torque increase. These designs are for motors with a high pole number. A general trend therefore seems to be that motors with high pole numbers have the greatest potential for torque increase. But note that the torque gain is very non-linearly dependent on the initial motor design. The major differences in releasing an extra dimension in the lamination design (compared to the state of the art) at least demonstrate that a more complete redesign of the lamination can make a big difference.

Beside torque improvement, multi-phase motors offer some efficiency increase. According to one paper, the six-phase induction motor with pure sinusoidal current offers 6.7% lower copper loss in the stator. An infinite number of phases give 8.5% reduction in copper loss. But it is assumed that the end turn is not extended even though the multi-phase winding has a higher pitch factor. This effect again increases the copper loss, so all in all the gain might be minimal. The calculations are done analytically. In another example the efficiency is measured to be lower for a six-phase motor with 3rd harmonic current injection than for a six-phase motor with pure sinusoidal current (which by the way is measured to be nearly identical to a three phase motor with sinusoidal current) at all working points beside overload. So it is mainly because of the 3rd harmonic current injection that the efficiency is lower. Redesigning with full freedom to change lamination dimensions could probably increase the efficiency at least to the same level as without 3rd harmonic current injection.

In the third chapter of the thesis a multi-winding (*MWI*) model for motors is described and evaluated. With this model the magnetic coupling between every single wire in the motor is calculated. The advantage of this is that the physical winding layout is used as input and with this option the number of phases can be random. The details in the model give the possibility to estimate all the copper loss and iron loss components in the machine. The calculations are based on a three-phase motor designed in the *SPEED* software, which ensures a calibrated starting point. Furthermore torque ripple caused by the winding layout can be calculated. Now it is possible to compare efficiency, torque ripple etc. of motors with different number of phases. It was found that a six-phase motor with sinusoidal supply has a 0.2% point higher efficiency and 40% lower torque ripple than a three-phase motor with sinusoidal supply. Increasing the slot width in the six-phase motor and injecting a 3rd harmonic voltage giving a 3rd harmonic current with 1/6 amplitude compared to the 1st harmonic current gives 0.3% point higher efficiency but only 10% lower torque ripple compared to the three phase motor. The efficiency improvements are very small so this does not give a valid reason for using multi-phase motors.

A six-phase motor with the exact same stator lamination and rotor as the three-phase motor is build. The only difference is the stator winding layout which now is six-phase. The six-phase induction motor is supplied via two standard three-phase Danfoss frequency converters. The six motor phases are star-connected and the

common star-point is returned to the *mid-point* of the *DC-link* capacitors. A *D-Space* system is used for control. With this configuration the motor can be supplied with a 3rd harmonic voltage/current together with a 1st harmonic voltage/current. Two cases with a simple fixed voltage/frequency ratio control algorithm are used for comparison between simulation and test. It was found that the *MWI* model of the motor showed satisfactory agreement with measurements in both cases.

In order to be able to supply completely sinusoidal currents a more advanced motor controller is build. This controller uses the well known vector control theory. A key to this theory is the transformation algorithm between rotating and stationary signals. In the case of a six-phase motor with a common return path three independent dq-axis exist, two dq-axis for 1st harmonic components and one dq-axis for the 3rd harmonic component. A simple rotor flux oriented control algorithm is used. The advantage with this approach is that the flux producing currents (i_{d1} and i_{d2}) and torque producing currents (i_{q1} and i_{q2}) are decoupled. The 3rd harmonic current components (i_{q0} and i_{d0}) are set to follow the current vector and is by default given an 1/6 amplitude compared to the 1st harmonic current. Six identical current controllers are designed using linear control design. The current references for torque producing current are controlled by a speed controller, which is also build using linear control design. The last controller that needs to be constructed is the *mid-point* controller. With this controller the *mid-point* potential in the *DC-link* capacitors is controlled by calculating a common voltage input adding to all six phase voltages. The state of the art is to build a seventh inverter branch with *PWM* modulation and an inductor to smooth the *PWM* voltage. Using the new control method these components can be saved. A drawback is that the *VA-rating* of the individual inverter switches need to be increased a little (depending i.e. on the demand for high torque at low speed), but the *VA-rating* of the whole inverter may not be affected compared to the need for an extra inverter branch. The strategy and test of the *mid-point* controller was also presented in two papers by the author [41] and [42].

It is important to note that the *mid-point* controller has to be calibrated together with the current controllers because they influence the *mid-point* controller. This is done in the second test session, where simulation results and test measurements are compared. The speed controller and the current controllers are also tested. A good agreement between simulation and measurements are found for all the controllers.

To demonstrate redundancy, one frequency converter is disabled online, resulting in disconnection of three motor phases. The motor is able to continue running, and in the test case even at the same speed because the load is relatively low. Only a small disturbance in speed is detected because the speed loop immediately detects the speed drop and increases the current reference to the remaining three phases. A three-phase induction motor would not be able to continue even if only one inverter phase fails. Compared to motors with several individual three-phase windings multi-phase motors also have some extra advantages. Since all the windings have a different vector angle, it is possible to make a rotating field if only two phases are operating. The torque production in this case could however be low if the angles

between the fail vectors are low, because the flux in space a vector diagram must be circular, and the peak current is limited. For other advantages see also 7.3.

Finally the motor is supplied only with a 3rd harmonic current to demonstrate the principles set up throughout the thesis. In this case the motor effectively has three times as many poles as the 1st harmonic, in this case six poles. The torque produced by the motor in the test case is 1.54Nm @ 1000RPM. The example serves to demonstrate the effect of injecting and using higher harmonic currents to produce torque.

7.2 Contributions

Throughout the thesis new ideas and contributions are described, analyzed and verified. In this section these contributions are listed.

- The maximum torque gain from a six-phase induction motor with 3rd harmonic current (equation (18) and Figure 18) is calculated with both the stator teeth and stator yoke as two independent degrees of freedom. Examples of torque gain for different Grundfos motors are listed in Figure 20.

- An extended multi-winding multi-phase model with iron loss estimation (equation (33)), and copper loss calculation for efficiency comparisons is documented in chapter 3 section 3.3. Some calculation examples are listed in Figure 38 and a more detailed table is to be found in Appendix E. One example with a six-phase motor is built and tested. The test results are compared with simulations, and satisfactory agreement is found (see section 4.3).

- A new controller which is able to stabilize the *mid-point* potential in the *DC-link* connected to the common star-point of a six-phase induction motor is analyzed, designed and tested (see 5.4, 6.4 and the papers [41] and [42]).

- An on-line disconnection of three out of six phases is forced to demonstrate a simple kind of redundancy (see 6.5). The motor is able to continue running with only a minor disturbance in the speed at the failure time (see Figure 80).

- The claimed effect of a 3rd harmonic current in a six-phase induction motor is demonstrated in a test setup. It is confirmed that a six-phase induction motor with only a 3rd harmonic current injected is able to produce usable torque (see 6.6).

- Physically based motor parameters for a six-phase motor are calculated in Appendix C, inserted in a dq-axis model and compared with the *MWI* with quite successful results (last section of Appendix C). With these calculations the six-phase dq-axis model can be used as an alternative to the *MWI* model. However, only for six-phase motors.

7.3 Conclusion

A table in Figure 85 summarizes and answers the question from the problem formulation in the case of three-, six- and nine-phase motors with three different kinds of supply: Sinusoidal voltage, Sinusoidal with 3rd harmonic current and Square-wave voltage.

		Number of phases		
Characteristics	Supply	Three-phase	Six-phase	Nine-phase
Redundancy	Arbitrary	Low	High	Highest
Relative VA-rating of individual switches		6	3	2
Winding		Standard	2x3 phases	3x3 phases
Bearing current due to common-mode voltage		High	Low	Low
Torque ripple	Sinusoidal	Medium	Low	Low
Efficiency		Medium	Medium	Medium
VA-rating of inverter		Medium	Medium	Medium
Lamination design		Standard	Standard	Standard
Torque gain from third harmonic current	Sinusoidal with third harmonic current	No	Yes	Yes
Need return wire and mid-point potential control		Yes	Yes	No
Torque ripple		High	Low	Low
Efficiency		Low	Medium	Medium
VA-rating of inverter		High	Medium	Low
Lamination design		Redesigned	Redesigned	Redesigned
Torque gain from third harmonic current	Square voltage (floating star point)	No	No	No
Torque ripple		High	Medium	Medium
Efficiency		Low	Medium	Medium
Switch loss in inverter		Low	Low	Low
VA-rating of inverter		High	High	High
Lamination design		Standard	Standard	Standard

Figure 85 Comparison between three-, six- and nine-phase induction motors with three kinds of supply.

The blue boxes represent cases that are not studied in details in this thesis, mainly because the nine-phase motor lamination has not been redesigned to include the effect of longer end-windings, lamination redesign (in the case with 3rd harmonic current) and the number of slots. If the motor is redesigned according to the same rules as for the six-phase motor (see section 2.3) the characteristics are probably nearly identical to the six-phase motor.

The star-point connected three-phase motor has no redundancy to failures in the phase wires. If one phase wire or inverter branch fails, the motor will only be able to produce a rotating field, if the star-point of the stator-wires are connected back i.e. to the *DC-link mid-point* potential. If on the other hand three of the phase-wires or inverter branches in a six-phase motor are failing, the motor will run even without a return path. If a return path exists the motor is able to produce torque even if four phase failures occur. In a nine-phase motor the numbers are six (no return path) and

seven (with return path). It is important to note that, to form a rotating field in the motor, two phases with different angles are needed. This is a particularity for the multi-phase motor.

The *VA-rating* of the inverter is not affected much if the supply is sinusoidal, but the individual switch rating is inversely proportional to the number of phases. If a 3rd harmonic current is injected in the six-phase motor, the *VA-rating* will be decreased to some extent, because the star-point is not floating, so space vector modulation is not possible. On the other hand the stator voltage will have a 3rd harmonic component, but not necessarily in phase with the 1st harmonic component. The last effect is in the case with square-wave voltage supply. In this case the current will have a high peak value even with multiple phases, but on the other hand the switching-loss will be dramatically reduced, enabling a higher current load.

The efficiency is not affected much. It is in the test examples a little better when going to six and nine-phase motors, but only 0.2-0.6% point depending on the shape of the voltage or current used as supply.

The torque ripple is lower when increasing the number of phases, but a normal three-phase induction motor with sinusoidal supply already has relatively low torque ripple compared to other motor types. In the test case the torque ripple is about 5%. Other kinds of motors like i.e. the switch reluctance drive could have 100% torque ripple as a comparison [39].

A main conclusion is therefore that multi-phase motors only improve the general characteristics of induction motor drives slightly. The most important gains when going into multiple phases are: high redundancy, low torque ripple and low bearing current. Note that the lower bearing current is not verified in this thesis (see 7.5). The drawback in general is a slightly more complex inverter and controller.

When injecting 3rd harmonic currents to get extra peak torque the drawback is a slightly more complex controller, more copper is necessary and redesign of the motor geometry is most likely needed.

7.4 Recommendations for industry applications

The power rating usually separates the most important characteristics of motor drives. Therefore the advice for multi-phase motors is also separated according to the drive size.

7.4.1 Small motor drives

In small drives high redundancy is usually not a major problem, so in this case the extra redundancy is probably not worth the extra cost of gate drivers and more computation power needed in multi-phase motors.

Torque ripple is amongst others a source of acoustic noise, and small motor drives are in many cases placed near people. In these cases multi-phase motors could be an option to reduce noise. But torque ripple is not the only source for acoustic noise production, and as mentioned in the summary the torque ripple is usually not severe in a standard sinusoidal supplied three-phase motor, so a thorough analysis comparing all the other characteristics must be executed before a final selection. Low torque ripple is important in servo applications like robots, where fast dynamics and low inertia are important characteristics. Vibrations can reduce lifetime and limit the bandwidth of servo drives.

The resistance and leakage inductance in small motors are in general higher than in large motors [10]. Therefore the overload (peak torque) is relatively low in small motors [18]. So in applications where relatively small motors and high peak torque are needed (i.e. drives for transportation or applications with high friction starting torque) the gain from 3rd harmonic current injection is valuable. As a general rule of thumb the torque gain potential is highest if the number of poles in the motor is high.

So for small motor drives the recommendation is not clear and no general conclusion can be made. A case to case study has to be made.

7.4.2 Larger motor drives

Large motor drives are usually a part of big production units like power plant pumps, paper mills, ship propulsions etc., where a high degree of redundancy is valuable or maybe even critical. In the mentioned cases it is of great importance that service can be scheduled, to avoid unintended stop of production. It is also always better to continue at partly loaded conditions than to close completely down. Extra computation power and gate drivers usually constitute a small part of the price of the complete motor-drive so multi-phase motors offer redundancy nearly for free in large motor-drives.

The values of maximum breakdown voltage and maximum current rating for silicon switches grow all the time, but are still a major challenge at high power levels, and the use of parallel and series coupled switches is still very attractive and widely used in high power motor-drives. Multi-phase motors offer a way to segment the power to several switches so the individual switch *VA-rating* is kept low. The load is shared equally between the switches, and a high degree of freedom to balance the load differently is also possible.

Torque ripple is not so important in large motor-drives, because the ripple frequency is usually very high compared to the slow dynamics of large systems. But as mentioned at small motor-drives, torque ripple is also a source of acoustic noise, so in the cases where this is problematic multi-phase motors can solve parts of the problem.

For larger motor-drives multi-phase motors generally have some nice features that are available for a relatively low extra cost. So the future for multi-phase induction motors is expected to be brightest for larger motor drives.

7.5 Future work

In this final section of the conclusion, ideas and perspectives for future work with multi-phase motors is given. These ideas and perspectives are given in the list below:

1. In chapter 2 the torque gain from a six-phase induction motor with 3^{rd} harmonic current injection is evaluated. This gain is found on the basis of an optimization process with stator teeth width and stator inner diameter as two degrees of freedom. Other dimensions could be set free especially it could be interesting to extend the optimization to include the stator slot-depth. In other words the torque gain could be extended even further by a more complete redesign of the lamination.

2. Construct a more advanced error handling algorithm to improve redundancy in a multi-phase motor. One of the problems with the present speed controller is that the factor from current reference to torque is changed if a phase fails. Therefore the speed loop has to increase the proportional gain through the controller to keep the same performance. In the case of the six-phase motor with third harmonic current, another problem is to decide if the third harmonic current has to be reduced or maybe completely turned of. If i.e. three phases in the same group are failing at the same time, a third harmonic current will only produce pulsating torque, so it has to be completely of.

3. Analyze different modulation strategies and switch patterns amongst others to minimize common mode voltage, which will reduce bearing currents. The number of switch states in an n-phase motor is 2^n. If the star-point of the motor is floating, this means n different voltage vector levels. Therefore the freedom to select vectors grows rapidly when the number of phases increases. This freedom can be used to decrease the switch frequency or to minimize the maximum dv/dt.

4. Extend the *MWI* model from two to m poles and include skewing in the model. Some of the *MWI* model is not dependent on the number of poles, but a symmetry assumption is used when the g function equation (27) is set up. Therefore the g function has to be reconstructed. The torque calculation is also changed because electrical speed and mechanical speed are no longer equivalent. The g function also has to be changed to include skew. The shape of the g function will be smoother with rounded corners.

5. A square wave supplied multi-phase drive naturally gives low switching loss at least at full load/speed. On the other hand the *VA-rating* due to peak

currents has to be higher than a comparable sinusoidal drive. The peak current increase is however reduced when the number of phases is increased. At the same time voltage amplitude change is necessary to make an effective variable speed drive, so either a variable *DC-link* is needed or *PWM* modulation is necessary at partly loaded situations. Both increase the switching losses. The number of possible switch states is 2^n where n is the number of phases, so in many ways the multi-phased motor can be compared to multi-level inverters. This minimizes the need for very fast switching frequencies. It seams to be reasonable that the size of the switching devices decreases as the number of phases is increased if the supply is square wave and only a very slow switching frequency is necessary.

6. It is recommended to incorporate the design rules outlined in chapter 2 in the *SPEED* program so that when designing an induction motor the torque gain by injecting a 3^{rd} harmonic component can be estimated. If the application calls for a high torque, the gain and guidance for a lamination reconstruction can very quickly be estimated. It is important to realize that the existing guide is limited to two degrees of freedom (tooth-width and inner diameter), so an optimization afterwards is advisable. This optimization can only be done if the existing *SPEED* software is upgraded to calculate on multi-phases motors. One way to invoke this is to use the *MWI* model. Extra benefits using the general *MWI* model is that it is able to calculate effects of asymmetries in the winding, broken rotor bars, winding harmonics, flux-density in the teeth and yoke etc.

References

[1] R. O. C. Lyra. ”Torque Density Improvement in a Six-Phase Induction Motor with 3rd harmonic Current Injection.” PhD. thesis, University of Wisconsin – Madison, 2002.

[2] H. A. Toliyat, T. A. Lipo, J. C. White “Analysis of concentrated winding induction machines for adjustable speed drive applications Part 1 (Motor analysis).” IEEE transactions on energy conversion, Vol. 6 No. 4, December 1991.

[3] H. A. Toliyat, T. A. Lipo, J. C. White “Analysis of concentrated winding induction machines for adjustable speed drive applications Part 2 (Motor design and performance).” IEEE transactions on energy conversion, Vol. 6 No. 4, December 1991.

[4] R. O. C. Lyra, T. A. Lipo “Torque Density Improvement in a Six-Phase Induction Motor with 3rd harmonic Current Injection.” Industry Applications Conference, 2001. Thirty-Sixth IAS Annual Meeting. Conference Record of the 2001 IEEE, On page(s): 1779 - 1786 Vol. 3, 30 Sept.-4 Oct. 2001

[5] Borealis Chorus motor tutorial “http://www.chorusmotors.gi/technology/motortutorial1.pdf” sited November 21, 2003.

[6] S. Williamson, S. Smith “Pulsating torque and losses in multiphase induction machines” IEEE transactions on industrial applications, Vol. 39, No. 4, July/August 2003.

[7] D. W. Novotny, T. A. Lipo “Vector control and dynamics of AC drives” Oxford Science publications. ISBN: 0-19-856439-2. First published 1996.

[8] K. Ogata “Modern control engineering” 2.ed. University of Minnesota. ISBN 0-13-598731-8, 1990.

[9] P. C. Sen “Principles of Electric Machine and Power Electronics” 2.ed. ISBN 0-471-02295-0, 1997.

[10] T. A. Lipo “Introduction to AC Machine Design” Vol. 1., University of Wisconsin. Printed and bound at the University of Wisconsin, Madison WI, 1996.

[11] P. Vas “Sensorless vector and direct torque control” Oxford science publications. ISBN: 0-19-856465-1, 1998.

[12] T. A. Lipo “A d-q model for six phase induction machines” ICEM pp 860, part 2, 1980.

[13] K. J. Åström, B. Wittenmark “Computer-controlled systems – Theory and design” 2. ed., ISBN: 0-13-172784-2, 1990.

[14] J. W. Kolar, H. Ertl, F. C. Zach “Minimizing the Current Harmonics *RMS* Value of Thee-phase *PWM* Converter Systems by Optimal and Suboptimal Transition between Continous and Discontinuous Modulation” Proceedings of the 22nd IEEE Power Electronics Specialists Conference, Vol. 1, pp 372-381, 1991.

[15] A. M. Hava, R. J. Kerkman, T. A. Lipo ”A High Performance Generalized Discontinous *PWM* Algorithm” Proceedings of the 12th IEEE Applied Power Electronics Conference and Exposition, Vol. 2, pp 886-894, 1997.

[16] A. M. Hava, R. J. Kerkman, T. A. Lipo ”Simple Analytical and Graphical Methods for Carrier-Based *PWM-VSI* Drives” IEEE Transactions on Power Electronics, Vol. 14, no. 1, pp 49-61, January 1999.

[17] P. C. Krause, O. Wasynczuk, S. D. Sudhoff “Analysis of electrical machinery” IEEE Press. ISBN: 0-7803-1101-9, 1994.

[18] L. W. Match, J. D. Morgan. “Electromagnetic and electromechanical machines” John Wiley & Sons. 3rd edition, 1987.

[19] P. Vadstrup “Multiwinding modelling of Induction Motors”. Grundfos A/S, 2002.

[20] Personal discussion with Jan Balle Nielsen from Grundfos A/S, November 28, 2005.

[21] http://www.grundfos.com Grundfos SQ-Flex submersible pump with segmented stator. Sited 2002.

[22] http://www.exlar.com/products/rotary/SLM/slm_oview.html sited November 28, 2005.

[23] http://www.designnews.com/article/CA234387.html sited November 28, 2005.

[24] http://www.danfossdrives.com/literature/fcm300fs.pdf Danfoss drives VLT drivemotor FCM 300 series.

[25] S. Z. Jiang, K. T. Chau, C. C. Chan ” Spectral Analysis of a New Six-Phase Pole-Changing Induction Motor Drive for Electric Vehicles” IEEE Transactions On Industrial Electronics, Vol. 50, No. 1, February 2003

[26] M. Mori, T. Mizuno, T. Ashikaga, I. Matsuda “A Control Method of An Inverter-Fed Six-Phase Pole Change Induction Motor for Electric Vehicles” Power Conversion Conference - Nagaoka 1997, Proceedings of the Volume 1, Page(s):25 - 32, 3-6 Aug. 1997

[27] M. B. R. Correa, C. B. Jacobina, C. R. da Silva, A. M. N. Lima, E. R. C. da Silva “Six-phase AC drive system with reduced common-mode voltage” Electric Machines and Drives Conference, 2003. IEMDC'03. IEEE International Volume 3, Page(s):1852 - 1858, 1-4 June 2003

[28] U. C. Mupambireyi, N. P. D. Schouten, B. M. Gordon, R. A. McMahon “High phase number induction motor drives for battery applications” Power Electronics and Variable Speed Drives, 2000. Eighth International

Conference on (IEE Conf. Publ. No. 475), Page(s):229 – 234, 18-19 Sept. 2000

[29] G. Oriti, L. Julian, T. A. Lipo "An inverter/motor drive with common mode voltage elimination" Industry Applications Conference, 1997. Thirty-Second IAS Annual Meeting, IAS '97., Conference Record of the 1997 IEEE Volume 1, Page(s):587 - 592, 5-9 Oct. 1997

[30] H. Razik "Modelling of double star induction motor for diagnosis purpose" Electric Machines and Drives Conference, 2003. IEMDC'03. IEEE International Volume 2, Page(s):907 - 912, 1-4 June 2003

[31] N. P. D. Schouten, B. M. Gordon, R. A. McMahon, M. S. Boger "Integrated drives using high voltage power ICs" Power Electronics and Variable Speed Drives, 2000. Eighth International Conference on (IEE Conf. Publ. No. 475), Page(s):554 – 559, 18-19 Sept. 2000

[32] N. P. D. Schouten, N. G. Damasius, R. A. McMahon "Drive concepts using single chip inverters" Industry Applications Conference, 2001. Thirty-Sixth IAS Annual Meeting. Conference Record of the 2001 IEEE Volume 3, Page(s):1715 - 1720, 30 Sept.-4 Oct. 2001

[33] K. G. King, "A three phase transistor class-B inverter with sinewave output and high efficiency," in Inst. Elect. Eng. Conf. Pub. 123, 1974.

[34] P. Hansen, F. Blaabjerg, J. K. Pedersen, E. Ritchie, " Calorimetric Measuring Systems for Characterizing High Frequency Power Losses in Power Electronic Components and Systems" IAS, Industry Applications Conference, Volume: 2 On page(s): 1368 – 1376, 13-18 Oct. 2002.

[35] P. V. Andersen "El-Ståbi" Teknisk forlag, 2. edition, ISBN: 87-571-1607-5, 1993.

[36] N. Tesla induction motor picture from the WEB-page: http://www.ingenious.org.uk/See/Tradeandindustry/FuelandPower/ found by searching for Tesla, sited 22/11-2005.

[37] Danfoss Drives A/S "Facts worth knowing about frequency converters", ISBN: 87-87411-22-9, 1998

[38] I. Boldea, S. A. Nasar "The Induction Machine Handbook" CRC press ISBN: 0-8493-0004-5, 2001.

[39] T. J. E. Miller "Brushless Permanent-Magnet and Reluctance Motor Drives" Clarendon press – Oxford, ISBN: 0-19-859369-4, 1989

[40] H. A. Toliyat "Analysis of Concentrated Winding Inductance and Reluctance Machines for Adjustable Speed Drive Applications" Ph.D. thesis, University of Wisconsin - Madison, 1991.

[41] F. B. Bendixen, F. Blaabjerg, P. O. Rasmussen "Den multi-fasede motor – et alternativ til den klassiske motor" Teknisk nyt special no. 36, Page 28-31, december, 2003.

[42] F. B. Bendixen, F. Blaabjerg, P. O. Rasmussen, K. Krabbe "Controlling the Dc-link Midpoint Potential in a Six-phase Motor-drive" 35th IEEE PESC, Aachen Germany, Page 476, 20-25 June, 2004.

Glossary of symbols

Chapter	*Variable*	*Description*
	DC-link	*The link connecting the rectifier part with the inverter in a frequency converter.*
	D-Space	*Real-time flexible control board with stand alone CPU for computer (see http://www.dspace.de/ww/de/gmb/home.cfm).*
	Matlab	*Mathematically based high level programming language by MathWorks. See www.matlab.com*
	mid-point	*When two capacitors are series connected in the DC-link, the mid-point or mid-point potential is the electrical point or electrical potential connecting the two capacitors.*
	MMF	*Magneto motive force.*
	MWI	*Multi winding model. A motor model where the winding layout is taken into consideration. This model is very useful to calculate on multiphase motors and to examine higher harmonics. See: Chapter 3 and reference [19] & [40].*
	PWM	*Pulse width modulation.*
	RMS	*Root mean square value.*
	Simulink	*Advanced simulation program for Matlab by MathWorks. See www.simulink.com*
	SPEED	*A commercial available motor design software program. See: http://www.speedlab.co.uk/software.html*
	SWOT	*Strength, weakness, opportunity and treat are four categories used for fast evaluation and comparison of topologies.*
	U/f control	*A simple but effective method for control of induction motors, where the voltage amplitude is changed proportionally with the frequency to maintain a constant fluxdensity in the motor.*
	VA-rating	*The maximum allowed apparent power rating. Calculated using the peak current and peak voltage of the inverter.*
	VSI	*Voltage source inverter. Frequency converter with voltage output.*

2	η_{gap}	*Rotor efficiency as seen from air-gap i.e. including rotor iron, copper and stray load losses.*
2	$\cos\phi_{gap}$	*Cosine to angle between rotor current and rotor voltage.*
2	τ_s	*Stator slot pitch width.*
2	τ_{sn}	*Stator slot pitch width new design.*
2	γ	*Stator slot pitch factor.*
2	γ_n	*Stator slot pitch factor new design.*
2	γ	*Stator slot pitch factor.*
2	γ_n	*Stator slot pitch factor new design.*
2	ϕ	*Angular position along the air-gap.*
2	γ	*Tooth width ratio.*
2	γ_n	*Tooth width ratio in new design.*
2	τ_s	*Tooth plus slot width.*
2	τ_{sn}	*Tooth plus slot width in new design.*
2	b_0	*Stator slot width.*
2	b_{0n}	*Stator slot width new design.*
2	B_{gl}	*Air-gap peak flux density.*
2	d_{cs}	*Stator yoke thickness.*
2	d_{csn}	*Stator yoke thickness in new design.*
2	D_{is}	*Stator inner diameter.*
2	D_{isn}	*Stator inner diameter in new design.*
2	F_0	*Zero sequence MMF.*
2	I_3	*3^{rd} harmonic stator current.*
2	k	*Flux reduction factor due to 3^{rd} harmonic current.*
2	k_1	*1^{st} harmonic factor including pitch, distribution, slot opening, and skew.*
2	k_{is}	*Stator lamination stacking factor.*
2	$K_{s(rms)}$	*RMS current per unit length of stator circumference.*
2	l_e	*Effective motor length.*
2	N_s	*Number of turns in a slot.*
2	t_0	*Stator tooth width.*
2	t_{0n}	*Stator tooth width new design.*
2	T_e	*Air-gap torque*
2	θ	*Angular position of the electrical field.*
3	$\Delta\theta_x$	*The angular difference between slot x and x+1.*
3	μ_0	*Vacuum permability.* $\pi \cdot 4 \cdot 10^{-7}$
3	ψ_r	*A vector with all the rotor flux linkages in each rotor loop.*
3	ω_r	*The angular rotor speed.*
3	θ_r	*The position difference between stator and rotor.*
3	θ_{r1}	*The position of the first rotor loop, seen from a stator fixed position.*
3	θ_{r2}	*The position of the second rotor loop, seen from a stator fixed position.*

3	θ_{rj}	The position of the individual rotor loops. $\theta_{r(m+1)} = \theta_{r1}$
3	θ_s	The position of the individual full pitch winding loops, seen from a stator fixed position.
3	ψ_s	A vector with the stator flux linkages in each stator phase.
3	θ_{sw}	The position of the stator windings. In symmetry: $(k-1)\frac{2\pi}{n}$ Where: k is the stator slot number. n is the number of stator slots.
3	A_{stator_yoke}	Area of the stator yoke. Length of stator times stator yoke width.
3	B_{rtpk}	The peak flux density in the rotor teeth.
3	B_{rtpkr}	Reference value of peak flux density in the rotor teeth taken from the three phased reference simulation.
3	B_{stpk}	The peak flux density in the stator teeth.
3	B_{stpkr}	Reference value of peak flux density in the stator teeth taken from the three phased reference simulation.
3	B_{sypk}	The peak flux density in the stator yoke.
3	B_{sypkr}	Reference value of peak flux density in the stator yoke taken from the three phased reference simulation.
3	d	The width of the air-gap.
3	f	The number of stator phases.
3	i	The stator phase number.
3	i_r	A vector with all the rotor loop currents (see Figure 23).
3	Iron	Reference value of complete calculation of iron loss taken from the SPEED program.
3	i_s	A vector with the stator currents in each phase.
3	j	The rotor loop number.
3	J	Moment of inertia. (In test case 0.0025kg*m^2 noload and 0.0050kg*m^2 loaded with DC-motor)
3	K_l	The common inductance constant.
3	l	The length of the rotor.
3	L_{rs}	Magnetic coupling matrix from the stator currents to rotor flux.
3	L_{rsji}	Magnetic coupling matrix from the stator currents to rotor flux, matrix element j,i.
3	l_{slx}	The leakage inductance in phase x.
3	L_{sr}	Magnetic coupling matrix from the rotor currents to stator flux.
3	L_{sr}	Magnetic coupling matrix from the rotor currents to stator flux.
3	L_{srij}	Magnetic coupling matrix from the rotor currents to stator flux, matrix element i,j.
3	L_{ss}	Magnetic coupling matrix between the individual stator phases.
3	m	The number of rotor loops, slots or bars.

3	*M*	*Electromagnetic torque.*
3	M_L	*Load torque.*
3	*n*	*The number of stator slots.*
3	N_{sx}	*The column vector with the winding function for phase x [19]. It is the accumulated sum (where the mean value is removed) of a column vector with the number of wires in each slot in phase x (called w_{sik} in equation (25)). See also Figure 22.*
3	*P*	*The number of poles.*
3	*ra*	*The radius to the air-gap.*
3	r_b	*Resistance in one rotor bar.*
3	r_e	*Resistance in one rotor endring.*
3	Ro_{Tooth}	*Reference value of iron loss in the rotor tooth taken from SPEED.*
3	R_r	*The resistance matrix for the rotor. See definitions in Figure 23.* $\begin{bmatrix} 2\cdot(r_b+r_e) & -r_b & 0 & \cdots & -r_b \\ -r_b & 2\cdot(r_b+r_e) & -r_b & \cdots & 0 \\ 0 & -r_b & 2\cdot(r_b+r_e) & \cdots & 0 \\ \vdots & \vdots & \vdots & \ddots & \vdots \\ -r_b & 0 & 0 & \cdots & 2\cdot(r_b+r_e) \end{bmatrix}$
3	R_s	*The resistance matrix for the stator.* $\begin{bmatrix} r_s & 0 & 0 \\ 0 & r_s & 0 \\ 0 & 0 & r_s \end{bmatrix}$
3	*SLL*	*Reference value of stray load loss in the motor taken from the SPEED program.*
3	St_{Tooth}	*Reference value of iron loss in the stator tooth taken from SPEED.*
3	St_{Yoke}	*Reference value of iron loss in the stator yoke taken from SPEED.*
3	u_s	*The voltage drop across a stator phase winding.*
3	w_{sik}	*The number of stator windings from each phase (i) in each individual stator slot (k).*
4	U_{dc}	*DC-link voltage. See Figure 58b for definitions.*
4	U_m	*Voltage across lower capacitor in DC-link. See Figure 58b for definitions.*
5	$\lvert i_{mr} \rvert$	*Rotor magnetizing current.*
5	$e(\omega_r \cdot i_d)$	*Electromotive force. Voltage drop across the magnetizing inductance.*
5	θ	*Angular position of the electrical field.*
5	γ	*The angle between the 3rd harmonic and the 1st harmonic component (see 5.3.2).*
5	$\theta(t)$	*Position of the current vector as a function of time.*

5	ω_e	*Applied field speed to the stator windings.*
5	σ_r	*Rotor leakage factor. Rotor leakage inductance divided by magnetizing inductance.*
5	ω_r	*The angular rotor speed.*
5	ω_s	*Slip speed.*
5	*a,b,c*	*Three groups of phases with common third harmonic current phase.*
5	*B*	*Viscous friction. (In test case $3.5*10^{-4}$J*s at noload and $3.25*10^{-2}$J*s at load)*
5	*C*	*Size of capacitors.*
5	C_m	*Lower capacitor in Figure 58b.*
5	C_{min}	*Minimum capacitor size.*
5	C_p	*Upper capacitor in Figure 58b.*
5	$f_{a,b,c}$	*The rotating abc components.*
5	f_{d0}	*The stationary d or flux producing components of the 3rd harmonic.*
5	$f_{d1,d2}$	*The stationary d or flux producing components of the 1st harmonic. 1 for abc and 2 for xyz.*
5	f_{q0}	*The stationary q or torque producing components of the 3rd harmonic.*
5	$f_{q1,q2}$	*The stationary q or torque producing components of the 1st harmonic. 1 for abc and 2 for xyz.*
5	$f_{x,y,z}$	*The rotating xyz components.*
5	h_d	*The d axis component of h.*
5	h_q	*The q axis component of h.*
5	*i*	*Stator current.*
5	i_0	*Current returning from the star-point of the motor.*
5	I_{1max}	*Maximum amplitude of the 1st harmonic stator current.*
5	I_{3max}	*Maximum amplitude of the 3rd harmonic stator current.*
5	i_d	*The 1st harmonic component of d-axis current. Flux producing axis.*
5	i_{d0}	*3rd harmonic stator current in the d-axis.*
5	i_{error}	*The reference current subtracted with the measured current.*
5	i_q	*The 1st harmonic component of the q-axis current. Torque producing axis.*
5	i_{q_ref}	*Reference current to the inner current loop.*
5	i_{q0}	*3rd harmonic stator current in the q-axis.*
5	i_{sx}	*Flux-producing stator current component.*
5	i_{sy}	*Torque producing stator current component.*
5	*j*	*The complex operator.*
5	*J*	*Moment of inertia. (In test case 0.0025kg*m^2 noload and 0.0050kg*m^2 loaded with DC-motor)*
5	k_t	*Torque constant going from q-axis current to torque. (In test case 0.28A/Nm)*

5	L'_s	*Transient stator inductance =* $L_m + L_{sl} - L_m^2 / (L_m + L_{rl})$ *[6].* *(In test case* $0.3049+0.01814-0.3049^2/(0.3049+0.01455)= 0.03199$ *H)*
5	L'_{s3}	*Transient stator inductance =* $L_{m3} + L_{ls3} - L_{m3}^2 / (L_{m3} + L_{lr3})$ *[6].* *(In test case* $0.06420+0.01814-0.06420^2/(0.06420+0.02629)=0.03679$H)
5	L_{lr}	*The leakage inductance in the rotor.*
5	L_m	*The magnetizing inductance between stator and rotor.*
5	L_r	*Self inductance of the rotor, transformed to stator side parameter. Equal to the rotor leakage plus the magnetizing inductance.*
5	P	*The number of poles.*
5	R_r	*Rotor resistance matrix.*
5	r_r	*Rotor resistance.*
5	r_s	*Stator resistance in one phase. (In test case 4.719Ω)*
5	s	*The differential operator (d/dt).*
5	T	*Shaft torque.*
5	t_e	*Electrical torque.*
5	T_r	*Rotor time constant =* L_r/R_r.
5	T_s	*Time constant for stator.* $T_s=L_s/R_s$
5	T_s'	*Transient time constant for stator.* $T_s'=L_s'/R_s$ *Where:* $L_s'=L_s-L_m^2/L_r$
5	U_0	*Voltage in the lower capacitor at the time zero.*
5	u_{dc}	*Potential in dc-link.*
5	u_{dx}	*Direct component of stator decoupling voltage.*
5	u_{dy}	*Quadrature component of stator decoupling voltage.*
5	u_m	*Potential across lower capacitor.*
5	$u_{mi\ ref}$	*Directly integrated potential across lower capacitor.*
5	u_{ref}	*Reference voltage to the motor.*
5	U_{rip}	*Acceptable voltage ripples at the applied field speed.*
5	u_{sx}	*Direct component of stator voltage.*
5	$\hat{u}_{sx}$	*Direct component of stator voltage drop across resistance and leakage.*
5	u_{sy}	*Quadrature component of stator voltage.*
5	$\hat{u}_{sy}$	*Quadrature component of stator voltage drop across resistance and leakage.*
5	v	*Stator voltage.*
5	x,y,z	*Three groups of phases with common third harmonic current phase.*
5	ω_{mr}	*Angular speed of the rotor-flux-oriented reference frame.*
5	ω_r	*The angular rotor speed.*
5	ω_{r_error}	*The reference minus the measured angular speed.*

6	a,b,c	Three groups of phases with common third harmonic current phase.
6	i_0	Current returning from the star-point of the motor.
6	i_d	The 1^{st} harmonic component of d-axis current. Flux producing axis.
6	i_{d0}	3^{rd} harmonic stator current in the d-axis.
6	i_{d1}	The 1^{st} harmonic component of d-axis current for phase group abc.
6	i_{d2}	The 1^{st} harmonic component of d-axis current for phase group xyz.
6	i_q	The 1^{st} harmonic component of the q-axis current. Torque producing axis.
6	i_{q0}	3^{rd} harmonic stator current in the q-axis.
6	i_{q1}	The 1^{st} harmonic component of the q-axis current for phase group abc.
6	i_{q2}	The 1^{st} harmonic component of the q-axis current for phase group xyz.
6	U_m	Voltage across lower capacitor in DC-link. See Figure 58b for definitions.
6	x,y,z	Three groups of phases with common third harmonic current phase.
B	i_d	The 1^{st} harmonic component of d-axis current. Flux producing axis.
B	i_q	The 1^{st} harmonic component of the q-axis current. Torque producing axis.
B	Jl	Inertia of load.
B	Jm	Inertia of motor.
B	K	Common inductor constant.
B	KOB	Resistance matrix for coupling of star-point.
B	Lrr	Rotor to rotor inductance matrix.
B	Lss	Stator to stator inductance matrix.
B	p	Number of polepairs.
B	rb	Rotor bar resistance vector.
B	rea	Endring resistance vector in end a.
B	reb	Endring resistance vector in end b.
B	rs	Stator phase resistance vector.
B	vr	Angle vector with positions of rotorbars.
B	vs	Angle vector with positions of statorslots.
B	Ws	Winding distribution matrix for each phase and slot.
B	x0	Initial condition of states.
C	γ	The angle between the 3^{rd} harmonic and the 1^{st} harmonic component (see 5.3.2).
C	λ,i	Refers to flux-linkage and current respectively. Same sub notation as described in equation (64) & (65).
C	μ_0	Vacuum permability. $\pi \cdot 4 \cdot 10^{-7}$

C	*a,b,c*	*Three groups of phases with common third harmonic current phase.*
C	*d*	*The width of the air-gap.*
C	*f*	*The number of stator phases.*
C	K_l	*The common inductance constant.*
C	k_{r_RS}	*Transformation factor from rotor to stator side.*
C	k_{s1}	*Winding factor for rotor winding.*
C	k_{w1}	*Winding factor for stator winding.*
C	*l*	*The length of the rotor.*
C	l_{bar}	*Rotor-bar leakage.*
C	l_{bar_ex}	*Extended rotor-bar leakage.*
C	l_{end}	*Rotor-end-ring leakage.*
C	L_{lm}	*Leakage inductance in each axis of the stator. 1^{st} harmonic system.*
C	L_{lr}	*Leakage inductance in rotor phase. 1^{st} harmonic system.*
C	L_{lr3}	*Leakage inductance in rotor phase. 3^{rd} harmonic system.*
C	L_{ls}	*Leakage inductance in each stator phase. 1^{st} harmonic system.*
C	L_m	*Magnetising inductance for each axis. 1^{st} harmonic system.*
C	L_{m3}	*Magnetising inductance for each axis. 3^{rd} harmonic system.*
C	*m*	*The number of rotor loops, slots or bars.*
C	*P*	*The number of poles.*
C	*ra*	*The radius to the air-gap.*
C	r_{bar}	*Rotor-bar resistance.*
C	r_{bar_ex}	*Extended rotor-bar resistance.*
C	r_{end}	*Rotor-end-ring resistance.*
C	r_r,r_{r3}	*Rotor resistance of the first and the 3^{rd} harmonic system.*
C	r_s	*Stator resistance in one phase. (In test case 4.719Ω)*
C	T_{ph}	*Number of series connected turns per phase.*
C	v,λ,i	*Refers to voltage, fluxlinkage and current respectively.*
C	*Wsn*	*Winding distribution vector for phase n in each slot.*
C	*x,y,z*	*Three groups of phases with common third harmonic current phase.*
C	x_0	*The 3^{rd} harmonic system of x.*
C	x_1,x_2	*The first and the second three phase system of x.*
C	x_3	*The 3^{rd} harmonic system.*
C	x_q,x_d	*Stands for q and d axis respectively of x.*
C	x_q,x_d	*Stands for q and d axis respectively.*
C	x_r	*Stands for rotor.*
C	x_s	*Stands for stator component of x.*

A. Test system

In this Appendix the test system is described. First some pictures of the system are presented together with comments. Next the control diagrams from *Simulink* is shown and discussed. At last the control cockpit is pictured and notes are made.

Pictures of test system

The first picture (Figure 86) shows the complete test system. The test bench is on the right and the computer on the table together with different voltage supplies. On the floor a transformer ensures galvanic isolation from the grid (done to minimize noise). In the top of the picture there are three motor drives hanging on the wall. The measuring system is placed on the table to the left.

Figure 86	Complete test system with six-phase induction motor, 2x3-phase Danfoss VLT, measurement board and a *D-Space* control computer.

Figure 87 shows a close up picture of the test bench, the DC-supply to the VLT's (gray circle) and the rectification of three phases (orange circle) with grid filter (purple circle) and series connected resistors (green circle). There are extra resistors in series to protect the three-phase rectifier from high inrush currents from the VLT's. The grid filter is inserted to reduce noise from/to the grid.

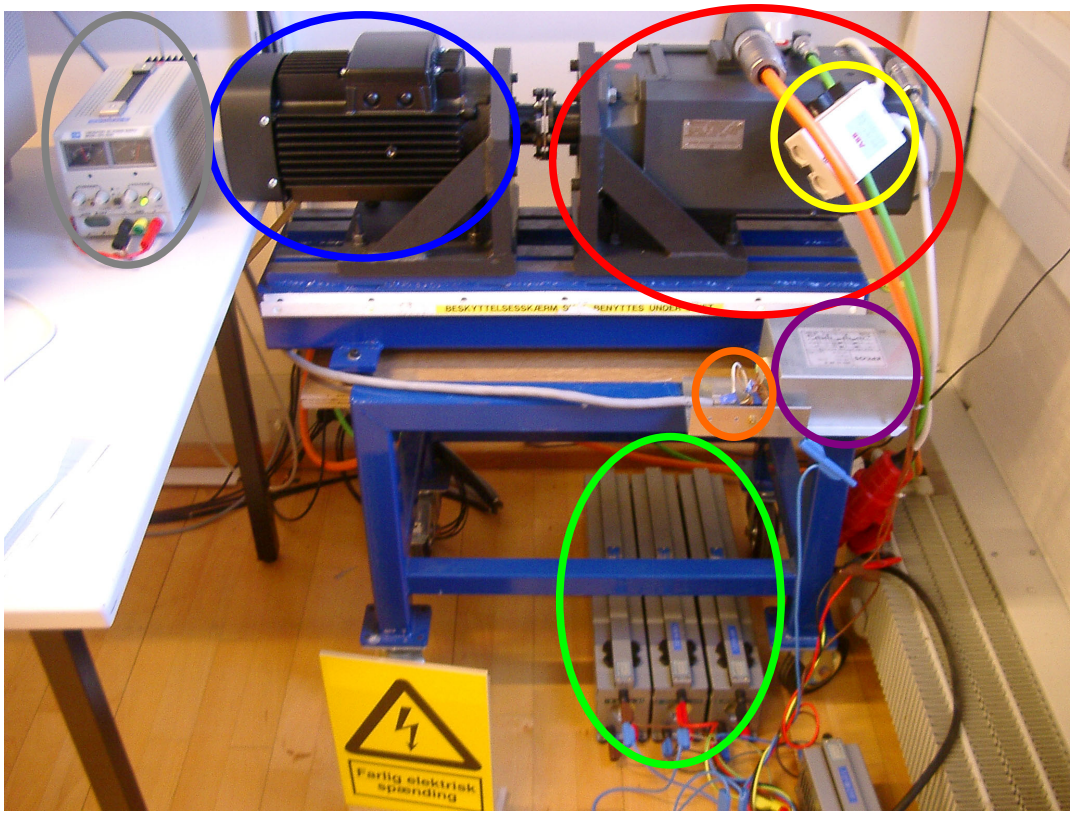

Figure 87	Test bench with the six-phase induction motor MG-100 from Grundfos (blue) and PMSM load motor from Siemens (red). There is a three phase on/off switch (yellow), three resistors for inrush damping of currents (green), an input filter to minimize grid disturbances (purple) and a rectifier (orange). At last there is a 24V DC supply (gray) for the two VLT's.

The three motor drives are shown on the picture in Figure 88. In the right the motor drive to the load motor is shown, it is a four quadrant drive that returns most of the generated power back to the grid. It was experienced that this drive makes a lot of air borne electrical field noise. Therefore the measuring system (Computer, voltage supplies and LEM-modules) was grounded to the drive. The two VLT's supplying the six-phase motor are in the left side of the picture. They have common *DC-link*

and DC-midpoint voltage (which demanded a small operation to establish). They are equipped with a special control-circuit, made by Aalborg University. One control-circuit only needs four optical signals. Three *PWM* signals and an enable signal. The three other *PWM* signals (to the lower switches) are computed internally. A 1.5µs dead time is used to prevent short circuit. Further more the phase currents are monitored by this control board and a protection procedure disable the VLT at overload current.

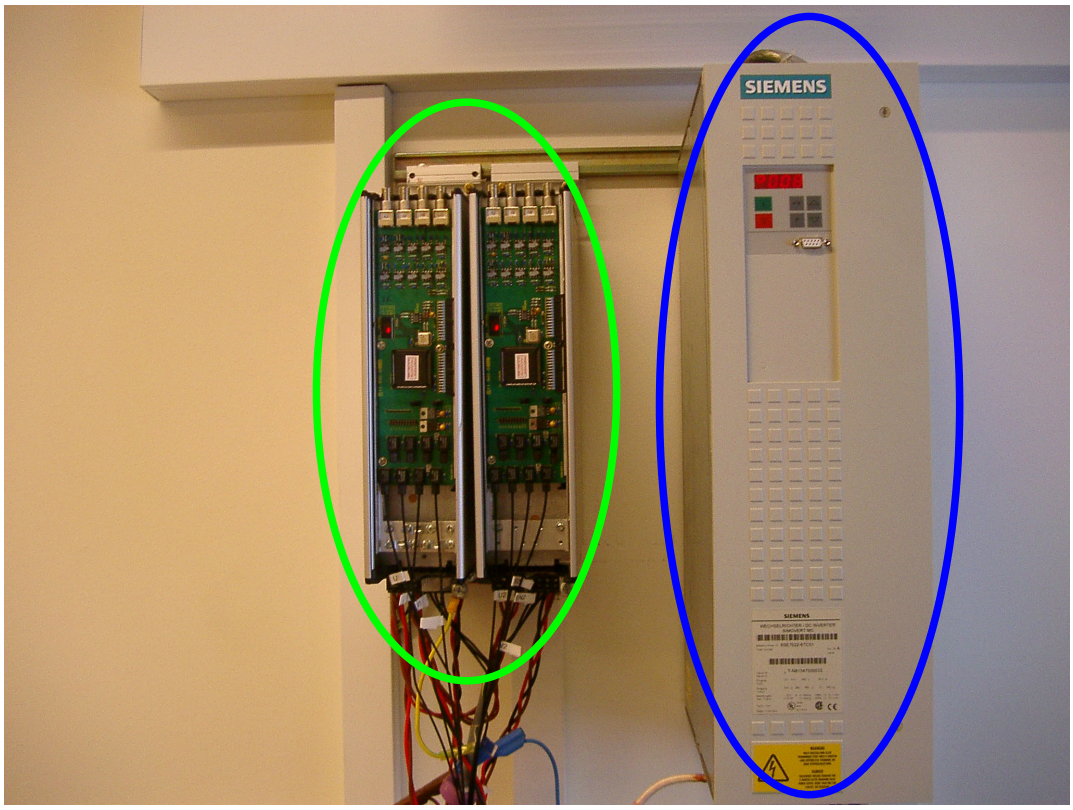

Figure 88	Two Danfoss VLT's 5004 (3.1 and 4.3KVA) (green) with connected *DC-link* capacitors and the Siemens drive for the load motor (blue).

The current and voltage measuring system is pictured on Figure 89. The power from the VLT's comes in with the left cable and goes out to the motor in the cable to the right. In-between (green circle) six LEM modules measure the six phase currents. If a zero current exist it will be the sum of the phase currents, therefore it is not measured instead it is calculated by the *D-Space* system. All the available A/D channels to the measuring system are also in use. But it gives some problems, because a common mode current (noise) will be multiplied with six on the zero current. A ferrite core is therefore placed around each cable to minimize common mode currents. The red and blue circle marks the DC-midpoint and *DC-link* voltage

measurements. The voltages are measured by the current flowing through a known resistor with a LEM-module. The reason is to ensure galvanic isolation. The eight LEM-modules output eight currents (yellow circle) that are transferred to the measurement condition unit (green circle in Figure 90). It is usually less noise to transport current than voltages. The two last BNC connections contain +/-15V supply for the LEM modules (shown on Figure 90 with a red circle).

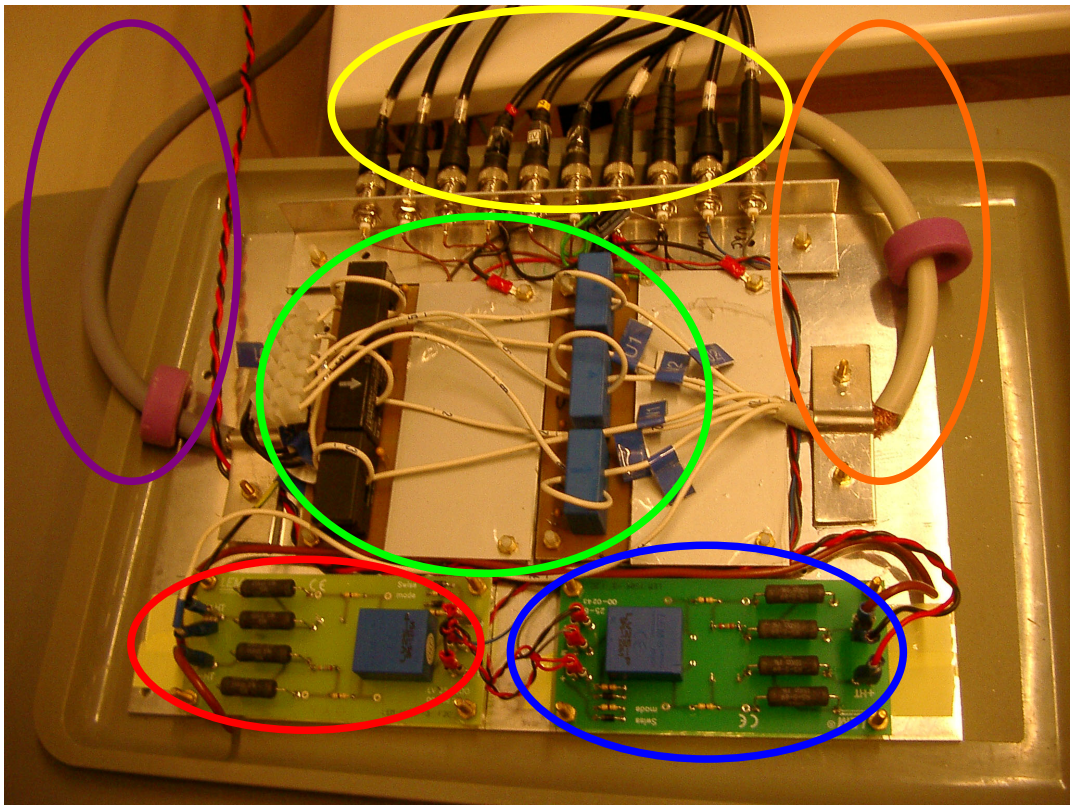

Figure 89	Six LEM modules to measure the six motor currents (green). *DC-link* voltage (blue) and *DC-link* midpoint voltage (red) measuring boards using LEM modules to ensure galvanic isolated measurements. Coaxial connections for signal transport and supply (yellow). Input cable from VLT's (purple) and output to the motor (orange).

The measured currents from the LEM modules go into a measurement conditioning rack (green circle on Figure 90). Signals to and from the load drive are also connected to the rack. The *PWM* and enable signals for the VLT's are output from the rack via optical fibers. The rack is supplied with power from a voltage supply (yellow circle). The rack has a I/O, analog/digital cable connection directly to the *D-Space* board on the AT-bus in the PC (blue circle). The acoustic noise from the

motor is heavy this is due to the 5kHz switching frequency of the converters, so a hearing protector (purple) is nice to wear.

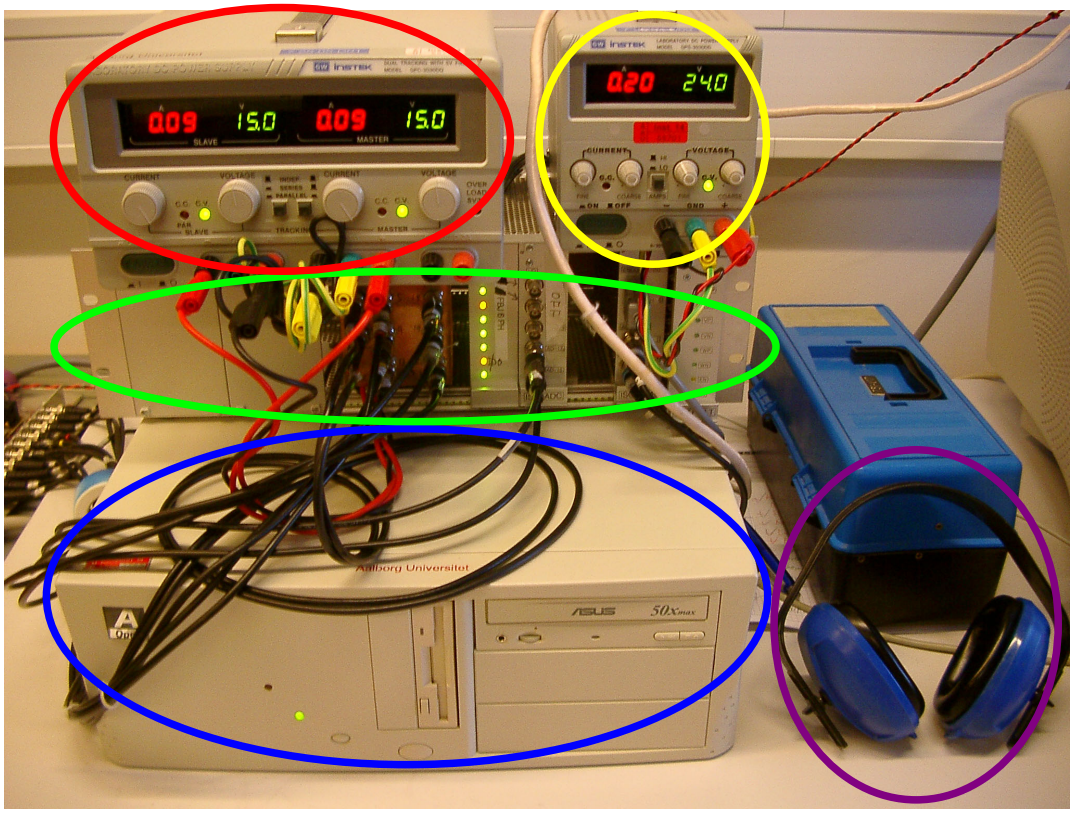

Figure 90	LEM module supply (red), signal conditioning rack (green) supply (yellow) and PC with *D-Space* board (blue). Audible noise reduction equipment (purple).

The *D-Space* card has two processors, generally speaking one for signal processing and one for calculations, and it is controlled with a PC. The card is able to run autonomous and it doesn't rely on the PC's CPU processor. The board runs in a real-time environment and the PC runs windows. This is smart because real-time evaluation need to be very fast and reliable which is possible with the *D-Space* card, and the computer need human interaction (see Figure 91), flexibility and has to run multiple tasks at the same time, which is possible with windows.

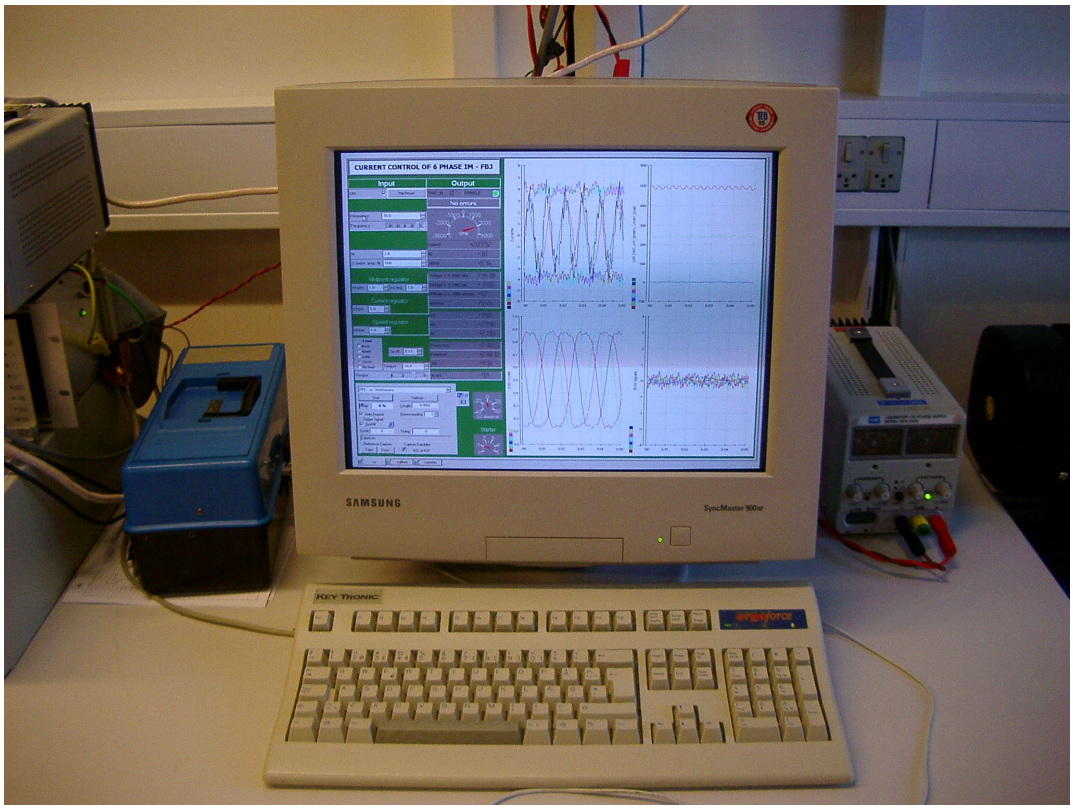

Figure 91	Screen shot with the motor running in current control mode.

Control diagrams in *Simulink*

The *D-Space* code is generated from *Matlab*/*Simulink* block diagrams. The control diagrams build in *Matlab*/*Simulink* are described in this section.

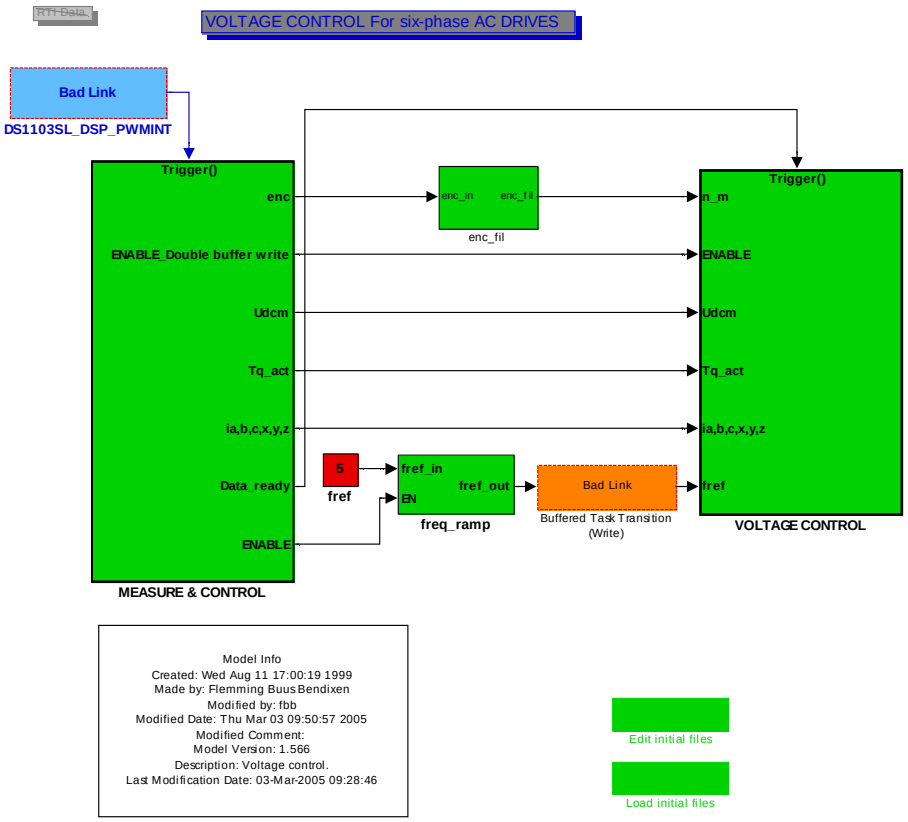

Figure 92 Interrupt control diagram.

The different tasks are triggered by an interrupt procedure (see Figure 92). During a zero vector the “measuring & control” block is triggered, when this block has finished one sample the control system is triggered. The frequency reference is also set and rate limited in this view (the block is opened in Figure 93). It is necessary to limit the frequency change rate during deceleration, because the power direction has to go from the inverter to the motor. If the power is drawn from the motor, the *DC-link* voltage will increase, because the energy has no other place to go. Normally a DC-chopper or active rectifier is used in this case, but it was not done in this project. The deceleration limit was set experimentally to 10Hz/s. This was enough to avoid over-voltage in the *DC-link*. At this rate the motor just slowly dissipate the stored rotation energy. Acceleration is not a problem if the current is limited and controlled (see chapter 5 & 6). But if a simple voltage controller with fixed U/f ratio is used (see chapter 4), fast accelerations will demand very high currents, which will trip the current protection system, so an acceleration limitation has to be used in this case.

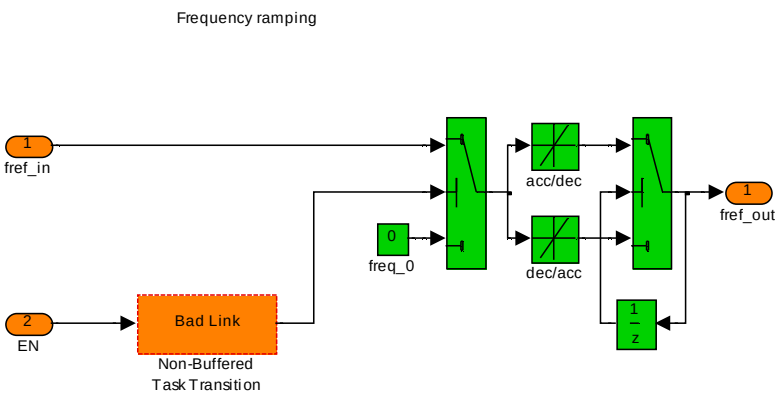

Figure 93	Reference frequency rate limitation diagram.

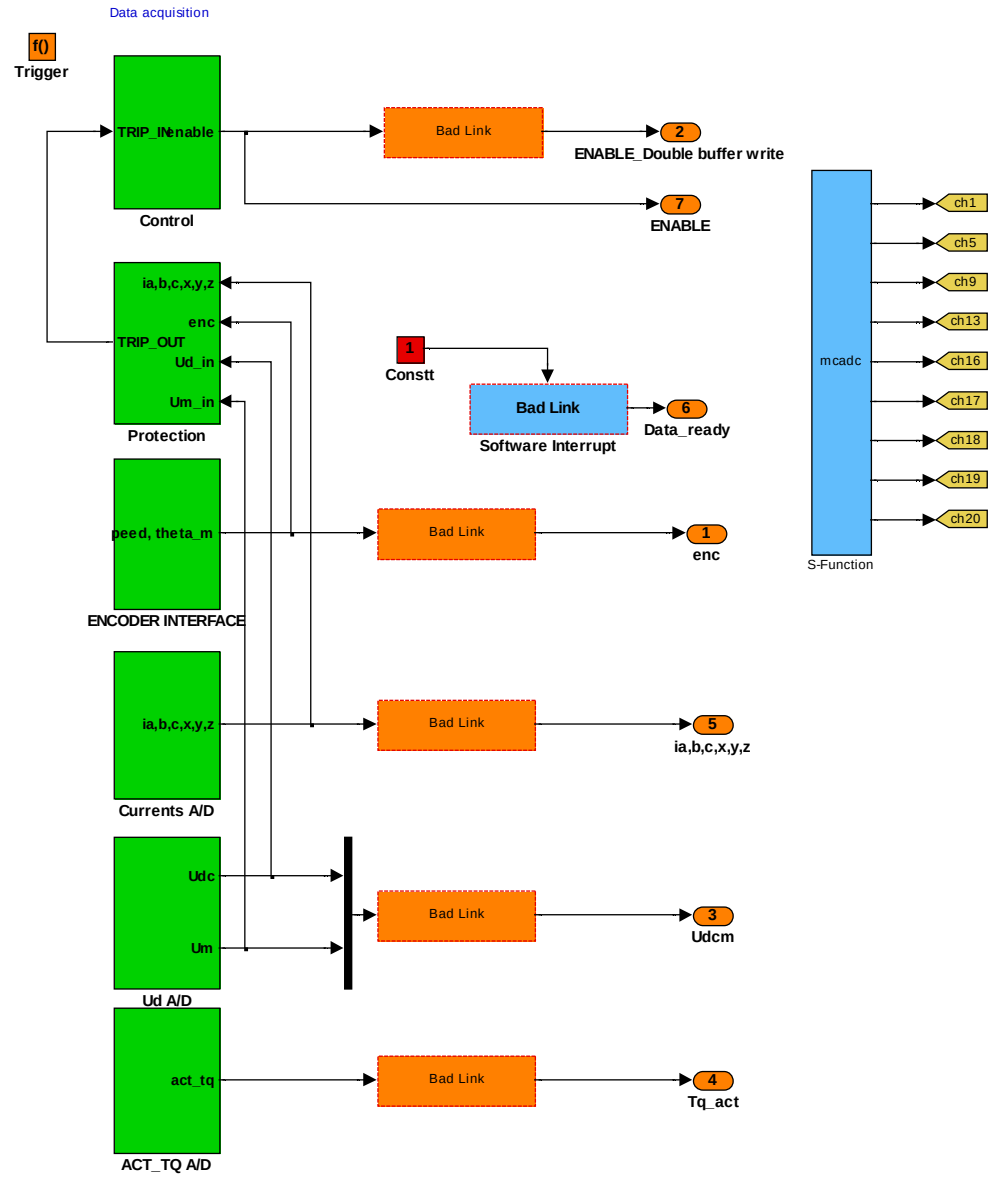

Figure 94 Data acquisition diagram.

The data acquisition diagram (see Figure 94) is in the block “measure & control” block. This block links the measurements (“Ud A/D”, “Currents A/D” and “ENCODER INTERFACE”) to the “Protection” system. The block also contains “mcadc”, that is an s-function written to convert the nine A/D channels at the best possible timing. “ACT_TQ A/D” is scaling of the measured torque from the Siemens load drive.

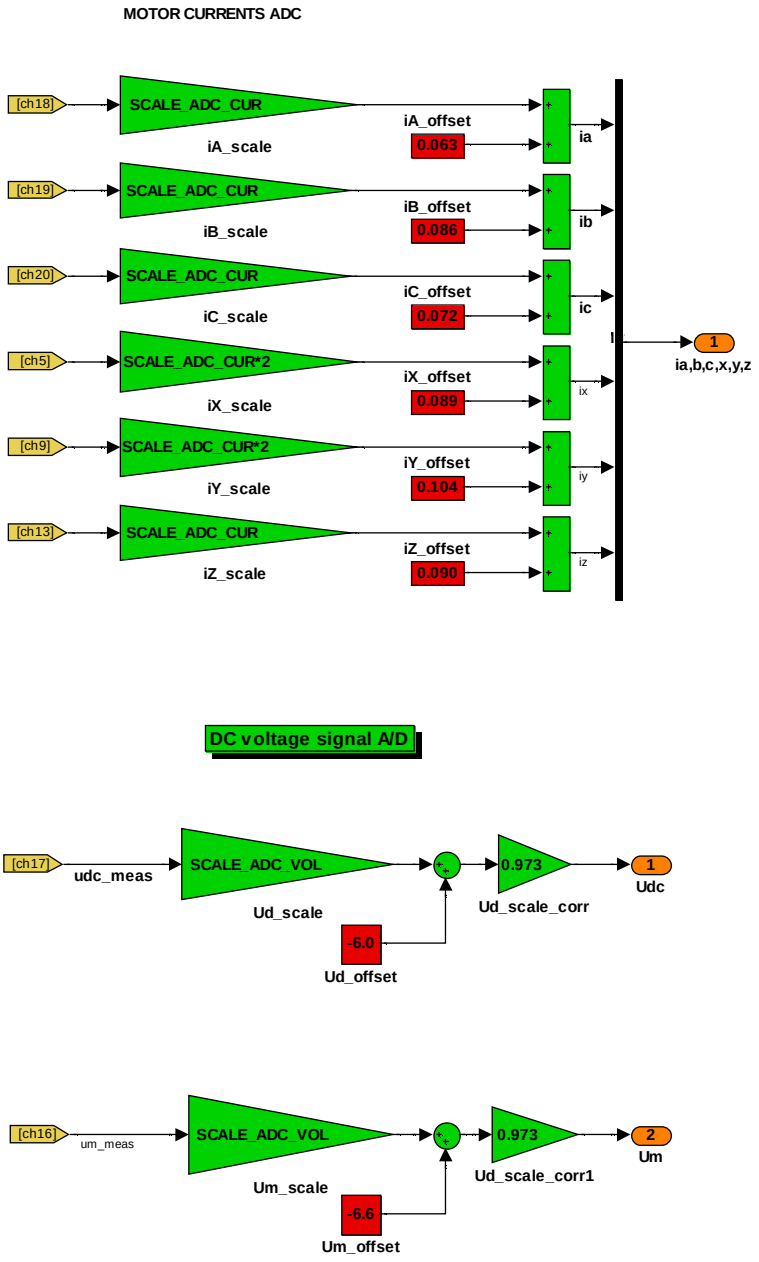

Figure 95	Measurement conditioning diagram of currents (top) and voltages (bottom).

"Currents A/D" and "Ud A/D" (see Figure 95) scale and calibrate the measured currents and voltages.

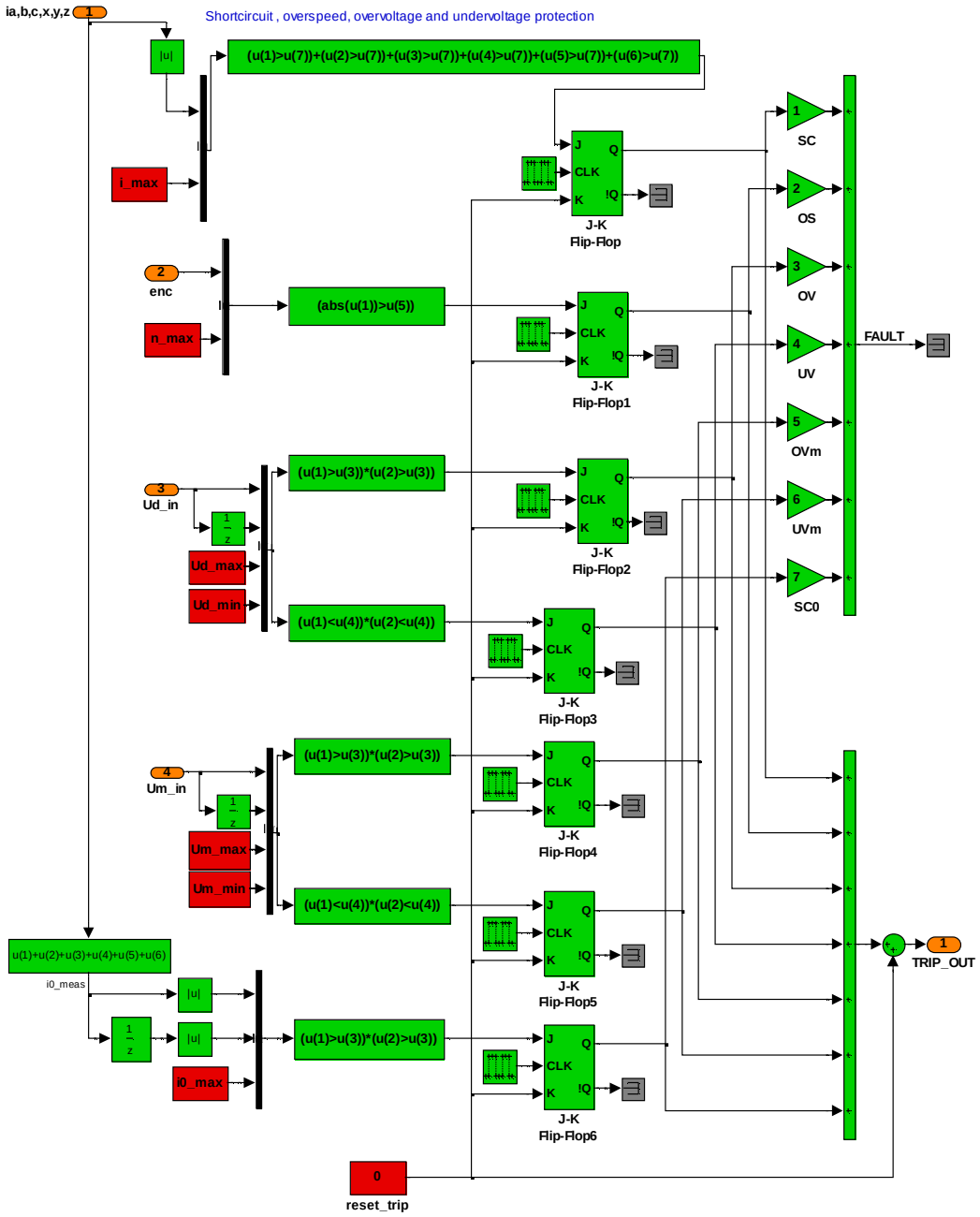

Figure 96 | Protection system diagram.

In the “Protection” block the measurements are monitored. If the absolute value of one of the six phase currents, the zero current or the speed is higher than a certain limit, the controller is stopped. The controller is also stopped if the *DC-link* or the

DC-midpoint voltage is outside certain limits. If an error occurs a fault message can be generated from the fault number.

In Figure 97 a simple *U/f control* diagram is shown. This diagram is inside the "Voltage control" block in Figure 92. The general idea is to calculate the *PWM* output to the VLT's and the torque reference to the load. Measurements are filtered according to the necessary control bandwidth and noise level, in the blocks "butter". In this simple controller the only measurement that is used is the *DC-link* voltage, which is used to calculate the duty cycle. The rest of the measurements are only used for readout and graphs for the *D-Space* user. Two key blocks are the transformation blocks. They rotate voltage and current vectors back and forth between rotating and stationary values (see 5.2.1 & 5.3.1). The rotation angle is the integral of the field speed, which is set from the reference frequency. This means that the voltage amplitude of the first and 3rd harmonic can now be given (preferably as a constant times the frequency to fix the flux level in the motor). The duty cycle goes into a *D-Space* block that generates the *PWM* output to the VLT's.

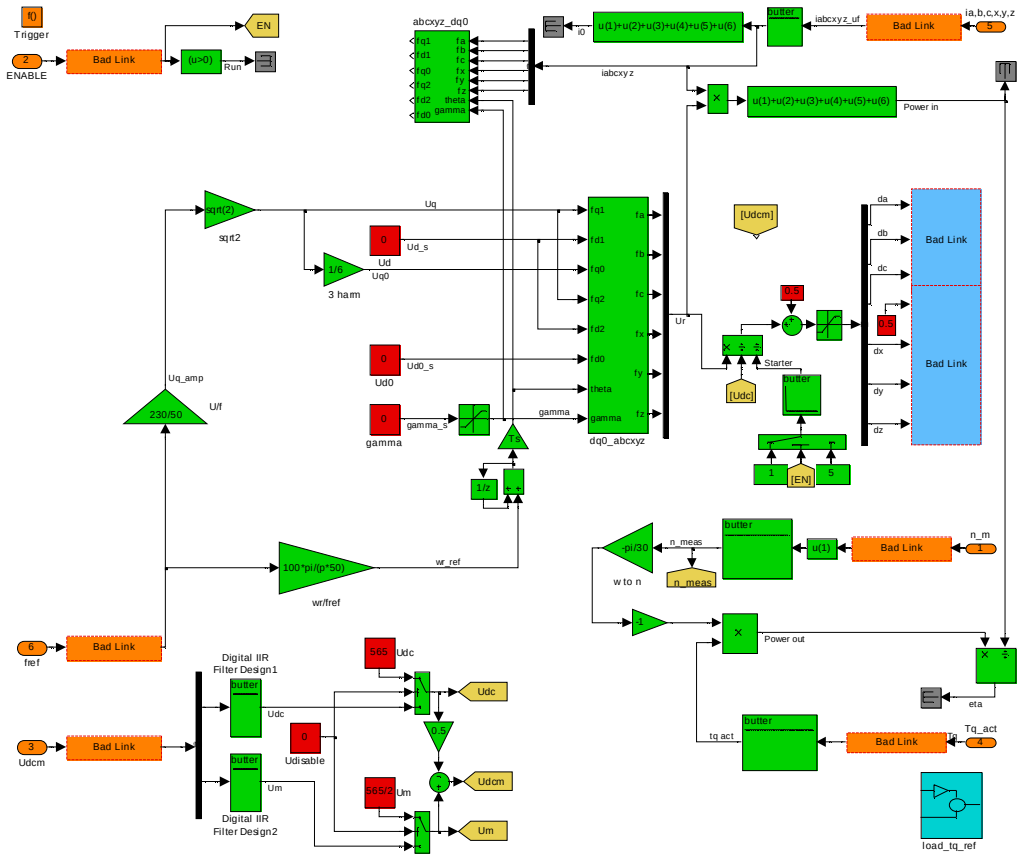

Figure 97	Voltage control diagram.

Instead of the *U/f controller* (Voltage control block) just mentioned, a more advanced current controller can be implemented. This block is shown in Figure 98. A detailed description of the control procedure is discussed in 5. The general idea is to control and limit the phase currents and to have a speed loop to control the speed.

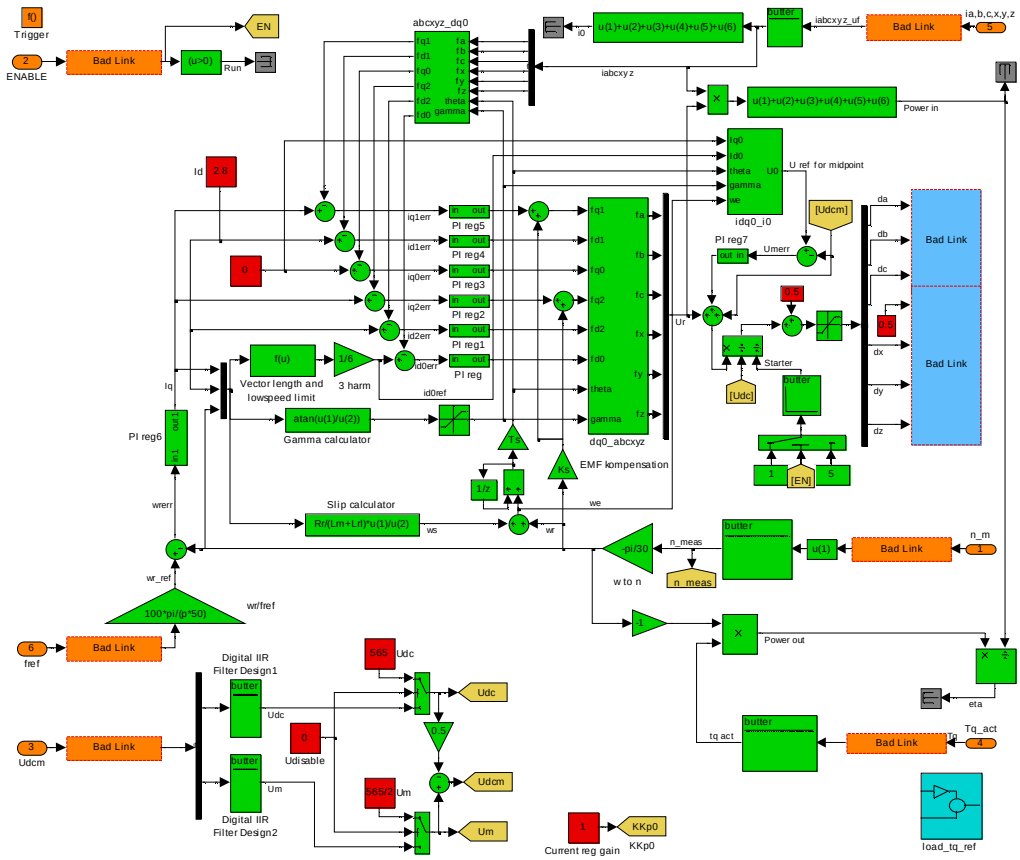

Figure 98 Current control diagram.

The last block to bring up is called “load_tq_ref” (see Figure 99), it exist in both the voltage and current control block diagrams. This block gives the possibility to make the load machine simulate different loads or applications. The idea is to make the load torque speed dependent, and to scale and calibrate the output torque. The load settings are linear, quadratic, cubic and constant torque dependency of speed.

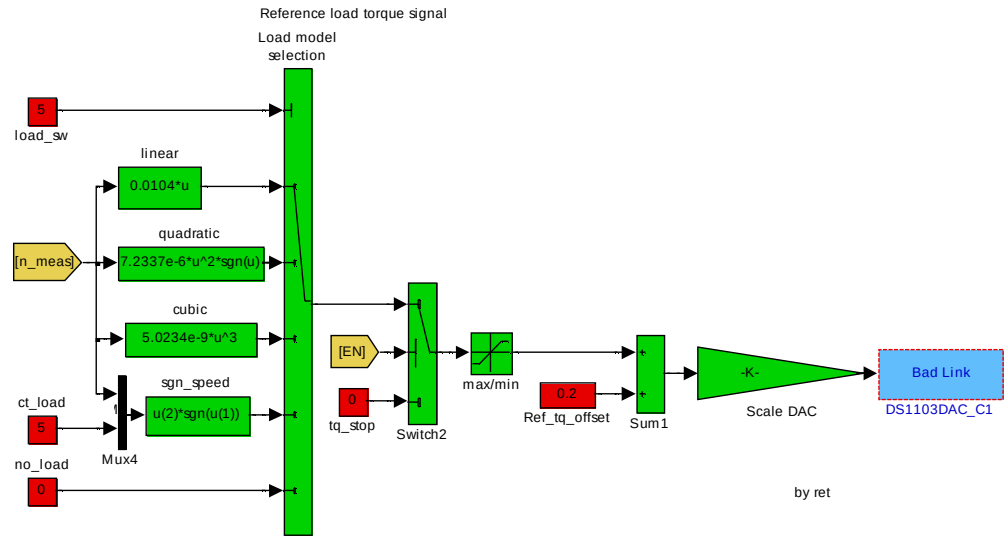

Figure 99 Load torque conditioning diagram.

Control desktop cockpit views

When the code is generated it is run on the *D-Space* card and the link to *Matlab*/*Simulink* can be broken (alternatively *Matlab*/*Simulink* can be used to control parameters, gain and so on). The *D-Space* system has a human interface to control the test online. This works generally speaking as a cockpit. The cockpit is programmed for the individual application. Constants and gain blocks in *Simulink* can be altered during operation. This provides the inputs to the test system. The signals can be displayed as output from *Simulink* in a variety of ways including digital and analog readouts, graphs aso.

There are four cockpit views build for controlling the six-phase motor. There is one view for voltage control (Figure 101), current control (Figure 102), calibration (Figure 100) and extra signals (not shown).

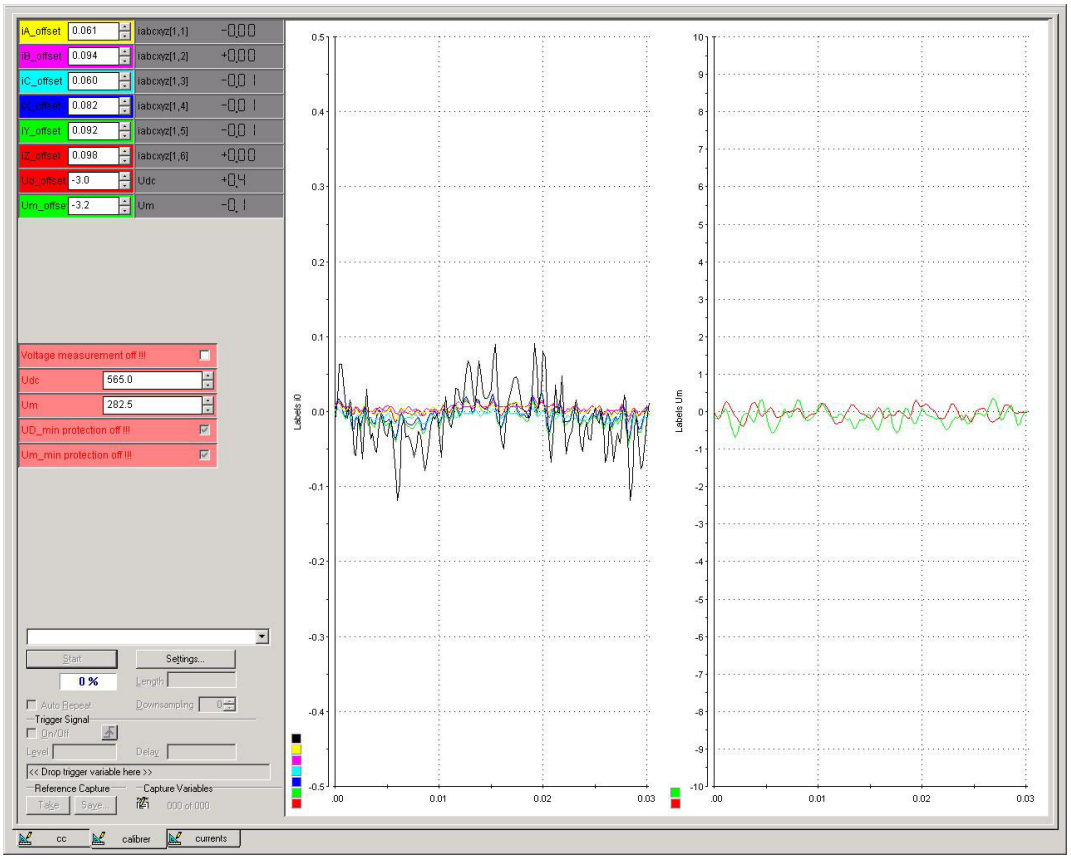

Figure 100 | Calibration view build in the *D-Space* control desktop.

On the calibration view (see Figure 100) the offset of the six currents and the two voltages are entered. When this calibration takes place the *DC-link* voltage should be short circuited.

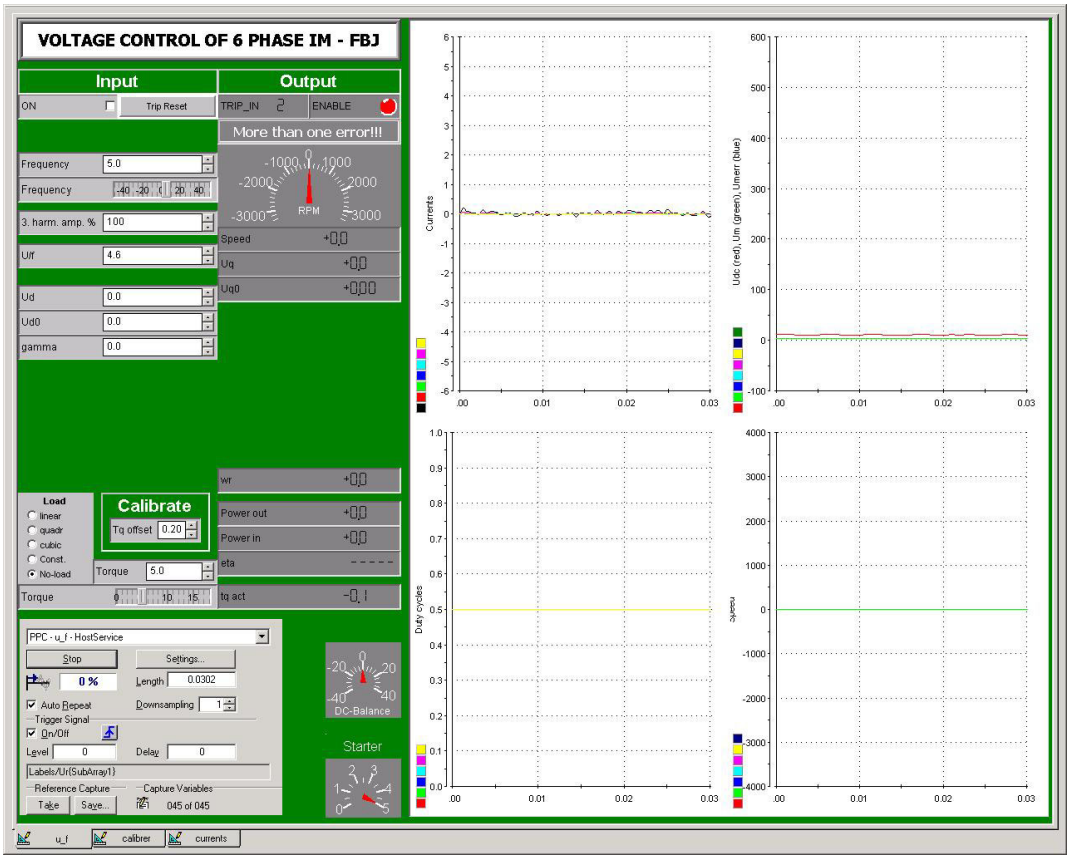

Figure 101 | Voltage control view build in *D-Space*.

The voltage control view (Figure 101) is used if *U/f control* is required. The current control view (Figure 102) is used if current control is required. On both views inputs are light gray (placed on the left) and readouts are dark gray (placed on the right). The graphs on the *U/f controller* show the six phase currents, the zero current, the *DC-link* voltage, the DC-midpoint voltage, the duty cycles and the speed. The graphs on the current controller show the six phase currents, the zero current, the *DC-link* voltage, the DC-midpoint voltage, the duty cycles, the error signals from the six current controllers and the error signal from the speed controller.

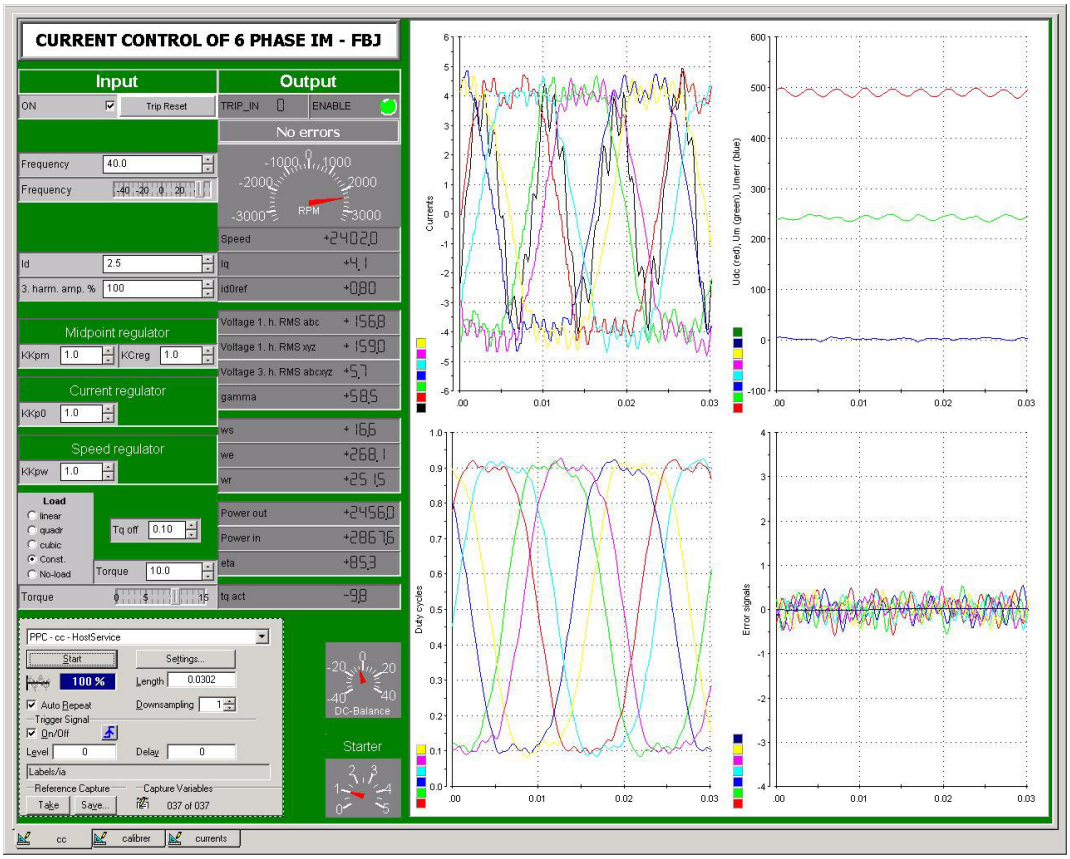

Figure 102	Current control view build in *D-Space*.

B. Simulation software

The simulation software used for verification of the control system and verification of the *MWI* model are described in this Appendix.

The *MWI* model

The *MWI* model of an n-phase motor described in 3.3 is implemented in a C file and compiled to a block in *Simulink*. This is done to make the simulation as fast as possible and at the same time keep the flexibility and transparency of *Simulink* blocks. The main part of the program is written by Pierre Vadstrup and Grundfos Management A/S has all the copyright, therefore the C-code is not shown here. The time dependent input to the block is a stator voltage vector and the torque. The fixed input parameters are: *Ws, vs, vr, K, Lss, Lrr, rs, rb, rea, reb, Jm+Jl, p, x0, KOB*. The outputs from the model are stator current, rotor current, air-gap torque, speed and position.

Complete simulation block diagram

Now the complete block diagram can be presented. The simulation program is build in the *Matlab*/*Simulink* environment. The block diagram is shown in figure 6.

Generally the block diagram is build like mentioned in the main chapters of the thesis. The green blocks symbolize what happens in the controller (see chapter 5). The orange blocks in the right is the output from the motor model. The blue blocks model hardware components like i.e. the motor, load, inverter and a disturbance of the zero current. The disturbing DC current is introduced to test the midpoint regulator (see section 6.4). The motor model is the high order model described in chapter 3. A dq-axis model of the motor (see Appendix C) is not used for simulation purpose, only for the design of the controllers.

The EMF feed forward compensation is as mentioned in the current controller section 5.3.5 a function of both magnetizing current (flux) and rotor speed (ω_r). This is not implemented in the simulation program because i_d is assumed to be constant. But if i_d is changed during operation (i.e. to minimize iron loss during part load) the performance of the controller can be improve if the current dependency is included in the voltage compensation.

The currents i_q and i_d can be changed in steps, pulsed or constant. Furthermore the active current i_q can be controlled by the speed controller.

The transportation delay is introduced to avoid algebraic loops, which speed up simulation time considerably. The transportation delay can also be seen as a simple model of a motor cable. The delay time is set to 2µs or 100 times as fast as the switching frequency for the inverter, so it has almost no effect on the performance. In comparison the dead-time between upper and lower switching is 1.5µs.

In the simulation diagram a pump is used as load for the six-phase induction motor. This is just to try the simulation program with a realistic application. Furthermore load torque pulses or measured torque from a file can be used as input to the simulation.

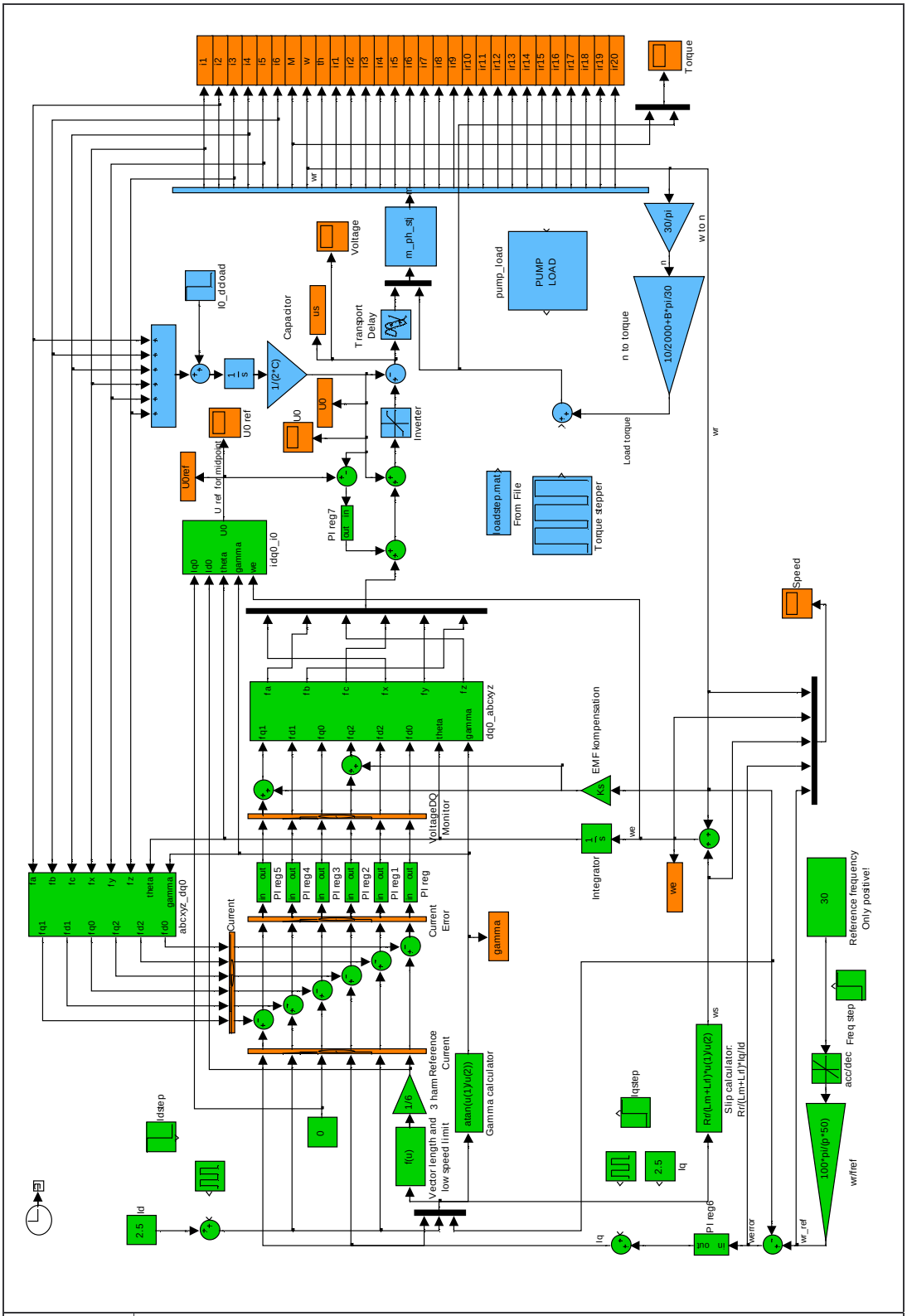

Figure 103 | *Simulink* block diagram for control system and motor model.

Steady state values from dynamic simulations

SPEED to Excel

The basis form all the simulation is a static calculation of the motor parameters for a three-phased motor. In Grundfos the simulation software *SPEED* is used for these calculations. The *SPEED* parameters are copied into an Excel sheet, where the multi winding model parameters are calculated. In the Excel sheet the parameters are categorized in the four main groups:

1. **General information**. The values in this part are mainly about the winding design, and refer to the *SPEED* calculation.
2. **Calculation results from SPEED**. This part contains data about the calculated characteristic for the motor.
3. **Parameters from SPEED**. This part contains calculated parameters for the motor like for example the equivalent circuit parameters.
4. **Parameters for multi winding model**. The parameters in point 3 have to be recalculated to be usable for the multi winding model. This is done in the fourth part.

The Excel sheet for the example is in Appendix D. Here 3, 6, 12, 5 and 9 phase-motors are presented. The numbers in the sheet have different colors dependent on where they come from. The green color numbers comes directly from the *SPEED* calculation. Yellow numbers are calculated in the sheet, where the equation is shown in the equation column. If a multi phase motor has to be calculated a three-phase calculation is always the basis. The blue colored numbers are directly copied from the three-phased calculation, assuming that the multiphase motor has the same characteristic. The red numbers are more complex changes from the three phase case, i.e. the resistances are calculated using the *SPEED* software. But in most cases an equation to calculate the red numbers also exist, assuming linearity with number of phases. In the sheet it is also possible to change the number of slots in both the rotor and stator. The assumptions are relatively simple but they are necessary because *SPEED* is not able to make calculations on multiphase motors. Therefore a motor design program able to design a multiphase motor more correctly is required. It would therefore be advisable to extend the *SPEED* model to include the *MWI* model so that the best from both models can be combined in a strong motor design software.

Excel to M-file

The calculated parameters from the Excel file (number 4 in the above section) are now copied into the m-file. Here the winding design (the number of wires in each slot for each phase) has to be defined. The matrices *Lss* and *Lrr* are setup on the basis of parameters from Excel. Finally the starting values for the integration variables in the differential equations are initialized.

The power supply input for the motor

In another m-file the supply for the motor is chosen. There exist a range of different supplies to try (see 3.3.4).

Steady state output variables

When the supply is configured the simulation can be run. After the simulation has reached the steady state condition, which in the test example means a stable speed, the steady state variables can be extracted, calculated and inserted in an Excel sheet for comparison with other simulations (see Appendix E). The torque is calibrated so the output power is very close to nominal 3kW.

To compare motors with different number of phases and different supply, it is essential to calculate all the relevant steady state variables. The outputs from the simulations are e.g. the *RMS* value of the 1st harmonic of the voltage and current and the *RMS* value of the torque ripple. Therefore an FFT analysis of the phase voltage, phase current and the shaft torque is made.

List of steady state variables calculated after simulation

Both the input and output steady state variables are explained under the following points. The variables are used in the table in Appendix E:

- **Sim. Prog.:** The simulation program used for the simulations. Basically there are only two programs the *SPEED* program and the *MWI* model. There is only one simulation from the *SPEED* program, and this simulation is used for reference purpose only. The simulations with the text “Multiwinding” are all done with the star-point of the motor connected to the midpoint of the DC voltage capacitor. The simulations with the text “M_ph_stj” could be a simulation both with the star-point connected and with the star-point floating. More information about the coupling can be seen on the parameter “Source”.
- **Source:** The input source for the simulation (see 3.3.4).
- **Ph:** The number of phases.
- **U 1.h:** Amplitude of the 1st harmonic of the phase voltage.
- **I 1.h:** Amplitude of the 1st harmonic of the phase current.
- **I RMS:** Root mean square value of the phase current.
- **I p:** Peak value of the phase currents.
- **U fp:** Peak value of the phase voltages.

- **RPM:** Speed of the rotor.
- **St. Cu loss:** The *RMS* value of the stator currents squared and multiplied with the stator resistances.
- **Ro. Cu loss:** The *RMS* value of the circulating rotor currents squared and multiplied with the rotor end-ring resistances, plus the *RMS* value of the current in the bars (the sum of the currents in the two loops on each side of the bar) squared multiplied with the resistance in the bars. See Figure 23.
- **Torq:** The mean value of the air-gap torque. To calculate the torque on the shaft the windage, mechanical friction and iron loss has to be subtracted from the air gap torque.
- **Torque ripple:** Torque ripple on the motor shaft (see 3.3.3).
- $\mathbf{B}_{rtpk}$**:** Peak value of flux density in the rotor tooth (see 3.3.3).
- $\mathbf{B}_{stpk}$**:** Peak value of flux density in the stator tooth (see 3.3.3).
- $\mathbf{B}_{sypk}$**:** Peak value of the flux density in the stator yoke (see 3.3.3).
- **R:** A check of the flux density values compared to the reference values from the reference simulation. If an R is returned it means that one or more of the flux densities are higher than in the reference simulation. If + is returned then the input voltage can be increased with some percent (see the parameter "%").
- **%:** An estimate of how much the voltage has to be increased/decreased before all the calculated flux densities (stator yoke, stator teeth and rotor teeth) still will be lower than the flux densities in the reference simulation.
- **S:** Returns an S, if one of the flux densities becomes higher than the saturation value of iron, in this case set to 1.9T. Otherwise returns nothing. R, % and S are used to calibrate the input voltage to a realistic value, where the calculations can be compared.
- **Cu loss:** The sum of "St. Cu loss" and "Ro. Cu loss".
- **Fe:** The iron loss in the motor can be estimated on the basis of the three above mentioned peak flux densities in the motor, the calculation of iron loss is shown in equation (33) and explained in 3.3.3.
- **P2 w.loss:** The air-gap power. Calculated from "Torq" multiplied by "RPM", which is converted to radians pr. second.
- **P2 shaft:** The shaft power. Calculated as "P2 w.loss" minus "Fe" and the mechanical friction taken from the *SPEED* calculation.

- **I RMS 3-ph:** The *RMS* value of the current, if the motor were three phased. Calculated as "I *RMS*" times "Ph" divided by three.
- **I p 3-ph:** The peak value of the current, if the motor were three phased. Calculated as "I p" times "Ph" divided by three.
- **Eta:** The efficiency of the motor. "P2 shaft" divided by the sum of "P2 w. loss" and "Cu loss".
- **Sim:** The simulation number.
- **Notes:** Notes to the simulation
- **VA peak:** The peak phase voltage times the peak phase ampere rating of the converter.

Simulation steps

The following is a list of the explained steps necessary to make the comparisons simulation:

1. Extract parameters from three-phase calculation in *SPEED* software.
2. Calculate parameters for multiphase motor in Excel file.
3. Setup and run initialization file in *Matlab*.
4. Chose supply type and make reference voltage or current in *Matlab*.
5. Run simulation in *Simulink*.
6. Extract steady state characteristics for the motor and the inverter in *Matlab*.
7. Store the results in Excel for comparison this is done automatically with *Matlab*.

C. dq-axis model of six-phase induction motor

In this Appendix a simpler motor model than the *MWI* model analyzed in chapter 3 is set up. The traditional dq-axis model of an induction motor is expanded to six phases in [1]. The six-phase dq-axis model, which includes 3rd harmonic current, is presented. At last the motor parameters for the six-phase model are calculated and the model is compared to the multiwinding model mentioned in chapter 3.

Six-phase dq-axis model with 3rd harmonic included

Just like a three phase asynchronous motor the six-phase motor can be modelled using a dq-axis model. A model was presented in 2002 [1]. The characteristic transient voltage and flux equations of a six-phase induction motor are presented in equation (64), (65), (66) and (67). The equations are shown in a reference frame rotating with the speed ω see Figure 52.

$$\begin{bmatrix} v_{sq1} \\ v_{sd1} \\ v_{sq0} \\ v_{sq2} \\ v_{sd2} \\ v_{sd0} \end{bmatrix} = \frac{d}{dt}\begin{bmatrix} \lambda_{sq1} \\ \lambda_{sd1} \\ \lambda_{sq0} \\ \lambda_{sq2} \\ \lambda_{sd2} \\ \lambda_{sd0} \end{bmatrix} + \omega\begin{bmatrix} \lambda_{sd1} \\ -\lambda_{sq1} \\ 0 \\ \lambda_{sd2} \\ -\lambda_{sq2} \\ 0 \end{bmatrix} + 3\omega\begin{bmatrix} 0 \\ 0 \\ \lambda_{sd0} \\ 0 \\ 0 \\ -\lambda_{sq0} \end{bmatrix} + \begin{bmatrix} r_s & 0 & 0 & 0 & 0 & 0 \\ 0 & r_s & 0 & 0 & 0 & 0 \\ 0 & 0 & r_s & 0 & 0 & 0 \\ 0 & 0 & 0 & r_s & 0 & 0 \\ 0 & 0 & 0 & 0 & r_s & 0 \\ 0 & 0 & 0 & 0 & 0 & r_s \end{bmatrix}\begin{bmatrix} i_{sq1} \\ i_{sd1} \\ i_{sq0} \\ i_{sq2} \\ i_{sd2} \\ i_{sd0} \end{bmatrix} \quad (64)$$

Where:	***Var***	***Description***
	v,λ,i	*Refers to voltage, fluxlinkage and current respectively.*
	r_s	*Stator resistance in one phase. (In test case 4.719Ω)*
	x_s	*Stands for stator component of x.*
	x_q,x_d	*Stands for q and d axis respectively of x.*
	x_0	*The 3rd harmonic system of x.*
	x_1,x_2	*The first and the second three phase system of x.*

$$\begin{bmatrix} v_{rq} \\ v_{rd} \\ v_{rq3} \\ v_{rd3} \end{bmatrix} = \frac{d}{dt}\begin{bmatrix} \lambda_{rq} \\ \lambda_{rd} \\ \lambda_{rq3} \\ \lambda_{rd3} \end{bmatrix} + (\omega-\omega_r)\begin{bmatrix} \lambda_{rd} \\ -\lambda_{rq} \\ 0 \\ 0 \end{bmatrix} + 3(\omega-\omega_r)\begin{bmatrix} 0 \\ 0 \\ \lambda_{rd3} \\ -\lambda_{rq3} \end{bmatrix} + \begin{bmatrix} r_r & 0 & 0 & 0 \\ 0 & r_r & 0 & 0 \\ 0 & 0 & r_{r3} & 0 \\ 0 & 0 & 0 & r_{r3} \end{bmatrix}\begin{bmatrix} i_{rq} \\ i_{rd} \\ i_{rq3} \\ i_{rd3} \end{bmatrix} \quad (65)$$

Where:	***Var***	***Description***
	v,λ,i	*Refers to voltage, fluxlinkage and current respectively.*
	r_r,r_{r3}	*Rotor resistance of the first and the 3rd harmonic system.*
	x_r	*Stands for rotor.*
	x_q,x_d	*Stands for q and d axis respectively.*
	x_3	*The 3rd harmonic system.*

Note that in equation (65) the equation for the zero sequence system is not included like shown in [1], instead the zero sequence is modeled in 5.4.5.

$$\begin{bmatrix} \lambda_{sq1} \\ \lambda_{sd1} \\ \lambda_{sq0} \\ \lambda_{sq2} \\ \lambda_{sd2} \\ \lambda_{sd0} \\ \lambda_{rq} \\ \lambda_{rd} \\ \lambda_{rq3} \\ \lambda_{rd3} \end{bmatrix} = L_{dq} \begin{bmatrix} i_{sq1} \\ i_{sd1} \\ i_{sq0} \\ i_{sq2} \\ i_{sd2} \\ i_{sd0} \\ i_{rq} \\ i_{rd} \\ i_{rq3} \\ i_{rd3} \end{bmatrix} \tag{66}$$

$$L_{dq} = \begin{bmatrix} L_{ls}+L_{lm}+L_m & 0 & 0 & L_{lm}+L_m & 0 & 0 & L_m & 0 & 0 & 0 \\ 0 & L_{ls}+L_{lm}+L_m & 0 & 0 & L_{lm}+L_m & 0 & 0 & L_m & 0 & 0 \\ 0 & 0 & L_{ls}+L_{m3} & 0 & 0 & 0 & 0 & 0 & cL_{m3} & sL_{m3} \\ L_{lm}+L_m & 0 & 0 & L_{ls}+L_{lm}+L_m & 0 & 0 & L_m & 0 & 0 & 0 \\ 0 & L_{lm}+L_m & 0 & 0 & L_{ls}+L_{lm}+L_m & 0 & 0 & L_m & 0 & 0 \\ 0 & 0 & 0 & 0 & 0 & L_{ls}+L_{m3} & 0 & 0 & -sL_{m3} & cL_{m3} \\ L_m & 0 & 0 & L_m & 0 & 0 & L_{lr}+L_m & 0 & 0 & 0 \\ 0 & L_m & 0 & 0 & L_m & 0 & 0 & L_{lr}+L_m & 0 & 0 \\ 0 & 0 & cL_{m3} & 0 & 0 & -sL_{m3} & 0 & 0 & L_{lr3}+L_{m3} & 0 \\ 0 & 0 & sL_{m3} & 0 & 0 & cL_{m3} & 0 & 0 & 0 & L_{lr3}+L_{m3} \end{bmatrix}$$

Where:	*Var*	*Description*
	λ,i	*Refers to flux-linkage and current respectively. Same sub notation as described in equation (64) & (65).*
	L_{ls}	*Leakage inductance in each stator phase. 1st harmonic system.*
	L_{lr}	*Leakage inductance in rotor phase. 1st harmonic system.*
	L_{lr3}	*Leakage inductance in rotor phase. 3rd harmonic system.*
	L_{lm}	*Leakage inductance in each axis of the stator. 1st harmonic system.*
	L_m	*Magnetising inductance for each axis. 1st harmonic system.*
	L_{m3}	*Magnetising inductance for each axis. 3rd harmonic system.*

$$\begin{aligned} s &= \sin(3\gamma) \\ c &= \cos(3\gamma) \end{aligned} \tag{67}$$

Where:	*Var*	*Description*
	γ	*The angle between the 3rd harmonic and the 1st harmonic component (see 5.3.2).*

State-space model

The voltage and flux equations can also be written in State Space, like shown in equation (68).

$$\frac{d}{dt}\begin{bmatrix}\lambda_{sq1}\\ \lambda_{sd1}\\ \lambda_{sq0}\\ \lambda_{sq2}\\ \lambda_{sd2}\\ \lambda_{sd0}\\ \lambda_{rq}\\ \lambda_{rd}\\ \lambda_{rq3}\\ \lambda_{rd3}\end{bmatrix} = \left(-\Omega - R\cdot L_{dq}^{-1}\right)\begin{bmatrix}\lambda_{sq1}\\ \lambda_{sd1}\\ \lambda_{sq0}\\ \lambda_{sq2}\\ \lambda_{sd2}\\ \lambda_{sd0}\\ \lambda_{rq}\\ \lambda_{rd}\\ \lambda_{rq3}\\ \lambda_{rd3}\end{bmatrix} + I\cdot\begin{bmatrix}v_{sq1}\\ v_{sd1}\\ v_{sq0}\\ v_{sq2}\\ v_{sd2}\\ v_{sd0}\\ v_{rq}\\ v_{rd}\\ v_{rq3}\\ v_{rd3}\end{bmatrix}$$

$$\begin{bmatrix}i_{sq1}\\ i_{sd1}\\ i_{sq0}\\ i_{sq2}\\ i_{sd2}\\ i_{sd0}\\ i_{rq}\\ i_{rd}\\ i_{rq3}\\ i_{rd3}\end{bmatrix} = L_{dq}^{-1}\begin{bmatrix}\lambda_{sq1}\\ \lambda_{sd1}\\ \lambda_{sq0}\\ \lambda_{sq2}\\ \lambda_{sd2}\\ \lambda_{sd0}\\ \lambda_{rq}\\ \lambda_{rd}\\ \lambda_{rq3}\\ \lambda_{rd3}\end{bmatrix} + 0\cdot\begin{bmatrix}v_{sq1}\\ v_{sd1}\\ v_{sq0}\\ v_{sq2}\\ v_{sd2}\\ v_{sd0}\\ v_{rq}\\ v_{rd}\\ v_{rq3}\\ v_{rd3}\end{bmatrix} \qquad (68)$$

Where Ω and R are defined in equation (69) and (70) respectively.

$$\Omega = \begin{bmatrix} 0 & \omega & 0 & 0 & 0 & 0 & 0 & 0 & 0 & 0 \\ -\omega & 0 & 0 & 0 & 0 & 0 & 0 & 0 & 0 & 0 \\ 0 & 0 & 0 & 0 & 0 & 3\omega & 0 & 0 & 0 & 0 \\ 0 & 0 & 0 & 0 & \omega & 0 & 0 & 0 & 0 & 0 \\ 0 & 0 & 0 & -\omega & 0 & 0 & 0 & 0 & 0 & 0 \\ 0 & 0 & -3\omega & 0 & 0 & 0 & 0 & 0 & 0 & 0 \\ 0 & 0 & 0 & 0 & 0 & 0 & 0 & (\omega-\omega_r) & 0 & 0 \\ 0 & 0 & 0 & 0 & 0 & 0 & -(\omega-\omega_r) & 0 & 0 & 0 \\ 0 & 0 & 0 & 0 & 0 & 0 & 0 & 0 & 0 & 3(\omega-\omega_r) \\ 0 & 0 & 0 & 0 & 0 & 0 & 0 & 0 & -3(\omega-\omega_r) & 0 \end{bmatrix} \quad (69)$$

$$R = \begin{bmatrix} r_s & 0 & 0 & 0 & 0 & 0 & 0 & 0 & 0 & 0 \\ 0 & r_s & 0 & 0 & 0 & 0 & 0 & 0 & 0 & 0 \\ 0 & 0 & r_s & 0 & 0 & 0 & 0 & 0 & 0 & 0 \\ 0 & 0 & 0 & r_s & 0 & 0 & 0 & 0 & 0 & 0 \\ 0 & 0 & 0 & 0 & r_s & 0 & 0 & 0 & 0 & 0 \\ 0 & 0 & 0 & 0 & 0 & r_s & 0 & 0 & 0 & 0 \\ 0 & 0 & 0 & 0 & 0 & 0 & r_r & 0 & 0 & 0 \\ 0 & 0 & 0 & 0 & 0 & 0 & 0 & r_r & 0 & 0 \\ 0 & 0 & 0 & 0 & 0 & 0 & 0 & 0 & r_{r3} & 0 \\ 0 & 0 & 0 & 0 & 0 & 0 & 0 & 0 & 0 & r_{r3} \end{bmatrix} \quad (70)$$

The equations can also be presented in an electrical diagram, which is shown in Figure 104, Figure 105, Figure 106 and Figure 107.

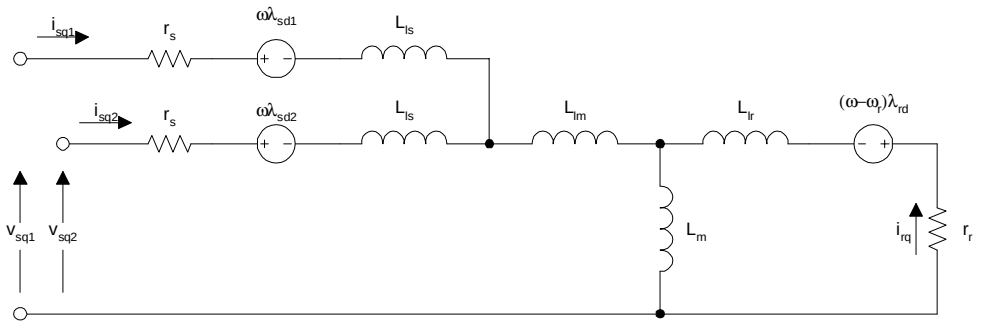

Figure 104	q-axis model of six-phase motor. For fundamental components.

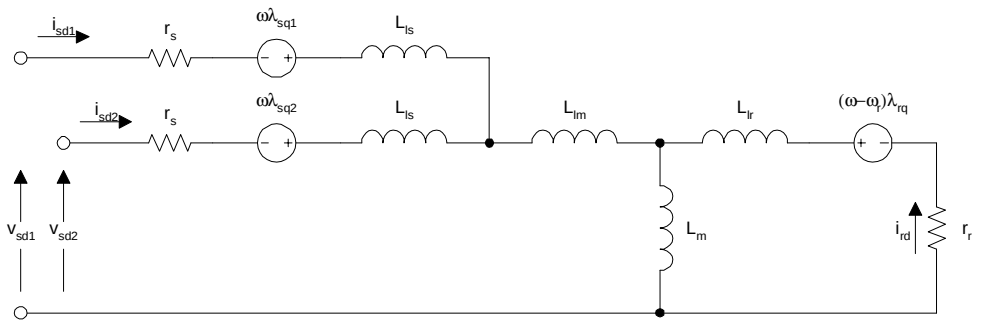

Figure 105	d-axis model of six-phase motor. For fundamental components.

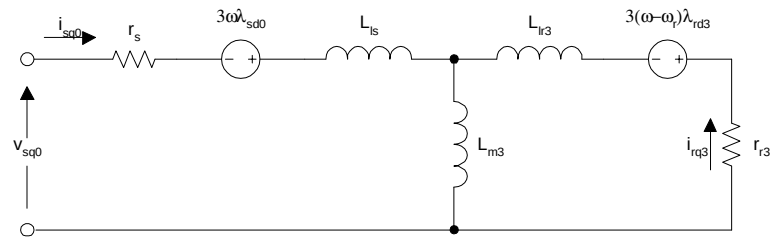

Figure 106	q-axis model of six-phase motor. For 3rd harmonic components with $\gamma=0$.

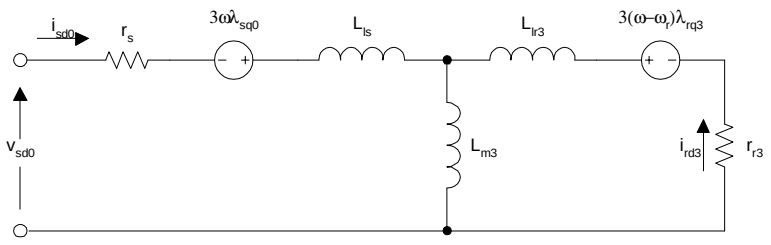

Figure 107	d-axis model of six-phase motor. For 3rd harmonic components with γ=0.

The shaft torque is shown in equation (71).

$$T_e = \left(\frac{P}{2}\right)\left(\frac{3}{2}\right)L_m\left(\left(i_{sq1}+i_{sq2}\right)\cdot i_{rd}-\left(i_{sd1}+i_{sd2}\right)\cdot i_{rq}\right)+ \left(\frac{P}{2}\right)(3)L_{m3}\left(\cos(3\gamma)\cdot\left(i_{sq0}\cdot i_{rd3}-i_{sd0}\cdot i_{rq3}\right)-\sin(3\gamma)\cdot\left(i_{sd0}\cdot i_{rd3}-i_{sq0}\cdot i_{rq3}\right)\right) \quad (71)$$

Where:	***Var***	***Description***
	P	*The number of poles.*

With these equations the six-phase induction motor can be simulated, and a controller can be designed using linear control theory.

Calculation of motor parameters from multiwinding model

The multiwinding model introduced in chapter 3 can be used for verifying the dq-axis model and the parameters in the six-phase dq-axis model presented just above. This means that the relative complicated physically based multiwinding model is simplified considerably, which is a great advantage when dimensioning the controller later in the chapter.

The *MWI* model is simulated in *Simulink* running at no-load and blocked rotor conditions, with fixed dq-axis voltages to the motor, and the steady state dq-axis currents are calculated. The model is linear, because the speed is fixed (see equation (68)), which makes it possible to use super positioning. This means that the 1st harmonic and the 3rd harmonic components can be calculated independent of each other.

Parameter calculation

For the 1st harmonic the following parameters have to be found: R_s, L_{ls}, L_{lm}, L_m, L_{lr} and R_r. For the 3rd harmonic only the parameters: L_{m3}, L_{lr3} and R_{r3} have to be found, since $R_{s3}=R_s$ and $L_{ls3}=L_{ls}$.

To find the rotor parameters three general expressions are first described here. The general expression, for transformation of rotor parameters to the stator side T-equivalent diagram for an induction motor, is shown in equation (72). This expression is merged between the two different sources [18] and the *SPEED* software.

$$k_{r\_RS} = \frac{4 \cdot f \cdot T_{ph}^{\,2} \cdot k_{w1}^{\,2}}{m \cdot k_{s1}^{\,2}} \tag{72}$$

Where:	***Var***	***Description***
	k_{r_RS}	*Transformation factor from rotor to stator side.*
	f	*The number of stator phases.*
	T_{ph}	*Number of series connected turns per phase.*
	k_{w1}	*Winding factor for stator winding.*
	k_{s1}	*Winding factor for rotor winding.*

The second general expression is the conversion of rotor end-ring resistance to rotor-bar resistance (73). After this the rotor-bar resistance is just extended with an equivalent value for the end-ring [10].

$$r_{bar\_ex} = r_{bar} + \frac{r_{end}}{2\left(\sin\left(\frac{\pi \cdot P}{2 \cdot m}\right)\right)} \tag{73}$$

Where:	***Var***	***Description***
	r_{bar_ex}	*Extended rotor-bar resistance.*
	r_{bar}	*Rotor-bar resistance.*
	r_{end}	*Rotor-end-ring resistance.*
	P	*The number of poles.*
	m	*The number of rotor loops, slots or bars.*

The last general expression (74) is for the conversion of rotor end-ring leakage to rotor-bar leakage combined with an expression of the zig-zag lekage inductance [10], [18].

$$l_{bar\_ex} = l_{bar} + \frac{l_{end}}{2\left(\sin\left(\frac{\pi P}{2m}\right)\right)} + \frac{\pi}{2} K_l \left(\frac{1}{m \cdot \sin\left(\frac{3\pi P}{2m}\right)^2} - \frac{{k_{s1}}^2 \cdot m}{f} \right) \quad (74)$$

Where:	Var	Description
	l_{bar_ex}	*Extended rotor-bar leakage.*
	l_{bar}	*Rotor-bar leakage.*
	l_{end}	*Rotor-end-ring leakage.*
	P	*The number of poles.*
	m	*The number of rotor loops, slots or bars.*

K_l is the common inductance constant shown in equation (75).

$$K_l = \frac{ra \cdot l \cdot \mu_0}{d} \quad (75)$$

Where:	Var	Description
	ra	*The radius to the air-gap.*
	l	*The length of the rotor.*
	d	*The width of the air-gap.*
	μ_0	*Vacuum permability.* $\pi \cdot 4 \cdot 10^{-7}$

R_s is the same as the one used in the *MWI*. In both models this value is calculated as an external value using *SPEED*.

L_{ls} is the same as the one used in the *MWI*. In both models this value is calculated as an external value using *SPEED*.

L_{lm} is the common leakage inductance between the two three phase systems. In the *MWI* all inductances that do not connect across the air-gap have to be set externally before simulation. In both the *MWI* and the dq-axis model, it is therefore chosen to set this value to zero. The value L_{lm} is calculated analytically in [12].

L_m is the magnetizing inductance. This inductance is placed where the two three phase systems have been connected (see Figure 104 and Figure 105). This means that the inductance is common for both systems, and it can be calculated like the magnetizing inductance for an equivalent three phase winding. This can be found by using super positioning of the windings (or the *MMF*) like this *a*+*x*, *b*+*y* and *c*+*z*. The result is divided by 2, and the inductance is found using equation (31).

L_{lr} is the rotor leakage inductance for the 1st harmonic. This value is calculated by transforming the leakage inductance on the rotor bars and end-rings to a common leakage inductance seen from the stator side. This involves two different processes. First a process of converting the end-ring leakage to an extra bar leakage (74) and second a process of converting the bar leakage inductance to the stator side (72).

R_r is the rotor resistance for the 1st harmonic. This value is calculated by transforming the resistance inductance on the rotor bars and end-rings to a common resistance inductance seen from the stator side. This involves two different processes. First a process of converting the end-ring resistance to an extra bar resistance (74) and second a process of converting the bar resistance inductance to the stator side (72).

L_{m3} is the magnetizing inductance for the 3rd harmonic. Just like the 1st harmonic magnetizing inductance, L_{m3} can be found using super positioning. Here the 3rd harmonic is in phase for *abc* and *xyz*, so the two phases used for the 3rd harmonic is $a+b+c$ and $x+y+z$. The result is divided by 3, and the inductance is found using equation (31).

L_{lr3} is calculated in exactly the same way as L_{lr}. The only thing to remember is that the 3rd harmonic is a 6/3=2 phase model and it has 2*3=6 poles. The number of series connected turns is calculated by using super positioning in the same way as done when finding L_{m3}. This is because the 3rd harmonic is in phase for phase a, b and c and another phase for x, y and z, so the two phase model of the 3rd harmonic has the windings $(W_{sa}+W_{sb}+W_{sc})/3$ and $(W_{sx}+W_{sy}+W_{sz})/3$ (see also Figure 22).

R_{r3} is calculated in exactly the same way as R_{lr}. The only thing to remember is that the 3rd harmonic is a 6/3=2 phase model and it has 2*3=6 poles. The number of series connected turns is calculated by using super positioning in the same way as done when finding L_{m3}. This is because the 3rd harmonic is in phase for phase *a*, *b* and *c* and another phase for *x*, *y* and *z*, so the two phase model of the 3rd harmonic has the windings $(W_{sa}+W_{sb}+W_{sc})/3$ and $(W_{sx}+W_{sy}+W_{sz})/3$ (see also Figure 22).

Test Case

The parameter values for the dq-axis or state-space model are summarised in the equations in (76).

$$
\begin{aligned}
R_s &= R_{s3} = 4{,}7188 \\
L_{ls} &= L_{ls3} = 0{,}018136 \\
L_{lm} &= 0 \\
L_m &= 0{,}3049 \\
L_{lr} &= 0{,}01455 \\
R_r &= 1{,}383 \\
L_{m3} &= 0{,}06420 \\
L_{lr3} &= 0{,}02629 \\
R_{r3} &= 2{,}139
\end{aligned}
\tag{76}
$$

Using the test case as example, a locked rotor and a no load simulation is performed using the *MWI* model. The simulation is linear, therefore the arbitrary simple voltage vector [100 0 100 100 0 0] are used as input. This vector gives 100V in the three q axis, 2 first and 1 3rd harmonic voltages. This voltage vector is transformed using the transformation matrix [Eq. (43)] to *abc-xyz* values and used as input to the *MWI* model. After the *MWI* model the six stator currents are transformed back to the dq-axis reference frame. The simulation circuit looks like shown in Figure 108.

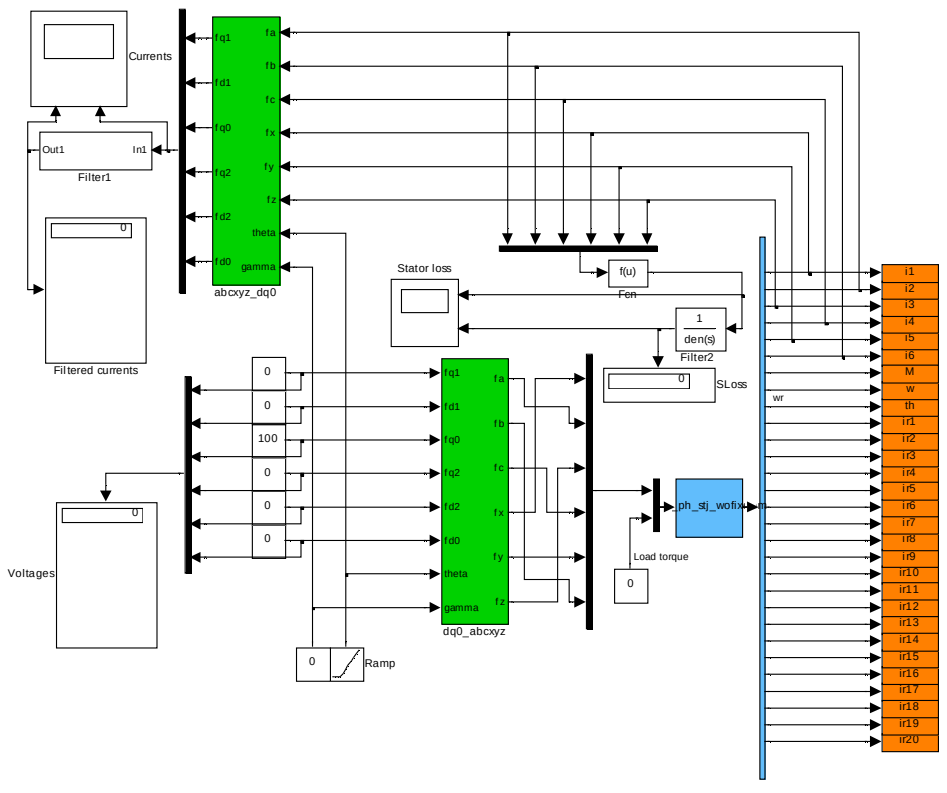

Figure 108	*MWI* model of six-phase motor with dq-axis as input and output. Used for comparison with dq-axis model.

The SS model can also be used to find the steady state currents. First the working point (ω_r) for the machine is selected, then the DC-gain (or steady state amplification) is found using the matlab function “dcgain”. These gain values are then multiplied with the voltage vector and then the steady state currents are found. The resulting six currents from both the *MWI* and the DQ/SS model are compared in the following table:

Blocked rotor currents	**DQ/SS model**	**MWI**	**Diff %**
i_{q1}	2.7692	2.81	1.5
i_{d1}	5.5311	5.537	0.1
i_{q0}	0.46829	0.4505	-3.8
i_{q2}	2.7692	2.815	1.7
i_{d2}	5.5311	5.553	0.4
i_{d0}	2.8038	2.737	-2.4

No-load currents	DQ/SS model	MWI	Diff %
i_{q1}	0.012115	0.01182	-2.4
i_{d1}	0.50655	0.5006	-1.2
i_{q0}	0.078075	0.07878	0.9
i_{q2}	0.012115	0.01187	-2.0
i_{d2}	0.50655	0.5006	-1.2
i_{d0}	1.2839	1.289	0.4

The two models doesn't fit exactly, the biggest difference is 3.8%. One reason for the difference is that the currents from the *MWI* model are filtered mean values. But, since the dq-axis model is only used to design the controller, it doesn't need to be very precise. In any case the controller need to be robust to parameter changes, so the controller need to work with i.e. 30% parameter change, and the model parameters are well within this range.

D. Motor data

On the next two pages is a list with motor data for 3, 5, 6, 9 and 12 phased induction motors most of the parameters are generated with the *SPEED* program.

General information

Name	Description	3 ph.	3 ph. Hot	3 ph. 3h. Hot	6 ph.	6 ph. 3h. Hot	12 ph.	5 ph.	9 ph.	Units	Equation	Note
Slots	Number of slots in stator	24	24	24	24	24	24	20	18			
R_Bars	Number of slots in rotor	20	20	20	20	20	20	16	14			
TC	Number of windings/slot	39	39	39	78	78	156	78	156		TC*Phaser/3*24/Slots	
Tph	Windings/phase	156	156	156	156	156	156	156	156			
kw1	Windingfactor for stator	0.9577	0.9577	0.9577	0.9577	0.9577	0.9577	0.9577	0.9577			
ks1	Windingfactor for rotor	0.9936	0.9936	0.9936	0.9936	0.9936	0.9936	0.9936	0.9936			
Tph1	1. Harm Windingfactor	149.4012	149.4012	149.4012	149.4012	149.4012	149.4012	149.4012	149.4012		Tph*kw1	Compare to Tph1 in SPEED
Phaser	Number of phases	3	3	3	6	6	12	5	9			
Poles	Pole number	2	2	2	2	2	2	2	2			
Ber. Nr.	Calculation number	6279	6279	6279	6979	6979	-	-	-			
Viklingsskema	Winding sheet	(Se 6279)	(Se 6279)	(Se 6279)	96485055	96485055	-	-	-			
SFillHBL	Fillfactor CU	74.1	74.1	74.1	76.2	76.2	76.2	76.2	76.2	%		
Tråd diameter	Winding diameter	(3x0,67)	(3x0,67)	(3x0,67)	2x0,56	2x0,56	0,56	-	-	mm		
Ordrenummer	Order number	85805810	85805810	85805810	-	-	-	-	-			

Calculation results from SPEED

Name	Description	3 ph.	3 ph.	3 ph. 3h.	6 ph.	6 ph. 3h.	12 ph.	5 ph.	9 ph.	Units	Equation	Note
rpm	Mechanical speed	2908	2908	2908	2908	2908	2908	2908	2908	RPM		
Pelec	Power input to motor	3448	3448	3448	3448	3448	3448	3448	3448	W		
WCuR	Cobberloss rotor	97.2843	97.2843	97.2843	97.2843	97.2843	97.2843	97.2843	97.2843	W		
	Ironloss + SLL stator yoke	37.8037	37.8037	37.8037	37.8037	37.8037	37.8037	37.8037	37.8037	W		
	Ironloss + SLL stator tooth	19.3223	19.3223	19.3223	19.3223	19.3223	19.3223	19.3223	19.3223	W		
	Ironloss + SLL rotor tooth	5.8243	5.8243	5.8243	5.8243	5.8243	5.8243	5.8243	5.8243	W		Both rotor tooth and rotor tooth top
Wiron	Ironloss	49.0002	49.0002	49.0002	49.0002	49.0002	49.0002	49.0002	49.0002	W		
Wsll	Stray load loss	63.5645	63.5645	63.5645	63.5645	63.5645	63.5645	63.5645	63.5645	W		
Wwf	Vent. loss and rotational loss	32.8862	32.8862	32.8862	32.8862	32.8862	32.8862	32.8862	32.8862	W		
Wekstra	Extra loss	145.4509	145.4509	145.4509	145.4509	145.4509	145.4509	145.4509	145.4509	W	Pkorr-PowerSh=Wiron+Wsll+Wwf	
PowerSh *	Shaft power	3012	2987	3000	3012	2990	3012	3012	3012	W	Pelec-Wiron-Wsll-Wwf-WCuS-WCuR	Compare to PowerSh
PowerSh	Shaft power	3010	3010	3010	3010	3010	3010	3010	3010	W		
Pgab	Airgab power	3142	3117	3130	3142	3120	3142	3142	3142	W	Pelec-Wiron-Wsll-WCuS	
Pkorr	Shaft power and extra loss	3156	3156	3156	3156	3156	3156	3156	3156	W	PowerSh+Wiron+WsllH+Wwf	Including iron- and frictional loss
TorqSh	Shaft torque	9.8854	9.8854	9.8854	9.8854	9.8854	9.8854	9.8854	9.8854	Nm	PowerSh*30/(rpm*pi)	Compare to TorqSh
Torqkorr	Torque including extra loss	10.3631	10.3631	10.3631	10.3631	10.3631	10.3631	10.3631	10.3631	Nm	Pkorr*30/(rpm*pi)	Including iron- and frictional loss
Ttab	Torque loss	0.4776	0.4776	0.4776	0.4776	0.4776	0.4776	0.4776	0.4776	Nm	Torqkorr-TorqSh	Iron- and frictional loss
Brtpk	Peakfluxdensity in rotor teeth	1.6505	1.6505	1.6505	1.6505	1.6505	1.6505	1.6505	1.6505	T		
Bstpk	Peakfluxdensity in stator teeth	1.5425	1.5425	1.5425	1.5425	1.5425	1.5425	1.5425	1.5425	T		
Bsypk	Peakfluxdensity in stator yoke	1.5098	1.5098	1.5098	1.5098	1.5098	1.5098	1.5098	1.5098	T		
Iph1	RMS fase current	5.6854	5.6854	5.6854	2.8427	2.8427	1.4214	3.4112	1.8951	A rms	Iph1*3/Phaser	
IL1	RMS line current	5.6854	5.6854	5.6854	2.8427	2.8427	1.4214	3.4112	1.8951	A rms	Iph1*3/Phaser	Starpoint connected motor
WCuR	Cobberloss rotor	97.28	97.28	97.28	97.28	97.28	97.28	97.28	97.28	W		
WCuS	Cobberloss stator	193.64	218.28	205.39	193.64	215.28	193.64	193.64	193.64	W	Iph1^2*R1*Phaser	Compare to WCuS !

Parameters from SPEED

Name	Description	3 ph.	3 ph.	3 ph. 3h.	6 ph.	6 ph. 3h.	12 ph.	5 ph.	9 ph.	Units	Equation	Note
Lstk	Stack length	140	140	140	140	140	140	140	140	mm		
LB	Length of rotorbar	140.4801	140.4801	140.4801	140.4801	140.4801	140.4801	140.4801	140.4801	mm		Compare to Lstk
Abar	Area of one rotorbar	71.0652	71.0652	71.0652	71.0652	71.0652	71.0652	88.8315	101.5217	mm^2	for N rotorbars: Abar*20/R_Bars	
RhoBar	Resistivity Alu bar	3.7942E-08	3.7942E-08	3.7942E-08	3.7942E-08	3.7942E-08	3.7942E-08	3.7942E-08	3.7942E-08	Ohm*m		
RhoEndring	Resistivity Alu endring	3.7942E-08	3.7942E-08	3.7942E-08	3.7942E-08	3.7942E-08	3.7942E-08	3.7942E-08	3.7942E-08	Ohm*m		
RotorOD	Rotor outer diameter	74.3	74.3	74.3	74.3	74.3	74.3	74.3	74.3	mm		
TW_S	Stator tooth width	3.6	3.6	3.08	3.6	3.08	3.6	4.32	4.8	mm	for M statorbars: TW_S*24/Slots	
TW_R	Rotor tooth width	4	4	3.42	4	3.42	4	5	5.714285714	mm	for N rotorbars: TW_R*20/R_Bars	
SYoke	Stator yoke width	15.625	15.625	15.625	15.625	15.625	15.625	15.625	15.625	mm		
RYoke	Rotor yoke width	4.45	4.45	4.45	4.45	4.45	4.45	4.45	4.45	mm		
Gap	Airgab length	0.35	0.35	0.35	0.35	0.35	0.35	0.35	0.35	mm		
RotJ	Moment of inertia	0.0025	0.0025	0.0025	0.0025	0.0025	0.0025	0.0025	0.0025	kg*m^2		
kC	Carter factor	1.3961	1.3961	1.3961	1.3961	1.3961	1.3961	1.3961	1.3961			
kXm	Factor for elongation of Xm	1.8639	1.8639	1.8639	1.8639	1.8639	1.8639	1.8639	1.8639			
f	Frequence	50	50	50	50	50	50	50	50	Hz		
R1	Stator resistance/phase	1.9969	2.251	2.118	3.9938	4.4400	7.9876	3.3282	5.9907	Ohm	for X phase: R1*Phaser/3	Because the area is halfed.
Xm	Main inductance	95.7897	95.7897	95.7897	95.7897	95.7897	95.7897	95.7897	95.7897	Ohm		
X1sat	Stator leakage induktans/phase	2.8487	2.8487	2.8487	5.6974	5.6974	11.3948	4.7478	8.5461	Ohm	for X phase: X1sat*Phaser/3	
X2sat	Rotor leakage induktans/phase	2.9977	2.9977	2.9977	5.9954	5.9954	11.9908	4.996166667	8.9931	Ohm	for X phase: X2sat*Phaser/3	
X_rotor	X2sat transformed to rotor side	1.17E-04	1.17E-04	1.17E-04	1.17E-04	1.17E-04	1.17E-04	1.17E-04	1.17E-04	Ohm		
X2slot	Rotor leakage in slots/bar	0.7464	0.7464	0.7464	0.7464	0.7464	0.7464	0.7464	0.7464	Ohm		
X2end	Rotor leakage in endring	0.2706	0.2706	0.2706	0.2706	0.2706	0.2706	0.2706	0.2706	Ohm		
X2diff	Extra leakage in slots/bar	1.2412	1.2412	1.2412	1.2412	1.2412	1.2412	1.2412	1.2412	Ohm		
Rbar	Resistance in rotor bars	1.0174	1.0174	0.9223	1.0174	0.9223	1.0174	1.0174	1.0174	Ohm		
REndRing	Resistance in endrings	0.2746	0.2746	0.2746	0.2746	0.2746	0.2746	0.2746	0.2746	Ohm		
R2	Total rotor resistance	1.2920	1.2920	1.1969	1.2920	1.1969	1.2920	1.2920	1.2920	Ohm	Rbar+REndRing	Compare to R2 in speed

Parameters for multi winding model

Name	Description	3 ph.	3 ph.	3 ph. 3h.	6 ph.	6 ph. 3h.	12 ph.	5 ph.	9 ph.	Units	Equation	Note
r	Radius to middel of airgab	37.3250	37.3250	37.3250	37.3250	37.3250	37.3250	37.3250	37.3250	mm	(RotorOD+Gap)/2	
L	Length of rotor	140	140	140	140	140	140	140	140	mm	Lstk	
d	Airgab	0.35	0.35	0.35	0.35	0.35	0.35	0.35	0.35	mm	Gap	
Jm	Moment of inertia	0.0025	0.0025	0.0025	0.0025	0.0025	0.0025	0.0025	0.0025	kg*m^2	RotJ	
k	Airgab correction	0.3843	0.3843	0.3843	0.3843	0.3843	0.3843	0.3843	0.3843		1/(kC*kXm)	Must be changed until Xm fits
n	Stator slots	24	24	24	24	24	24	20	18		Slots	
m	Rotor slots	20	20	20	20	20	20	16	14		R_Bars	
wl	Wires/slot	39	39	39	78	78	156	78	156		TC	
p	Number of polepairs	1	1	1	1	1	1	1	1		Poles/2	
ws *	Transformation factor	191.7718	191.7718	182.5891	191.7718	182.5891	191.7718	191.7718	191.7718		(Rbar/(3/4*pi^2/m*rb))^0,5	
ws	Transformation factor	191.4488	191.4488	191.4488	191.4488	191.4488	191.4488	191.4488	191.4488		(omr/(3/4*pi^2/m))^0,5	
omr *	Transformation factor stator/rotor	13611.3268	13611.3268	12339.0276	13611.3268	12339.0276	13611.3268	17014.1585	19444.7525		3/4*pi^2/m*ws^2	Compare to omr
omr	Transformation factor stator/rotor	13565.5141	13565.5141	13565.5141	13565.5141	13565.5141	13565.5141	16956.8926	19379.3058		(kw1^2*Tph^2)/(ks1^2*m*Poles)*24	Compare to kr_RS
lm	Main inductance	0.2033	0.2033	0.2033	0.2033	0.2033	0.2033	0.2033	0.2033	H	2/3*Xm/(2*pi*f)	Compensate until k fits!
Lsl	Stator leakage inductance	0.009068	0.009068	0.009068	0.018135	0.018135	0.036271	0.015113	0.027203	H	X1sat/(2*pi*f)	
Lrl	Rotor leakage inductance	0.009542	0.009542	0.009542	0.019084	0.019084	0.038168	0.015903	0.028626	H	X2sat/(2*pi*f)	
rs	Resistance statorwinding	1.9969	2.251	2.118	3.9938	4.44	7.9876	3.3282	5.9907	Ohm	R1	
Lb	Leakage rotor bars	6.3990E-07	6.3990E-07	6.3990E-07	1.3433E-06	1.3433E-06	2.7501E-06	8.8707E-07	1.4327E-06	H	(X2sat-X2end)/(2*pi*f*omr)	Is compensated for ERB
Lea	Leakage rotor endring 1	3.1077E-09	3.1077E-09	3.1077E-09	3.1077E-09	3.1077E-09	3.1077E-09	3.8666E-09	4.4016E-09	H	X2end*2*sin(pi*Poles/(m*2))^2/(2*pi*f*omr)	
Leb	Leakage rotor endring 2	3.1077E-09	3.1077E-09	3.1077E-09	3.1077E-09	3.1077E-09	3.1077E-09	3.8666E-09	4.4016E-09	H	X2end*2*sin(pi*Poles/(m*2))^2/(2*pi*f*omr)	
rb *	Rotor bar resistance	7.4999E-05	7.4999E-05	6.7989E-05	7.4999E-05	6.7989E-05	7.4999E-05	5.9999E-05	5.2499E-05	Ohm	Rbar/omr	Compare to rb
rb	Rotor bar resistance	7.4747E-05	7.4747E-05	7.4747E-05	7.4747E-05	7.4747E-05	7.4747E-05	5.9797E-05	5.2323E-05	Ohm	RhoBar*LB/Abar	Calculated from area aso.
re	Rotor endring resistance	9.9074E-07	9.9074E-07	9.9074E-07	9.9074E-07	9.9074E-07	9.9074E-07	1.2327E-06	1.4032E-06	Ohm	REndRing*2*sin(pi*Poles/(m*2))^2/(omr)	
rea	Rotor endring resistance 1	9.9074E-07	9.9074E-07	9.9074E-07	9.9074E-07	9.9074E-07	9.9074E-07	1.2327E-06	1.4032E-06	Ohm	re	
reb	Rotor endring resistance 2	9.9074E-07	9.9074E-07	9.9074E-07	9.9074E-07	9.9074E-07	9.9074E-07	1.2327E-06	1.4032E-06	Ohm	re	

E. Static results from dynamic simulations

On the next two pages the steady state results of a range of different simulations are presented:

Comparation of motors with different number of phases and different supply.

Extra loss

Iron	49.00 W
SLL	63.56 W
Wwf	32.89 W
Sum	145.45 W

Distribution of Fe

St.Yoke	37.8	no unit
St.Tootl	19.3	no unit
Ro.Too	5.8	no unit

P2 shaft=P2 w.loss-Wwf-Fe

$$FE=(Iron+SLL)\cdot\frac{Ro.Tooth\left(\frac{Brtpk}{Brtpkr}\right)^2+St.Tooth\left(\frac{Bstpk}{Bstpkr}\right)^2+St.Yoke\left(\frac{Bsypk}{Bsypkr}\right)^2}{Ro.Tooth+St.Tooth+St.Yoke}$$

Test of induction level

+ =	Voltage can be incr. comp. to ref.	
R =	Induction to high comp. to ref.	
=	Within tolerence	0.04 T
S =	Saturated	1.90 T
		2.1 %

Colours

Yellow is stored simulations
Blue is simulation results from Speed
Green is the reference simulation

Sort by R, Source, Ph

Sim. Prog.	Source	Ph	U 1.h	I 1.h	I RMS	I p	U fp	RPM	St. Cu	Ro. Cu	Torq	Torq. rip	Brtpk	Bstpk	Bsypk	R	%	S	Cu loss	Fe	P2 w.loss	P2 shaft	I RMS 3-ph	I p 3-ph	Eta	Sim	Notes	VA peak
Multiwinding	Sinus	3	325	8.29	5.87	8.67	325	2920	206	88	10.14	0.589	1.76	1.63	1.44	0			294	113	3101	2955	5.87	8.67	87.1	2		2820
Multiwinding	Dead	12	315	1.98	1.54	3.05	250	2914	228	95	10.08	0.539	1.37	1.26	1.47	-2			323	97	3076	2946	6.16	12.21	86.7	18		3053
Multiwinding	Dead	6	318	4.04	3.04	5.60	260	2915	220	93	10.11	0.679	1.42	1.32	1.46	-1			313	99	3086	2955	6.07	11.21	86.9	14		2914
Multiwinding	Dead	3	322	8.35	6.11	11.48	290	2915	227	99	10.11	1.510	1.70	1.57	1.41	2			326	107	3086	2946	6.11	11.48	86.4	6		3330
M_ph_stj	Deadstj	12	315	2.00	1.52	2.89	301	2913	230	95	10.36	0.338	1.37	1.27	1.46	-2			325	97	3161	3031	6.07	11.55	86.9	32		3476
M_ph_stj	Deadstj	6	320	4.13	3.06	4.80	362	2912	223	98	10.36	0.581	1.54	1.43	1.42	1			321	101	3161	3027	6.12	9.61	86.9	27		3477
M_ph_stj	Deadstj	5	321	4.91	3.64	6.64	366	2913	221	95	10.33	0.729	1.45	1.35	1.44	0			316	98	3153	3022	6.06	11.06	87.1	40	statorslots=20, rotorbars=16	4046
M_ph_stj	Deadstj	3	321	8.34	6.09	11.33	338	2916	227	99	10.36	1.438	1.69	1.57	1.41	2			326	106	3165	3026	6.09	11.33	86.7	25		3826
Multiwinding	Deadx2	12	319	2.02	1.52	3.07	260	2914	217	94	10.06	0.649	1.42	1.31	1.44	0			311	97	3071	2941	6.06	12.29	87.0	20		3195
M_ph_stj	Deadx2	9	336	2.66	1.99	4.65	281	2920	209	89	10.15	0.770	1.53	1.42	1.47	-2			297	105	3102	2964	5.96	13.95	87.2	45	statorslots=18, rotorbars=14	3920
M_ph_stj	Deadx2stj	9	336	2.69	2.00	3.65	396	2919	210	90	10.36	0.725	1.60	1.48	1.45	-1			300	106	3166	3027	5.99	10.96	87.3	44	statorslots=18, rotorbars=14	4342
M_ph_stj	Deadx2stj	6	338	3.93	2.94	5.99	418	2923	209	85	10.32	0.566	1.69	1.56	1.43	1			293	108	3159	3018	5.88	11.98	87.4	29		5011
M_ph_stj	Deadx2stj	5	309	5.17	3.73	7.01	427	2904	232	106	10.38	0.630	1.73	1.61	1.27	1			338	97	3156	3027	6.21	11.69	86.6	41	statorslots=20, rotorbars=16	4995
Multiwinding	Sinus	12	339	1.97	1.40	2.35	339	2922	187	85	10.11	0.402	1.78	1.64	1.45	-1			272	115	3092	2944	5.59	9.41	87.5	16		3194
M_ph_stj	Sinus	9	342	2.65	1.90	3.78	342	2922	194	87	10.07	0.423	1.77	1.64	1.45	-1			281	115	3080	2933	5.69	11.34	87.3	42	statorslots=18, rotorbars=14	3882
Multiwinding	Sinus	6	339	3.95	2.80	4.41	339	2923	188	83	10.14	0.338	1.79	1.66	1.46	-2			271	116	3104	2955	5.60	8.82	87.6	10		2993
M_ph_stj	Sinus	5	335	4.84	3.44	5.59	335	2921	197	87	10.07	0.515	1.76	1.63	1.44	0			284	113	3081	2935	5.73	9.32	87.2	37	statorslots=20, rotorbars=16	3125
Multiwinding	Sinus	3	325	8.29	5.87	8.67	325	2920	206	88	10.14	0.589	1.76	1.63	1.44	0			294	113	3101	2955	5.87	8.67	87.1	2		2820
M_ph_stj	Sinusstj	12	339	1.98	1.40	2.35	385	2921	189	86	10.36	0.044	1.77	1.64	1.45	-1			274	115	3169	3022	5.61	9.40	87.8	31		3620
M_ph_stj	Sinusstj	9	342	2.65	1.89	3.54	423	2921	194	87	10.36	0.133	1.77	1.64	1.45	-1			281	114	3168	3021	5.68	10.62	87.6	43	statorslots=18, rotorbars=14	4491
M_ph_stj	Sinusstj	6	335	4.00	2.84	4.40	385	2921	193	86	10.35	0.036	1.76	1.63	1.44	0			279	113	3166	3020	5.67	8.80	87.7	39		3391
M_ph_stj	Sinusstj	5	335	4.86	3.44	5.40	390	2920	197	87	10.38	0.198	1.76	1.63	1.44	0			285	112	3173	3028	5.74	8.99	87.6	38	statorslots=20, rotorbars=16	3509
M_ph_stj	Sinusstj	3	325	8.32	5.88	8.51	359	2920	207	89	10.36	0.536	1.76	1.63	1.44	0			296	112	3167	3021	5.88	8.51	87.3	21		3056
Multiwinding	Square	12	306	1.97	1.57	3.70	240	2908	248	100	10.12	0.481	1.31	1.21	1.43	0			348	92	3082	2957	6.29	14.80	86.2	17		3552
Multiwinding	Square	6	306	3.97	3.21	7.28	240	2909	255	100	10.06	0.712	1.31	1.22	1.43	0			355	92	3064	2938	6.42	14.55	85.9	12		3492
M_ph_stj	Squarestj	3	319	8.48	6.18	10.85	375	2916	229	100	10.38	1.436	1.75	1.62	1.41	0			329	109	3169	3026	6.18	10.85	86.5	22		4063
M_ph_stj	U3h6m10	6	325	4.03	2.93	4.14	291	2917	206	90	10.09	0.470	1.53	1.42	1.45	-1			296	103	3082	2946	5.86	8.28	87.2	51		2411
M_ph_stj	U3h6m25	6	325	4.03	2.93	3.96	305	2917	206	90	10.10	0.487	1.58	1.47	1.45	-1			296	105	3085	2947	5.86	7.92	87.2	48		2413
M_ph_stj	U3h6m75	6	325	4.03	2.93	4.68	344	2917	206	91	10.12	0.539	1.75	1.62	1.42	1			296	110	3090	2947	5.86	9.37	87.0	47		3221
M_ph_stj	U3h6p0	9	325	2.72	1.99	3.62	282	2914	214	96	9.98	0.675	1.49	1.38	1.42	1			309	99	3046	2914	5.97	10.86	86.9	54	Lavt startmoment	3060
M_ph_stj	U3h6p0	6	325	4.03	2.93	4.29	282	2917	205	90	10.09	0.507	1.51	1.40	1.45	-1			296	102	3083	2948	5.86	8.58	87.3	46		2418
M_ph_stj	U3h6p0	5	325	4.89	3.56	5.37	282	2916	211	92	10.07	0.581	1.51	1.40	1.45	-1			303	102	3077	2942	5.94	8.95	87.1	52		2521

Comparation of motors with different number of phases and different supply.

Extra loss

Iron	49.00 W
SLL	63.56 W
Wwf	32.89 W
Sum	145.45 W

Distribution of Fe

St.Yoke	37.8 no unit
St.Tooth	19.3 no unit
Ro.Tooth	5.8 no unit

P2 shaft=P2 w.loss-Wwf-Fe

$$FE=(Iron+SLL)\cdot\frac{Ro.Tooth\left(\frac{Brtpk}{Brtpkr}\right)^2+St.Tooth\left(\frac{Bstpk}{Bstpkr}\right)^2+St.Yoke\left(\frac{Bsypk}{Bsypkr}\right)^2}{Ro.Tooth+St.Tooth+St.Yoke}$$

Test of induction level

+	=	Voltage can be incr. comp. to ref.
R	=	Induction to high comp. to ref.
	=	Within tolerence 0.04 T
S	=	Saturated 1.90 T
		2.1 %

Colours

Yellow is stored simulations
Blue is simulation results from Speed
Green is the reference simulation

Sort by R, Source, Ph

Multiwinding	Sinus	3	325	8.29	5.87	8.67	325	2920	206	88	10.14	0.589	1.76	1.63	1.44		0		294	113	3101	2955	5.87	8.67	87.1	2		2820
Sim. Prog.	**Source**	**Ph**	**U 1.h**	**I 1.h**	**I RMS**	**I p**	**U fp**	**RPM**	**St. Cu**	**Ro. Cu**	**Torq**	**Torq. rip**	**Brtpk**	**Bstpk**	**Bsypk**	**R**	**%**	**S**	**Cu loss**	**Fe**	**P2 w.loss**	**P2 shaft**	**I RMS 3-ph**	**I p 3-ph**	**Eta**	**Sim**	**Notes**	**VA peak**
M_ph_stj	U3h6p0	3	312	8.48	6.20	8.52	270	2914	231	97	10.13	0.489	1.51	1.40	1.42		1		328	99	3090	2958	6.20	8.52	86.5	53		2305
M_ph_stj	U3h6p0stj	9	332	2.70	1.98	3.62	385	2916	209	93	10.36	0.586	1.58	1.47	1.44		0		302	104	3164	3027	5.93	10.87	87.3	55		4182
M_ph_stj	U3h6p10	6	325	4.02	2.93	4.43	291	2917	205	90	10.12	0.500	1.54	1.42	1.45		-1		295	103	3091	2955	5.85	8.86	87.3	50		2578
M_ph_stj	U3h6p25	6	325	4.03	2.93	4.61	305	2917	205	90	10.09	0.498	1.59	1.47	1.45		-1		296	105	3082	2944	5.86	9.23	87.2	49		2813
Multiwinding	XDeadx2	12	314	2.05	1.54	3.00	255	2909	223	99	10.07	0.609	1.39	1.29	1.41		2		322	93	3068	2942	6.15	12.02	86.8	19		3064
M_ph_stj	XSinus	5	335	4.82	3.43	5.70	335	2921	196	87	10.24	1.300	1.76	1.63	1.44		0		283	113	3133	2987	5.72	9.51	87.4	36	statorslots=20, rotorbars=18	3186
M_ph_stj	XSinusstj	3	329	8.47	5.99	8.76	384	2920	215	87	10.36	0.544	1.74	1.61	1.44		0		302	112	3169	3024	5.99	8.76	87.1	35	rotorbars=10	3362
Multiwinding	Dead	3	278	9.63	6.95	11.78	250	2880	291	136	10.04	1.339	1.42	1.31	1.18	+	18		428	74	3029	2922	6.95	11.78	84.5	4		2944
Multiwinding	Dead	3	300	8.89	6.45	11.61	270	2901	252	114	10.05	1.397	1.56	1.44	1.29	+	10		366	90	3053	2930	6.45	11.61	85.7	5		3135
M_ph_stj	Deadstj	3	276	9.65	6.95	11.65	302	2880	294	137	10.35	1.242	1.42	1.31	1.17	+	19		431	74	3122	3015	6.95	11.65	84.9	23		3523
M_ph_stj	Deadx2stj	6	286	4.59	3.36	6.21	333	2885	272	126	10.36	0.592	1.40	1.29	1.18	+	18		398	74	3132	3025	6.71	12.43	85.7	28		4144
Multiwinding	Sinus	6	325	4.09	2.90	4.57	325	2916	201	92	10.10	0.413	1.70	1.58	1.39	+	3		293	106	3083	2945	5.80	9.14	87.2	9		2972
M_ph_stj	Sinusstj	12	325	2.05	1.45	2.43	373	2914	203	95	10.37	0.046	1.69	1.56	1.38	+	4		297	104	3165	3028	5.81	9.73	87.5	30		3632
M_ph_stj	Sinusstj	6	325	4.11	2.91	4.49	377	2915	203	93	10.37	0.046	1.70	1.58	1.39	+	3		296	106	3166	3028	5.82	8.98	87.4	24		3390
Multiwinding	Dead	6	357	3.73	2.85	5.66	290	2934	193	73	10.16	0.615	1.61	1.49	1.65	R	-15		266	127	3123	2963	5.69	11.32	87.4	13		3284
M_ph_stj	Deadstj	6	357	3.80	2.85	4.46	391	2932	194	77	10.36	0.594	1.73	1.61	1.62	R	-12		271	129	3182	3020	5.71	8.91	87.5	26		3480
Multiwinding	Deadx2	3	324	7.41	8.27	21.27	500	2932	399	114	10.04	4.017	2.56	2.37	1.25	R	-45	S	513	146	3082	2903	8.27	21.27	80.8	7		10635
Multiwinding	Deadx2	3	290	8.14	8.35	21.06	450	2911	406	132	10.04	3.493	2.22	2.05	1.11	R	-26	S	538	111	3062	2918	8.35	21.06	81.1	8		9476
M_ph_stj	Deadx3stj	6	342	3.85	3.12	8.41	474	2928	233	86	10.41	0.865	1.95	1.81	1.38	R	-11	S	320	118	3193	3042	6.25	16.82	86.6	34		7979
Multiwinding	Sinus	12	354	1.91	1.35	2.31	354	2929	176	77	10.11	0.372	1.86	1.72	1.52	R	-6		253	126	3102	2943	5.42	9.24	87.7	15		3266
SPEED	Sinus	3	325	8.04	5.69	8.04	325	2908	194	97	10.36	-	1.65	1.54	1.51	R	-5		291	115	3156	3008	5.69	8.04	87.3	1		2615
Multiwinding	Square	6	344	3.61	3.03	7.82	270	2931	227	77	10.16	0.691	1.50	1.39	1.65	R	-15		304	121	3120	2965	6.06	15.64	86.6	11		4222
Multiwinding	Square	3	318	7.99	6.66	14.66	250	2921	272	103	10.12	2.007	1.50	1.39	1.52	R	-5		375	108	3094	2953	6.66	14.66	85.1	3		3665
M_ph_stj	Squarestj	12	318	1.91	1.50	3.57	315	2916	237	92	10.36	0.269	1.38	1.28	1.50	R	-4		329	101	3164	3030	6.01	14.27	86.7	33		4501
M_ph_stj	SinusV	3	325	8.35	5.91	8.71	325	2904	236	106	10.17	0.581	1.75	1.62	1.43		1		342	111	3092	2949	5.91	8.71	85.9	56	Winding a)	2834
M_ph_stj	U3h6p0V	3	312	8.52	6.24	8.69	270	2904	248	108	10.11	0.499	1.78	1.65	1.41		-1		355	104	3074	2937	6.24	8.69	85.6	57	Small teeth winding a)	2351
M_ph_stj	SinusV	6	338	3.99	2.83	4.43	338	2906	227	102	10.13	0.351	1.77	1.64	1.44		0		329	114	3084	2938	5.66	8.86	86.1	58	Winding b)	2996
M_ph_stj	U3h6p0V	6	325	4.05	2.95	4.35	282	2907	232	101	10.12	0.530	1.76	1.63	1.44		0		333	106	3080	2941	5.91	8.70	86.2	59	Small teeth winding b)	2451
M_ph_stj	U3h6p0V	6	325	4.06	2.96	4.36	282	2899	248	110	10.04	0.557	1.50	1.39	1.44		0		358	100	3046	2913	5.92	8.71	85.6	60	Winding b)	2454
M_ph_stj	U3h6p0V	6	328	4.37	3.18	4.65	285	2899	270	120	11.02	0.632	1.77	1.64	1.45		-1		390	114	3346	3200	6.37	9.29	85.6	61	Winding b)	2644